Nitrogen cycling in the subtropical southeast Atlantic and southwest Indian Oceans as recorded by the nitrogen isotopes of modern planktic foraminifera

Thesis presented for the Degree of

DOCTOR OF PHILOSOPHY

in the Department of Oceanography

UNIVERSITY OF CAPE TOWN

Robyn L. L. Granger

Supervisors: A/Prof. Sarah Fawcett, Dr. Sandi Smart, and Dr. Alan Foreman

May 2023

Plagiarism Declaration

I, Robyn Leigh Lindiwe Granger, know the meaning of plagiarism and declare that all of the work in the document, save for that which is properly acknowledged, is my own.

Robyn Granger

Abstract

Despite the importance of nitrogen (N) for ocean productivity, and the long history of using fossil foraminifera to reconstruct past ocean conditions, it is only in recent years, due to methodological advances, that the nitrogen isotope ratio (δ^{15}N) of foraminifera has become a viable proxy for past marine nutrient cycling. Organic N trapped within planktic foraminifer shells is protected from bacterial degradation, with its δ^{15}N recording the processes acting on the upper-ocean N pool. This thesis examines the relationship between local biogeochemical cycling and foraminifera tissue- and shell-bound δ^{15}N in the greater Agulhas Current system and southeast Atlantic Ocean, focusing on the implications for reconstructing Agulhas leakage (i.e., the transfer of Indian Ocean waters into the Atlantic). Past fluctuations in this important component of the Atlantic Meridional Overturning Circulation, whereby warm, saline Agulhas waters are transported to the North Atlantic along its upper limb, have been tied to global glacial-interglacial cycles, highlighting the region's sensitivity to large-scale climate change. The work detailed in this thesis includes the first foraminifer-bound δ^{15}N ground-truthing studies from the southeast Atlantic and the Agulhas Current regions and examines the extent to which the unique δ^{15}N signature of Indian Ocean nitrate is preserved in the tissue and shells of foraminifera living in Agulhas leakage features (e.g., eddies). The isotopes of several forms of N, including nitrate, particulate organic N, size-fractionated zooplankton biomass, living foraminifera tissue and shell N, and fossil foraminifera, were measured and interpreted in the context of coincident hydrographic measurements to determine the controls on the δ^{15}N of foraminifera and their potential food sources.

The data presented here reveal that mixed layer nitrate δ^{15}N was noticeably lower within an Agulhas eddy than it was for the surrounding Cape Basin waters, a characteristic that was likely inherited from low thermocline nitrate δ^{15}N produced in the region of leakage origin, the Agulhas Current System. Similarly, the δ^{15}N of foraminifera inhabiting the Agulhas eddy was found to be low relative to foraminifera under background southeast Atlantic conditions, despite foraminifera in the Agulhas Current System displaying on average a higher δ^{15}N than was recorded by foraminifera inhabiting the eddy. The data therefore suggest that anticyclonic eddies "leaking" into the region from the Indian Ocean maintain a low-δ^{15}N environment that sustains the growth of foraminifera for several months, and that N_2 fixation and/or recycling of low-δ^{15}N ammonium within the eddy environment likely contributed to lowering of foraminifer-δ^{15}N. That foraminifer-δ^{15}N is

on average 2-3 ‰ lower in Agulhas leakage than in the southeast Atlantic suggests that enduring periods of increased leakage could result in relatively low-δ^{15}N material being transferred to the sediment and recorded.

A comparison of data from the southeast Atlantic and Agulhas regions to previous ground-truthing studies from the Sargasso Sea and Southern Ocean reveals similarities in both foraminifer tissue-shell δ^{15}N relationships and inter-species δ^{15}N differences. For instance, symbiont-hosting foraminifera are consistently lower in δ^{15}N than deeper-dwelling, symbiont-barren individuals at the same location due to the symbiont's ability to recycle low-δ^{15}N ammonium. Also consistent with previous studies is the positive correlation observed between fossil foraminifera from core tops and modern shell- and biomass δ^{15}N in the Atlantic, despite sediment being derived from multiple locations within the Cape Basin. This study adds to burgeoning efforts to ground-truth the foraminifer-δ^{15}N palaeoproxy and supports the argument that the δ^{15}N of living foraminifera, which is set by both the local N supply and N-cycling processes, can be deduced from foraminifera shell-bound δ^{15}N in the sediment record. Furthermore, the work detailed in this thesis examines how the unique δ^{15}N of the nitrate and biological community of a particular water mass might be leveraged to reconstruct past variations in Agulhas leakage.

Acknowledgements

I've been writing this PhD for roughly one fifth of my life. When put like that, it's not that surprising to look back and realise that a whole village of people have contributed to my work, both professionally or personally. First, thanks must go to my supervisors, Assoc. Prof. Sarah Fawcett, Dr. Sandi Smart and Dr. Alan Foreman, without whom this work would not be possible. Thank you for encouraging me during this journey, investing in me, and providing your expertise in this weirdly niche field that brings me joy. Sandi, you were particularly instrumental in mentoring me, providing as much personal support as professional, and I hope to someday pay it forward by being some other student's 'Sandi.'

Special thanks must go to the Environmental Geochemistry Group at the Max Planck Institute for Chemistry for allowing me use of their laboratories, but also for teaching me various methods, including me in lab meetings, and never failing to collect me for the 'lunch train!' I especially appreciate Dr. Alfredo Martinez-Garcia for making time to discuss my results with me, and Florian Rubach for putting up with all my questions - also, I'm sorry I nearly gave you a heart attack over that gas bottle. Thanks too to Max Planck-adjacent academics, Drs. Alex Auderset and Jesse Farmer, for proof reading sections, checking up on me, and reassuring me that imposter syndrome doesn't mean that I'm a genuine imposter.

To my UCT colleagues, both those who have graduated before me and those who have yet to graduate, thank you for inspiring me and commiserating with me. To my friends, ditto. My level of appreciation for all the prayers you've prayed for me is matched only by my appreciation for your senses of humour. Julz, thanks for being my friend/sister/partner in crime for the better part of two decades, despite my refusing to watch Star Wars.

I'm also extremely grateful to my flatmates who have put up with me during my PhD. Kerry, Miriam and Sarah - I definitely lucked out with you all. Thank you for making home a place I always love coming back to, for watching Bones with me, teaching me about astronomy, and for always making me laugh by reading out your students' funniest answers on papers that each of you were grading.

Sven, thank you for understanding me, and for your tireless efforts to make my life easier.

Adi P., thank you for all you have done for me, for sharing your wisdom, building my confidence, and teaching me the value of earnest leadership.

Finally, thank you to my family. Mom, Dad, Jess, Nan and all the rest... I could not have done this without your support. There really aren't words to describe how much your unconditional love means to me. But that's okay, because I think you already know.

And of course, I'd like to thank these last few years in general, for being some of my most memorable. The City of Cape Town's desperate attempt to avoid running out of water taught me that solutions to even the most impossible of problems can always be found, through teamwork and thinking a little outside the box. COVID-19 showed me how societal norms can change in an instant, how to persevere through fear and doubt, and how something as simple as loneliness can truly affect day-to-day life. And of course, ESKOM.... where to start? I guess what the South African electricity crisis has really taught me is that the most important specification to look at when purchasing a new laptop is its battery power.

Contents

List of Figures

List of Tables

Chapter 1

Introduction and Literature Review

1.1 Introduction

The oceans around southern Africa are home both to a strong Eastern Boundary Current (the Benguela Current) in the South Atlantic Ocean, and a vigorous Western Boundary Current (the Agulhas Current), in the Indian Ocean Fig. 1.1. The cool Benguela Current flows north towards the equator, and the Agulhas Current flows polewards until it reaches the the African cape, whereupon it loops back eastwards as the Agulhas Return Current, forming part of the southern boundary of the Indian Ocean Subtropical Gyre (Lutjeharms, 1981; Nelson and Hutchings, 1983; Shannon and Nelson, 1996; Hutchings et al., 2009; Beal et al., 2011). The proximity of both the Benguela and Agulhas systems to the Subtropical Front and Southern Ocean adds further complexity to the region when investigating climate variability, but also presents several opportunities for palaeoceanographic research (e.g., Peeters et al., 2004), as interactions between the ocean systems are thought to play a major role in global climate changes (Winter and Martin, 1990; Biastoch et al., 2008; Beal et al., 2011). The goal of this thesis is to assist palaeoceanographic research in the South Atlantic and South Indian Oceans. This will be achieved through studying how biogeochemical cycling processes lead to nitrogen isotope variability in planktic foraminifera and their surroundings, and subsequently assessing whether nitrogen isotopes in the sedimentary record can serve as a reliable indicator of past alterations in thermocline nitrate and marine productivity in this region.

1.2 The Biological Pump

The Atlantic Meridional Overturning Circulation (AMOC) Fig. 1.2 refers to the Atlantic component of the global ocean conveyor-belt, and facilitates inter-hemispheric transfer of oceanic heat and salt through the interactions of surface, thermocline and deep currents, playing an essential role in Earth's climate system (Gordon, 1986; Buckley and Marshall, 2016; Thornalley et al., 2018). Deep southward export of cool North Atlantic Deep Water (NADW) is compensated by the northward flow of warm, salty surface and intermediate

waters which undergo cooling and further evaporation before subducting and contributing to NADW formation (Kuhlbrodt et al., 2007; Garzoli and Matano, 2011). The depth and strength of overturning fluctuates over time, which has implications for global climate changes due to the close relationship between AMOC circulation and nutrient cycling, including the biological pump (Völker and Köhler, 2013; Hertzberg et al., 2016; Valley et al., 2017).

The biological pump is a term used to describe the marine biogeochemical processes which act to transfer carbon from the ocean's surface to the deep ocean (Volk and Hoffert, 1985; Martin et al., 1987). Dissolved inorganic matter is fixed by phytoplankton in the euphotic surface waters into particulate organic matter (POM) and biominerals, which are either grazed upon by zooplankton, or are transported out of the upper ocean (Boyd et al., 2019; Nowicki et al., 2022; Siegel et al., 2023). Once phytoplankton die, their biomass sinks out of the euphotic zone and is decomposed into inorganic forms; some is recycled back into the euphotic layer as dissolved inorganic carbon, and some (usually larger, more rapidly sinking) particles 'escape' and sink to the deep ocean or sea floor as marine snow (McCave, 1975; Suess, 1980; Billett et al., 1983; Martin et al., 1987; Alldredge and Silver, 1988; Henson et al., 2012; Devries et al., 2012). This deeper remineralization results in a more efficient biological pump, as more carbon is removed from surface waters, and less recycled nutrients are available to support new phytoplankton growth (Ito and Follows, 2005; Boyd et al., 2019; Devries et al., 2012). When nutrients remain unused in the euphotic layer, less carbon is sequestered into the deep ocean and the biological pump is less efficient, driving an increase in atmospheric CO_2 (Broecker, 1982; Broecker and Peng, 1987; Sigman and Boyle, 2000; Ito and Follows, 2005; Schmittner and Galbraith, 2008; Schmittner and Somes, 2016). A less efficient pump has been associated with past deglacial events (e.g., Heinrich Stadial 1, $\sim$ 14,500 - 18,000 years before present (BP)), and is thought to have been triggered as a result of a slowdown in the AMOC (Gherardi et al., 2009; Oppo et al., 2015; Bauska et al., 2016; Hertzberg et al., 2016), given that an increase in atmospheric CO_2 has been shown to drive an increase in global temperatures (Petit et al., 1999; Kohfeld and Ridgwell, 2009). The suggestion that biological pump efficiency is a primary driver of atmospheric CO_2 variability therefore points to AMOC being a vital mechanism responsible for modulating CO_2 over time (Schmittner and Galbraith, 2008; Hertzberg et al., 2016).

1.3 Agulhas Leakage and the Atlantic Meridional Overturning Circulation

One of the key components that influences AMOC is the transport of warm, salty water from the Indian to the Atlantic Ocean, a process known as Agulhas leakage (Lutjeharms, 2006; Beal et al., 2011; Van Sebille et al., 2015). This largely occurs through mesoscale eddies which propagate into the Cape Basin from the east, and continue northwards as

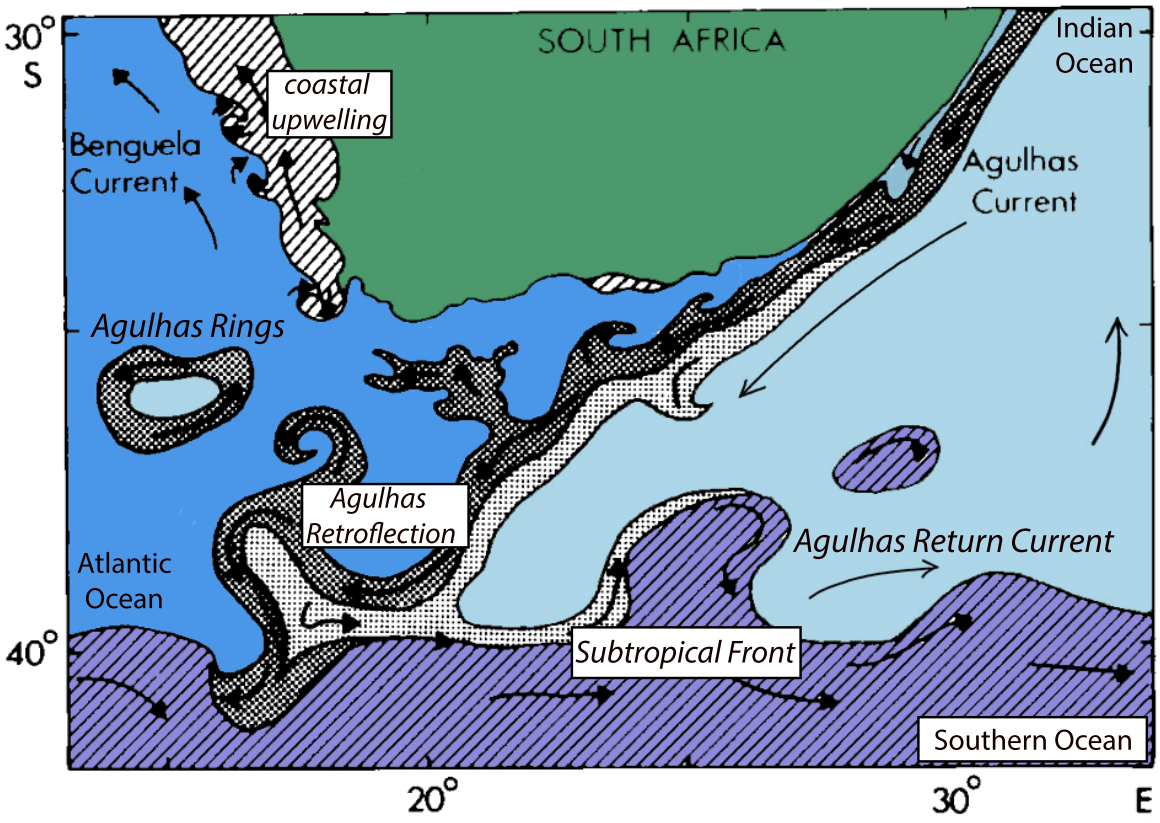

Figure 1.1: Schematic of the ocean systems and their important features surrounding Southern Africa, adapted from Hutchings et al. (1986).

part of the upper limb of the AMOC (Beal et al., 2011; Rühs et al., 2013). Leakage through the Indian-Atlantic oceanic gateway is the sole mechanism by which Indian Ocean waters enter the Atlantic (Lutjeharms, 2006; Beal et al., 2011).

Over orbital to millennial timescales, changes in leakage volume can affect the formation of NADW, whilst fluctuations in leakage over decadal timescales contribute to AMOC variability (Biastoch et al., 2008; Caley et al., 2011; Simon et al., 2013). The most accepted interpretation of millennial-scale fluctuations in Agulhas leakage volume is that changes appear to be driven primarily by latitudinal shifts in the mid-latitude westerly wind belt as well as through the modification of wind intensity (Bard and Rickaby, 2009; Durgadoo et al., 2013; Simon et al., 2013; Biastoch et al., 2015; Cheng et al., 2018; Tim et al., 2019). Most palaeoceanographic records suggest that a poleward (equatorward) shift in the wind belt results in an increase (decrease) in Agulhas leakage and a decrease (increase) in wind intensity (Peeters et al., 2004; Marino et al., 2013), although opinions differ as to which exerts more control on AMOC. Rapid warming and salinification of surface waters in the region of the Indo-Atlantic gateway are thought to have been a response to the wind shifts and subtropical front migration associated with early stages of glacial terminations (Peeters et al., 2004; Martínez-Méndez et al., 2010; Dyez et al., 2014; Kasper et al., 2014; Koutsodendris et al., 2014; Petrick et al., 2015a; Simon et al., 2015). The negative buoyancy associated with leaked Indian Ocean waters is thought to

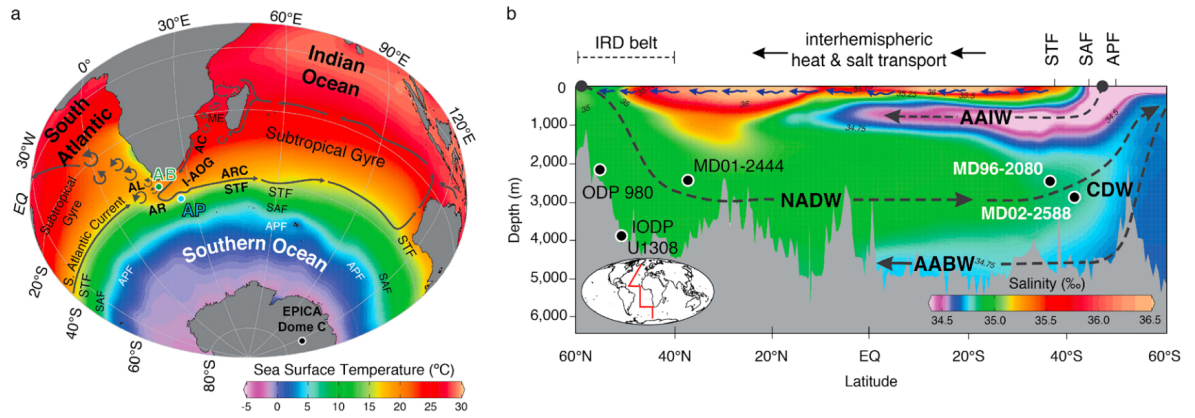

Figure 1.2: Maps showing the influence of Agulhas leakage on the Atlantic Meridional Overturning Circulation (a) Mean annual sea surface temperature (Schlitzer, 2012), with arrows indicating mean surface circulation, including anticyclonic eddies moving westwards into the South Atlantic at the Agulhas Retroflection (AR). (b) Meridional cross-section of the North and South Atlantic basins (Schlitzer, 2012), indicating the northwards transport of surface and subsurface waters, and the southwards transport of North Atlantic Deep Water (NADW). The high salinity input at the surface north of the Subtropical Front (STF) is a result of Agulhas leakage. Figure is from Marino et al. (2013)

have triggered the resumption of convective overturning during periods of weak circulation (through the subduction of surface waters in the North Atlantic close to Greenland, Iceland and Norway) (Dyez et al., 2014; Koutsodendris et al., 2014), which helps to kick start a sluggish or inactive AMOC at the end of an ice age (Peeters et al., 2004; Dickson et al., 2010; Martínez-Méndez et al., 2010; Dyez et al., 2014; Kasper et al., 2014; Petrick et al., 2015a).

Understanding the relationship between Agulhas leakage and the AMOC over shorter (i.e., decadal and interannual) timescales is important for accurately projecting future climate change. On a decadal timescale, multi-proxy records suggest that Atlantic circulation has slowed over the last 150 years, and that it is declining more rapidly under the present day conditions than during the previous 1,500 years (Robson et al., 2016; Thornalley et al., 2018; Caesar et al., 2021). Initial modelling studies have shown that leakage responds to hemispheric changes in the winds on a decadal scale, with an increased volume of Agulhas leakage occurring in response to the progressive poleward migration of westerlies over the past three to four decades (Biastoch et al., 2009; Rouault et al., 2010). However, a further model has proposed the opposite effect, whereby a decrease in leakage is a response to a poleward shift in westerlies, (Durgadoo et al., 2013). These competing hypotheses underscore the complexity of Agulhas leakage and its links to climate changes at various time scales.

1.4 The challenge of reconstructing Agulhas leakage

Given the importance of Agulhas leakage to AMOC, a system which influences the efficiency of the biological pump, reconstructing leakage can provide meaningful information

about global ocean circulation and ocean-atmosphere climate changes. However, the relationship between Agulhas leakage and the AMOC, and the interaction between the South Atlantic and Indian Oceans, is not straightforward, and interpreting proxy records of leakage is difficult. For example, sea surface temperature (SST) and sea surface salinity, both considered to be proxy measures of Agulhas leakage (Martínez-Méndez et al., 2010; Caley et al., 2011; Marino et al., 2013; Dyez et al., 2014; Biastoch et al., 2015; Simon et al., 2015; Petró et al., 2016), appear to be offset from one another during some periods over the last 500,000 years, with the timing of increased salinity better matching the onset of deglaciation, whilst the SST increase is delayed (Kasper et al., 2014; Petrick et al., 2015a). A further complication to accurate interpretation is the potential discrepancy between when large changes in leakage volume occurred, relative to when Agulhas waters entered the north Atlantic. Recent speculation is that the release of Indian Ocean waters may initially lead to the development of a saline pool in the western Atlantic, before the original leaked waters are 'released' to the north Atlantic in pulses (Ballalai et al., 2019). Yet other studies have demonstrated the potential of Agulhas Current salinity or temperature changes upstream of the Indian-Atlantic gateway region to alter leakage properties without affecting the volume entering the Cape Basin, which can lead to confusion in interpreting records from the South Atlantic (Caley et al., 2011; Petrick et al., 2015b; Simon et al., 2015).

Furthermore, Agulhas anticyclonic eddies – the primary mode of Agulhas leakage – are not passive transporters of Indian Ocean waters, but actively modify regional biological production through upwelling, downwelling, and lateral advection (Lehahn et al., 2011; Wallschuss et al., 2022). Recent studies suggest that present-day Agulhas eddies absorb between 20% and 30% more CO_2 than their surroundings, thus contributing to the gas's removal from the atmosphere (Orselli et al., 2019a,b; Ford et al., 2022). This could lead to an underestimation of the efficiency of the biological pump when reconstructing climate conditions, if interpretations are reliant solely on salinity or temperature proxies. The aforementioned studies therefore serve to raise the question of how best to identify leakage, its impact on the biological pump, and highlight the need to better understand the processes that drive it.

1.5 The marine nitrogen cycle and nitrogen isotopes

One way in which past changes in productivity might be constructed is through examining changes to the marine nitrogen (N) cycle Fig. 1.3. Bioavailable N is required for primary productivity, but it is limited throughout much of the surface ocean (Menzel and Ryther, 1961; Thomas, 1966; John H. Ryther and Dunstan, 1971). N-cycling processes that add or remove bioavailable N to the euphotic layer help modulate the strength and efficiency of the biological pump (Raimbault et al., 1999; Yool et al., 2007; Sigman and Hain, 2012; Emerson and Yang, 2022). New N enters the marine environment through N_2 fixation, a

process performed by marine microorganisms known as N-fixers, or diazotrophs (e.g., the cyanobacterium Trichodesmium) (Dugdale and Goering, 1967; Sohm et al., 2011; Zehr and Ward, 2002a) that creates bioavailable N whilst removing CO_2 from the atmosphere (Carpenter and Price, 1977; Zehr and Ward, 2002b). Removal of fixed N from the ocean occurs via denitrification and anammox, which convert the fixed forms of N to N_2 or N_2O gas, which is ultimately released to the atmosphere (Cline and Kaplan, 1975; Ganeshram et al., 1995).

Past N-cycling processes can be reconstructed is through stable isotope analysis. There are two stable isotopes of N: ^{14}N and ^{15}N, which make up 99.63% and 0.37% of the planet's total N, respectively, and isotopic fractionation occurs as a result of differences in the reaction rates between two isotopes for a given process (Mariotti et al., 1981). During the assimilation of nitrate by phytoplankton, the degree of discrimination occurring between the two N isotopes can be defined as:

$$\varepsilon = \left[{}^{14}k/{}^{15}k - 1\right] \times 1000 \tag{1.1}$$

where ε is referred to as the isotope effect, and ^{14}k and ^{15}k represent the reaction rates of ^{14}N and ^{15}N, respectively. Nitrogen isotopes composition/ratios are written in delta notation, δ^{15}N, expressed in parts per thousand (per mille, ‰), relative to N_2 in air. All the aforementioned N-cycling processes (N_2 fixation, denitrification, assimilation and nitrification) are subject to varying degrees of kinetic isotope fractionation, which combine to leave an isotopic imprint on the remaining nitrate and the organic matter from which it is produced (Hoering and Ford, 1960; Miyake and Wada, 1967; Wada, 1980; Goering et al., 1990; Montoya, 1994; Altabet and Francois, 1994; Altabet et al., 1999).

To interpret the δ^{15}N of nitrate or particulate organic nitrogen (PON), a model is often used to provide a framework for understanding how nitrate is consumed by phytoplankton over time (Casciotti, 2016). The Rayleigh model is one such simplified approach (Sigman and Casciotti, 2009). It assumes that the rate of consumption by phytoplankton is proportional to the fraction of remaining available nitrate in the euphotic zone, given a finite nutrient supply (Sigman et al., 1999). This is a good approximation of many ocean systems, including the South Atlantic (Louanchi and Najjar, 2000; Sato and Polito, 2014), where the surface ocean receives nitrate during a season (e.g., during winter, where decreased stratification leads to upward mixing of subsurface nutrients into the euphotic zone; Sarmiento et al. 2004), and little to no nutrients during the season of nitrate uptake that follows (e.g., spring and summer) (Sigman et al., 1999). When using the Rayleigh model (Fig. 1.4), ε remains constant, and a constant δ^{15}N is assumed for the initial nitrate source. Under these conditions, the δ^{15}N of the reactant (nitrate) can then be approximated as:

$$\delta^{15}\mathrm{N}_{reactant} = \delta^{15}\mathrm{N}_{initial} - \varepsilon \times \ln(f) \tag{1.2}$$

where $\delta^{15}\mathrm{N}_{initial}$ is the δ^{15}N of the initial supply of nitrate available to be consumed and

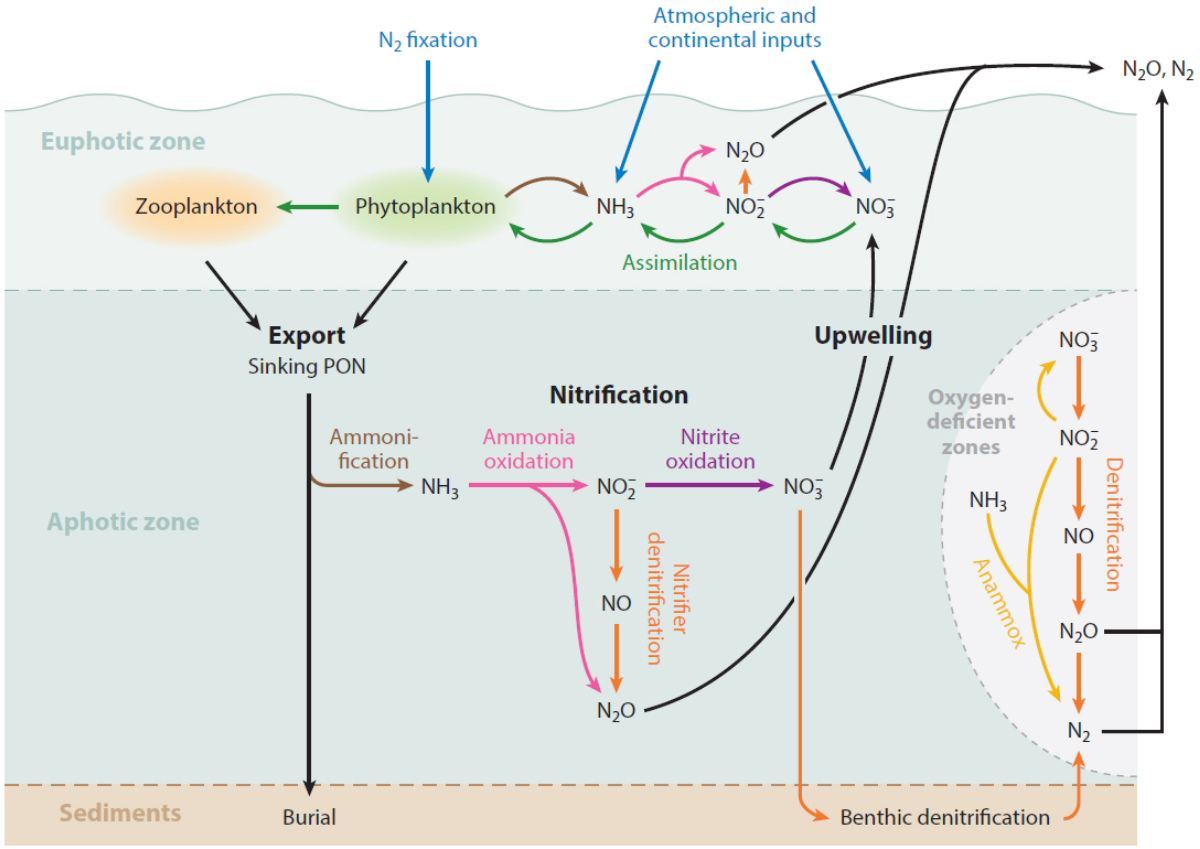

Figure 1.3: Overview of the marine nitrogen cycle, showing the processes associated with the inputs (N_2 fixation and continental inputs), losses (denitrification) and internal cycling (assimilation and nitrification) of bioavailable nitrogen. Figure is from Casciotti (2016).

f refers to the fraction of the supply that remains. Nitrate assimilation by phytoplankton exponentially discriminates against ^{15}N with an estimated global average of between 4 and 6 ‰, and the nitrate (and the PON subsequently produced from it) becomes enriched as the remaining nitrate pool is used up. (Wada and Hattori, 1978; Sigman et al., 1999).

The instantaneous $\delta^{15}N$ of PON is a measure of the isotopic value at a specific point, and is consistently offset by the amount of the isotope effect, whereas the integrated $\delta^{15}N$ is a reflection of the total accumulated PON pool. The two are calculated as follows:

$$\delta^{15}N_{instantaneous} = \delta^{15}N_{reactant} - \varepsilon \tag{1.3}$$

$$\delta^{15}N_{integrated} = \delta^{15}N_{initial} + \varepsilon \times \left[\frac{f}{1-f}\right] \times \ln(f) \tag{1.4}$$

Because of the isotope effect (i.e., discrimination against ^{15}N), partial consumption of the available nitrate produces PON with a lower $\delta^{15}N$ than that of the original nitrate supply, whilst complete utilisation of the available nitrate causes $\delta^{15}N$ of the final particulates increasingly resemble that of the original supply (Altabet, 1988; Francois and Altabet, 1992). If nitrate is completely consumed, the $\delta^{15}N$ of the particulate organic N will be equal to that of the original supply, and no isotope effect will be expressed.

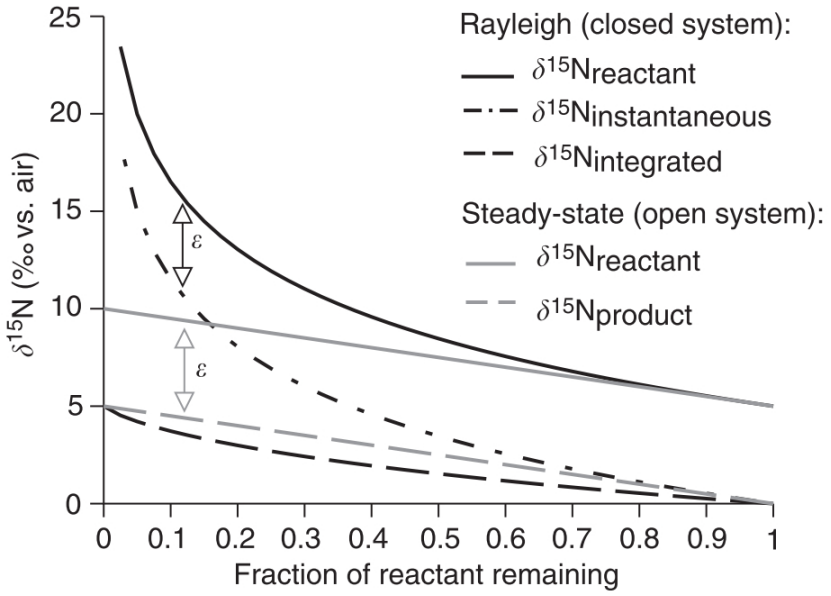

Figure 1.4: Graph showing the effect of nitrate assimilation on δ^{15}N using the Rayleigh (closed nitrate pool) and Steady state (continuous nitrate supply) models. This example uses an isotope effect (ε) of 5 ‰ and an initial δ^{15}N of 5 ‰ for the reactant (nitrate). ε approximates the difference between the reactant N and product N (particulate organic nitrogen) in the case of the instantaneous product. Figure is from Sigman and Casciotti (2009).

Therefore, PON δ^{15}N variation in N-limiting oligotrophic regions (low latitudes and subtropical gyres) should reflect changes in the δ^{15}N of the source (Altabet, 1988; Francois and Altabet, 1992).

Heterotrophic zooplankton inherit the δ^{15}N of the PON they consume, plus additional δ^{15}N elevation due to trophic enrichment (Minagawa and Wada, 1984). After death, some material sinks to the seafloor and is buried, where the isotopic signal can be preserved in the sediment (Francois and Altabet, 1992; Altabet and Francois, 1994). Reconstructing changes in past δ^{15}N is therefore a useful approach with which palaeoceanographic changes in the marine N cycle can be analysed.

In order to understand the reasons for sedimentary δ^{15}N variation at a site over glacial-interglacial time frames, it is crucial to determine the dominant N processes present in the modern system. Isolating the important N-cycling processes in a marine system and investigating their potential influences on δ^{15}N, not only provides insight into how the system might respond to future changes over time, but also allows for better global recognition of N-cycling processes when interpreting δ^{15}N variability in the sediment record (Sigman and Casciotti, 2009).

Many studies attribute the increased efficiency associated with glacial periods (e.g., the Last Glacial Maximum) to a decrease in denitrification and/or enhanced N_2 fixation increasing the relative consumption of fixed N in the surface ocean (McElroy, 1983; Altabet et al., 1995; Ganeshram et al., 1995; Broecker, 1998; Archer and Winguth, 2000; Eugster et al., 2013; Landolfi et al., 2021). Others propose that the increased biological pump

efficiency during glacial periods was the result of more complete utilization of the available N pool in high latitude regions that (under present-day conditions) contain excess nitrate (Sigman and Boyle, 2000; Martínez-García et al., 2014). Utilization of marine N, referred to as assimilation, is carried out by microorganisms (e.g., phytoplankton), and nitrate, ammonium, and nitrite are all forms which have the potential to be assimilated (Wada and Hattori, 1978; Waser et al., 1998). Nitrate (and to a lesser degree, ammonium) tend to be more abundant in the water column, due to nitrite's role as a transient intermediate during nitrification, the process whereby bacteria oxidise ammonium to nitrate (Ward et al., 1982; Ward, 2008; Ryabenko, 2013; Kits et al., 2017). Increasing N utilization during the glacial periods could have been achieved through the addition of iron (a limiting trace metal in the Southern Ocean that is necessary for primary production; Trull et al. 2008; Martínez-García et al. 2014; Studer et al. 2015), or by increasing stratification, which consequently lowered the rate of nutrient transport to the euphotic layer (Sigman et al., 2000).

Bulk sediment analysis of δ^{15}N has until recently been the primary method of generating palaeoceaongraphic records of N variability (e.g., Freudenthal et al., 2001; Jenkyns et al., 2001; Robinson and Meyers, 2002; Galbraith et al., 2013). In high nutrient regions where N is not limiting (e.g., the Southern Ocean), δ^{15}N variability in sediments may reflect the degree of nitrate consumption, from which the efficiency of global biogeochemical cycling could be inferred (Sigman and Casciotti, 2009; Martínez-García et al., 2014). In oligotrophic regions where N is a limiting factor in primary production, changes in sedimentary δ^{15}N primarily reflect changes in N sources (Ren et al., 2012a; Kast et al., 2019). Because essentially all surface nitrate is consumed on an annual basis, it is expected that variation in the δ^{15}N of exported material in these regions is a good approximation of changes in the δ^{15}N supply (Sigman and Casciotti, 2009).

However, bulk particle δ^{15}N has been shown to undergo isotopic alteration upon sinking out of the euphotic zone, as ^{14}N is preferentially removed during decay, and prolonged sinking of particles, or exposure at the sediment-water interface can significantly alter the original δ^{15}N signal (Wada, 1980; Altabet et al., 1991; Altabet and Francois, 1994, 2001; Lehmann et al., 2002; Lourey et al., 2003; Gaye-Haake et al., 2005; Robinson et al., 2012). It is difficult to assess whether alterations to bulk sediment δ^{15}N have been consistent over time; consequently, it has proven challenging to account for or accurately constrain additional fractionation effects that accompany the decomposition of material (Lehmann et al., 2002; Robinson et al., 2012).

To minimize the additional fractionation on δ^{15}N that occurs after particulates sink out of the euphotic zone, research has begun to focus on using the δ^{15}N of microfossils (diatoms and foraminifera) as a proxy for nutrient cycling in the ocean (Ren et al., 2009). Diatoms and foraminifera also record past environmental conditions, but appear to be less affected by degradation due to the organic N being preserved within a biomineral matrix (Altabet, 1988; Freudenthal et al., 2001; Ren et al., 2009; Mompeán et al., 2016; Martínez-García et al., 2022). Initially suggested as a solution by (Altabet and Curry, 1989), foraminifera-

bound δ^{15}N was largely dismissed as too labour intensive to be practical, since thousands of shells were required for a single measurement. The advent of new technologies has allowed for the development of viable new proxy methods which require fewer specimens per sample measurement. This is particularly relevant for the foraminfera-bound nitrogen isotope proxy, which is reliant on accurate measurements from very small amounts of organic N (Ren et al., 2009). Trace amounts of amino acids are incorporated into the calcium carbonate tests (shells) during their construction, as organic material is used to create the template upon which calcification can occur (King and Hare, 1972; Schiebel et al., 2018). It is primarily this N, trapped between test layers, that is preserved upon the foraminifer's death. Because δ^{15}N is preserved during trophic transfer, foraminifera δ^{15}N should in theory reflect the δ^{15}N of consumed PON, which in turn is an indication of the N-cycling processes involved in the PON's production. Foraminifera-bound δ^{15}N variation in the fossil record therefore has the potential to reflect changes in the relative consumption of total nitrate available, and/or changes in the nitrate source (ie. whether nitrate in the euphotic zone available for productivity is primarily due to the upwelling of preformed nitrate or due to N_2 fixation).

1.6 Foraminifera as δ^{15}N recorders

Foraminifera are a group of heterotrophic unicellular protists whose influence on the palaeoclimatic record to date has been immeasurable (Kucera, 2007; Schiebel et al., 2018). Arguably the backbone of palaeoceanography, foraminifera are responsible for many, if not most, of the marine reconstructions we have today. Their calcite shells are ideal candidates for several proxy methods (e.g., δ^{18}O and Mg/Ca are used for reconstructing temperature; LeGrande et al. 2004; Jonkers et al. 2013), whilst a species' presence or absence can signify changes in the water column. Advantages of using planktic (subsisting in the water column) foraminifera in palaeoceanographic reconstructions include that they are abundant throughout the world's oceans, have existed for millions of years, possess narrow temperature preferences, are relatively large (in comparison to diatoms), and there are a manageable number of taxonomic species, allowing for both spatial and temporal comparisons (Robinson et al., 2023). Planktic foraminifera live their entire lives in the mid to upper water column before sinking to the seafloor after death, and their isotopic makeup can be seen as reflective of their habitat, in addition to species-specific traits (e.g., diet and physiology).

Features common to all species of foraminifera include pseudopodia, apertures, and a shell ('test') to which chambers are added as the foraminifera grows (Hemleben et al., 1989; Goldstein, 1999). Organelles and fibrillar bodies make up the cytoplasm inside the test, whilst the pseudopodia (thin rhizopodia strands made up of stretched cytoplasm) extend from the aperture away from the organism to collect food, aid mobility, and assist in reproduction (Hemleben et al., 1989; Goldstein, 1999; Kucera, 2007). Pseudopodia

activity decreases prior to new chamber formation, as a cytoplasmic bulge emerges to form the primary organic sheet. The sheet serves as the template upon which calcification occurs, resulting in a new chamber wall which is subsequently thickened by further calcification over several days (Bé et al., 1979; Kimoto, 2015). The calcium carbonate shells produced in this way are responsible for up to 60% of the total deep marine calcite budget (Schiebel, 2002; Bird et al., 2020). Species are typically classified through shell morphology. Features such as chamber size and shape, spiral form, the presence of spines or keels, wall thickness, and number and size of apertures, help to distinguish individual planktic species (i.e., morphotypes), of which there are roughly 50 in the modern ocean (and several hundred in the known fossil record spanning from the mid-Jurassic until the present day) (Kucera, 2007; Schiebel et al., 2018).

Planktic foraminifera have a wide range of feeding mechanisms, including grazing on phytoplankton and/or detritus, carnivory, and symbiosis (Hemleben et al., 1989; Goldstein, 1999; Sen Gupta, 2003; Kucera, 2007). Non-spinose species such as *Globorotalia truncatulinoides* and *Globorotalia tumida* are more passive feeders, dwelling deeper in the water column (> 200 m) and relying on sinking or suspended debris and bacteria as a food source (Hemleben et al., 1989; Sen Gupta, 2003). Photosymbiosis (endosymbiosis with autotrophic algae; Takagi et al. 2019) allows for some foraminifera species to receive fixed carbon and nitrogen from the algae, whilst additionally engaging in carnivory or consuming suspended particulate organic matter (Lee et al., 1965; Bé and Anderson, 1976; Gastrich, 1987; Bird et al., 2017). The symbiotic relationship can be obligatory (e.g., *Orbulina universa*, *Globigerinoides ruber*, *Trilobus sacculifer*, *Globigerinella siphonifera*) or facultative (e.g. *Globorotalia inflata*, *Globorotalia menardii* and *Neogloboquadrina dutertrei*), where the latter is not required for the foraminifer's survival (Hemleben et al., 1989; Takagi et al., 2019). Most species utilize more than one feeding strategy. Carnivory is especially important to spinose symbiont-bearers, who prey upon a wide range of zooplankton, including copepods, amphipods, pteropods, crustaceans, and tintinids (Bé and Hutson, 1977; Hemleben et al., 1989).

Most foraminifera have a monthly reproductive cycle and lifespan, although the deep-dweller *G. truncatulinoides* appears to reproduce annually (Hemleben et al., 1985; Schiebel and Hemleben, 2005). During its lifetime, *G. truncatulinoides* migrates vertically up to several hundred metres (Lohmann and Schweitzer, 1989); some studies suggest that reproduction occurs during late winter at depth, with juveniles ascending in the water column through mixing and innate buoyancy control (Bé and Ericson, 1963; Schiebel, 2002; Margaritelli et al., 2020), whereas other research proposes the ascension of adults before the spring bloom, prior to the release of gametes (Schiebel and Hemleben, 2005).

However, additional potential sources of δ^{15}N variation need to be considered. Interpretation of foraminifera-bound δ^{15}N requires an in-depth knowledge of regional nutrient cycling, local water mass transport, and an understanding of foraminifera morphology, life cycles, habitat preferences and food strategies (Ren et al., 2012b). Initial work us-

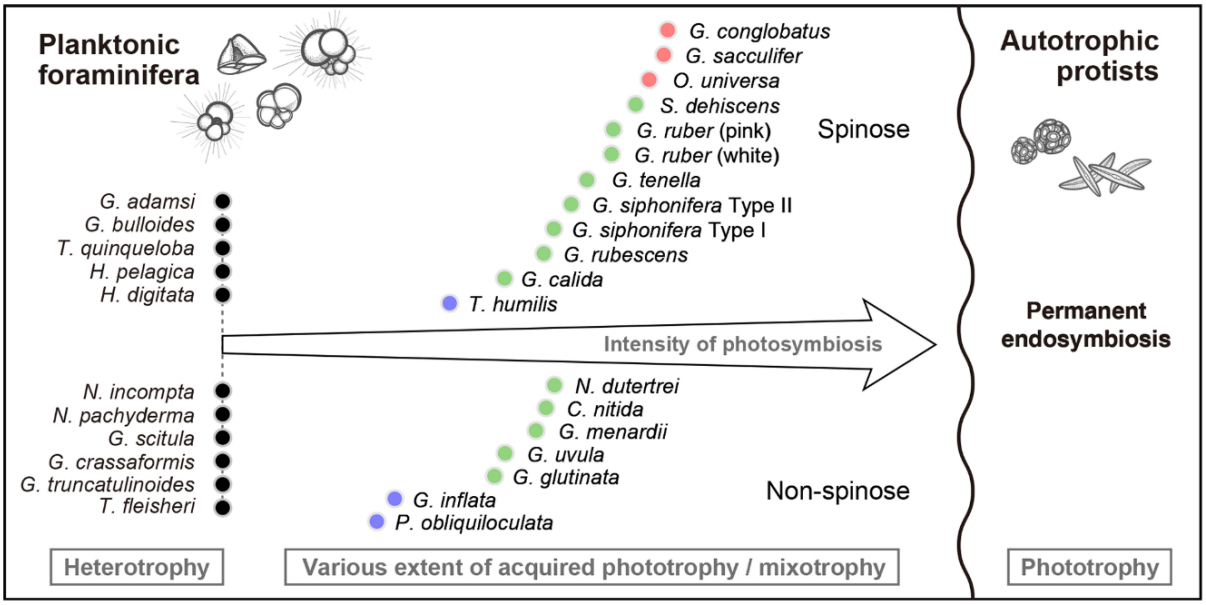

Figure 1.5: A conceptual diagram from Takagi et al. (2019), showing the reliance of foraminifera on symbionts. Colours represent clusters of similar species (determined by the fraction of individuals with symbionts, the relationship between test size and chlorophyll a content, the ratio of chlorophyll a to biomass, and the maximum potential for photosynthetic activity).

ing foraminifera-bound δ^{15}N in downcore reconstructions has been promising, which has served to highlight the need for ground-truthing studies in order to determine the relationship between foraminifera and nitrate under different ocean conditions. Robinson et al. (2023) summarize how ongoing calibration research is focused on three main questions: (1) is the shell-bound δ^{15}N a good reflection of foraminifer tissue δ^{15}N; (2) is the δ^{15}N of living foraminifera preserved in the fossil shells; and (3) what processes influence the δ^{15}N of foraminifera?

Tissue δ^{15}N refers to the isotopic composition of living foraminifera biomass (i.e., not preserved in the fossil record), whereas shell-bound δ^{15}N refers to measurements acquired from the N trapped between shell layers, which is the fraction that remains post-deposition. Initial measurements from the Sargasso Sea and Southern Ocean have observed, on average, little to no difference between tissue and shell-bound δ^{15}N (Smart et al., 2018, 2020), which appears promising for point (1). Regarding point (2), comparisons between foraminifer δ^{15}N in living and core-top (recent sediment) measurements are limited, but thus far suggest only minimal alteration ($\sim$0.6 ‰ increase) in the δ^{15}N of fossil shells relative to living ones (Ren et al., 2012b; Smart et al., 2018). Point (3) requires a more regionally-specific approach in order to determine what N-cycling processes are dominant in driving changes in modern foraminiferδ^{15}N at a specific location. Research in the low-latitude ocean shows that the δ^{15}N of foraminifera track the δ^{15}N of thermocline nitrate, with symbiont-hosting species closely matching the actual value (Ren et al., 2009, 2012b). Changes in foraminifera δ^{15}N in the Southern Ocean track PON δ^{15}N variation, which seems to be seasonally decoupled from nitrate δ^{15}N (Smart et al., 2020). The decoupling can be explained by an increase in ammonium recycling

during late summer lowering the δ^{15}N of PON and foraminifera, whereas higher levels of degradation during austral winter raise PON and foraminifer δ^{15}N (Smart et al., 2020).

These studies demonstrate the importance of ground-truthing the method in quantifying as much variability as possible, to better explain long-term trends in downcore reconstructions. This includes researching the effect of biogeochemical cycling at both intra- and inter-annual time scales in multiple regions, dominated by different N-cycling processes. Within each environment, the relationship between the tissue- and shell-bound δ^{15}N of each species of foraminifera to the δ^{15}N of mixed layer and/or thermocline nitrate should be established, paying close attention to species-specific habitat preferences and diets, as a species' seasonal preference can influence how we interpret δ^{15}N in the fossil record.

1.7 Structure of this thesis

The work presented in this thesis focuses on broadening the understanding of biogeochemical cycling in the southeast Atlantic and southwest Indian Ocean regions through nitrate isotopes, and introduces the idea of using nitrogen isotopes in foraminifera as a method for reconstructing Agulhas leakage. The thesis explores the advantages and challenges of using nitrogen isotopes in planktic foraminifera as an indicator of past environmental change, and synthesizes palaeo-proxy ground-truthing efforts (including this research and existing studies) across the world's oceans.

Chapter 2 focuses on establishing the driving processes of nitrogen cycling in the southeast Atlantic and determining the relationship between the δ^{15}N of upper ocean nitrate and that of planktic foraminifera living in the region today. The chapter also documents the finding that isotopically distinct Agulhas eddies transporting Indian Ocean waters into the South Atlantic can impact the local δ^{15}N signal of both nitrate and the biological community, thus raising the possibility of utilizing fossil shell-bound δ^{15}N as a proxy for past leakage variation. Questions addressed in this chapter are:

1. What is the relationship between foraminifer tissue δ^{15}N and thermocline nitrate δ^{15}N in the southeast Atlantic?

2. Do nitrate and foraminifer δ^{15}N within a mature 'leaked' Agulhas eddy remain isotopically distinct from background Atlantic conditions?

Chapter 3 investigates how biogeochemical cycling influences foraminifer δ^{15}N in the Agulhas Current System. Analysing foraminifera from this region provides an opportunity to resolve several questions raised in Chapter 2 regarding the fidelity of foraminifer δ^{15}N in the Agulhas eddy with respect to the original source of Agulhas leakage. The chapter explores the impact of two adjacent, isotopically-distinct thermocline nitrate sources on foraminifer assemblages and tissue δ^{15}N. Key questions include:

1. How does foraminifer tissue-bound δ^{15}N from the Agulhas Current System compare to that which was measured in the Agulhas eddy?

2. What is the relationship between the δ^{15}N of foraminifer tissue, PON, and thermocline nitrate in the Agulhas Current System?

Chapter 4 focuses on ground-truthing the relationship between modern and fossil foraminifer δ^{15}N in the southeast Atlantic, and assesses whether modern the shell-bound δ^{15}N in this region is correlated to tissue δ^{15}N. Additionally, findings from the southeast Atlantic are compiled with existing data from other regions to analyze broader-scale trends. Key questions addressed include:

1. What is the relationship between modern tissue- and shell-bound δ^{15}N in both the southeast Atlantic regions?

2. What is the relationship between modern and core-top shell-bound δ^{15}N?

3. Is there evidence of spatial variability in the δ^{15}N of fossil foraminifera within the southeast Atlantic?

Chapter 5 reviews the main conclusions of this study and highlights potential avenues for future foraminifera shell-bound δ^{15}N research.

References

Alldredge, A. L. and Silver, M. W. (1988). Characteristics, dynamics and significance of marine snow. *Progress in Oceanography*, 20:41–82.

Altabet, M. A. (1988). Variations in nitrogen isotopic composition between sinking and suspended particles: implications for nitrogen cycling and particle transformation in the open ocean. *Deep Sea Research Part A, Oceanographic Research Papers*, 35(4):535–554.

Altabet, M. A. and Curry, W. B. (1989). Testing models of past ocean chemistry using foraminifera 15N/14N. *Global Biogeochemical Cycles*, 3(2):107–119.

Altabet, M. A., Deuser, W. G., Honjo, S., Stienen, C., and Stienent, C. (1991). Seasonal and depth-related changes in the source of sinking particles in the North Atlantic. *Nature*, 354(November):136–139.

Altabet, M. A. and Francois, R. (1994). Sedimentary nitrogen isotopic ratio as a recorder for surface ocean nitrate utilization. *Global Biogeochemical Cycles*, 8(1):103–116.

Altabet, M. A. and Francois, R. (2001). Nitrogen isotope biogeochemistry of the Antarctic polar frontal zone at 170°W. *Deep-Sea Research Part II: Topical Studies in Oceanography*, 48(19-20):4247–4273.

Altabet, M. A., Francois, R., Murray, D. W., and Prell, W. L. (1995). Climate-related variations in denitrification in the Arabian Sea from sediment15N/14N ratios. *Nature*, 373(6514):506–509.

Altabet, M. A., Pilskaln, C., Thunell, R., Pride, C., Sigman, D., Chavez, F., and Francois, R. (1999). The nitrogen isotope biogeochemistry of sinking particles from the margin of the eastern North Pacific. *Deep-Sea Research Part I: Oceanographic Research Papers*, 46(4):655–679.

Archer, D. and Winguth, A. (2000). What caused the glacial/interglacial atmospheric pCO2 cycles? *Reviews of Geophysics*, 38(2):159–189.

Ballalai, J. M., Santos, T. P., Lessa, D. O., Venancio, I. M., Chiessi, C. M., Johnstone, H. J., Kuhnert, H., Claudio, M. R., Toledo, F., Costa, K. B., and Albuquerque, A. L. S. (2019). Tracking Spread of the Agulhas Leakage Into the Western South Atlantic and Its Northward Transmission During the Last Interglacial. *Paleoceanography and Paleoclimatology*, 34(11):1744–1760.

Bard, E. and Rickaby, R. E. (2009). Migration of the subtropical front as a modulator of glacial climate. *Nature*, 460(7253):380–383.

Bauska, T. K., Baggenstos, D., Brook, E. J., Mix, A. C., Marcott, S. A., Petrenko, V. V., Schaefer, H., Severinghaus, J. P., Lee, J. E., and Thiemens, M. H. (2016).

Carbon isotopes characterize rapid changes in atmospheric carbon dioxide during the last deglaciation. *Proceedings of the National Academy of Sciences of the United States of America*, 113(13):3465–3470.

Bé, A. W. H. and Anderson, O. R. (1976). Gametogenesis in Planktonic Foraminifera. *Science*, 192(4242):890–892.

Bé, A. W. H. and Ericson, D. B. (1963). Aspects of Calcification in Planktonic Foraminifera (Sarcodinia). *Annals of the New York Academy of Sciences*, 109(1):65–81.

Bé, A. W. H., Hemleben, C., Anderson, O. R., and Spindler, M. (1979). Chamber Formation in Planktonic Foraminifera. *Micropaleontology*, 25(3):294.

Bé, A. W. H. and Hutson, W. H. (1977). Ecology of Planktonic Foraminifera and Biogeographic Patterns of Life and Fossil Assemblages in the Indian Ocean. *Micropaleontology*, 23(4):369.

Beal, L., De Ruijter, W. P., Biastoch, A., Zahn, R., Cronin, M., Hermes, J., Lutjeharms, J. R., Quartly, G., Tozuka, T., Baker-Yeboah, S., Bornman, T., Cipollini, P., Dijkstra, H., Hall, I., Park, W., Peeters, F. J., Penven, P., Ridderinkhof, H., and Zinke, J. (2011). On the role of the Agulhas system in ocean circulation and climate. *Nature*, 472(7344):429–436.

Biastoch, A., Boening, C. W., and Lutjeharms, J. R. (2008). Agulhas leakage dynamics affects decadal variability in Atlantic overturning circulation. *Nature*, 456(November):489–492.

Biastoch, A., Boening, C. W., Schwarzkopf, F. U., and Lutjeharms, J. R. (2009). Increase in Agulhas leakage due to poleward shift of Southern Hemisphere westerlies. *Nature*, 462(November):495–499.

Biastoch, A., Durgadoo, J. V., Morrison, A. K., Van Sebille, E., Weijer, W., and Griffies, S. M. (2015). Atlantic multi-decadal oscillation covaries with Agulhas leakage. *Nature Communications*, 6:1–7.

Billett, D. S., Lampitt, R. S., Rice, A. L., and Mantoura, R. F. (1983). Seasonal sedimentation of phytoplankton to the deep-sea benthos.

Bird, C., Darling, K. F., Russell, A. D., Davis, C. V., Fehrenbacher, J., Free, A., Wyman, M., and Ngwenya, B. T. (2017). Cyanobacterial endobionts within a major marine planktonic calcifier (Globigerina bulloides, Foraminifera) revealed by 16S rRNA metabarcoding. *Biogeosciences*, 14(4):901–920.

Bird, C., LeKieffre, C., Jauffrais, T., Meibom, A., Geslin, E., Filipsson, H. L., Maire, O., Russell, A. D., and Fehrenbacher, J. S. (2020). Heterotrophic Foraminifera Capable of Inorganic Nitrogen Assimilation. *Frontiers in Microbiology*, 11(December):3076.

Boyd, P. W., Claustre, H., Levy, M., Siegel, D. A., and Weber, T. (2019). Multi-faceted particle pumps drive carbon sequestration in the ocean. *Nature*, 568(7752):327–335.

Broecker, W. S. (1982). Ocean chemistry during glacial time. *Geochimica et Cosmochimica Acta*, 46:1689–1705.

Broecker, W. S. (1998). Paleocean circulation during the Last Deglaciation: A bipolar seesaw? *Paleoceanography*, 13(2):119.

Broecker, W. S. and Peng, T. H. (1987). The ocean salt pump: does it contribute to the glacial-interglacial difference in atmosphere CO2 content? *Global Biogeochemical Cycles*, 1(3):251–259.

Buckley, M. W. and Marshall, J. (2016). Observations, inferences, and mechanisms of the Atlantic Meridional Overturning Circulation: A review. *Reviews of Geophysics*, 54(1):5–63.

Caesar, L., McCarthy, G. D., Thornalley, D., Cahill, N., and Rahmstorf, S. (2021). Current Atlantic Meridional Overturning Circulation weakest in last millennium. *Nature Geoscience*, 14(3):118–120.

Caley, T., Kim, J. H., Malaizé, B., Giraudeau, J., Laepple, T., Caillon, N., Charlier, K., Rebaubier, H., Rossignol, L., Castañeda, I. S., Schouten, S., and Sinninghe Damsté, J. S. (2011). High-latitude obliquity as a dominant forcing in the Agulhas current system. *Climate of the Past*, 7(4):1285–1296.

Carpenter, E. J. and Price, C. C. (1977). Nitrogen fixation, distribution, and production of Oscillatoria (Trichodesmium) spp. in the western Sargasso and Caribbean Seas. *Limnology and Oceanography*, 22(1):60–72.

Casciotti, K. L. (2016). Nitrogen and Oxygen Isotopic Studies of the Marine Nitrogen Cycle. *Annual Review of Marine Science*, 8(1):379–407.

Cheng, Y., Beal, L. M., Kirtman, B. P., and Putrasahan, D. (2018). Interannual Agulhas leakage variability and its regional climate imprints. *Journal of Climate*, 31(24):10105–10121.

Cline, J. D. and Kaplan, I. R. (1975). Isotopic fractionation of dissolved nitrate during denitrification in the eastern tropical north pacific ocean. *Marine Chemistry*, 3(4):271–299.

Devries, T., Primeau, F., and Deutsch, C. (2012). The sequestration efficiency of the biological pump. *Geophysical Research Letters*, 39(13):1–5.

Dickson, A. J., Leng, M. J., Maslin, M. A., Sloane, H. J., Green, J., Bendle, J. A., McClymont, E. L., and Pancost, R. D. (2010). Atlantic overturning circulation and

Agulhas leakage influences on southeast Atlantic upper ocean hydrography during marine isotope stage 11. *Paleoceanography*, 25(3):1–14.

Dugdale, R. C. and Goering, J. J. (1967). Uptake of new and regenerated forms of nitrogen in primary productivity. *Limnology & Oceanography*, 12(2):196–206.

Durgadoo, J. V., Loveday, B., Reason, C., Penven, P., and Biastoch, A. (2013). Agulhas Leakage Predominantly Responds to the Southern Hemisphere Westerlies. *Journal of Physical Oceanography*, 43:2113–2131.

Dyez, K. A., Zahn, R., and Hall, I. R. (2014). Multicentennial Agulhas leakage variability and links to North Atlantic climate during the past 80,000-years. *Paleoceanography*, 29(12):1238–1248.

Emerson, S. and Yang, B. (2022). The Ocean's Biological Pump: In Situ Oxygen Measurements in the Subtropical Oceans. *Geophysical Research Letters*, 49(21).

Eugster, O., Gruber, N., Deutsch, C., Jaccard, S. L., and Payne, M. R. (2013). The dynamics of the marine nitrogen cycle across the last deglaciation. *Paleoceanography*, 28(1):116–129.

Ford, D. J., Tilstone, G. H., Shutler, J. D., Kitidis, V., Sheen, K. L., Dall'olmo, G., and Orselli, I. B. M. (2022). Mesoscale eddies enhance the air-sea CO 2 sink in the South Atlantic Ocean.

Francois, R. and Altabet, M. A. (1992). Glacial to interglacial changes in surface nitarte utilization in the Indian sector of the Southern Ocean as recorded by sediment δ15N. *Paleoceanography*, 7(5):589–606.

Freudenthal, T., Wagner, T., Wenzhöfer, F., Zabel, M., and Wefer, G. (2001). Early diagenesis of organic matter from sediments of the eastern subtropical Atlantic: Evidence from stable nitrogen and carbon isotopes. *Geochimica et Cosmochimica Acta*, 65(11):1795–1808.

Galbraith, E. D., Kienast, M., Albuquerque, A. L., Altabet, M. A., Batista, F., Bianchi, D., Calvert, S. E., Contreras, S., Crosta, X., De Pol-Holz, R., Dubois, N., Etourneau, J., Francois, R., Hsu, T. C., Ivanochko, T., Jaccard, S. L., Kao, S. J., Kiefer, T., Kienast, S., Lehmann, M. F., Martinez, P., McCarthy, M., Meckler, A. N., Mix, A., Möbius, J., Pedersen, T. F., Pichevin, L., Quan, T. M., Robinson, R., Ryabenko, E., Schmittner, A., Schneider, R., Schneider-Mor, A., Shigemitsu, M., Sinclair, D., Somes, C. J., Studer, A. S., Tesdal, J. E., Thunell, R. C., and Terence Yang, J. Y. (2013). The acceleration of oceanic denitrification during deglacial warming. *Nature Geoscience*, 6(7):579–584.

Ganeshram, R. S., Pedersen, T. F., Calvert, S. E., and Murray, J. W. (1995). Large changes in oceanic nutrient inventories from glacial to interglacial periods.

Garzoli, S. L. and Matano, R. P. (2011). The South Atlantic and the Atlantic Meridional Overturning Circulation. *Deep-Sea Research Part II: Topical Studies in Oceanography*, 58(17-18):1837–1847.

Gastrich, M. (1987). Ultrastructure of a new intracellular symbiotic alga found within planktonic foraminifera. *Journal of Phycology*, 25:623–632.

Gaye-Haake, B., Lahajnar, N., Emeis, K. C., Unger, D., Rixen, T., Suthhof, A., Ramaswamy, V., Schulz, H., Paropkari, A. L., Guptha, M. V., and Ittekkot, V. (2005). Stable nitrogen isotopic ratios of sinking particles and sediments from the northern Indian Ocean. *Marine Chemistry*, 96(3-4):243–255.

Gherardi, J. M., Labeyrie, L., Nave, S., Francois, R., McManus, J. F., and Cortijo, E. (2009). Glacial-interglacial circulation changes inferred from231Pa/ 230Th sedimentary record in the North Atlantic region. *Paleoceanography*, 24(2):1–14.

Goering, J., Alexander, V., and Haubenstock, N. (1990). Seasonal variability of stable carbon and nitrogen isotope ratios of organisms in a North Pacific Bay. *Estuarine, Coastal and Shelf Science*, 30(3):239–260.

Goldstein, S. T. (1999). Foraminifera: A biological overview. *Modern Foraminifera*, pages 37–55.

Gordon, A. L. (1986). Interocean exchange of thermocline water. *Journal of Geophysical Research*, 91(C4):5037.

Hemleben, C., Spindler, M., and Anderson, O. R. (1989). *Modern Planktonic Foraminifera.* Springer-Verlag, New York, 1 edition.

Hemleben, C., Spindler, M., Breitinger, I., and Deuser, W. G. (1985). Field and laboratory studies on the ontogeny and ecology of some globorotaliid species from the Sargasso Sea off Bermuda. *Journal of Foraminiferal Research*, 15(4):254–272.

Henson, S. A., Sanders, R., and Madsen, E. (2012). Global patterns in efficiency of particulate organic carbon export and transfer to the deep ocean. *Global Biogeochemical Cycles*, 26(1):1–14.

Hertzberg, J. E., Schmidt, M. W., Bianchi, T. S., Smith, R. K., Shields, M. R., and Marcantonio, F. (2016). Comparison of eastern tropical Pacific TEX86 and Globigerinoides ruber Mg/Ca derived sea surface temperatures: Insights from the Holocene and Last Glacial Maximum. *Earth and Planetary Science Letters*, 434:320–332.

Hoering, T. C. and Ford, H. T. (1960). The Isotope Effect in the Fixation of Nitrogen by Azotobacter. *J. Am Chem Soc.*, 82:376–378.

Hutchings, L., Armstrong, D. A., and Mitchell-Innes, B. A. (1986). The frontal zone in the southern benguela current. *Elsevier Oceanography Series*, 42(C):67–94.

Hutchings, L., van der Lingen, C. D., Shannon, L. J., Crawford, R. J. M., Verheye, H. M. S., Bartholomae, C. H., van der Plas, A. K., Louw, D., Kreiner, A., Ostrowski, M., Fidel, Q., Barlow, R., Lamont, T., Coetzee, J., Shillington, F. A., Veitch, J. A., Currie, J. C., and Monteiro, P. M. S. (2009). The Benguela Current: An ecosystem of four components. *Progress in Oceanography*, 83(1-4):15–32.

Ito, T. and Follows, M. J. (2005). Preformed phosphate, soft tissue pump and atmospheric CO2. *Journal of Marine Research*, 63(4):813–839.

Jenkyns, H., Gröcke, D. R., and Hesselbo, S. (2001). Nitrogen isotope evidence for water mass denitrification during the early Toarcian (Jurassic) oceanic anoxic event. *Paleoceanography*, 16(6):593–603.

John H. Ryther and Dunstan, W. M. (1971). Nitrogen, phosphorus, and eutrophication in the coastal marine environment. *Science*, 171:1008–1014.

Jonkers, L., Jiménez-Amat, P., Mortyn, P. G., and Brummer, G. J. A. (2013). Seasonal Mg/Ca variability of N. pachyderma (s) and G. bulloides: Implications for seawater temperature reconstruction. *Earth and Planetary Science Letters*, 376:137–144.

Kasper, S., van der Meer, M. T. J., Mets, A., Zahn, R., Sinninghe Damsté, J. S., and Schouten, S. (2014). Salinity changes in the Agulhas leakage area recorded by stable hydrogen isotopes of C37 alkenones during Termination I and II. *Climate of the Past*, 10:251–260.

Kast, E. R., Stolper, D. A., Auderset, A., Higgins, J. A., Ren, H., Wang, X. T., Martínez-García, A., Haug, G. H., Sigman, D. M., and Stopler, D. (2019). Nitrogen isotope evidence for expanded ocean suboxia in the early Cenozoic. *Science*, 364(6438):386–389.

Kimoto, K. (2015). *Marine protists: Diversity and dynamics.*

King, K. and Hare, P. E. (1972). Amino Acid Composition of the Test as a Taxonomic Character for Living and Fossil Planktonic Foraminifera. *Micropaleontology*, 18(3):285.

Kits, K. D., Sedlacek, C. J., Lebedeva, E. V., Han, P., Bulaev, A., Pjevac, P., Daebeler, A., Romano, S., Albertsen, M., Stein, L. Y., Daims, H., and Wagner, M. (2017). Kinetic analysis of a complete nitrifier reveals an oligotrophic lifestyle. *Nature*, 549(7671):269–272.

Kohfeld, K. E. and Ridgwell, A. (2009). Glacial-Interglacial Variability in Atmospheric CO2. *Surface ocean-lower atmosphere process*, 187:252–286.

Koutsodendris, A., Pross, J., and Zahn, R. (2014). Exceptional Agulhas leakage prolonged interglacial warmth during MIS 11c in Europe. *Palaeoceanography*, 29:1062–1071.

Kucera, M. (2007). Chapter Six Planktonic Foraminifera as Tracers of Past Oceanic Environments. *Developments in Marine Geology*, 1(November 2017):213–262.

Kuhlbrodt, T., Griesel, A., Montoya, M., Levermann, A., Hofmann, M., and Rahmstorf, S. (2007). On the driving processes of the Atlantic meridional overturning circulation. *Reviews of Geophysics*, 45(2):1–32.

Landolfi, A., Rabouille, S., and Mouriño-Carballido, B. (2021). Evolution of the nitrogen cycle and its influence on the biological sequestration of CO2 in the ocean. *Frontiers in Marine Science*, 8:1–2.

Lee, J. J., Freudenthal, H., Kossoy, V., and Bé, A. W. H. (1965). Cytological Observations on Two Planktonic Foraminifera, Globigerina bulloides and Globigerinoides ruber. *J. Protozool.*, 12:531–542.

LeGrande, A. N., Lynch-Stieglitz, J., and Farmer, E. C. (2004). Oxygen isotopic composition of Globorotalia truncatulinoides as a proxy for intermediate depth density. *Paleoceanography*, 19(4):1–7.

Lehahn, Y., D'Ovidio, F., Lévy, M., Amitai, Y., Heifetz, E., Ovidio, F., Lévy, M., Amitai, Y., and Heifetz, E. (2011). Long range transport of a quasi isolated chlorophyll patch by an Agulhas ring. *Geophysical Research Letters*, 38(16):1–6.

Lehmann, M. F., Bernasconi, S. M., Barbieri, A., and McKenzie, J. A. (2002). Preservation of organic matter and alteration of its carbon and nitrogen isotope composition during simulated and in situ early sedimentary diagenesis. *Geochimica et Cosmochimica Acta*, 66(20):3573–3584.

Lohmann, G. P. and Schweitzer, P. N. (1989). Globorotalia truncatulinoides' growth and chemistry as probes of the past thermocline: 1. Shell size. *Palaeoceanography*, 5(1):55–75.

Louanchi, F. and Najjar, R. G. (2000). A global monthly climatology of phosphate, nitrate, and silicate in the upper ocean: Spring-summer export production and shallow remineralization. *Global Biogeochemical Cycles*, 14(3):957–977.

Lourey, M. J., Trull, T. W., and Sigman, D. M. (2003). Sensitivity of δ15N of nitrate, surface suspended and deep sinking particulate nitrogen to seasonal nitrate depletion in the Southern Ocean. *Global Biogeochemical Cycles*, 17(3):1–18.

Lutjeharms, J. R. (1981). Features of the southern Agulhas Current circulation from satellite remote sensing. *South African Journal of Science*, 77(May):231–236.

Lutjeharms, J. R. (2006). *The Agulhas Current*. Springer-Verlag, Berlin Heidelberg, 1 edition.

Margaritelli, G., Lirer, F., Schroeder, K., Alberico, I., Dentici, M. P., and Caruso, A. (2020). Globorotalia truncatulinoides in Central - Western Mediterranean Sea during the Little Ice Age. *Marine Micropaleontology*, 161(September):101921.

Marino, G., Zahn, R., Ziegler, M., Purcell, C., Knorr, G., Hall, I. R., Ziveri, P., and Elderfield, H. (2013). Agulhas salt-leakage oscillations during abrupt climate changes of the Late Pleistocene. *Paleoceanography*, 28(3):599–606.

Mariotti, A., A, Germon, J. C., Hubert, P., Kaiser, P., Letolle, R., and Tardieux, A. (1981). Experimental determination of nitrogen kinetic isotope fractionation: some principles: illustration for the denitrification and nitrification processes. *Plant and Soil*, 62(3):413–430.

Martin, J. H., Knauer, G. A., Karl, D. M., and Broenkow, W. W. (1987). VERTEX: carbon cycling in the northeast Pacific. *Deep Sea Research Part A, Oceanographic Research Papers*, 34(2):267–285.

Martínez-García, A., Jung, J., Ai, X. E., Sigman, D. M., Auderset, A., Duprey, N. N., Foreman, A., Fripiat, F., Leichliter, J., Lüdecke, T., Moretti, S., and Wald, T. (2022). Laboratory Assessment of the Impact of Chemical Oxidation, Mineral Dissolution, and Heating on the Nitrogen Isotopic Composition of Fossil-Bound Organic Matter. *Geochemistry, Geophysics, Geosystems*, 23(8):1–23.

Martínez-García, A., Sigman, D. M., Ren, H., Anderson, R. F., Straub, M., Hodell, D. A., Jaccard, S. L., Eglinton, T. I., and Haug, G. H. (2014). Iron fertilization of the Subantarctic ocean during the last ice age. *Science (New York, N.Y.)*, 343(6177):1347–50.

Martínez-Méndez, G., Zahn, R., Hall, I. R., Peeters, F. J., Pena, L. D., Cacho, I., Negre, C. C. C. C., and Méndez, G. M. (2010). Contrasting multiproxy reconstructions of surface ocean hydrography in the Agulhas Corridor and implications for the Agulhas Leakage during the last 345,000 years. *Paleoceanography*, 25:1–12.

McCave, I. N. (1975). Vertical flux of particles in the ocean. *Deep-Sea Research and Oceanographic Abstracts*, 22(7):491–502.

McElroy, M. B. (1983). Marine biological controls on atmospheric CO2 and climate.

Menzel, D. W. and Ryther, J. H. (1961). Nutrients limiting the production of phytoplankton in the Sargasso sea, with special reference to iron. *Deep Sea Research (1953)*, 7(4):276–281.

Minagawa, M. and Wada, E. (1984). Stepwise enrichment of 15N along food chains: Further evidence and the relation between 15N and animal age. *Geochimica et Cosmochimica Acta*, 48(5):1135–1140.

Miyake, Y. and Wada, E. (1967). The Abundance Ratio of 15N/14N in Marine Environments. *Records of Oceanographic Works*, 9(1):37–53.

Mompeán, C., Bode, A., Gier, E., and McCarthy, M. (2016). Bulk vs. amino acid stable N isotope estimations of metabolic status and contributions of nitrogen fixation to size-fractionated zooplankton biomass in the subtropical N Atlantic. *Deep-Sea Research Part I: Oceanographic Research Papers*, 114:137–148.

Montoya, J. (1994). Nitrogen Isotope Fractionation in the Modern Ocean: Implications for the Sedimentary Record. In Zahn, R., editor, *Carbon Cycling in the Glacial Ocean: Constraints on the Ocean's Role in Global Change*, volume I 17, pages 259–279. Springer-Verlag.

Nelson, G. and Hutchings, L. (1983). The Benguela upwelling area. *Progress in Oceanography*, 12(3):333–356.

Nowicki, M., DeVries, T., and Siegel, D. A. (2022). Quantifying the carbon export and sequestration pathways of the ocean's biological carbon pump. *Global Biogeochemical Cycles*.

Oppo, D. W., Curry, W. B., and McManus, J. F. (2015). What do benthic δ13C and δ18O data tell us about Atlantic circulation during Heinrich Stadial 1? *Paleoceanography*, 30(4):353–368.

Orselli, I. B., Goyet, C., Kerr, R., de Azevedo, J. L., Araujo, M., Galdino, F., Touratier, F., and Garcia, C. A. (2019a). The effect of Agulhas eddies on absorption and transport of anthropogenic carbon in the South Atlantic Ocean. *Climate*, 7(6):1–25.

Orselli, I. B., Kerr, R., Azevedo, J. L., Galdino, F., Araujo, M., and Garcia, C. A. (2019b). The sea-air CO2 net fluxes in the South Atlantic Ocean and the role played by Agulhas eddies. *Progress in Oceanography*, 170(2018):40–52.

Peeters, F. J., Acheson, R., Brummer, G.-J. A., De Ruijter, W. P., Schneider, R., Ganssen, G. M., Ufkes, E., and Kroon, D. (2004). Vigorous exchange between the Indian and Atlantic oceans at the end of the past five glacial periods. *Nature*, 430(7000):661–5.

Petit, J. R., Jouzel, J., Raynaud, D., Barnola, J. M., Basile, I., Bender, M., Chappellaz, J., Davis, M., Delaygue, G., Delmotte, M., Kotlyakov, V. M., Legrand, M., Lipenkov, V. Y., Loriu, C., Pepin, L., Ritz, C., Saltzman, E., and Stievenard, M. (1999). Climate and atmospheric history of the past 420,000 years from the Vostok ice core, Antarctica. *Nature*, 399:429–436.

Petrick, B. F., McClymont, E. L., Felder, S., Rueda, G., Leng, M. J., and Rosell-Melé, A. (2015a). Late Pliocene upwelling in the Southern Benguela region. *Palaeogeography, Palaeoclimatology, Palaeoecology*, 429:62–71.

Petrick, B. F., McClymont, E. L., Marret, F., Meer, M. T. J., and van der Meer, M. T. J. (2015b). Changing surface water conditions for the last 500ka in the Southeast Atlantic: Implications for variable influences of Agulhas leakage and Benguela upwelling. *Paleoceanography*, 17(9):8092.

Petró, S. M., Pivel, M. A. G., Coimbra, J. C., and Mizusaki, A. M. P. (2016). Paleoceanographic changes through the last 130 ka in the western South Atlantic based on planktonic foraminifera. *Revista Brasileira de Paleontologia*, 19(1):3–14.

Raimbault, P., Slawyk, G., Boudjellal, B., Coatanoan, C., Coste, B., Garcia, N., Moutin, T., and Pujo-pay, M. (1999). Carbon and nitrogen uptake and export in the equatorial Pacific at 150W: Evidence of an efficient regenerated production cycle. *Journal of Geophysical Research*, 104(C2):3341–3356.

Ren, H., Sigman, D. M., Chen, M. T., and Kao, S. J. (2012a). Elevated foraminifera-bound nitrogen isotopic composition during the last ice age in the South China Sea and its global and regional implications. *Global Biogeochemical Cycles*, 26(1):1–13.

Ren, H., Sigman, D. M., Meckler, A. N., Plessen, B., Robinson, R., Rosenthal, Y., and Haug, G. H. (2009). Foraminiferal isotope evidence of reduced nitrogen fixation in the ice age Atlantic Ocean. *Science*, 323(5911):244–248.

Ren, H., Sigman, D. M., Thunell, R. C., and Prokopenko, M. G. (2012b). Nitrogen isotopic composition of planktonic foraminifera from the modern ocean and recent sediments. *Limnology and Oceanography*, 57(4):1011–1024.

Robinson, R., Kienast, M., Luiza Albuquerque, A., Altabet, M. A., Contreras, S., De Pol-Holz, R., Dubois, N., Francois, R., Galbraith, E. D., Hsu, T. C., Ivanochko, T., Jaccard, S., Kao, S. J., Kiefer, T., Kienast, S., Lehmann, M. F., Martinez, P., McCarthy, M., Möbius, J., Pedersen, T. F., Quan, T. M., Ryabenko, E., Schmittner, A., Schneider, R., Schneider-Mor, A., Shigemitsu, M., Sinclair, D., Somes, C. J., Studer, A. S., Thunell, R. C., and Yang, J. Y. (2012). A review of nitrogen isotopic alteration in marine sediments. *Paleoceanography*, 27(PA4203):1–13.

Robinson, R. and Meyers, P. A. (2002). Biogeochemical changes within the Benguela Current upwelling system during the Matuyama Diatom Maximum: Nitrogen isotope evidence from Ocean Drilling Program Sites 1082 and 1084. *Paleoceanography*, 17(4):1–10.

Robinson, R., Smart, S. M., Cybulski, J. D., McMahon, K. W., Marcks, B., and Nowakowski, C. (2023). Insights from Fossil-Bound Nitrogen Isotopes in Diatoms, Foraminifera, and Corals. *Annual Review of Marine Science*, 15(1):1–24.

Robson, J., Ortega, P., and Sutton, R. (2016). A reversal of climatic trends in the North Atlantic since 2005. *Nature Geoscience*, 9(7):513–517.

Rouault, M., Pohl, B., and Penven, P. (2010). Coastal oceanic climate change and variability from 1982 to 2009 around South Africa. *African Journal of Marine Science*, 32(2):237–246.

Rühs, S., Durgadoo, J. V., Behrens, E., and Biastoch, A. (2013). Advective timescales and pathways of Agulhas leakage. *Geophysical Research Letters*, 40:3997–4000.

Ryabenko, E. (2013). Stable Isotope Methods for the Study of the Nitrogen Cycle. In Zambianchi, E., editor, *Topics in Oceanography*, pages 1–40. InTech.

Sarmiento, J. L., Gruber, N., Brzezinski, M. A., and Dunne, J. P. (2004). High-latitude controls of thermocline nutrients and low latitude biological productivity. *Nature*, 427(6969):56–60.

Sato, O. T. and Polito, P. S. (2014). Observation of South Atlantic subtropical mode waters with Argo profiling float data. *Journal of Geophysical Research: Oceans*, 119:2860–2881.

Schiebel, R. (2002). Planktic foraminiferal sedimentation and the marine calcite budget. *Global Biogeochemical Cycles*, 16(4):3–1.

Schiebel, R. and Hemleben, C. (2005). Modern planktic foraminifera. *Paläontologische Zeitschrift*, 79(1):135–148.

Schiebel, R., Smart, S. M., Jentzen, A., Jonkers, L., Morard, R., Meilland, J., Michel, E., Coxall, H. K., Hull, P. M., de Garidel-Thoron, T., Aze, T., Quillévéré, F., Ren, H., Sigman, D. M., Vonhof, H. B., Martínez-García, A., Kučera, M., Bijma, J., Spero, H. J., and Haug, G. H. (2018). Advances in planktonic foraminifer research: New perspectives for paleoceanography. *Revue de Micropaleontologie*, 61(3-4):113–138.

Schlitzer, R. (2012). Ocean Data View.

Schmittner, A. and Galbraith, E. D. (2008). Glacial greenhouse-gas fluctuations controlled by ocean circulation changes. *Nature*, 456(7220):373–376.

Schmittner, A. and Somes, C. J. (2016). Complementary constraints from carbon (13C) and nitrogen (15N) isotopes on the glacial ocean's soft-tissue biological pump. *Paleoceanography*, 31(6):669–693.

Sen Gupta, B. K. (2003). *Modern Foraminifera*, volume 36.

Shannon, L. V. and Nelson, G. (1996). The Benguela: Large Scale Features and Processes and System Variability. In Wefer, G., Berger, W., Siedler, G., and Webb, D., editors, *The South Atlantic*, pages 163–210. Springer, Berlin.

Siegel, D. A., Devries, T., Cetinić, I., and Bisson, K. M. (2023). Quantifying the Ocean's Biological Pump and Its Carbon Cycle Impacts on Global Scales. *Annual Review of Marine Science*, 15:329–356.

Sigman, D. M. and Boyle, E. A. (2000). Glacial/Interglacial Variations In Atmospheric Carbon Dioxide. *Nature*, 407(6806):859–869.

Sigman, D. M. and Casciotti, K. (2009). Nitrogen Isotopes in the Ocean. *Encyclopedia of Ocean Sciences*, (Ms 632):1884–1894.

Sigman, D. M. and Hain, M. P. (2012). The Biological Productivity of the Ocean. *Nature Education*, 3(6):1–16.

Sigman, D. M., M. A, A., McCorkle, D. C., Francois, R., and Fischer, G. (1999). The δ15N of nitrate in the Southern Ocean: Nitrate consumption in surface waters. *Global Biogeochemical Cycles*, 13(4):1149–1166.

Sigman, D. M., Mccorkle, D. C., Francois, R., and Fischer, G. (2000). The d15N of nitrate in the Southern Ocean: Nitrogen cycling and circulation in the ocean interior. *Journal of Geophysical Research*, 105(C8):19599–19614.

Simon, M., Arthur, K., Hall, I. R., Peeters, F. J., Loveday, B. R., Barker, S., Ziegler, M., and Zahn, R. (2013). Millennial-scale Agulhas Current variability and its implications for salt-leakage through the Indian–Atlantic Ocean Gateway. *Earth and Planetary Science Letters*, 383:101–112.

Simon, M. H., Ziegler, M., Bosmans, J., Barker, S., Reason, C. J., and Hall, I. R. (2015). Eastern South African hydroclimate over the past 270,000 years. *Scientific Reports*, 5:1–19.

Smart, S. M., Fawcett, S. E., Ren, H., Schiebel, R., Tompkins, E. M., García, A. M., Stirnimann, L., Roychoudhury, A., Haug, G. H., and Sigman, D. M. (2020). The Nitrogen Isotopic Composition of Tissue and Shell-Bound Organic Matter of Planktic Foraminifera in Southern Ocean Surface Waters. *Geochemistry, Geophysics, Geosystems*, 21:1–29.

Smart, S. M., Ren, H., Fawcett, S. E., Schiebel, R., Conte, M., Rafter, P. A., Ellis, K. K., Weigand, M. A., Oleynik, S., Haug, G. H., and Sigman, D. M. (2018). Ground-truthing the planktic foraminifer-bound nitrogen isotope paleo-proxy in the Sargasso Sea. *Geochimica et Cosmochimica Acta*, 235:463–482.

Sohm, J. A., Hilton, J. A., Noble, A. E., Zehr, J. P., Saito, M. A., and Webb, E. A. (2011). Nitrogen fixation in the South Atlantic Gyre and the Benguela Upwelling System. *Geophysical Research Letters*, 38(16):1–6.

Studer, A. S., Sigman, D. M., Martínez-García, A., Benz, V., Winckler, G., Kuhn, G., Esper, O., Lamy, F., Jaccard, S. L., Wacker, L., Oleynik, S., Gersonde, R., and Haug, G. H. (2015). Antarctic Zone nutrient conditions during the last two glacial cycles. *Paleoceanography*, 30:845–862.

Suess, E. (1980). Particulate organic carbon fux in the oceans - surface productivity and oxygen utilization. *Nature*, 288:260–263.

Takagi, H., Kimoto, K., Fujiki, T., Saito, H., Schmidt, C., Kucera, M., and Moriya, K. (2019). Characterizing photosymbiosis in modern planktonic foraminifera. *Biogeosciences*, 16(17):3377–3396.

Thomas, W. H. (1966). Surface nitrogenous nutrients and phytoplankton in the northeastern tropical Pacific Ocean. *Limnology & Oceanography*, 11(3):393–400.

Thornalley, D., Delia, W., Ortega, P., Robson, J. I., Brierley, C. M., Davis, R., Hall, I. R., Moffa-sanchez, P., Rose, N. L., Spooner, P. T., Yashayaev, I., and Keigwin, L. D. (2018). Atlantic overturning during the past 150 years. *Nature*, 556(7700):227–230.

Tim, N., Zorita, E., Emeis, K.-c., Schwarzkopf, F. U., Biastoch, A., and Hunicke, B. (2019). Analysis of the position and strength of westerlies and trades with implications for Agulhas leakage and South Benguela upwelling. *Earth System Dynamics*, 10:847–858.

Trull, T. W., Davies, D., and Casciotti, K. L. (2008). Insights into nutrient assimilation and export in naturally iron-fertilized waters of the Southern Ocean from nitrogen, carbon and oxygen isotopes. *Deep-Sea Research Part II: Topical Studies in Oceanography*, 55(5-7):820–840.

Valley, S., Lynch-Stieglitz, J., and Marchitto, T. M. (2017). Timing of Deglacial AMOC Variability From a High-Resolution Seawater Cadmium Reconstruction. *Paleoceanography*, 32(11):1195–1203.

Van Sebille, E., Scussolini, P., Durgadoo, J. V., Peeters, F. J., Biastoch, A., Weijer, W., Turney, C., Paris, C. B., and Zahn, R. (2015). Ocean currents generate large footprints in marine palaeoclimate proxies. *Nature Communications*, 6:1–8.

Volk, T. and Hoffert, M. I. (1985). Ocean carbon pumps: analysis of relative strengths and efficiencies in ocean-driven atmospheric CO2 changes. In Sundquist, E. and Broecker, W., editors, *The Carbon Cycle and Atmospheric CO2: Natural Variations Archaean to Present*, volume 32, pages 99–110. DC: Am. Geophys. Union, Washington.

Völker, C. and Köhler, P. (2013). Responses of ocean circulation and carbon cycle to changes in the position of the Southern Hemisphere westerlies at Last Glacial Maximum. *Paleoceanography*, 28(4):726–739.

Wada, E. (1980). Nitrogen isotope fractionation and its significance in biogeochemical processes occurring in marine environments. *Isotope marine chemistry*, pages 375–398.

Wada, E. and Hattori, A. (1978). Nitrogen isotope effects in the assimilation of inorganic nitrogenous compounds by marine diatoms. *Geomicrobiology Journal*, 1:85–101.

Wallschuss, S., Mdutyana, M., Parrott, R. G., Forrer, H. J., Roman, R., Walker, D., Ansorge, I., and Fawcett, S. E. (2022). The Influence of Agulhas Leakage on Primary Production and Nitrogen Cycling in the Southeastern Atlantic Ocean. *Journal of Geophysical Research: Oceans*, 127:1–26.

Ward, B. B. (2008). *Nitrification in Marine Systems*.

Ward, B. B., Olson, R. J., and Perry, M. J. (1982). Microbial nitrification rates in the primary nitrite maximum off southern California. *Deep Sea Research Part A, Oceanographic Research Papers*, 29(2):247–255.

Waser, N. A., Yin, K., Yu, Z., Tada, K., Harrison, P. J., Turpin, D. H., and Calvert, S. E. (1998). Nitrogen isotope fractionation during nitrate, ammonium and urea uptake by marine diatoms and coccolithophores under various conditions of N availability. *Marine Ecology Progress Series*, 169:29–41.

Winter, A. and Martin, K. (1990). Late Quaternary History of the Agulhas Current. *Palaeoceanography*, 5(4):479–486.

Yool, A., Martin, A. P., Fernández, C., and Clark, D. R. (2007). The significance of nitrification for oceanic new production. *Nature*, 447(7147):999–1002.

Zehr, J. P. and Ward, B. B. (2002a). Nitrogen Cycling in the Ocean : New Perspectives on Processes and Paradigms MINIREVIEW Nitrogen Cycling in the Ocean : New Perspectives on Processes and Paradigms. *Applied and environmental microbiology*, 68(3):1015–1024.

Zehr, J. P. and Ward, B. B. (2002b). Nitrogen Cycling in the Ocean: New Perspectives on Processes and Paradigms. *Applied and environmental microbiology*, 68(3):1015–1024.

Chapter 2

Tracking Agulhas leakage in the South Atlantic using modern planktic foraminifera nitrogen isotopes

Abstract

The volume of water transported into the South Atlantic from the Indian Ocean via "Agulhas leakage" modulates global ocean circulation and has been linked to glacial-interglacial climate cycles. However, constraining past Agulhas leakage remains a challenge. Using new measurements from the modern South Atlantic, we propose that the nitrogen isotope ratio of organic matter preserved in the shells of fossil planktic foraminifera could be used to infer past changes in Agulhas leakage. Along a winter transect of the Cape Basin that intersected a mature Agulhas eddy, we measured the nitrogen and oxygen isotope ratios (δ^{15}N and δ^{18}O) of nitrate and the δ^{15}N of suspended particles, bulk zooplankton, and foraminifera (tissue and shells). Mixed-layer nitrate-, zooplankton-, and foraminifera-δ^{15}N were 2-3 ‰ lower in the eddy than the background Atlantic even though the δ^{15}N of the underlying thermocline nitrate was indistinguishable. We suggest that the δ^{15}N of eddy-N reflects Agulhas Current thermocline nitrate, which is ~ 2 ‰ lower in δ^{15}N than South Atlantic thermocline nitrate due to N_2 fixation occurring in the Indian Ocean. Further lowering of foraminifera δ^{15}N may have occurred during eddy transport due to *in-situ* N_2 fixation and/or recycling of low-δ^{15}N ammonium. The absence of low-δ^{15}N Agulhas nitrate in the eddy thermocline can be explained by the lower density of Agulhas thermocline and mixed-layer waters relative to the Cape Basin mixed layer. Agulhas thermocline waters are transported into the mixed layer of migrating eddies, where isotope fractionation during phytoplankton nitrate assimilation rapidly increases the δ^{15}N of the nitrate within. The low δ^{15}N of eddy foraminifera, apparent even after several months of eddy migration across the Cape Basin, suggests that fossil foraminifer-bound δ^{15}N may record variations in past Agulhas leakage.

2.1 Introduction

The southeast Atlantic Ocean is important for global ocean-atmosphere dynamics because it hosts the transport of heat and salt from the Indian to the Atlantic Oceans, which is fundamental to the Atlantic Meridional Overturning Circulation (AMOC) (Fig. 1; Gordon 1986; De Ruijter et al. 1999; Garzoli and Matano 2011; Rühs et al. 2013). Warm, saline upper Indian Ocean waters enter the South Atlantic via large anticyclonic eddies, jets, and filaments that flow into the Cape Basin (Duncombe Rae, 1991; van Ballegooyen et al., 1994; Schouten et al., 2000); this "Agulhas leakage" is the only pathway for Indian Ocean waters into the Atlantic (Gordon, 1986; De Ruijter et al., 1999; Beal et al., 2011; Rühs et al., 2013). The Cape Basin is bordered by the highly productive Benguela upwelling system to the east and the oligotrophic South Atlantic subtropical gyre to the north and west (Fig. 1; Stramma and Peterson 1989; Garzoli and Gordon 1996). Along with being regularly infiltrated by Agulhas eddies, the Cape Basin imports and modifies mode- and intermediate waters originating in the Southern Ocean, thereby acting as a conduit for equatorward-flowing nutrients (Sarmiento et al., 2004; Garzoli and Matano, 2011).

The spawning of Agulhas eddies occurs at the Agulhas Retroflection, where the zero wind stress curl and southward inertia cause the current to loop back on itself, anticyclonically, and form the eastward-flowing Agulhas Return Current (Gordon et al., 1987; Lutjeharms and Valentine, 1984; De Ruijter et al., 1999; Beal et al., 2011). Although most Agulhas Current waters are subsequently recirculated into the southwest Indian Ocean subgyre (Stramma and Lutjeharms, 1997; De Ruijter et al., 1999; Hermes et al., 2007), some water escapes at the Retroflection to form mesoscale anticyclonic eddies (the largest termed "Agulhas rings"; Lutjeharms and Stockton 1987), which then either dissipate in the Cape Basin or continue past the Walvis Ridge into the southwest Atlantic, occasionally even entering the North Atlantic (Goni et al., 1997; Arhan et al., 1999; Schouten et al., 2000).

Once in the Cape Basin, Agulhas eddies rapidly lose the warm temperatures of their (sub)tropical Indian Ocean source waters (Goni et al., 1997; Olson et al., 1992; Schouten et al., 2000; Schmid et al., 2003). They can nonetheless be identified by a characteristic positive sea-surface height anomaly (SSHA) associated with convergence at their centres, as well as by their elevated salinity, which persists on advective timescales (Gordon and Huber, 1990; van Ballegooyen et al., 1994; Schouten et al., 2000). The export of relatively saline waters from the Indian Ocean by Agulhas eddies contributes to the densification and subduction of surface waters in the North Atlantic (through the formation of North Atlantic Deep Water (NADW); Gordon et al. 1992; Donners et al. 2005; Garzoli and Matano 2011), which leads to freshly oxygenated deep waters spreading southwards via the AMOC (Gordon, 1986; Rintoul, 1991; Wefer et al., 1996; Garzoli and Matano, 2011; Ferreira and Kerr, 2017). It has been suggested that decreased Indo-Atlantic exchange during ice ages inhibited NADW production, weakening the AMOC, while a deglacial increase in Agulhas leakage may have helped to re-establish warmer interglacial conditions

by strengthening the AMOC (Berger and Wefer, 2002; Weijer et al., 2002; Knorr and Lohmann, 2003; Peeters et al., 2004). Long-term variability in Agulhas leakage thus has global-scale climate implications (Schouten et al., 2000; Van Aken et al., 2003; Beal et al., 2011).

Past variations in Agulhas leakage have been reconstructed from assemblages of planktic foraminifera, single-celled zooplankton with calcite shells that can be preserved in seafloor sediments for millions of years post deposition (Bé and Hutson, 1977; Schiebel and Hemleben, 2005). This approach relies on the sedimentary ratio of (sub)tropical Indian Ocean species (termed "Agulhas leakage fauna") to species better adapted to cooler South Atlantic conditions as an indicator of the strength of leakage (Peeters et al., 2004; Lončarić, 2006; Caley et al., 2014). The idea is that foraminifera originating in (sub)tropical Indian Ocean waters are transported via Agulhas eddies into the South Atlantic where they sink and accumulate on the seafloor; and that the stronger the Agulhas leakage, the more abundant the (sub)tropical foraminifera in the sediments relative to the temperate Atlantic species (Peeters et al., 2004; Martínez-Méndez et al., 2010; Caley et al., 2011, 2012).

Attempts to ground-truth this assemblage-based approach using modern foraminifera indicate that it works well for young Agulhas eddies ($<$ 9 months old) located relatively close to the Agulhas Current Retroflection (Peeters et al., 2004; Caley et al., 2014). However, foraminifer species collected from a mature Agulhas eddy ($>$ 10 months old) in the Cape Basin were found to be indistinguishable from the species sampled in South Atlantic waters outside the eddy (Lončarić, 2006). The implication of this finding is that although conditions within an Agulhas eddy may initially favour (sub)tropical foraminifera, changes in the eddy environment with time (e.g., rapid heat loss; van Ballegooyen et al., 1994) prevent their sustained growth, allowing them to be succeeded by temperate Atlantic species that are better adapted to the ambient conditions (Lončarić, 2006). This pattern of succession will ultimately be communicated to the sediment record, with temperate foraminifera potentially overwhelming the Agulhas assemblage and, by extension, the evidence of leakage. There is thus a need for alternative proxies that better preserve the signal of Agulhas leakage, especially beyond the region of eddy formation.

A potential candidate proxy for tracking Agulhas leakage is the nitrogen (N) isotopic composition of organic matter encased within the calcite tests of planktic foraminifera (i.e., foraminifer-bound δ^{15}N, where δ^{15}N (in ‰ *versus* N_2 in air) = $[(^{15}N/^{14}N)_{sample}/(^{15}N/^{14}N)_{air}$ - 1] $\times$ 1000). Bulk sedimentary N isotopes are often unreliable because the original upper-ocean δ^{15}N signal imprinted on particulate organic N (PON) can be altered during particle sinking or at the sediment-water interface, particularly in the less-productive (i.e., low flux) open ocean, and/or be overwhelmed by contaminating inputs (e.g., fluvial or laterally transported sediments), including in more productive coastal waters (Altabet and Francois, 2001; Holmes et al., 2002; Robinson et al., 2012). The organic matter bound within foraminifer shells appears far less vulnerable to such diagenetic change and/or con-

tamination (Altabet and Francois, 1994; Meckler et al., 2011). During chamber formation, foraminifera precipitate calcite onto an organic sheet containing N-rich amino acids (Bé and Tolderlund, 1971; King and Hare, 1972; Hemleben et al., 1977; Spero and Williams, 1988). This organic material ends up encased within the foraminifer calcite matrix (Bé et al., 1979; Hemleben et al., 1985) where the composition appears largely protected from alteration (Martínez-García et al., 2022), including during sinking and burial in marine sediments (King and Hare, 1972; Robbins and Brew, 1990; Ren et al., 2009, 2012; Smart et al., 2018), where it can be preserved unaltered for millions of years (Kast et al., 2019; Auderset et al., 2022).

An assumption inherent to applications of foraminifer-bound δ^{15}N to sediment records is that the δ^{15}N of the organic N encased within a foraminifer shell is a good indicator of the ecology and environment experienced during the organism's lifetime (which can range from two weeks to a year, depending on the species (Bé et al., 1979). Recent comparisons of the δ^{15}N of foraminifer tissue and shells have revealed a near 1:1 relationship and relatively consistent offsets between the two in the mixed layer (average offsets $\sim$1.0 ‰, Ren et al. 2012; Smart et al. 2018, 2020; Robinson et al. 2023). Additionally, foraminifer-bound δ^{15}N appears to change only slightly between the mixed layer (i.e., living foraminifera) and twilight zone (sinking foraminifera recovered via sediment trap, increasing by 0.6 ‰ between the upper 200 m and 500 m in the subtropical Sargasso Sea), and then remains constant until foraminifera are incorporated into the sediments (Ren et al., 2012; Smart et al., 2018). In low-latitude regions where the concentration of surface-water nitrate is always low (i.e., oligotrophic), there is a strong link between foraminifer-bound δ^{15}N and the δ^{15}N of thermocline nitrate supplied to the surface annually (Ren et al., 2009, 2012; Smart et al., 2018). By contrast, in the high-latitudes where phytoplankton do not fully consume surface-layer nitrate, foraminifer-bound δ^{15}N is expected to reflect the extent of nitrate drawdown (Martínez-García et al., 2014; Ren et al., 2015). This is because isotope fractionation during nitrate assimilation causes phytoplankton biomass δ^{15}N to rise as the nitrate concentration declines (Altabet and Francois, 1994; Sigman et al., 1999), such that more complete nitrate consumption should increase foraminifer-bound δ^{15}N. However, a recent ground-truthing study from the Southern Ocean showed that the δ^{15}N of modern foraminifer tissue (i.e., the non-calcified biomass of living foraminifera; FT-δ^{15}N) is more strongly linked to the δ^{15}N of PON than to the δ^{15}N of nitrate on a seasonal basis (Smart et al., 2020).

On an annual basis, the δ^{15}N of symbiont-bearing foraminifera (shells and tissue) in the low-latitude ocean (Sargasso and South China Seas) has been shown to record the δ^{15}N of shallow thermocline nitrate almost without offset, while the δ^{15}N of foraminifera without symbionts is generally 1-2 ‰ higher (Ren et al., 2009; Smart et al., 2018). On shorter timescales, both foraminifer-bound δ^{15}N and FT-δ^{15}N also reflect changes in upper ocean N cycling (Smart et al., 2018, 2020). Because individual foraminifera often live for just a few weeks to months, the δ^{15}N of living organisms may record multiple environ-

mental processes, which could yield similar or opposing isotopic signatures. Interpreting variations in fossil foraminifer-bound δ^{15}N thus requires knowledge of regional and global nutrient cycling, water mass properties including thermocline and sub-thermocline nitrate δ^{15}N, and foraminifer ecology at the species level.

Given the demonstrated sensitivity of foraminifer δ^{15}N to thermocline nitrate in the low-latitude ocean (Ren et al., 2009, 2012; Schiebel et al., 2018), we propose that foraminifer-bound δ^{15}N is a potentially viable proxy for monitoring Agulhas leakage into the South Atlantic. While both the South Atlantic and Indian Oceans rely on Subantarctic Mode Water (SAMW) as the ultimate source of their mixed-layer nitrate (Rintoul and Trull 2001; Sarmiento et al. 2004; Palter et al. 2010; Marshall et al. 2023), the δ^{15}N of nitrate in the thermocline of the subtropical Indian Ocean is substantially lower than that observed in the subtropical South Atlantic ($< 5.4\,‰$ *versus* $\sim 6.8\,‰$; This difference has been explained as the result of N_2 fixation in the Indian but not in the subtropical South Atlantic (Moore et al. 2009; Raes et al. 2015; Landolfi et al. 2018; Harms et al. 2019; Marshall et al. 2023), which introduces bioavailable N to the upper water column that is low in δ^{15}N (-2-$0\,‰$; Carpenter et al. 1997; Hoering and Ford 1960; Minagawa and Wada 1986). In other ocean regions that host significant rates of N_2 fixation, such as the (sub)tropical North Atlantic, the low δ^{15}N of thermocline nitrate is passed on to phytoplankton (Fawcett et al., 2011, 2014; Van Oostende et al., 2017) and zooplankton (Somes et al., 2010; Loick-Wilde et al., 2016), including foraminifera (Ren et al., 2012; Smart et al., 2018). We thus expect the PON produced from the consumption of the nitrate in Agulhas waters (including Agulhas eddies), as well as the foraminifera reliant thereon, to be lower in δ^{15}N than foraminifera from the Cape Basin. For a δ^{15}N-based leakage proxy to add value beyond existing proxies, a distinct δ^{15}N signature must persist in foraminifer-bound N regardless of changes in the eddy foraminifer species composition (i.e., a major limitation of the assemblage-based proxy; Lončarić 2006).

Here, we investigate the potential utility of foraminifer-bound δ^{15}N as a proxy for Agulhas leakage and lay the ground-work for its application to palaeoceanographic records from the Cape Basin. We present measurements of nitrate isotope ratios for samples collected in 2015 and 2017 along a transect extending from the west coast of South Africa, across the Cape Basin, and into the South Atlantic subtropical gyre that intersected Agulhas eddies. For the 2017 cruise, we also measured the δ^{15}N of various forms of PON and of the tissue and shells of living planktic foraminifera captured in surface net tows, both within an Agulhas eddy and in the "background" (i.e., non-eddy) South Atlantic. We compare our data to new nitrate isotope measurements from the Agulhas Current (Marshall et al., 2023) and confirm that its thermocline nitrate is low in δ^{15}N compared to the δ^{15}N of nitrate in SAMW and the Cape Basin thermocline. Our results show that foraminifera living in Agulhas eddies have a unique and persistent δ^{15}N signature which we suggest/propose could be leveraged to reconstruct Agulhas leakage in the past.

2.2 Methods

2.2.1 Shipboard sampling

The South Atlantic Meridional Overturning Circulation Basin-wide Array (SAMBA) is a zonal transect of moorings along 34.5°S that was installed to measure basin-scale meridional transport of mass, heat, and salt (Morris et al., 2017). During a cruise in 2017 to service the eastern sub-array of SAMBA located off the coast of South Africa (i.e., east of 0°E), we sampled 21 conductivity-temperature-depth (CTD) hydrocast stations for a variety of physical, chemical, and biological parameters (Fig. 2.1). We supplemented this dataset with hydrographic, nutrient, and nitrate isotope measurements from five hydrocasts conducted along the same array in 2015 (Campbell, 2016, ; C1-C5 in Fig. 1). In both years, sampling occurred during austral winter (July) aboard the R/V *S.A. Agulhas II*, with water-column samples collected using Niskin bottles attached to a rosette equipped with Sea-bird CTD, oxygen, and fluorescence sensors that assisted in targeting specific features (e.g., the mixed layer depth (MLD) and depth of maximum fluorescence (F-max)). Sampling resolution was higher at the shallower depths (< 200 m) than deeper in the water column. In 2017, the cruise detoured south between 11.2°E and 14.3°E (to 35.5°S) to sample an anticyclonic Agulhas eddy (hereafter referred to as E1) that was tracked prior to and during the cruise using satellite altimetry (see below).

In July 2016, samples were collected for nutrients and nitrate isotopes aboard the R/V *S.A. Agulhas II* along the Agulhas System Climate Array (ASCA) transect in the southwest Indian Ocean that extends 300 km offshore of South Africa across the Agulhas Current Morris et al. 2017; Marshall et al. 2023). From these samples, a representative station (35.52°S; 28.77°E) located just offshore of the current core was selected for comparison with the SAMBA stations (yellow circle in Fig. 2.1). Samples were processed as described for the SAMBA collections (Marshall et al., 2023).

For both the 2015 and 2017 SAMBA datasets, MLD was calculated as the depth at which potential density exceeded the value at 25 m by 0.05 $\mathrm{kg.m^{-3}}$. These derived MLDs closely tracked the 26.1-26.2 $\mathrm{kg.m^{-3}}$ isopycnals that denote the top of the thermocline and yielded upper layers over which the nitrate concentrations were near-homogeneous (Fig. 2.2a, 2.2b).

All CTD stations were sampled for seawater nitrate+nitrite and nitrite concentrations, with five and 19 stations sampled for nitrate isotopes in 2015 and 2017, respectively. Water samples were collected in well-rinsed 50 mL Falcon tubes for nutrients and high-density polyethylene bottles for nitrate isotopes, with the latter immediately frozen at -20°C. The nitrate+nitrite concentrations were measured shipboard using a Lachat QuickChem flow injection autoanalysis platform (Grasshoff, 1976; Diamond, 1994) in a configuration with a detection limit of 0.1 μM. Nitrite concentrations were determined manually via the colorimetric method of Strickland and Parsons (1968) using a Thermo Scientific Genesys 30 visible spectrometer. Certified reference materials (JAMSTEC) were included in each ni-

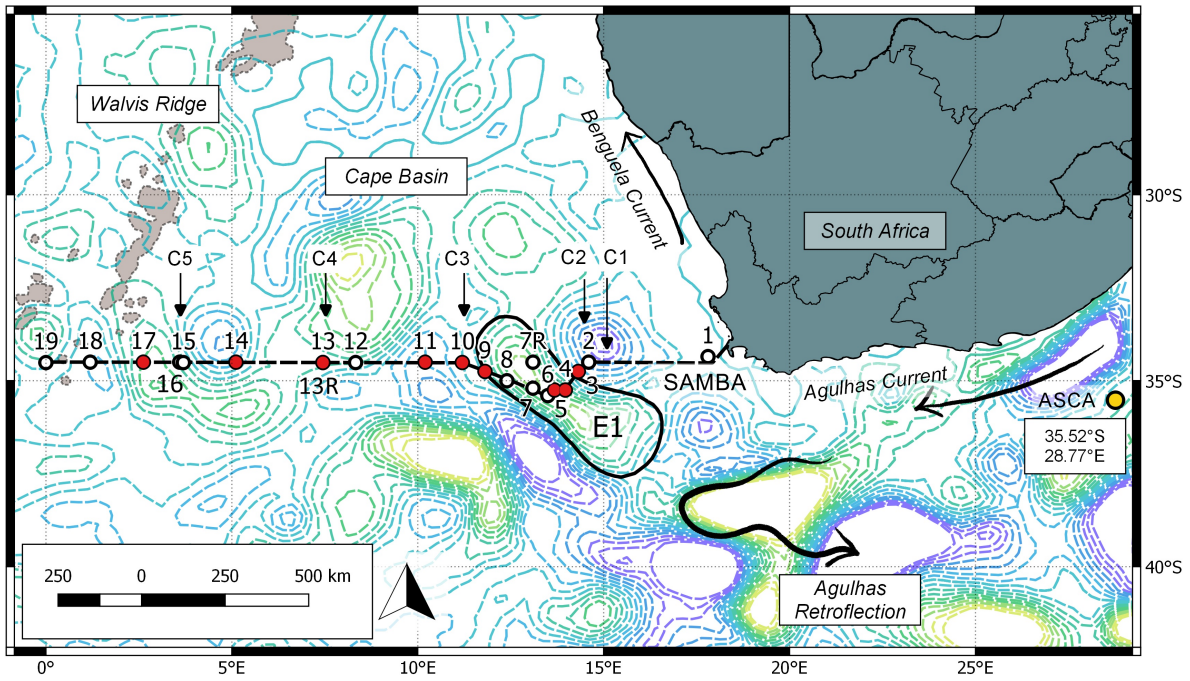

Figure 2.1: Cruise track followed by the R/V *S.A. Agulhas II* in July 2017 along the SAMBA line. Contour lines show sea surface height anomaly in reference to the geoid (SSALTO/DUACS product distributed by AVISO via the Copernicus Marine Environment Monitoring Service Lea et al. 2018, `http://marine.copernicus.eu`, 24 July 2017), with positive and negative anomalies shown by the light green and purple dashed lines, respectively. The outer edge of Agulhas eddy E1, as defined in section 2.4, is indicated by the thick black contour, and E1 is labelled on the map. Along the transect, the white circles represent stations sampled for nitrate concentration, isotopes, and particulate organic nitrogen; red circles show stations where foraminifera and bulk zooplankton were also collected using net tows. The positions of stations sampled in 2015 along the same 34.5°S transect (Campbell, 2016) are indicated by arrows and labelled as C1-C5, noting that the background SSHA does not apply to these stations.

trate+nitrite and nitrite run to ensure measurement accuracy. Nitrate-only concentrations were calculated as the difference between the nitrate+nitrite and nitrite concentrations.

In 2017, four to six bulk suspended PON samples were collected over the mixed layer (0-175 m) at all stations. We targeted the surface (< 10 m), the F-max, and two to four additional depths including the approximate MLD. At each depth, 4 L of seawater were filtered through pre-combusted (450°C for 8 hours) 0.3 μm glass fibre filters (GF-75s; Sterlitech) that were stored frozen in pre-combusted foil at −80°C until processing.

Living planktic foraminifera were collected at nine stations (Fig.1, red circles) using a double 1 m^2 250 μm-mesh plankton net, towed obliquely over the upper 200 m of the water column at 0.1-0.6 knots for an average of 40 minutes. On deck, 90% of each collection was preserved using 5-10% pH-buffered formalin and refrigerated at 4°C until processing, following the protocol of Smart et al. (2020) (modified from Ren et al. 2012). The remaining 10% was size-fractionated on board for later analysis of bulk zooplankton

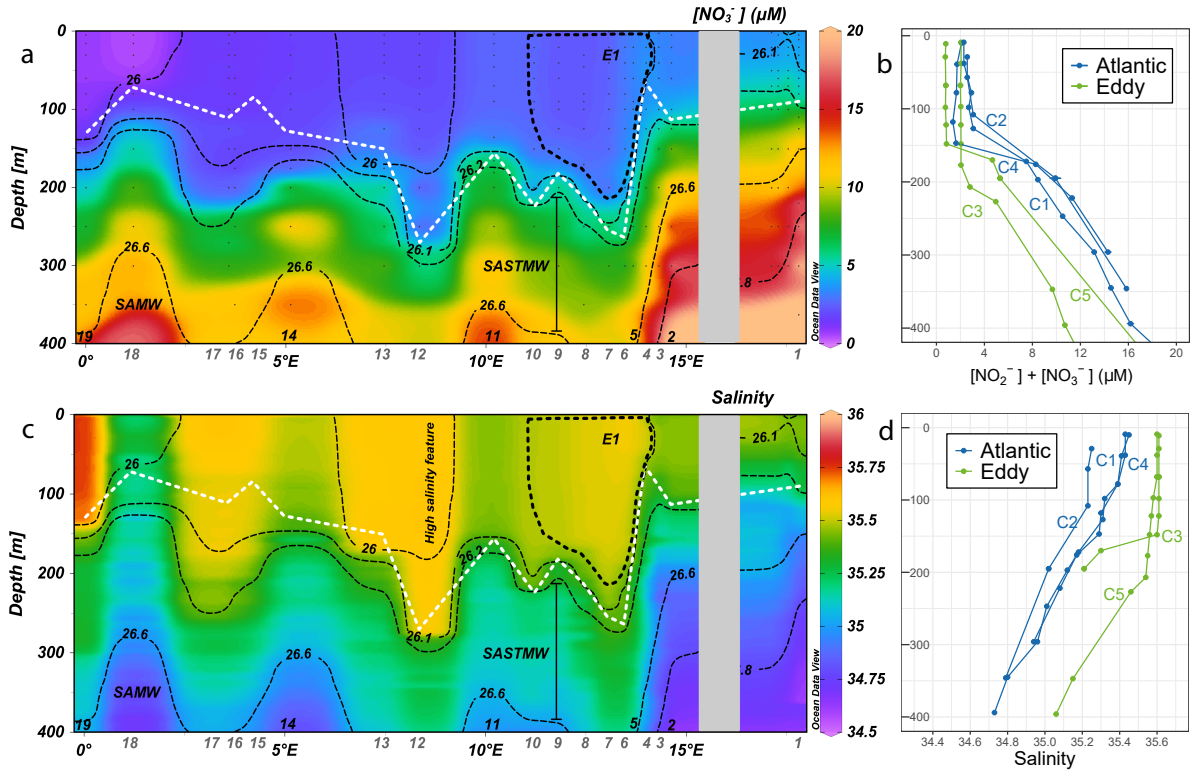

Figure 2.2: Section plots from the 2017 cruise showing a) nitrate concentrations and c) salinity overlaid with isopycnals (kg m^{-3}; dotted black contour lines). The approximate mixed layer depth is indicated by the dashed white line. Sampling stations are labelled on the bottom x-axis, and the location of Agulhas eddy E1 is shown by the dashed black polygon (labelled E1). Panels b) and d) show the vertical profiles of nitrate and salinity for the stations sampled in 2015, with the colours indicating whether those stations were located in background Atlantic- (blue) or Agulhas eddy waters (green) at the time of sampling.

δ^{15}N by sieving the material in series through nylon mesh sieves of 5000 μm, 2000 μm, 1000 μm, 500 μm, 250 μm, and 150 μm. The contents of each sieve were transferred to pre-combusted 0.7 μm glass fibre filters (GF/Fs) and frozen at −20°C until processing.

2.2.2 Foraminifera and bulk zooplankton sample preparation

Sample preparation took place in the Marine Biogeochemistry Lab at the University of Cape Town (UCT-MBL) and the Max Planck Institute for Chemistry (MPIC) in Mainz. Foraminifera were picked according to the methods outlined in Ren et al. (2012) and Smart et al. (2020). Briefly, formalin-preserved material was passed through a 1000 μm-mesh sieve to remove large zooplankton, then rinsed several times with deionized water. A density separation was subsequently performed using a 200 $g.L^{-1}$ NaCl solution before the foraminifer-containing material was rinsed again with de-ionized water and transferred to clean plastic petri dishes and the liquid was allowed to evaporate under a fume hood.

For tissue measurements, between three and 14 specimens of each species were picked, photographed (Olympus UC90 camera) and transferred to weighed, pre-combusted (500°C for 5 hours) 4 mL Wheaton vials. Picked foraminifera were rinsed with MilliQ water under an Olympus SZX16 (0.7X–11.5X) incident light microscope using a pipette to remove

residual nitrate and formalin (Ren et al., 2012; Smart et al., 2020), then the remaining liquid was removed and the samples were dried in a desiccator overnight. Specimens were weighed (Mettler Toledo XP6U comparator 7-digit microbalance), crushed in the vial with an ethanol-cleaned spatula and transferred to the freezer until oxidation. Shell samples were treated in the same way, using between 15 and 100 specimens per vial.

Thereafter, 1 mL of persulfate oxidising reagent (POR) was added to each tissue (1 g of four-times recrystallized potassium persulfate combined with 0.7 g NaOH and dissolved in 100 mL Milli-Q water) and shell sample (1.5 g potassium persulfate and 1.5 g NaOH dissolved in 100 mL Milli-Q water) to convert the organic N to nitrate, facilitated by autoclaving for 65 minutes at 120°C on a slow vent setting (Nydahl, 1978; Knapp et al., 2005). Samples were prepared in triplicate in different oxidation batches (with the exception of rare species), and POR blanks and a dilution series of the amino acid standards, USGS-40 and USGS-41 (Qi et al., 2003), were included in all batch runs. The blanks and standards were used to quantify the magnitude and δ^{15}N of the POR-associated N blank and to ensure complete oxidation (standards). After autoclaving, tissue samples were pH-adjusted to 5-7 using 4 N Optima grade HCl. For shell samples, the tissue-derived nitrate was removed by rinsing 4 times with Milli-Q water, with the remaining calcite left to dry overnight at 40°C following the method of Ren et al. (2009). Samples were then transferred to clean Wheaton vials to which 1 mL of HCl was added to release the calcite-bound organic N into solution. This organic N was oxidized to nitrate via the addition of POR (in this case, 0.7 g of potassium persulfate and 4 mL of 6.25 M NaOH in 96 mL Milli-Q), after which sample pH was adjusted to 5-7.

Size-fractionated zooplankton samples were prepared for N isotope analysis by freeze-drying at −80°C using a Scanvac Coolsafe. Where possible, the dried material was gently scraped from the GF/F into a tin cup and weighed. Between 0.125 and 0.750 mg of sample was analysed. Where scraping was not possible due to small particles adhering to the GF/F, filter quarters were inserted into tin cups and measured separately alongside blank pre-combusted filters. The bulk PON samples were prepared and subsequently analysed in the same way.

2.2.3 Particulate and nitrate isotope analysis

The concentration of nitrate resulting from the oxidation of foraminifer tissue and shells was measured by chemiluminescence (Braman and Hendrix, 1989; Ren et al., 2012). Nitrate was then quantitatively converted to N_2O gas via the denitrifier method (Sigman et al., 2001) and the δ^{15}N of the N_2O was measured by gas chromatography-isotope ratio mass spectrometry (GC-IRMS) at MPIC using a Thermo MAT253 with custom-built N_2O extraction and purification system (Weigand et al., 2016). N_2O isotope measurements were calibrated to N_2 in air using the nitrate reference materials, USGS-34 and IAEA-NO_3 (Gonfiantini et al., 1993; Böhlke et al., 2003). Measurements from each batch were corrected for the POR blank (which on average accounted for 0.7% of the N in the

foraminifer tissue samples and 10.7% of the N in the shell samples). The mean pooled standard deviation (1σ) for cleaning-and-oxidation replicates of the same sample was 0.03 for the tissue samples (n=188). The N content of the shell samples was not high enough to run replicates.

Seawater samples underwent nitrite removal via sulfamic acid addition (Granger and Sigman, 2009) prior to N and oxygen (O) isotope analysis since even very low concentrations of nitrite can significantly affect the measured δ^{15}N and δ^{18}O of nitrate+nitrite (where δ^{18}O (*versus* Vienna Standard Mean Ocean Water (VSMOW)) = $[(^{18}O/^{16}O)_{sample}/(^{18}O/^{16}O)_{VSMOW} - 1] \times 1000$), Casciotti and McIlvin 2007; Fawcett et al. 2015). The δ^{15}N and δ^{18}O of nitrate ($\delta^{15}N_{NO_3}$ and $\delta^{18}O_{NO_3}$) were subsequently determined using the denitrifier-IRMS method (Sigman et al., 2001; Casciotti et al., 2002; Weigand et al., 2016) at MPIC for the SAMBA 2017 samples and at Princeton University for the SAMBA 2015 samples. The pooled standard deviations for replicate measurements (n≥2) were 0.05 and 0.18 (n = 245) for δ^{15}N and δ^{18}O, respectively.

The nitrate N and O isotope data were used to calculate the parameter Δ(15-18) (equating to $\delta^{15}N_{NO_3} - \delta^{18}O_{NO_3}$; Sigman et al. 2005; Rafter et al. 2013). The ratio of the N and O isotope effects expressed during nitrate assimilation by phytoplankton is approximately 1:1 (Granger et al., 2004, 2010), such that assimilation does not alter nitrate Δ(15-18). By contrast, processes that produce nitrate have variable effects on its $\delta^{15}N_{NO_3}$ and $\delta^{18}O_{NO_3}$. This is because the δ^{15}N of nitrate resulting from subsurface nitrification depends on the δ^{15}N of the organic matter and ammonium being remineralized and nitrified, while the δ^{18}O of newly-nitrified nitrate is set by the δ^{18}O of seawater (plus an isotopic offset of $\sim$1.1 ‰; Sigman et al. 2005, 2009; Buchwald and Casciotti 2010; Boshers et al. 2019). As such, nitrate Δ(15-18) can be used to disentangle overlapping N cycle processes that cannot be diagnosed from measurements of $\delta^{15}N_{NO_3}$ or $\delta^{18}O_{NO_3}$ alone. For example, N_2 fixation introduces nitrate to the subsurface that is lower in δ^{15}N than deep-ocean nitrate, thus causing nitrate Δ(15-18) to decrease (e.g., Knapp et al. 2008; Marshall et al. 2023). Similarly, co-occurring partial nitrate assimilation and nitrification (e.g., at the base of the mixed layer), which has no net effect on the $\delta^{15}N_{NO_3}$ but causes $\delta^{18}O_{NO_3}$ to rise (because the δ^{18}O of newly-nitrified nitrate is higher than the δ^{18}O of the nitrate assimilated by phytoplankton), yields a decline in nitrate Δ(15-18) (Sigman et al., 2005; Wankel et al., 2007; Sigman et al., 2009; Rafter et al., 2013; Fawcett et al., 2015; Deman et al., 2021).

The δ^{15}N of bulk PON and size-fractionated zooplankton was measured in the Stable Light Isotope Laboratory at UCT using a Delta V Plus IRMS coupled to a Flash 2000 elemental analyzer. In-house standards calibrated against IAEA reference materials were run after every 5-8 samples and used to reference the measurements to atmospheric N_2. The detection limit for N was 1 μg and precision was < 0.2 ‰. On average, the filter blanks were 1.4% of the bulk zooplankton N concentration and 6.9% of the bulk PON. The pooled standard deviation for replicate samples was 0.18 ‰.

2.2.4 Satellite imagery and model products

Satellite altimetry was used alongside ship-board hydrographic and acoustic Doppler current profiler (ADCP) data to track an Agulhas eddy before and during the SAMBA 2017 cruise. A large asymmetrical eddy (E1) formed in December 2016 and was evident at the time of sampling as a closed-contour, positive surface height anomaly (SSHA) $> +7$ cm (CMEMS, Fig. 1). Within this contour, E1 was characterized by high sea-surface salinity ($> 35.5\,\mathrm{g.kg^{-1}}$), depressed isopycnals (Fig. 2.2c), and anticyclonic rotation (apparent in the ACDP data; Chen et al. 2021; Wallschuss et al. 2022). For the 2015 cruise, Agulhas eddies were identified post-cruise from elevated water temperatures (by as much as 4.7°C at 250 m), anticyclonic rotation (via ADCP), high mixed-layer salinity (Fig. 2.2d), and the depression of isopycnals in the upper water column. Two additional eddies (E2, 7.5-8.3°E and E3, 3.6-3.7°E) were identified by Wallschuss et al. (2022) along the 2017 transect. Our stations 12, 13, 13R, 15, and 16 were located with these features. However, we classify only station 12 (8.3°E) as an eddy station and refer to stations 13, 13R, 15, and 16 as 'mixed'. This decision was based on (1) reduced rotation at the mixed stations due to their being located at the eddy edges, and recognizing that the physical and biological properties at eddy edges can reflect either the eddy (e.g., station 3) or the background Atlantic (e.g., station 10); and (2) the low sampling resolution within E2 and E3, such that these features are not well defined (Wallschuss et al., 2022).

The CMEMS product, Global_Forecast_Bio_001_028, was used to visualize the seasonal cycle of surface (0.5 m) nitrate concentrations at four locations along 34.5°S over four years, encompassing the two cruises (2014 – 2018 at 0.25°E, 7.5°E, 10°E, and 13°E). This product uses the output from the PISCES model (Aumont et al., 2015), which simulates daily biogeochemical cycles of carbon and nutrients. The surface nitrate concentration is resolved at 0.25° horizontal resolution in the eddy-permitting model.

2.3 Results

2.3.1 Hydrography and the identification of eddy stations

Eddy stations were distinguished from the background Atlantic using a combination of altimetry, density, and salinity data, along with the derived MLDs. Agulhas eddies are characterized by anticyclonic rotation, positive SSHAs, and deep, low-density, high-salinity mixed layers (Schouten et al., 2000; Van Aken et al., 2003; Moutin and Prieur, 2012; Dufois et al., 2016). From our high resolution sampling in 2017 between stations 2 and 10 (14.6°E to 11.2°E), we determined that stations 4 to 9 were located within eddy E1, with the neighbouring stations on either side representing the eddy edges (Fig. 2.1 and 2.2). The most positive SSHA (+38 cm) was observed at station 7 (13.1°E), which was taken to represent the core of E1. As expected, the E1 mixed layer was more saline than the surrounding Atlantic stations (e.g., $35.55\,\mathrm{g.kg^{-1}}$ at station 5 *versus* $35.45\,\mathrm{g.kg^{-1}}$ at station

11; Fig. 2.2c).

Satellite imagery indicated the presence of an additional eddy-like feature just north of our transect, with station 12 sampling its southern edge (Fig. 2.1). Although station 12 was not located in the centre of this eddy, its high-salinity, low-density mixed layer evince a substantial influence of Agulhas leakage (Fig. 2.2). Additionally, its mixed layer was 277 m deep, leading us to classify station 12 as an eddy station. Agulhas leakage was less apparent at the neighbouring station 13 (and 13R; where "R" indicates "repeat" since station 13 was sampled on both the outbound and inbound legs of the cruise). Here, the isopycnals shoaled rapidly, leading to shallower mixed layers (158 m and 211 m). We classify these stations as "mixed", and as such, do not include them (or the E1 edge stations 3 and 10) in our comparisons of Atlantic *versus* eddy seawater characteristics.

At the trailing (i.e., eastern) edge of E1, a dipole effect was evident, with the cyclonic circulation of a non-Agulhas eddy to the east creating a steep gradient in SSHA (approximately 50 cm over 100 km between stations 2 and 4; Fig. 2.1). The interaction of E1 with the cyclone heavily influenced the physical and chemical characteristics of the water column, evinced by a sudden shoaling of the mixed layer (to 67 m) and nitracline at stations 3 to 5 compared to the stations in the centre of E1 (Fig. 2.2b).

The average MLD in E1 was significantly greater than the average Atlantic MLD across the 2017 transect (MLD = 218 ± 37 m (n = 5; stations 5 to 9) and 106 ± 40 m (n = 8; stations 2, 11, 14 to 19), respectively, Welch's t-test $p < 0.001$). Eddy station 4 was excluded from this analysis due to its much shallower mixed layer (67 m) resulting from isopycnal shoaling during interaction of the trailing edge of E1 with the cyclone to its east. The same trend of deeper in-eddy mixed layers was evident in the 2015 dataset, with an average MLD of 187 ± 32 m (n = 2) for the eddies (stations C3 and C5) and 139 ± 16 m (n = 3) for the Atlantic stations (C1, C2 and C4; Fig. 2.2b and 2.2d).

Using potential density, we identified several water masses in the upper 1000 m of the 2015 and 2017 transects. SAMW was evident between 26.6 and 27.0 $kg.m^{-3}$ ($\sim$350 to 750 m) and was overlaid by South Atlantic Subtropical Mode Water (SASTMW; 26.2 to 26.6 $kg.m^{-3}$; $\sim$200 to 350 m), which is formed through the modification of SAMW by mixing with less dense surface waters (Donners et al., 2005). In 2017, the surface waters overlying SASTMW had a potential density of 25.9 to 26.2 $kg.m^{-3}$, with the lightest waters encountered at the westernmost edge of the transect (i.e., station 19 in the subtropical gyre), as well as at mid-transect stations 12, 13, and 13R.

2.3.2 Seawater nitrate concentrations and isotopes

Mixed-layer nitrate concentrations were similar for the 2015 and 2017 transects ($< 4.1\,\mu$M in 2017 and $< 3.1\,\mu$M in 2015; Fig. 2.2a and 2.2b, S.1), with a consistent east-to-west decrease of $\sim 0.2\,\mu$M per degree of longitude (Fig. S.1). In E1, mixed-layer nitrate was on average $1.2\,\mu$M higher than background Atlantic levels. In 2015, the eddies were encountered further west along the transect, and eddy mixed-layer nitrate was on average

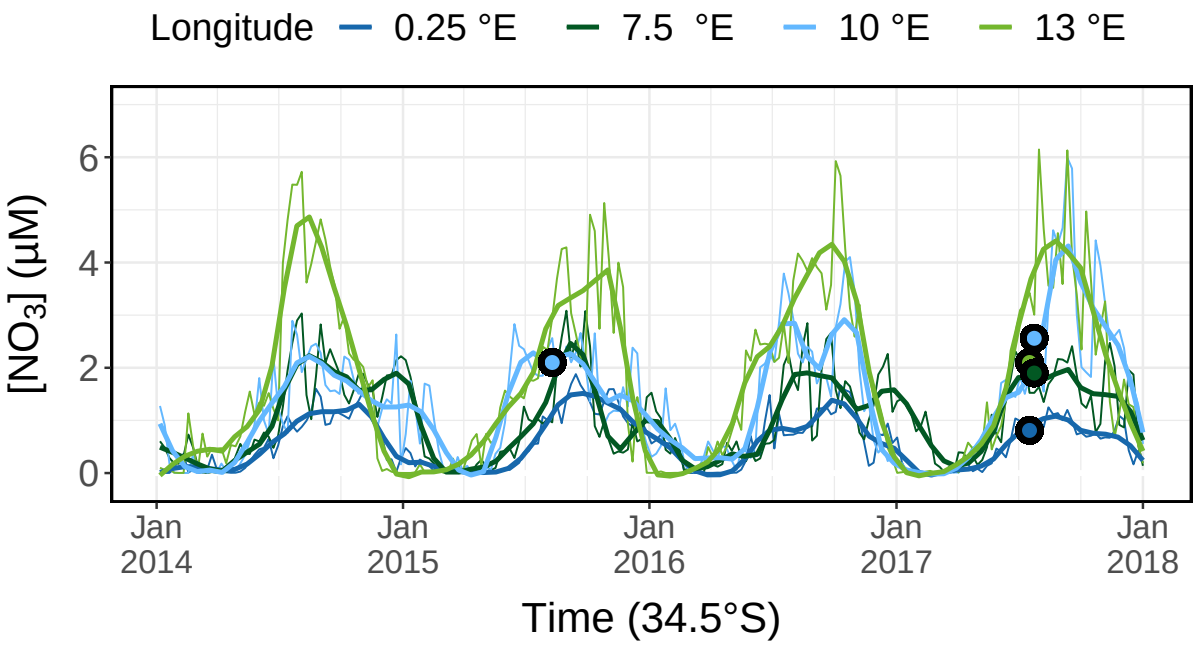

Figure 2.3: Surface (0.5 m) nitrate concentrations at four locations along the SAMBA transect (34.5°S; 0°E (dark blue), 7.5°E (dark green), 10°E (light blue), 13°E (light green)) between January 2014 and January 2018. The thin lines show monthly reanalysis data and the thick lines show smoothed data (moving average = 2 weeks) (`http://marine.copernicus.eu/documents/QUID/CMEMS-GLO-QUID-001-028.pdf`). Coloured circles show the surface nitrate concentrations measured at the corresponding locations during the 2015 and 2017 cruises.

0.7 μM lower than in the Atlantic mixed layer. Below the mixed layer, the nitrate concentration of SASTMW in 2017 was fairly uniform, averaging $8.6 \pm 2.3\,\mu$M (n = 12) for the Atlantic stations and $8.5 \pm 1.9\,\mu$M (n = 14) in E1. The mean value across the transect was $8.6 \pm 2.0\,\mu$M (n = 38), consistent with previous measurements of SASTMW in the southeast Atlantic ($8.7 \pm 2.6\,\mu$M; Flynn et al. 2020). The nitrate concentration of the underlying SAMW ranged from 11.3 to 23.6 μM (average of $16.7 \pm 3.7\,\mu$M, n = 27), with no significant difference between the Atlantic stations and E1. The nitrate concentrations determined in 2015 for these water masses were similar ($9.2 \pm 6.6\,\mu$M (n = 17) for SASTMW and $20.2 \pm 5.6\,\mu$M (n = 13) for SAMW).

Surface (0.5 m) nitrate data from CMEMS agree well with our measured concentrations (Fig. 2.3). The model time-series shows that our sampling took place during the nitrate resupply period, which begins in late autumn (April/May). Surface nitrate concentrations peak in spring (September), reaching 4 to 5 μM at 13°E, 2 to 4 μM at 10°E, 1 to 3 μM at 7.5°E, and 1 to 2 μM at 0°E, and nitrate is almost completely exhausted by late summer (March/April). Comparing the nitrate concentration data from 2015 and 2017 with the model output suggests that both samplings captured typical winter conditions in the southeast Atlantic, and that the two years can be analysed as a single, combined dataset. Thus, unless otherwise stated, further discussion of water masses and seawater nitrate isotopes refers to a composite of the 2015 and 2017 datasets.

The mean $\delta^{15}N_{NO_3}$ for SASTMW across the transect (eddy + Atlantic stations) was

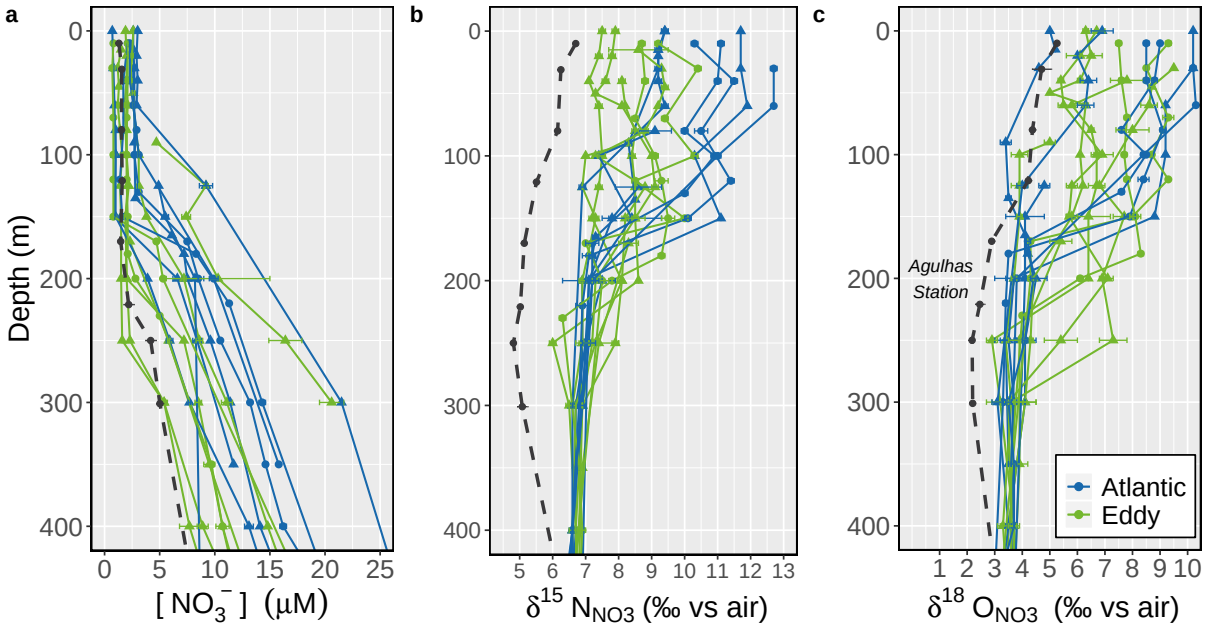

Figure 2.4: Depth profiles (0-400 m) of a) nitrate concentration, b) $\delta^{15}N_{NO_3}$, and c) $\delta^{18}O_{NO_3}$ for the SAMBA line stations sampled in 2015 and 2017, coloured by station type (blue = background Atlantic, green = Agulhas eddy). Also shown are data from a representative station located in the Agulhas Current (dashed black line; Marshall et al. 2023). Error bars show ±1 standard deviation of duplicate measurements.

6.9 ± 0.4 ‰ and the mean $\delta^{18}O_{NO_3}$ was 3.8 ± 0.6 ‰ (n = 51, Fig. 2.4). From the combined nitrate isotope dataset, we observe a clear difference between eddy and Atlantic $\delta^{15}N_{NO_3}$, but not $\delta^{18}O_{NO_3}$ (Fig. 2.4b and c). While $\delta^{15}N_{NO_3}$ increased from the thermocline (i.e., SASTMW) into the surface (< 20 m) at both the eddy and Atlantic stations, the magnitude of the increase was smaller at the eddy stations (average surface $\delta^{15}N_{NO_3} = 8.6 \pm 0.5$ ‰ and 10.3 ± 0.8 ‰ for the eddy (n = 19) and Atlantic stations (n = 40), respectively). Similarly, the concentration-weighted average mixed-layer $\delta^{15}N_{NO_3}$ for the eddy stations (calculated using 1 m gridded values) was 7.9 ± 0.7 ‰ (i.e., 1.0 ‰ higher than the thermocline $\delta^{15}N_{NO_3}$), while in the Atlantic mixed layer, $\delta^{15}N_{NO_3}$ averaged 9.6 ± 1.2 ‰ (i.e., 2.7 ‰ higher). In addition, some of the E1 profiles showed a negative $\delta^{15}N_{NO_3}$ deviation at the top of the thermocline (from 6.9 ‰ in SASTMW to as low as 6 ‰ at 230 to 250 m) that was not apparent at the Atlantic stations (nor in the $\delta^{18}O_{NO_3}$ data). Like the $\delta^{15}N_{NO_3}$, the $\delta^{18}O_{NO_3}$ also increased from the thermocline into the mixed layer, but by similar amounts at the eddy and Atlantic stations; averaged over the mixed layer, $\delta^{18}O_{NO_3}$ was elevated relative to the thermocline by 2.3 ± 1.3 ‰ at the eddy stations and 2.8 ± 2.1 ‰ at the Atlantic stations.

The difference between the thermocline-to-mixed-layer changes in $\delta^{15}N_{NO_3}$ and $\delta^{18}O_{NO_3}$ in the eddy *versus* Atlantic is highlighted by the nitrate Δ(15-18) profiles where the effect of nitrate assimilation on $\delta^{15}N_{NO_3}$ and $\delta^{18}O_{NO_3}$ has been removed (Fig. 2.5). Below the thermocline, all the seawater nitrate profiles converged on a Δ(15-18) of 3.2. At the eddy stations, Δ(15-18) then decreased over the thermocline and into the surface (average

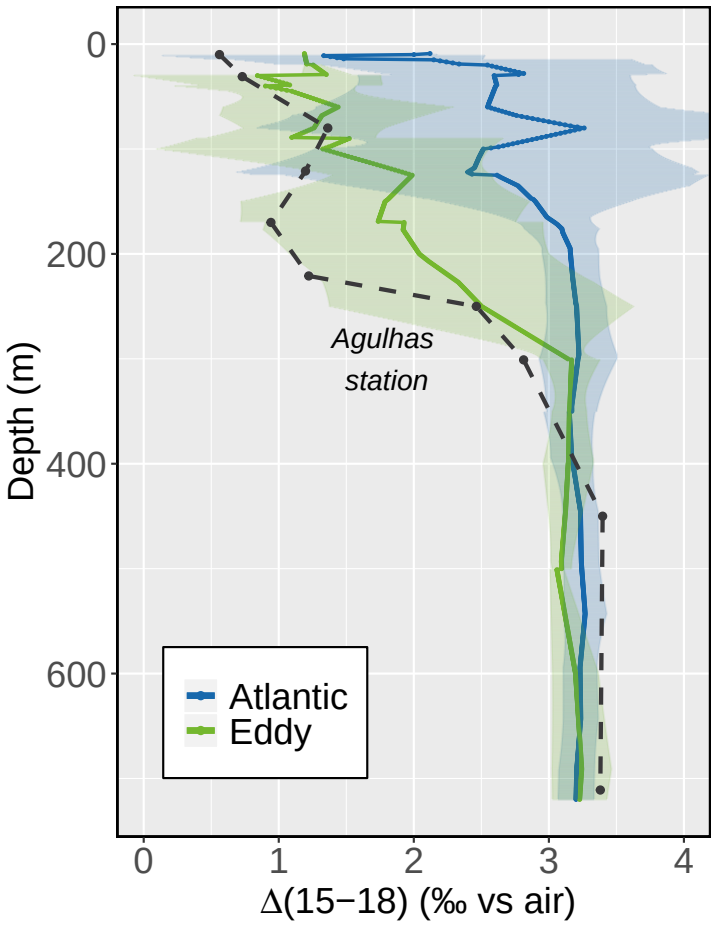

Figure 2.5: Average nitrate Δ(15-18) ($\delta^{15}N_{NO_3}$ – $\delta^{18}O_{NO_3}$) for the Atlantic and eddy stations gridded at 1 m intervals. Shaded areas show ±1 standard deviation of the combined 2015 and 2017 dataset. The black dashed line indicates the Δ(15-18) for the Agulhas Current profile shown in Fig. 2.4.

mixed-layer Δ(15-18) of 1.8 ± 1.2 ‰) whereas at the Atlantic stations, Δ(15-18) remained roughly constant between the thermocline and the surface (average mixed-layer Δ(15-18) of 3.0 ± 1.4 ‰).

In the Agulhas profile, the mixed layer had a density of 25.4 kg.m^{-3}, which was low compared to the Cape Basin mixed layer, and a nitrate concentration of 1.2 ± 0.1 μM, which was similar (Fig. 2.4a). While SAMW (26.6-27.0 kg.m^{-3}), with a core $\delta^{15}N_{NO_3}$ and $\delta^{18}O_{NO_3}$ of 6.9 ± 0.2 ‰ and 3.5 ± 0.2 ‰, respectively (Δ(15-18) of 3.4 ± 0.2 ‰) (Marshall et al., 2023), also underlies the Agulhas Current thermocline, $\delta^{15}N_{NO_3}$ decreased strongly into the thermocline (to reach a minimum of 4.9 ‰ at 250 m Fig. 2.4b) and $\delta^{18}O_{NO_3}$ decreased slightly (to reach a minimum of 2.2 at 250 m; Fig. 2.4c). The subsequent thermocline-to-mixed-layer increases in $\delta^{15}N_{NO_3}$ and $\delta^{18}O_{NO_3}$ were by 2.4 ‰ and 4.3 ‰, respectively (Fig. 2.5), similar to (although offset to lower absolute values, particularly for $\delta^{15}N_{NO_3}$) the increases observed in E1. As such, mixed-layer $\delta^{15}N_{NO_3}$ in the Agulhas profile (concentration-weighted average of 8.2 ± 0.8 ‰) was similar to that measured in the Cape Basin eddies and lower than in the Atlantic mixed layer (by 1.4 ‰), while its $\delta^{18}O_{NO_3}$ (concentration-weighted mixed-layer average of 7.2 ‰) overlapped with the lower

end of the mixed-layer values measured across the Cape Basin. The Δ(15-18) of nitrate averaged over the mixed layer of the Agulhas profile was 1.0 ± 0.3 ‰, which is 0.8 ‰ and 2.0 ‰ lower than the mixed-layer nitrate-Δ(15-18) observed at the eddy and Atlantic stations, respectively.

2.3.3 Foraminifera and particulate organic N isotopes

In our analysis of the foraminifera (tissue and shell) and particulate δ^{15}N data, we divide the stations into two groups, "eddy" and "Atlantic". We include the mid-transect "mixed" station 13 in the Atlantic group since, although it showed some properties consistent with an eddy-influenced environment (e.g., high salinity and positive SSHA), it was not enclosed by anticyclonic flow (Fig. 2.1). We also classify the leading edge of E1 (station 10) as Atlantic, as the upward-sloping isopycnals meant that Atlantic waters lay just below the surface (< 50 m) even as the surface waters showed some Agulhas influence. The trailing edge of E1 (station 3) is considered part of the eddy given its close proximity to the eddy centre (where retention of the eddy source waters is typically strongest; Wang et al. 2018) compared to the stations at the leading edge. We note that excluding these three stations (3, 10, and 13) from our analysis does not significantly alter the results. Standard deviations reported for foraminifera and particulate δ^{15}N reflect variability between sampled specimens (typically from multiple stations), rather than measurement replication.

2.3.3.1 Foraminifera abundance and size

Three dominant foraminifer species were present at all stations sampled in 2017; combined, the deeper-dwelling species, *Globorotalia inflata, Globorotalia truncatulinoides*, and *Globorotalia hirsuta* accounted for between 73% and 100% of the total foraminifera at each station (Fig. 2.6). Atlantic stations 17 (2.6°E) and 14 (5.1°E) were characterised by the highest relative abundances of spinose shallower-dwellers (*Globigerina bulloides, Orbulina universa*, and *Globigerina falconensis*) at 26.5% and 18.5% of the total foraminifera, respectively. In contrast, stations 13 (7.5°E) and 9 (11.8°E) comprised almost entirely of *G. inflata, G. hirsuta*, and *G. truncatulinoides*. We did not observe any of the typical subtropical species previously recorded in this region (e.g., *Globigerinoides ruber, Trilobus sacculifer, Globorotalia menardii*; Schiebel and Hemleben 2017), apart from a single *G. ruber* specimen at station 14.

Although the three deeper-dwelling species dominated the foraminiferal assemblage across the transect, their relative abundance varied, with *G. inflata* and *G. truncatulinoides* varying inversely (r2 = 0.89). *G. truncatulinoides* dominated the western section of the transect (e.g., 63% of the total assemblage at station 17 where *G. inflata* comprised just 7%), while *G. inflata* dominated in the east (e.g., 80% at E1 station 5 where *G. truncatulinoides* contributed only 7%). The contribution from *G. hirsuta* across the transect

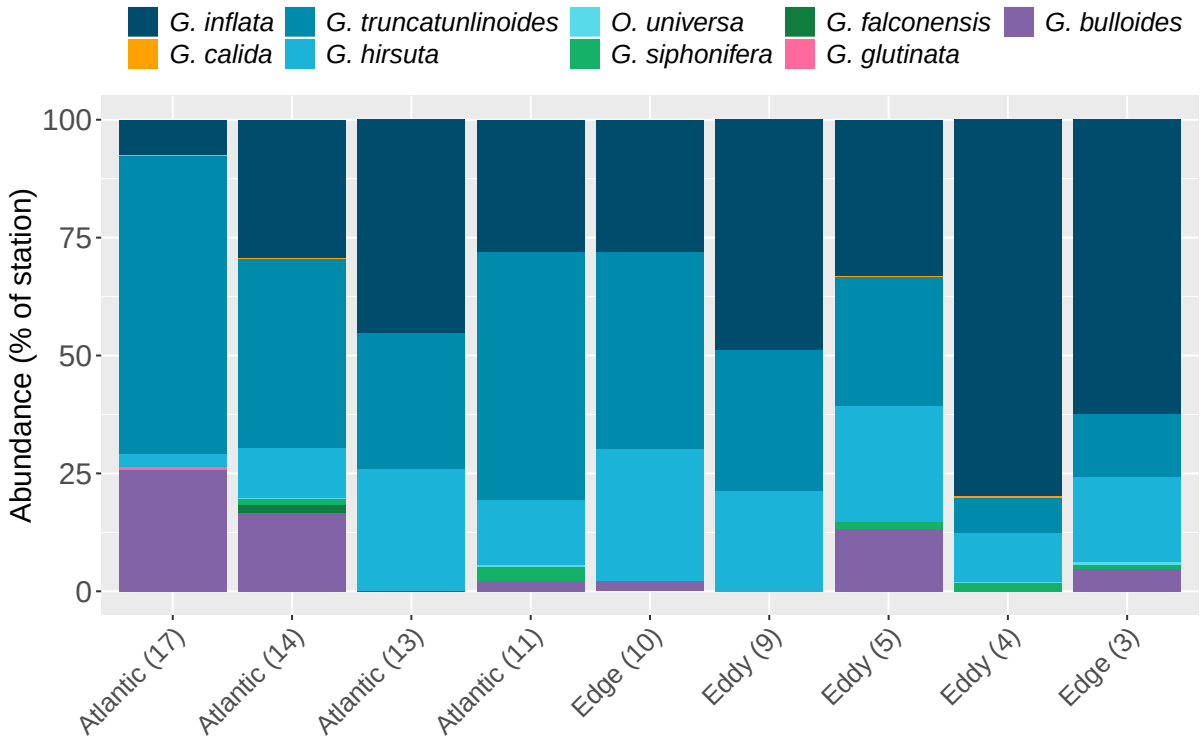

Figure 2.6: Relative abundance of different species of foraminifera from each net tow across the transect. Numbers in brackets indicate station numbers. Leading edge (10) is assigned to the Atlantic group while Trailing edge (3) is grouped with the eddy stations (see text for details).

was lower (3 to 28%; lowest in the Atlantic and highest at the leading edge of E1) and did not show a relationship with either *G. inflata* or *G. truncatulinoides* abundances. Most other species (*O. universa, Globigerinella calida, Globigerinella siphonifera*, and *G. bulloides*) were present in low numbers at several stations across the transect. *G. falconensis* was only present at two Atlantic stations (13 and 14), as was *G. glutinata* (stations 14 and 17).

G. truncatulinoides and *G. hirsuta* were the two largest species sampled across the transect (longest dimensions averaging $614 \pm 138\,\mu$m and $614 \pm 113\,\mu$m, respectively), followed by *G. inflata* ($507 \pm 78\,\mu$m). On average, all three of these species were larger at the Atlantic stations than in E1, although the differences were not statistically significant. The opposite trend was observed for the euphotic-dwelling *G. bulloides* and *O. universa*, which were on average slightly larger in E1 than in the Atlantic, although specimen numbers were too low to establish significance.

2.3.3.2 Foraminifer tissue nitrogen isotopes (FT-δ^{15}N)

For the eddy group, the overall FT-δ^{15}N (i.e., combining data from all species) ranged from 1.7 ‰ to 6.1 ‰, with a mean of 4.4 ± 1.2 ‰ (n=45; all sampled specimens) (Fig. 2.7a). FT-δ^{15}N was significantly higher ($p < 0.01$) at the Atlantic stations (range of 5.7 ‰ to 8.0 ‰, with a mean of 6.8 ± 0.6 ‰ (n=63)), and less variable (ranges of 2.3 ‰ in the

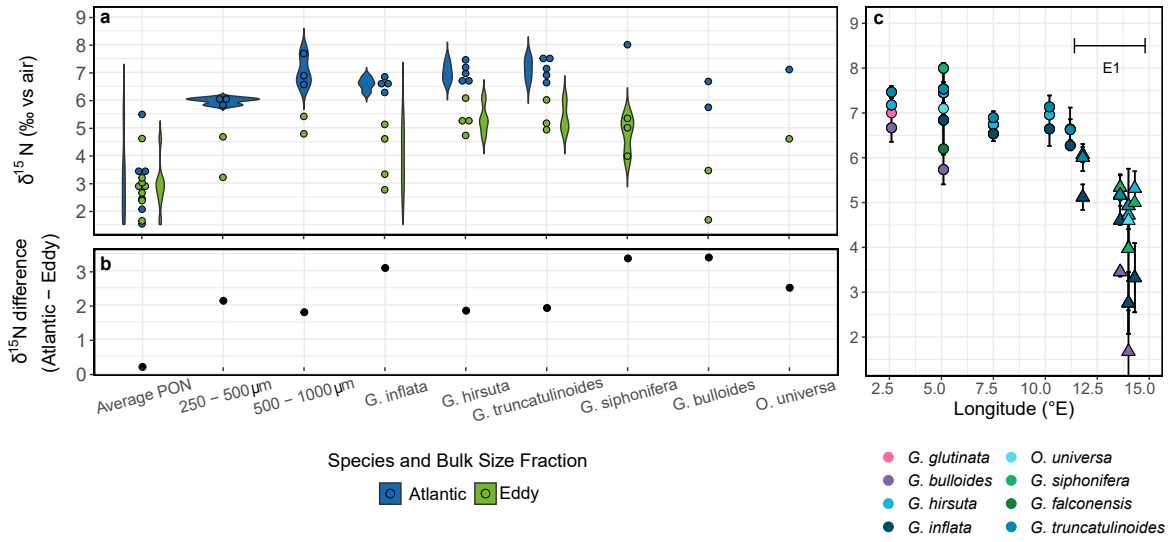

Figure 2.7: a) Violin plot showing the average, concentration-weighted δ^{15}N for mixed-layer PON, bulk zooplankton (250-500 μm and 500-1000 μm size classes), and foraminifer tissue (i.e., FT-δ^{15}N) for six species collected in the $0 \rightarrow 200$ m net tows in 2017. Circles represent the average FT-δ^{15}N measured in triplicate for each species at a single station, with the blue circles indicating Atlantic stations and the green circles showing the data from Agulhas eddy E1. The shapes behind or alongside the circles show the spread of the data; b) Average species-specific FT-δ^{15}N for each station sampled along the transect, with circles and triangles representing Atlantic and eddy stations, respectively. Error bars show standard deviation.

Atlantic *versus* 4.4 ‰ in the eddy). The same trends hold within most species (i.e., lower FT-δ^{15}N in the eddy than in the Atlantic samples; Fig. 2.7b). The mean FT-δ^{15}N of the highly abundant *G. inflata* was 6.7 ± 0.5 ‰ (n=14) and 3.6 ± 1.0 ‰ (n=12) in the Atlantic and eddy groups, respectively, while the less abundant *G. bulloides* had a mean FT-δ^{15}N of 6.3 ± 0.6 ‰ (n=4) at the Atlantic stations and 2.9 ± 0.9 ‰ (n=4) in the eddy. Where abundant enough to measure, G. siphonifera had a higher δ^{15}N in both the Atlantic and eddy samples relative to the other species (8.0 ± 0.1 ‰ (n = 3 samples from 1 station) and 4.6 ± 0.8 ‰ (n=7 samples from 3 stations), respectively). Additionally, *G. hirsuta* and *G. truncatulinoides* were consistently higher in δ^{15}N than the other species at all stations, with an average eddy FT-δ^{15}N of 5.3 ± 0.5 ‰ (n = 12) and 5.4 ± 0.7 ‰ (n = 9) and Atlantic FT-δ^{15}N of 7.1 ± 0.4 ‰ (n = 19) and 7.3 ± 0.5 ‰ (n = 19), respectively. Standard deviations reported here reflect variability between sampled specimens (typically from multiple stations), rather than measurement replication.

2.3.3.3 Foraminifer shell-bound nitrogen isotopes

Shell-bound δ^{15}N correlated well with FT-δ^{15}N for all species (r2 = 0.8, Fig. 2.8a) and was on average 1.3 ± 0.8 ‰ higher than FT-δ^{15}N for the same species at a given station. Shell measurements for the three species present at both the eddy and Atlantic stations (*G. truncatulinoides, G. hirsuta*, and *G. inflata*) yielded an average δ^{15}N of 6.3 ± 1.4 ‰ (n

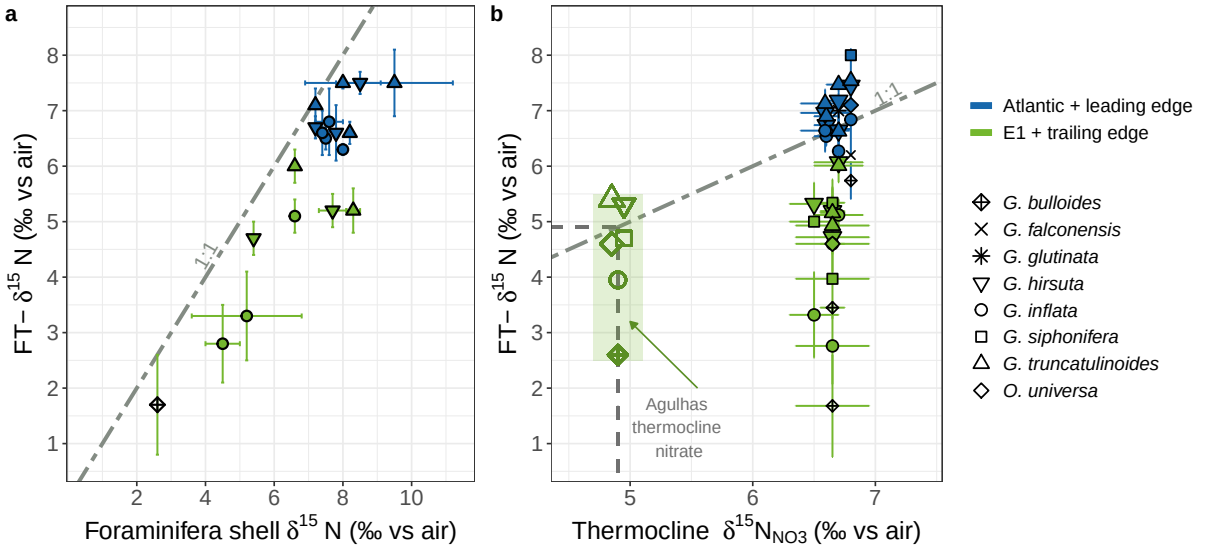

Figure 2.8: a) Cross-plot of FT-δ^{15}N *versus* foraminifera shell-bound δ^{15}N from the same net tows. Error bars indicate ± 1 standard deviation of repeat (duplicate or triplicate) oxidations + measurements of a single species at a particular station; b) Comparison of FT-δ^{15}N and thermocline $\delta^{15}N_{NO_3}$ (represented by the $\delta^{15}N_{NO_3}$ measurement from just below the mixed layer) across the transect. Blue shapes show nitrate and foraminifer measurements from the Atlantic stations and the leading edge of Agulhas eddy E1 while green shapes show data from within E1 and include the trailing edge station (see text for details). Error bars show ±1 standard deviation of triplicate measurements of the same foraminifer species at each station (y-axis) and duplicate nitrate isotope measurements from the same station and depth (x-axis). Shapes in the shaded green box indicate where the average eddy FT-δ^{15}N for each foraminifer species would be positioned if plotted *versus* the mean Agulhas thermocline $\delta^{15}N_{NO_3}$ (4.9 ‰). The dashed grey line in both figures indicates a slope of 1:1.

= 7) and 7.9 ± 0.7 ‰ (n = 11), respectively (i.e., an eddy-Atlantic difference of 1.3 ‰). The spread in the shell-bound δ^{15}N data was also greater for the eddy (2.4 ‰) than the Atlantic samples (1.3 ‰). Similar to FT-δ^{15}N, there was a larger difference between Atlantic and eddy shell samples for *G. inflata* than for *G. hirsuta* or *G. truncatulinoides* (the difference between Atlantic and eddy shell-bound δ^{15}N was 1.5 ‰ greater for *G. inflata* than for the latter two species; in the case of FT-δ^{15}N, the difference was 1.0 ‰).

2.3.3.4 Bulk zooplankton and particulate organic N

The δ^{15}N of the bulk zooplankton increased with increasing size-fraction, from a mean (for the combined eddy and Atlantic stations) of 5.8 ± 0.6 ‰ for the 250-500 μm size-class to 6.7 ± 1.2 ‰ for the 500-1000 μm size-class (Fig. 2.7a). Both the zooplankton size classes (chosen due to their containing the majority of the foraminifera and their larger prey) from the Atlantic stations had a higher δ^{15}N than their eddy counterparts. The 250-500 μm and 500-1000 μm fractions had a mean δ^{15}N of 6.0 ± 0.1 ‰ (n=3) and 7.2 ± 0.6 ‰ (n=3), respectively, at the Atlantic stations *versus* 3.9 ± 1.0 ‰ (n = 2) and 5.1 ± 0.4 ‰ (n=2) in the eddy. This equates to an Atlantic-to-eddy decline of 1.9 ‰ and 2.0 ‰ for the 250-500 μm and 500-1000 μm size classes, respectively, which is similar to the trend observed for the foraminifera.

We observed no difference in upper-ocean (0-100 m) PON concentrations between the

eddy and Atlantic stations ($0.3 \pm 0.04\,\mu$M (n = 7) and $0.3 \pm 0.4\,\mu$M (n = 6), respectively; Fig. 2.7). Similarly, there was no significant difference in the mean PON-δ^{15}N between the two groups ($2.8 \pm 1.6\,‰$ (n = 6) for the Atlantic and $2.5 \pm 0.7\,‰$ (n=7) for the eddy), although the Atlantic group exhibited larger within-group variability. Both the lowest mixed-layer average PON-δ^{15}N ($1.2 \pm 0.8\,‰$) and the highest ($5.5 \pm 0.9\,‰$) were measured at Atlantic stations.

2.3.3.5 Foraminifer tissue δ^{15}N *versus* seawater nitrate δ^{15}N

Because we have considerably more measurements (and replicate samples) of FT-δ^{15}N than of shell-bound δ^{15}N, we focus our comparison with $\delta^{15}N_{NO_3}$ on the FT-δ^{15}N data. We nonetheless expect the trends to hold for the shell data given their strong correlation with FT-δ^{15}N (Fig. 8a; Smart et al., 2018, 2020). Of all the species measured, *G. truncatulinoides*, *G. hirsuta*, and *G. inflata* were most similar in δ^{15}N to thermocline nitrate at the Atlantic stations (with the mean $\delta^{15}N_{NO_3}$ of SASTMW, the water mass just below the mixed layer, taken to represent thermocline nitrate). The combined average FT-δ^{15}N for *G. truncatulinoides* and *G. hirsuta* was $7.2 \pm 0.4\,‰$, compared to $6.9 \pm 0.4\,‰$ (or $7.0 \pm 0.3\,‰$ when comparing only the year from which net tows were collected, i.e. 2017) for thermocline nitrate (Fig. 2.8b).

The similarity of FT-δ^{15}N to $\delta^{15}N_{NO_3}$ did not extend to E1 where *G. truncatulinoides* and *G. hirsuta* had a combined FT-δ^{15}N that was on average $1.5\,‰$ lower than the local thermocline $\delta^{15}N_{NO_3}$ (mean FT-δ^{15}N = $5.3 \pm 0.6\,‰$ *versus* $6.8 \pm 0.6\,‰$ for eddy thermocline nitrate; Fig. 2.8b). Across all the eddy stations, *G. bulloides* and *G. inflata* showed the largest deviations in δ^{15}N from thermocline nitrate, with the minimum FT-δ^{15}N (as for all species) observed at station 4 in the centre of E1, resulting in a thermocline-to-FT-δ^{15}N difference of $5.0\,‰$ and $3.9\,‰$ for *G. bulloides* and *G. inflata*, respectively, at this station. Comparing the mean FT-δ^{15}N for eddy foraminifer species with the average $\delta^{15}N_{NO_3}$ of the Agulhas thermocline ($4.9\,‰$; Marshall et al. (2023), noting that Fig. 2.4b shows a representative offshore profile rather than the thermocline average shown by the green shading in Fig. 2.8b) reveals a strong similarity for *G. truncatulinoides* (mean eddy FT-δ^{15}N = $5.4 \pm 0.7\,‰$), *G. hirsuta* ($5.3 \pm 0.5\,‰$), *G. siphonifera* ($5.3 \pm 0.3\,‰$), and *O. universa* ($4.6 \pm$ NA ‰), while the remaining foraminifera were lower in FT-δ^{15}N than Agulhas thermocline nitrate ($3.6 \pm 1.0\,‰$ and $2.9 \pm 0.9\,‰$ for *G. inflata* and *G. bulloides*, respectively).

2.4 Discussion

2.4.1 Absence of Agulhas planktic foraminifer assemblages in the Cape Basin

No robust differences were observed in the foraminifer assemblage inside and outside Agulhas eddy E1. The known temperate winter species, *G. truncatulinoides* and *G. hirsuta*, dominated across the transect, while the more adaptable transitional species, *G. inflata*, appeared to favour the turbulence created by winter mixing and eddy vorticity (i.e., *G. inflata* increased in relative abundance at the trailing edge of E1; Deuser et al. 1981; Chapman 2010. This similarity in foraminifer community composition indicates that diagnosing Agulhas leakage through an abundance-based index is not always possible, particularly once Agulhas eddies have migrated some distance from the Retroflection region. Similar foraminifer species homogeneity has been observed for a mature (i.e., > 7 month old; Schouten et al. 2000; Froyland et al. 2015) Agulhas ring and its Cape Basin surrounds during late summer, with (sub)tropical/warm-water species *T. sacculifer* and *G. ruber* (both considered Agulhas Leakage fauna) dominating inside and outside the eddy (Lončarić, 2006).

Seasonality is likely the primary determinant of the "background" foraminifer assemblage of the Cape Basin (Van Aken et al., 2003; Peeters et al., 2004), as is the case for other ocean regions (Boltovskoy, 1994; Eguchi et al., 2003; Jonkers and Kučera, 2017). Recently-shed eddies can disrupt this scenario, however, as the upper-ocean temperatures of young Agulhas rings and eddies are warmer than in the Cape Basin, creating a temporary niche for (sub)tropical foraminifer species in the southeast Atlantic. Eddies located near the Retroflection tend to be relatively young (< 5 months) and in a stage of active decay characterized by large SST and SSH anomalies (Schouten et al., 2000). However, intense heat loss and advective mixing rapidly cool eddy surface waters, particularly as they near the South Atlantic subtropical gyre (Duncombe Rae, 1991; Goni et al., 1997; De Ruijter et al., 1999; Van Aken et al., 2003). The mean annual SST at 28°E in the Agulhas Current is $\sim$23°C (Garcia et al., 2019); further west and closer to the Retroflection at 18.5°E, this decreases to $\sim$19°C (Locarini et al., 2013). By the time E1 reached our transect position (7 to 8 months after shedding), its maximum SST had dropped to 16°C. Although within the temperature range determined under laboratory conditions to be acceptable to (sub)tropical foraminifer species (e.g., *T. sacculifer*, *G. ruber, N. dutertrei*; Bijma et al. 1990), the eddy SST was nonetheless below that considered optimal for these species to reproduce (i.e., above 20°C for all three species; Hecht 1976; Waterson et al. 2017). In the summer, however, SSTs in the Cape Basin rise above 20°C (Lea et al., 2018), adequate to at least temporarily sustain (sub)tropical populations imported by Agulhas rings (Peeters et al., 2004; Lončarić, 2006).

Among the (more temperate) foraminifer species present in E1, the variations in relative abundance might reflect their preferences for different hydrographic conditions (Feld-

meijer et al., 2015). The high percentage of *G. inflata* within and at the trailing edge of E1 relative to the Atlantic stations (Fig. 2.6) is consistent with previous assertions that this species is more tolerant of vertical mixing, cool waters, and rapidly changing conditions (Schiebel and Hemleben, 2017; Kretschmer et al., 2018). In contrast, *G. truncatulinoides* appears better adapted to less turbulent conditions as this species was most abundant at the stations near the more stable South Atlantic subtropical gyre. However, *G. truncatulinoides* is known to spend most of its life below the thermocline, ascending only during late winter/early spring for reproduction (Schiebel and Hemleben, 2005); it is possible that the deep eddy mixed layers displaced this species beneath the reach of our nets (towed over the upper 200 m).

2.4.2 Potential mechanisms for δ^{15}N differences in the southeast Atlantic and Agulhas eddies

2.4.2.1 Relative consumption of nitrate

As the dominant form of fixed N in the ocean, nitrate sets the baseline for the N isotope distributions in an ecosystem. The lower $\delta^{15}N_{NO_3}$ (and (Δ15-18)) evident in the mixed layer at the eddy stations relative to the background South Atlantic (8.2 ± 0.7 ‰ *versus* 10.2 ± 1.3 ‰ for $\delta^{15}N_{NO_3}$; Fig. 2.4b) suggests that the controls on the nitrate isotope distributions in eddy waters are distinct, and that eddies may receive a low-$\delta^{15}N_{NO_3}$ source that does not influence the mixed-layer of the surrounding Atlantic. Since the potential for isotopic alteration due to nitrite was eliminated by its removal prior to our measurement of the nitrate isotopes (Granger and Sigman, 2009), any differences in $\delta^{15}N_{NO_3}$ and $\delta^{18}O_{NO_3}$ between the eddy and background Atlantic must be due to processes that influence the nitrate pool. We examine these in detail below.

One mechanism that can cause mixed-layer $\delta^{15}N_{NO_3}$ to vary is the extent to which vertically-supplied nitrate is taken up by phytoplankton. Phytoplankton preferentially consume 14N-bearing nitrate, such that the $\delta^{15}N_{NO_3}$ of the residual nitrate pool rises as its concentration declines (Minagawa and Wada, 1986; Sigman et al., 1999). Thus, the more completely a particular supply of nitrate is consumed, the higher its $\delta^{15}N_{NO_3}$, and vice versa. It is therefore possible that the lower $\delta^{15}N_{NO_3}$ measured in the eddy mixed layer relative to that in the background Atlantic was due to less complete consumption of the same nitrate supply.

To a first approximation, the available nitrate concentration data appear consistent with this idea. An east-west gradient is apparent in both the 2015 and 2017 nitrate measurements, with surface nitrate concentrations declining near-linearly from the nearshore stations ($\sim 3\,\mu$M) to the most offshore station 19 ($0.8\,\mu$M at 0°E) (Fig. S.1). In 2017, E1 was located at the eastern edge of the transect and its mixed layer was characterized by higher nitrate concentrations than the background stations to the west (by $\sim 0.4\,\mu$M). One might thus conclude that the mixed-layer $\delta^{15}N_{NO_3}$ (and by extension the FT-δ^{15}N)

difference between the eddy and Atlantic stations can be explained by a lower degree of nitrate consumption to the east (eddy) *versus* the west (Atlantic) of the transect.

There are a number of reasons why this explanation is unlikely, however. First, our sampling occurred near the beginning of the nitrate resupply period (Fig. 2.3), such that the mixed layer nitrate concentration and $\delta^{15}N_{NO_3}$ should mainly reflect ongoing mixing of thermocline nitrate with a volume of nitrate-depleted surface water leftover from the previous growing season (i.e., late-summer/autumn). By contrast, because the lifetime of zooplankton and foraminifera is on the order of months (Montoya et al., 2002; Schiebel and Hemleben, 2005; Loick-Wilde et al., 2016), their biomass $\delta^{15}N$ will largely reflect the N consumed over the previous growing season, prior to the onset of nitrate resupply.

Second, the CMEMS concentration data indicate that the amount of nitrate supplied to the mixed layer is not the same across the transect (Fig. 2.3). Instead, the seasonal nitrate supply is higher nearer the coast, decreasing offshore (i.e., the maximum surface nitrate concentration, indicative of the nitrate available to phytoplankton at the beginning of the growing season (in September/October), averages 3.6 μM at 13°E *versus* 1.2 μM at 0.25°). Thus, even if our July nitrate concentrations do predominantly reflect consumption (rather than mixing), the fraction of the nitrate supply consumed (i.e., $[NO_3^-]_{(July,\ surface)}/[NO_3^-]_{(Sept/Oct,\ supply)}$) would be similar across the transect (64-67% remaining), rather than higher to the east than the west as would be required to explain the $\delta^{15}N_{NO_3}$ data by differential nitrate consumption.

Third, in the 2015 dataset, Agulhas eddies were encountered further west along the transect and their mixed-layer nitrate was on average 0.7 μM lower than in the Atlantic mixed layer. While this pattern is consistent with the zonal trend in nitrate concentration observed in 2017 (and in the CMEMS product), it would have resulted in a higher $\delta^{15}N_{NO_3}$ in the eddy- than the Atlantic mixed layers if driven by nitrate consumption, which is not what we observe. Instead, eddy mixed-layer $\delta^{15}N_{NO_3}$ in 2015 was 2.3 ‰ lower than the average Atlantic mixed-layer $\delta^{15}N_{NO_3}$, consistent with the eddy-Atlantic difference observed in 2017.

Finally, if the difference in the $\delta^{15}N_{NO_3}$ in the eddy *versus* the background Atlantic were due to nitrate consumption, the $\delta^{18}O_{NO_3}$ should be similarly variable since $\delta^{15}N_{NO_3}$ and $\delta^{18}O_{NO_3}$ increase proportionally during nitrate assimilation (Granger et al., 2004, 2010; Rohde et al., 2015). However, we observe a much smaller (statistically insignificant; $p = 0.2$) difference in the mean $\delta^{18}O_{NO_3}$ in the mixed layer of the eddy *versus* the background Atlantic (6.1 ± 1.3 ‰ *versus* 6.6 ± 2.1 ‰, Fig. S.2). Below the depth of winter mixing ($\sim$300 m), nitrate Δ(15-18) averages 3.2 ± 0.2 ‰ for all stations across the transect, consistent with previous observations for SAMW in the South Atlantic (Tuerena et al., 2015; Marconi et al., 2019; Flynn et al., 2020). At the background Atlantic stations, mixed-layer nitrate Δ(15-18) was 3.0 ± 1.4 ‰, indistinguishable from the subsurface nitrate and indicating that the seasonal supply and consumption of subsurface nitrate is the main driver of the nitrate isotope distributions at these stations (Granger et al., 2004;

Rafter et al., 2013). By contrast, nitrate Δ(15-18) in the eddies was low throughout the mixed layer (average of 1.8 ± 1.2 ‰ for the mixed layer and even lower for the upper 100 m, Δ(15-18) of 1.6 ± 1.7 ‰). Moreover, eddy nitrate Δ(15-18) was similar to the mean Δ(15-18) observed in the Agulhas Current thermocline and mixed layer (2.1 ‰ and 1.3 ‰, respectively; Fig. 5; (Marshall et al., 2023)). We thus conclude that a mechanism other than differential nitrate consumption is required to explain the lower $\delta^{15}N_{NO_3}$ and Δ(15-18) of nitrate in Agulhas eddies *versus* the background Atlantic.

2.4.2.2 Low thermocline nitrate δ^{15}N

N_2 fixation introduces organic N to the mixed layer that is low in δ^{15}N, −2 ‰ to 0 ‰ (Hoering and Ford, 1960; Minagawa and Wada, 1986). The subsequent sinking and remineralization (i.e., ammonification plus nitrification) of this organic N yields subsurface nitrate that is similarly low in δ^{15}N (Knapp et al. 2005, 2008; Marshall et al. 2023). By contrast, the δ^{18}O of newly nitrified nitrate is relatively high, as it is set by the δ^{18}O of seawater (∼0 ‰) plus an isotopic offset of ∼1.1 ‰ (Sigman et al., 2009; Boshers et al., 2019; Buchwald and Casciotti, 2013). As such, N_2 fixation causes both the $\delta^{15}N_{NO_3}$ and the Δ(15-18) of nitrate to decline (Sigman et al., 2009; Rafter et al., 2013). Data from the Agulhas Current (Fig. 4; Marshall et al. 2023) and the waters of the southern Indian Ocean (Harms et al., 2019) that ultimately feed the Agulhas Current reveal a low $\delta^{15}N_{NO_3}$ and Δ(15-18) throughout the thermocline (4.9 ‰ and 2.4 ‰, respectively) and low Δ(15-18) in the surface waters (1.3 ‰). The similarity of the eddy and Agulhas Current Δ(15-18) values strongly suggests that Agulhas leakage transports recently fixed nitrate from the South Indian Ocean into the Cape Basin, with potential vorticity and kinematic steering associated with the circulation of migrating eddies (Chelton et al., 2011; Condie and Condie, 2016) maintaining the isotopic distinction between the eddy and the surrounding south Atlantic.

Thermocline $\delta^{15}N_{NO_3}$ is robustly low across the Agulhas Current System (as exemplified by the black profile in Fig. 2.4b; Harms et al. 2019; Marshall et al. 2023) yet within the Agulhas eddies, subsurface $\delta^{15}N_{NO_3}$ is generally more similar to the $\delta^{15}N_{NO_3}$ of the South Atlantic thermocline. The absence of low-$\delta^{15}N_{NO_3}$ in the eddy thermocline can be attributed to the deep convective mixing typical of Agulhas eddies (Dufois et al., 2016; Olson et al., 1992; Schmitt and Olson, 1985), which likely entrains both mixed-layer and upper thermocline Agulhas Current nitrate into the eddy mixed layer (noting too, that Agulhas Current mixed-layer and thermocline waters are less dense than mixed-layer waters in the Cape Basin; 24.0-26.4 $kg.m^{-3}$ *versus* 26.0-26.2 $kg.m^{-3}$). Consumption of this nitrate by phytoplankton will rapidly raise its $\delta^{15}N_{NO_3}$ (and $\delta^{18}O_{NO_3}$), overprinting the low $\delta^{15}N_{NO_3}$ but not the low Δ(15-18) characteristic of the Agulhas Current thermocline (Sigman et al., 2009).

The low nitrate Δ(15-18) in the eddies may also be influenced by coupled partial nitrate assimilation and nitrification. If nitrate assimilation and nitrification co-occur

(e.g., at the base of the mixed layer; Fawcett et al. 2015; Marshall et al. 2023), the cycling between organic N and nitrate yields no net change in the $\delta^{15}N_{NO_3}$ of the combined (i.e., partially assimilated plus newly-nitrified) nitrate pool, provided N is neither lost nor gained (Rafter et al., 2013; Sigman et al., 2005, 2009). By contrast, assimilation is a sink for the O atoms in nitrate while nitrification is a source, with the $\delta^{18}O_{NO_3}$ reset by nitrification to the $\delta^{18}O$ of seawater plus an isotopic offset of $\sim$1.1 ‰ (Sigman et al., 2009; Buchwald and Casciotti, 2013; Boshers et al., 2019). The $\delta^{18}O_{NO_3}$ of newly nitrified nitrate thus ends up higher than the $\delta^{18}O_{NO_3}$ that was initially assimilated. As such, coupled partial nitrate assimilation and nitrification causes the $\delta^{18}O_{NO_3}$ of the combined nitrate pool to rise, which, along with no change in $\delta^{15}N_{NO_3}$ drives a decline in the Δ(15-18) of nitrate (Sigman et al., 2005; Wankel et al., 2007; Sigman et al., 2009; Rafter et al., 2013; Fawcett et al., 2015; Deman et al., 2021; Marshall et al., 2023). Nitrification of partially assimilated N at the base of the mixed layer could occur prior to and/or following eddy spawning, making the low-Δ(15-18) either a transported or an in situ signal, or both. Indeed, it has been suggested that some portion of the low-Δ(15-18) nitrate in the mixed layer and upper thermocline of the Agulhas Current derives from coupled partial nitrate assimilation and nitrification (Marshall et al., 2023). This signal is then transported (and possibly augmented) in Agulhas leakage. Coupled partial nitrate assimilation and nitrification cannot account for the entire lowering of the nitrate Δ(15-18), however, either in the Agulhas Current or in the eddy, as this mechanism does not lower $\delta^{15}N_{NO_3}$. Thus, there must be a role for N_2 fixation in driving the nitrate isotope distributions observed in Agulhas leakage.

2.4.2.3 *In-situ* drivers of eddy δ^{15}N variation

A final consideration is that that the $\delta^{15}N$ of PON and foraminifera within Agulhas eddies may decline during their migration into the South Atlantic (i.e., after spawning) in response to processes that further lower the $\delta^{15}N_{NO_3}$ and Δ(15-18) of eddy nitrate. Anticyclonic eddies in other subtropical and mid-latitude regions have been observed to host elevated rates of N_2 fixation (Holl et al., 2007; Fong et al., 2008; Löscher et al., 2016; Liu et al., 2020); similar conditions in the Cape Basin in summer and autumn (i.e., N-limited surface waters, a stoichiometric phosphorus excess relative to N, and surface temperatures $>$ 20°C) may be conducive to this process, provided the iron supply is sufficient (Deutsch et al., 2007; Marshall et al., 2023)). There is little evidence of N_2 fixation in the (sub)tropical South Atlantic, which has been attributed to iron limitation of diazotrophic plankton (Moore et al., 2009; Luo et al., 2012; Browning et al., 2017), but Agulhas eddies may host higher trace metal concentrations than the surrounding Atlantic because they include a significant contribution of southwest Indian Ocean coastal waters (Paul et al., 2015; Conway et al., 2016). However, that the $\delta^{15}N_{NO_3}$ and Δ(15-18) of nitrate in the eddy mixed-layer and thermocline is higher than in the Agulhas Current suggests that if N_2 fixation does occur in Agulhas eddies, its influence is minor compared

to the effect of horizontal and vertical mixing between the eddy and its surroundings, which may have been significant for E1 given its age (7 to 8 months) (Schouten et al., 2000). However, calculating the exact degree of mixing between E1 and its surroundings is beyond the scope of this study, given the difficulty in constraining variables in this region (e.g., identifying a completely leakage-free $\delta^{15}N_{NO_3}$ end-member in the southeast Atlantic is difficult to extract) using wintertime nitrate measurements from a single cruise.

Another *in-situ* mechanism that could act to lower foraminifer $\delta^{15}N$ is the recycling of low-$\delta^{15}N$ ammonium within the eddy. Recycled ammonium produced via zooplankton excretion and bacterial decomposition of organic matter has a lower $\delta^{15}N$ (by $\sim$5 ‰) than nitrate (Checkley and Miller, 1989; Mobius, 2013); when assimilated by phytoplankton, this ammonium will decrease the $\delta^{15}N$ of PON (Fawcett et al., 2011, 2014; Treibergs et al., 2014) and subsequently, the $\delta^{15}N$ of foraminifera (Smart et al., 2020). Enhanced reliance on regenerated N in anticyclonic eddies has previously been suggested to occur as a consequence of light limitation of phytoplankton induced by the characteristically deep mixed layers (Dortch, 1990; Siegel et al., 1995). Indeed, Wallschuss et al. (2022) measured nitrification rates in the mixed layer of E1 that were an order of magnitude higher than in the surrounding Atlantic. This finding indicates that (1) the deep eddy mixed layer environment was conducive to intense N recycling, and (2) the in-eddy phytoplankton were light-limited (a requirement for nitrifiers to outcompete phytoplankton), such that they would have been consuming regenerated N rather than nitrate, the latter being far more energetically expensive to assimilate than ammonium (Dortch, 1990). It is thus likely that ammonium recycling during eddy transit contributed to the low $\delta^{15}N$ of the foraminifera in E1.

Regardless of whether N_2 fixation or ammonium recycling were active during eddy transit, our nitrate isotope data strongly suggest that the $\delta^{15}N_{NO_3}$ and Δ(15-18) of mixed-layer nitrate in Agulhas leakage is strongly influenced by processes occurring in the Agulhas Current and its source waters, and as such, is distinct from that of the surrounding Cape Basin. While the low $\delta^{15}N_{NO_3}$ is rapidly eroded by isotopic fractionation associated with nitrate assimilation during eddy migration, it nonetheless influences the isotopic composition of other eddy N pools. Moreover, the low nitrate Δ(15-18) is retained, making this parameter a robust tracer of Agulhas leakage.

2.4.3 Controls on FT-$\delta^{15}N$

All the foraminifer species in E1 show a significantly lower FT-$\delta^{15}N$ than the Atlantic foraminifera (4.4 ± 1.2 ‰ *versus* 6.8 ± 0.6 ‰; Figs. 7 and 8). We observe the same trend for the foraminifer shells (6.3 ± 1.4 ‰ *versus* 7.9 ± 0.7 ‰), as well as for tissue and shell-bound N within individual species, suggesting that the eddy community was supported by a comparatively low-$\delta^{15}N$ diet. The similar Atlantic-to-eddy $\delta^{15}N$ decrease observed for bulk zooplankton within the size range of foraminifera (from 7.2 ± 0.6 ‰ to 5.1 ± 0.4 ‰) supports this notion. The nitrate supplied to the winter mixed layer of the South Atlantic

Table 2.1: Mean FT-δ^{15}N of the various foraminifer species measured in this study with their average living depth (*ALD, estimated from Peeters and Brummer 2002; Sousa et al. 2014; Rebotim et al. 2017; Schiebel and Hemleben 2017; Meilland et al. 2018, 2019; Lessa et al. 2020). ** *G. truncatulinoides* experiences large seasonal vertical displacement and can at times be found at depths > 600 m.

Species	Atlantic δ^{15}N (‰)	Eddy δ^{15}N (‰)	Estimate of ALD* (m)	Symbionts?
G. bulloides	6.3 ± 0.6	2.9 ± 0.9	0 - 100	No (unknown)
G. falconensis	6.2 ± 0.0	-	50 - 100	Facultative (unknown)
G. glutinata	7.0 ± *NA*	-	0 - 80	Facultative (chrysophytes)
G. hirsuta	7.1 ± 0.4	5.3 ± 0.5	100 - 200	No
G. inflata	6.7 ±0.5	3.6 ± 1.0	80 - 100	Facultative (chrysophytes)
G. siphonifera	8.0 ± 0.1	5.3 ± 0.3	80 - 100	Facultative (chrysophytes)
G. truncatulinoides	7.3 ± 0.5	5.4 ± 0.7	80 - 200 **	No
O. universa	7.1 ± *NA*	4.6 ± *NA*	70 - 100	Obligate (dinoflagellates)

was completely consumed by phytoplankton during the 2016-2017 spring/summer growing season preceding our sampling (Fig. 2.3). This nitrate consumption would have yielded mixed-layer PON that was similar in δ^{15}N to the subsurface nitrate supply (under ideal conditions where the δ^{15}N of the product tends to equal that of the original nitrate; Mariotti et al. 1981). In the eddy, therefore, the PON produced from the consumption of Agulhas nitrate would have been relatively low in δ^{15}N ($\sim$4.9 ‰) compared to PON in the waters outside that eddy that was fuelled by SASTMW ($\sim$6.9 ‰). Given that all foraminifera and zooplankton consume particulate N (be it phytoplankton, zooplankton, detritus or the microbial inhabitants thereof; Bé and Hutson 1977; Spindler et al. 1984; Uhle et al. 1997; Bird et al. 2020), those inhabiting the eddy would have incorporated the low δ^{15}N of Agulhas nitrate into their biomass. The lower FT-δ^{15}N (and shell-bound δ^{15}N) of foraminifera in the eddy *versus* the background Atlantic is thus consistent with the eddy fauna retaining the δ^{15}N of Agulhas thermocline nitrate while foraminifera in background Atlantic waters record the higher δ^{15}N of SASTMW. We note, however, that the measured δ^{15}N of mixed-layer PON at the time of sampling was not different between the eddy and Atlantic, which we largely ascribe to the shorter integration time for the suspended PON pool (mainly composed of phytoplankton) relative to zooplankton in general and foraminifera in particular (Altabet and McCarthy, 1985; Eppley et al., 1983; Fasham et al., 1990; Capone et al., 2008). This isotopic discrepancy is addressed in detail in section 2.4.3.1 below.

2.4.3.1 Interspecies relationships

The interspecies FT-δ^{15}N relationships are broadly consistent across the eddy and Atlantic stations and largely in agreement with previous observations (Ren et al., 2009, 2012; Li et al., 2019; Smart et al., 2018, 2020). Higher FT-δ^{15}N is associated with deep-dwelling non-spinose species (*G. truncatulinoides* and *G. hirsuta*, typically inhabiting

depths > 100 m, Table 2.1), the FT-δ^{15}N of *G. inflata* (a mid- to shallow-depth dwelling non-spinose species) is slightly lower (by 1 ‰ on average), and the FT-δ^{15}N observed for *G. bulloides* and *G. falconensis* (spinose shallow dwellers) is the lowest (on average 1.9 ‰ lower than the FT-δ^{15}N of *G. truncatulinoides*). This pattern closely resembles that seen in the Southern Ocean (where the FT-δ^{15}N of *G. truncatulinoides*/*G. hirsuta* > *G. inflata* > *G. bulloides*; Smart et al. 2020). Differences in FT-δ^{15}N among species are likely a reflection of both diet and species-specific metabolic processes. For example, *G. truncatulinoides* and *G. hirsuta* are thought to predominantly graze on sinking PON (Bé and Hutson, 1977; Sen Gupta, 2003), the δ^{15}N of which increases with depth as ^{14}N-bearing PON is preferentially decomposed by heterotrophic bacteria (Altabet, 1988; Mobius, 2013).

Interestingly, *G. siphonifera* had a FT-δ^{15}N that was similar to the deep-dwellers, despite its hosting symbionts (Gastrich, 1987; Faber et al., 1988), which might be expected to lower its FT-δ^{15}N (Ren et al., 2012). This observation is consistent with tissue and shell measurements from the Sargasso Sea, where *G. siphonifera* was observed to be as high or higher in FT-δ^{15}N than the deep-dwelling foraminifera (Smart et al., 2018). There, it was posited that the chrysophyte symbionts associated with *G. siphonifera* (a species that may dwell at sub-euphotic depths where light intensity is low; Rebotim et al. 2017; Meilland et al. 2019) might be less active in N cycling than the dinoflagellate symbionts present in *O. universa*, rendering *G. siphonifera* more reliant upon predation and leading to its higher trophic level. Higher-δ^{15}N food sources available at its slightly deeper dwelling depth may also contribute to *G. siphonifera*'s elevated δ^{15}N (Li et al., 2019). The largest discrepancy from previous work that we observe is for *O. universa* in the eddy (station 4; one of only two stations with sufficient *O. universa* specimens to measure FT-δ^{15}N). The dinoflagellate-bearing *O. universa* has been observed to be lower in δ^{15}N than non-symbiont-hosting species, explained by partial retention of low-δ^{15}N ammonium normally excreted by foraminifera (Uhle et al., 1999; Ren et al., 2012; Lekieffre et al., 2020). However, we measure an in-eddy FT-δ^{15}N for this species that is similar to the symbiont-barren, deep-dwelling *G. hirsuta* (i.e., high in δ^{15}N). By contrast, at station 14 outside the eddy, *O. universa* had similar FT-δ^{15}N (lower by 0.4 ‰) to *G. hirsuta*. The *O. universa* specimens in the eddy were roughly 20% larger in diameter than those collected from the Atlantic, and thus also higher in N content (6.6 vs 2.4 nmol N/individual on average). If a larger size implies a higher trophic level (e.g., more carnivorous), then trophic position might explain the higher δ^{15}N of *O. universa* in the eddy. However, larger *O. universa* individuals can also host more symbionts (Spero and Parker, 1985), which might instead be expected to lower their FT-δ^{15}N (by allowing them to retain more low-δ^{15}N ammonium; Ren et al. 2012; Lekieffre et al. 2020) relative to that of smaller individuals. To disentangle the relative importance of carnivory *versus* ammonium retention in setting the FT-δ^{15}N of *O. universa*, summertime sampling is needed as this is the season when *O. universa* (and other dinoflagellate-bearing foraminifer

species) should be most abundant (Deuser et al., 1981; Chapman, 2010; Friedrich et al., 2012).

The different amounts by which the FT-δ^{15}N (and shell-bound δ^{15}N) of the various foraminifer species are lower in the eddy than in the Atlantic (i.e., the "FT-δ^{15}N offset") could be the result of several environmental and/or ecological factors. The similar FT-δ^{15}N offset for the two non-spinose deep dwellers (1.9 ‰ and 1.8 ‰ for *G. truncatulinoides* and *G. hirsuta*, respectively) is likely explained by their similar depth habitat and a common food source. A larger FT-δ^{15}N offset was observed for *G. inflata* and *G. bulloides* (2.9 ‰ and 3.4 ‰, respectively). In nutrient-rich regions, these two species have been observed to live at similar depths, typically associated with the chlorophyll maximum (Mohtadi et al., 2007; Salgueiro et al., 2020; Zarkogiannis et al., 2020). Occupation of a similar depth habitat (and thus access to similar food sources) could explain the similar FT-δ^{15}N of *G. bulloides* and *G. inflata*.

To explain the larger FT-δ^{15}N offset of the remaining shallow- to intermediate-depth-dwellers (*O. universa* and *G. siphonifera*; 2.5 ‰ and 2.7 ‰, respectively) compared to the deeper dwellers, we consider differences in symbiotic activity, lifetime, and seasonality between the two groups (Anand et al., 2003; Lombard et al., 2011; Friedrich et al., 2012; Stainbank et al., 2019). For *O. universa* and *G. siphonifera*, a shift to greater reliance on symbiont-retained N inside the eddy could hypothetically lower their FT-δ^{15}N, which could amplify their FT-δ^{15}N offset relative to the deep-dwellers. Such a shift may occur because of a difference in foraminifer size or maturation stage. For the dinoflagellate-hosting *O. universa*, the occurrence of larger foraminifera inside the eddy is consistent with this explanation, as larger specimens tend to possess more symbionts (Spero and Parker, 1985; Hönisch et al., 2021), which could increase the amount of ^{14}N retained relative to individuals with fewer symbionts (as is the case with δ^{11}B, Hönisch and Hemming 2004; Henehan et al. 2013). However, we do not observe an increase in test size in *G. siphonifera* in E1 relative to the South Atlantic. Longer lifespans may also have contributed to the smaller offset measured in *G. truncatulinoides* and *G. hirsuta* (long-lived species that migrate several hundred metres during their lifetime (Hemleben et al., 1985; Lohmann and Schweitzer, 1989); for example, if these species had only recently entered the local mixed layer. In this case, the FT-δ^{15}N of *G. truncatulinoides* and *G. hirsuta* in the eddy would partly retain the higher δ^{15}N of their former diet (partially degraded subsurface PON) and not yet have fully taken on the (lower) δ^{15}N of their new mixed-layer food source. Deep-dwelling individuals could also have recently become mixed into the eddy due to the recent seasonal deepening of the mixed layer across the transect, thus incorporating foraminifera with a higher 'starting' FT-δ^{15}N than if the individuals had been consuming low FT-δ^{15}N throughout their lifetime.

2.4.3.2 In-eddy dynamics

FT-δ^{15}N was not uniform across the eddy, but was instead lowest closer to the eddy centre (i.e., near the SSHA maximum; station 5, Fig. 2.1, Fig. **??**) and near the trailing edge (stations 3 to 4). Across-eddy spatial patterns were observed for other properties, such as temperature and salinity, which were highest at the eddy centre, declining towards its edges (Fig. 2.2c). It is likely that the parameters measured at the centre of the eddy more closely reflect the eddy source region while the edges reflect enhanced mixing with the surrounding waters. Indeed, the transitional nature of eddy edges is well known, with seawater properties (and subsequently, the biological community) in eddies evolving over time to more closely resemble the eddy surroundings. The fact that our FT-δ^{15}N data show a spatial pattern across the eddy further supports the notion that the low FT-δ^{15}N of eddy foraminifera is due to the influence of Agulhas thermocline nitrate rather than to some mechanism ongoing across the Cape Basin. FT-δ^{15}N at station 3 at the trailing edge of E1 was similarly low to the FT-δ^{15}N measured in the centre of the eddy (4.1 ± 1.2 ‰ *versus* 5.0 ± 0.8 ‰), seemingly at odds with the explanation above. However, the trailing edge of E1 was located very close to the eddy centre, and possessed properties much more eddy-like than the leading edge (Fig. 2.1), such that despite the increased mixing expected at eddy edges, many of the foraminifera sampled in the station 3 net tow likely lived in close proximity to the eddy core for much of their lifetime.

2.4.3.3 Factors affecting the relationship between FT-δ^{15}N and $\delta^{15}N_{NO_3}$

The FT-δ^{15}N of several foraminifer species in the Atlantic closely approximated the $\delta^{15}N_{NO_3}$ of thermocline (i.e., SASTMW) nitrate. The three most abundant species (*G. truncatulinoides, G. hirsuta, G. inflata*; all deep and/or mid-depth dwellers) together had an average FT-δ^{15}N that was offset from the $\delta^{15}N_{NO_3}$ of thermocline nitrate by only 0.4 ± 0.3 ‰ (Fig. 2.8b). In the Sargasso Sea, a similar near-match between foraminifer tissue and thermocline $\delta^{15}N_{NO_3}$ has been observed, but there it was the euphotic-dwelling, symbiont-hosting species *G. ruber, T. sacculifer*, and *O. universa* were that were most similar to thermocline $\delta^{15}N_{NO_3}$, while the FT-δ^{15}N of the deep dwelling foraminifera was higher, by $\sim$1 ‰ (Smart et al., 2018). The same pattern has been observed in a comparison between thermocline nitrate and foraminifera-bound δ^{15}N from surface sediments across the low-mid latitude ocean (Ren et al., 2012a). These authors reasoned that the dinoflagellate symbionts in euphotic-dwelling foraminifer species were responsible for the similarity of FT-δ^{15}N to $\delta^{15}N_{NO_3}$, as they effectively lower FT-δ^{15}N through ammonium retention, counteracting the isotopic enrichment expected for a predator relative to its prey. In our study, the FT-δ^{15}N of the facultatively symbiotic species *G. inflata* and potentially symbiotic (Gastrich, 1987; Jonkers and Kučera, 2015) *G. falconensis* was slightly lower (0.5 to 0.8 ‰) than the $\delta^{15}N_{NO_3}$, seemingly at odds with these earlier findings. However, in the short-term, FT-δ^{15}N is set by the δ^{15}N of its diet and species-specific metabolism (i.e., specific trophic offset; affected by ammonium excretion, symbiont activity/exchanges

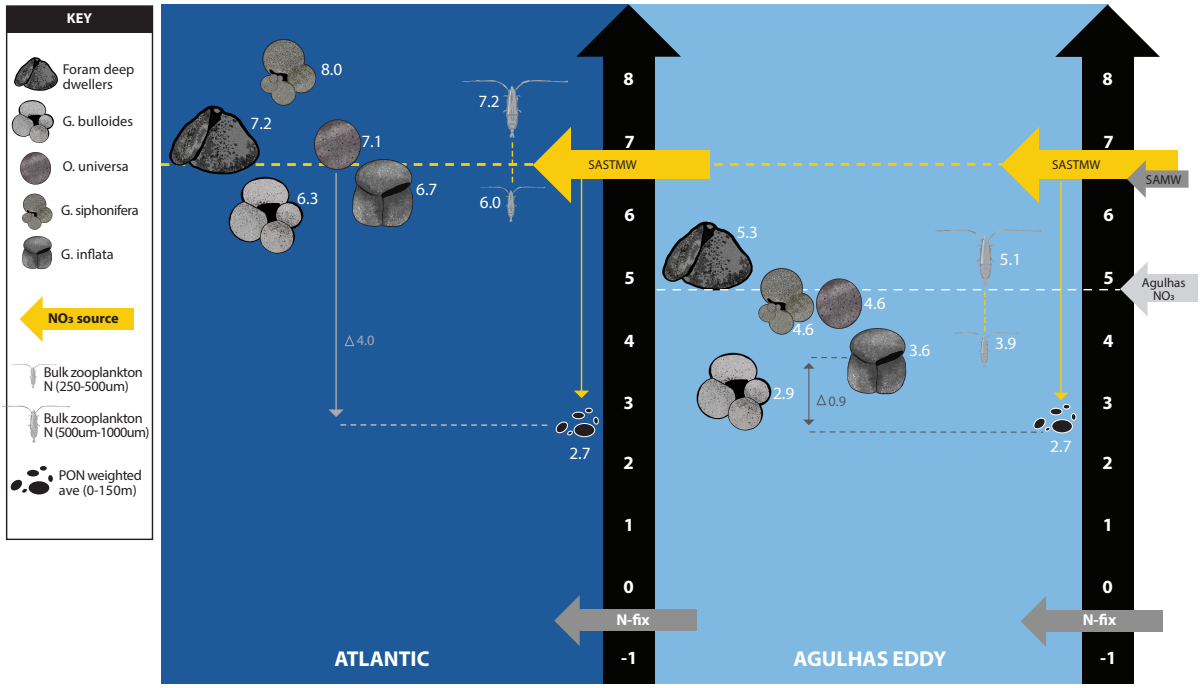

Figure 2.9: Schematic showing the nitrogen isotope dynamics that we propose were ongoing in a) the background Cape Basin and b) an Agulhas eddy that had migrated into the Cape Basin in 2017. The orange arrow and dashed line indicates South Atlantic Subtropical Mode Water (SASTMW, 6.9 ‰). The light grey arrow in panel b shows the mean $\delta^{15}N_{NO_3}$ of Agulhas Current nitrate (4.9 ‰, Marshall et al. 2023) and the darker grey arrow below it indicates the import of Subantarctic Mode Water (SAMW, 6.7 ‰), the ultimate source of nitrate to both the Cape Basin and Agulhas region. Suspended PON $\delta^{15}N$, bulk zooplankton $\delta^{15}N$ (for the 250-500 μm and 500-1000 μm size classes), and FT-$\delta^{15}N$ are indicated using images of the various species (see legend). Thin vertical lines are the calculated difference in $\delta^{15}N$ between one example foraminifer species (*G. inflata*) and suspended PON.

and/or direct ammonium assimilation (e.g., *G. bulloides* in culture; Bird et al. 2020) rather than by $\delta^{15}N_{NO_3}$ directly, with seasonal changes in PON $\delta^{15}N$ appearing to drive large deviations (as high as 4 ‰) in FT-$\delta^{15}N$ relative to both the annual average FT-$\delta^{15}N$ and the $\delta^{15}N_{NO_3}$ of the nitrate supply (Smart et al., 2020). As such, the fact that we only have winter FT-$\delta^{15}N$ in the South Atlantic may explain the apparently anomalous relationship of the FT-$\delta^{15}N$ of certain foraminifer species to $\delta^{15}N_{NO_3}$, with data from other seasons required to fully characterize the relationship.

The similarity between FT-$\delta^{15}N$ and thermocline $\delta^{15}N_{NO_3}$ observed at the Atlantic stations did not hold in the eddy. Here, FT-$\delta^{15}N$ was on average 2 ‰ lower than the $\delta^{15}N_{NO_3}$ of SASTMW nitrate underlying the mixed layer and was more similar to the $\delta^{15}N_{NO_3}$ of Agulhas thermocline nitrate ($\sim$4.9 ‰) (Fig. 2.9). As outlined in section 4.2 above, we suggest that as the eddy migrated into the South Atlantic, nitrate originating in the Agulhas Current thermocline (and mixed layer, although its concentration in this layer would have been extremely low; Marshall et al. 2023) was incorporated into the eddy's

deepening mixed layer where it would have been rapidly consumed by phytoplankton and thus integrated into the eddy's planktonic ecosystem. In other words, the waters underlying the eddy mixed layer at the time of sampling did not reflect the original nitrate supply to its surface ecosystem. Indeed, given the age of the eddy (7 to 8 months), along with its retentive anticyclonic circulation and the considerably longer lifetime of foraminifera compared to phytoplankton (i.e., PON), SASTMW nitrate likely contributed only minimally to the FT-δ^{15}N measured in the eddy.

2.4.3.4 Foraminifera δ^{15}N *versus* PON δ^{15}N

Above, we have compared FT-δ^{15}N to $\delta^{15}N_{NO_3}$. However, foraminifera do not consume nitrate, but rather the photosynthetic biomass generated from the assimilation of nitrate and other N forms, as well as heterotrophic and detrital organic matter (i.e., PON). Indeed, a recent study from the Southern Ocean showed that FT-δ^{15}N in the mixed layer is more closely tied to the δ^{15}N of PON than to $\delta^{15}N_{NO_3}$ on sub-annual timescales (Smart et al., 2020) As such, for the eddy foraminifera to acquire their lower FT-δ^{15}N, they would have had to consume a different (i.e., lower δ^{15}N) PON pool from the Atlantic foraminifera, which we propose derived from the assimilation of Agulhas-sourced nitrate. However, the measured δ^{15}N of upper mixed-layer PON in E1 is remarkably similar to the PON collected at the Atlantic stations (2.5 ± 0.7 ‰, n = 7 *versus* 2.8 ± 1.6 ‰, n = 6)).

To explain these suspended PON data, we consider the time over which the isotopic signal of different N pools integrates and examine the potential effect(s) of circulation and seasonality. Phytoplankton, a large component of the PON pool, live for hours to days, which allows for fairly rapid isotopic change (Pasquero, 2005; d'Ovidio et al., 2010; Treibergs et al., 2014). As such, suspended PON in the eddy may reflect phytoplankton N assimilation that has occurred recently (e.g., of vertically- or laterally-supplied SASTMW and/or shallower Cape Basin nitrate), while foraminifer shell δ^{15}N integrates the isotopic signal of all the PON consumed by the foraminifera over their lifetime (although the turnover time for biomass is unknown, and is likely shorter than the shell). The foraminifera chosen for isotope analysis in this study were adults, such that their FT-δ^{15}N also likely integrated over weeks to several months. One problem with this explanation, however, is that our sampling took place near the start of the nitrate resupply period in the Cape Basin (Fig. 2.3), meaning that any recent assimilation of SASTMW nitrate, accompanied by isotopic fractionation, would have yielded PON with a considerably lower δ^{15}N (by as much as 5 ‰, the expected isotope effect associated with nitrate assimilation; Sigman and Casciotti 2009) than that of SASTMW nitrate. Moreover, given the very deep mixed layers in the eddy ($\sim$250 m), which would have caused severe light limitation of phytoplankton (Wallschuss et al., 2022), along with the fact that nitrate is energetically expensive to assimilate (Dortch, 1990), it is unlikely that significant consumption of newly-supplied SASTMW was ongoing at the time of our study. Indeed,

direct measurements of N uptake in the eddy that occurred coincident with our sampling indicate that phytoplankton were supported near-exclusively by recycled N (Wallschuss et al., 2022).

Anticyclonic eddies can retain particles in the mixed layer for months as weak downwelling reduces the sinking flux and the closed circulation and inward surface convergence deter the loss of organisms through horizontal advection (Saino and Hattori, 1980; Condie and Condie, 2016; Cetina-Heredia et al., 2019; Sinha et al., 2019). Bacterial re-working of particles within the eddy would raise the δ^{15}N of PON over time (without the need for an additional supply of high $\delta^{15}N_{NO_3}$), bringing the originally lower-δ^{15}N PON in the eddy in line with the surrounding Atlantic PON (Altabet and McCarthy, 1985; Mobius, 2013; Mino et al., 2020). One might expect such a rise in PON δ^{15}N to also increase FT-δ^{15}N given the strong relationship between FT-δ^{15}N and PON δ^{15}N observed in the Southern Ocean (Smart et al., 2020), yet this is not what we observe. It is possible that at the time of our sampling, the eddy foraminifera had not consumed enough partially degraded PON to significantly raise their δ^{15}N. Additionally, some foraminifera (e.g., shallow-dwellers) may have fed preferentially on PON that was newly produced from the assimilation of nitrate with an isotope effect or low-δ^{15}N ammonium, or even assimilating some ammonium directly (e.g., *G. bulloides*) (Bird et al., 2020).

Without temporally-resolved measurements, it is difficult to draw robust conclusions regarding the dynamics of the eddy PON pool. However, even though the δ^{15}N of PON does not align with the trends observed in the $\delta^{15}N_{NO_3}$ and FT-δ^{15}N, the bulk δ^{15}N does (Fig. 2.7). It is thus possible that the zooplankton biomass (particularly in the 250 - 500 μm range, which has an N concentration 3- 4 times that of the $< 0.7\,\mu$m PON) as well as detritus in that size class and/or its microbial inhabitants more accurately represents the diet of the foraminifera than does the suspended PON. Not only will foraminifera consume other zooplankton (Bé and Hutson, 1977; Hemleben et al., 1989), but the zooplankton biomass integration time would have been similar to that of the foraminifera (Montoya et al., 2002; Loick-Wilde et al., 2016). As such, the bulk zooplankton δ^{15}N at the time of our sampling, which was lower in the eddy than the Atlantic due to the influence of Agulhas-derived nitrate, may be a better approximation than the δ^{15}N of suspended PON of the organic matter consumed by the foraminifera (Fig. S.3).

2.4.4 Potential for reconstruction of past Agulhas leakage from foraminifer-bound nitrogen isotopes

In this study, we found the $\delta^{15}N_{NO_3}$ of Agulhas eddy mixed-layer nitrate to be significantly lower than that of the surrounding Cape Basin, even after several months of eddy migration away from the Agulhas Retroflection. The δ^{15}N of foraminifera and bulk zooplankton was similarly low for populations sampled in the eddy compared to those collected from adjacent background Atlantic waters. We also observed a strong similarity between the FT-δ^{15}N of deep-dwelling foraminifera and thermocline $\delta^{15}N_{NO_3}$, with eddy foraminifera

recording the $\delta^{15}N_{NO_3}$ of Agulhas Current thermocline nitrate and Atlantic foraminifera more closely resembling local SASTMW. These findings have important implications for (1) palaeo-climate reconstructions in the Atlantic-Indian gateway region and (2) the implementation of the foraminifer-bound $\delta^{15}N$ proxy elsewhere in the ocean.

Our data show that foraminifera in Agulhas eddies retain the distinct $\delta^{15}N$ of Agulhas thermocline nitrate, itself the result of N_2 fixation in the southwest Indian Ocean (Harms et al. 2019; Marshall et al. 2023), which could be leveraged to trace Indo-Atlantic exchange through past climate transitions. Previous palaeoclimate studies have suggested that glacial-to-interglacial climate transitions were associated with increased leakage of Indian Ocean waters into the South Atlantic, which would have increased the salinity of waters returning to the North Atlantic, thus enhancing NADW subduction and strengthening the AMOC (Peeters et al., 2004; Franzese et al., 2006; Ballalai et al., 2019; Dickson et al., 2010; Caley et al., 2011; Marino et al., 2013; Simon et al., 2020). Studies of fossil foraminifera collected in sediment cores from the western continental shelf of South Africa reveal a higher abundance of (sub)tropical species (i.e., Agulhas leakage fauna) during glacial terminations, consistent with an increase in the strength of Agulhas leakage during this time (Peeters et al., 2004; Caley et al., 2014). From our FT-$\delta^{15}N$ results and the strong correlation of FT-$\delta^{15}N$ to shell-bound $\delta^{15}N$ observed here and elsewhere (Fig. 8a; Ren et al., 2012; Smart et al., 2018, 2020), we would expect these glacial-interglacial transitions to be characterized by comparatively low foraminifer-bound $\delta^{15}N$ in the southeastern Atlantic sediment record. Our samples were collected from a relatively mature Agulhas eddy and yet the isotopic influence of Agulhas nitrate was still clear in the FT-$\delta^{15}N$. This observation suggests that the foraminifera-$\delta^{15}N$ proxy has the potential to extend Agulhas leakage reconstructions beyond the retroflection region and into the offshore South Atlantic where Agulhas leakage fauna (e.g., *G. ruber, G. menardii, T. sacculifer*) no longer dominate surface waters due to temperature changes associated with eddy decay (Lončarić, 2006). One caveat to this idea is that the foraminifer-$\delta^{15}N$ leakage proxy relies on the $\delta^{15}N$ of Agulhas nitrate being distinct from that of the Cape Basin thermocline, as is the case today. Since Agulhas thermocline nitrate is low in $\delta^{15}N$ because of N_2 fixation, a past decrease in N_2 fixation in the southwest Indian Ocean would lead to higher-$\delta^{15}N$ nitrate in the Agulhas Current, which would be passed on to the upper-ocean ecosystem, including the foraminifera. Similarly, a past increase in N_2 fixation in the South Atlantic, which today hosts negligible rates of this process (Moore et al., 2009; Sohm et al., 2011), could have lowered the $\delta^{15}N$ of thermocline nitrate in the Cape Basin, weakening the $\delta^{15}N$ difference between Agulhas leakage and the surrounding Atlantic waters. Since N_2 fixation in the South Atlantic is currently strongly iron limited (Moore et al., 2009), one might be able to address the potential for its occurrence in the past through examination of proxies for iron supply (Wolff et al., 2006; Martínez-García et al., 2014). In addition, past variations in the $\delta^{15}N$ of Agulhas or south Atlantic nitrate endmembers could be reconstructed by analysing foraminifera-bound $\delta^{15}N$ in sediment

records from these regions. If the variability of these endmembers through time is known, foraminifera-bound δ^{15}N measurements on sediment records located in the Agulhas leakage region could provide detailed reconstruction of past changes in Agulhas leakage.

2.5 Conclusions

We measured the δ^{15}N and δ^{18}O of nitrate and the δ^{15}N of PON, bulk zooplankton, and foraminifera in an anticyclonic eddy that had pinched off the Agulhas Current, as well as in the surrounding (i.e., "background") southeast Atlantic, to assess their utility as a tool for identifying Agulhas leakage into the Cape Basin. Nitrate supplied to the mixed layer across the Cape Basin in winter and early spring is exhausted during the spring-summer growing season, limiting the extent, on an annual basis, to which isotope fractionation during nitrate consumption is imprinted on $\delta^{15}N_{NO_3}$ or the δ^{15}N of the organisms consuming this nitrate. We therefore attribute the low δ^{15}N of anticyclonic Agulhas eddies to the retention of Agulhas-sourced nitrate, which is low in δ^{15}N and Δ(15-18) as a result of N_2 fixation in the southwest Indian Ocean (Harms et al. 2019; Marshall et al. 2023. This low δ^{15}N signal is retained in the δ^{15}N of foraminifera and other zooplankton inhabiting the eddy even after the δ^{15}N of eddy mixed-layer nitrate is raised by isotopic fractionation during phytoplankton nitrate assimilation and mixing with the higher-δ^{15}N nitrate of the Cape Basin. We attribute the different δ^{15}N trends in mixed-layer nitrate, PON, bulk zooplankton, and foraminifera to the different isotopic integration times of these N pools. Foraminifera and zooplankton inhabiting Agulhas eddies appear to retain the low δ^{15}N of Agulhas thermocline nitrate for several months, despite ongoing exchange with the surrounding Cape Basin and changes in the dominant foraminifer species in the eddy driven by rapid surface heat loss that renders eddy waters unsuitable for Agulhas fauna (Gordon et al., 1987; Gordon and Haxby, 1990; Lončarić, 2006). These findings are of particular relevance for tracking Agulhas leakage some distance beyond the Agulhas Retroflection – the rapid decrease in eddy temperatures post-eddy spawning (De Ruijter et al., 1999; Van Aken et al., 2003) leads to faunal assemblages in Agulhas leakage quickly becoming more similar to those in the surrounding Atlantic, to the extent that it becomes challenging to distinguish leakage based only on the presence and/or relative abundance of Agulhas fauna (Lončarić, 2006).

Our data add to a growing body of work showing a strong (near 1:1) correlation between tissue- and shell-bound foraminifer δ^{15}N and confirm previous assertions that foraminifer-bound δ^{15}N can be used to track the δ^{15}N of thermocline nitrate in the low-latitude open ocean (Ren et al., 2012; Smart et al., 2018). However, our observations differ from previous findings in that it is the deep-dwelling, non-symbiont hosting foraminifer species rather than the shallow-dwelling, dinoflagellate-bearers that most closely match the δ^{15}N of thermocline nitrate, at least during winter when our sampling occurred. The implication is that deep-dwelling foraminifera are faithful recorders of the subsurface

nitrate supply to the South Atlantic mixed layer during winter. Future studies seeking to use FT-δ^{15}N to reconstruct thermocline $\delta^{15}N_{NO_3}$ in the South Atlantic should avoid Cape Basin sediments as we hypothesize these will be influenced by the isotopic signal of Agulhas leakage.

Future investigations into spring and summer N dynamics in the Cape Basin would be useful for assessing the relationships among summer foraminifer species composition, foraminifer δ^{15}N, and shallow thermocline nitrate, as well as for determining the relative importance of seasonal fluxes (and consequently, the dominant δ^{15}N signals) reaching the sea floor (as per Smart et al. 2020). For example, the available data suggest that *G. truncatulinoides* is most abundant in winter (Lohmann and Schweitzer, 1989; Steinhardt et al., 2015; Rebotim et al., 2017); as such, shell measurements of this species from sedimentary archives may reflect changes in winter conditions rather than an annual average. Additionally, isotope measurements in the Agulhas Current System (i.e., of PON and foraminifera prior to the formation of eddies) would provide important end-member information that would assist in interpreting Agulhas eddy N isotope dynamics, as would observations from newly-formed Agulhas eddies. Comparing the results of the present study with such data would also allow us to disentangle imported signals from in situ eddy processes that may alter nitrate and particle δ^{15}N, such as in-eddy N_2 fixation and ammonium recycling that could have contributed to the low FT-δ^{15}N measured in the mature Agulhas eddy.

Acknowledgements

We are grateful to the Captain and crew of the R/V *S.A. Agulhas II* for their efforts during both the 2015 and 2017 SAMBA cruises, and would like to thank Chief Scientists I. Ansorge and M. van den Berg, and the Department of Forestry, Fisheries and Environment: Oceans and Coasts for providing the nets used during the 2017 voyages. We are also grateful to B. Hinnenberg, J. Luyt, I. Newton, S. Oleynik, F. Rubach and R. Schiebel for laboratory and technical expertise, H. Forrer, P. Kenemy and K. Spence, for help with sampling, and J. Magner for assistance with Figure 9. This work was supported by the South African Department of Science and Innovation (DSI) through their SEAmester programme (`seamester.co.za`), the South African National Research Foundation through grants 129320 and 116142 to SEF and grants 112379 and 121126 to R. Granger, the University of Cape Town through a VC Future Leaders 2030 award and Research Committee Equipment grant to SEF, and by the African Academy of Sciences/ Royal Society through a FLAIR Fellowship to SEF. The 2017 SAMBA nitrate and foraminifera nitrogen isotope analyses were funded by the Max Planck Society (MPG). The authors also acknowledge the DSI's Biogeochemistry Research Infrastructure Platform (BIOGRIP; `www.biogrip.ac.za`).

Supplementary data

Nitrate isotope data for SAMBA 2017 can be found online at `https://doi.org/10.5281/zenodo.7648606`.

Supplementary Figures

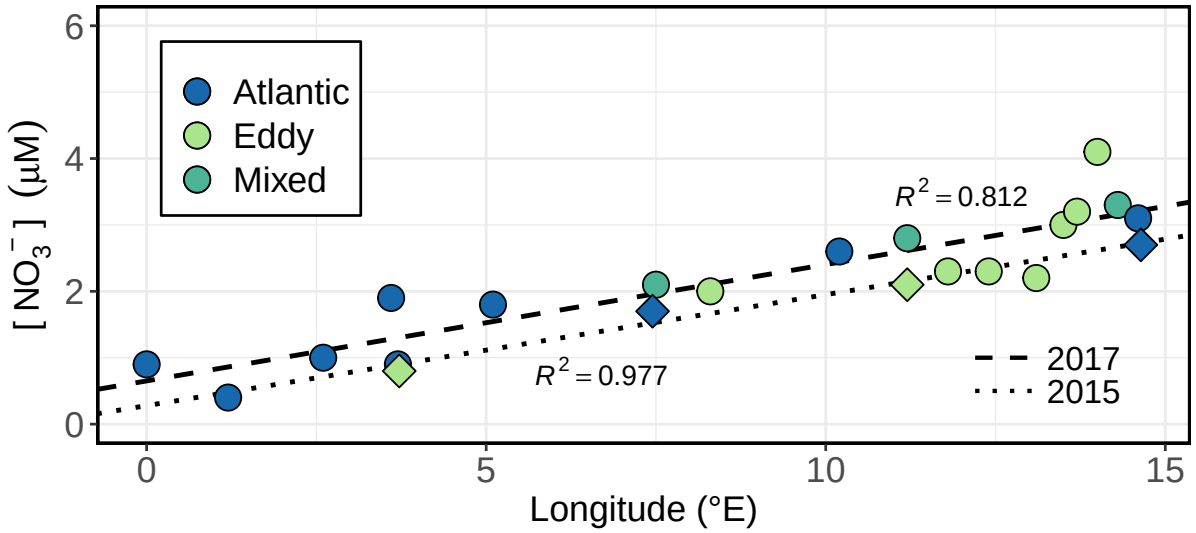

Figure S.1: Surface nitrate concentrations across the SAMBA transect in 2015 and 2017. Blue points show Atlantic stations, light green points represent eddy stations, and dark green points refer to mixed stations (stations with properties characteristic to both Atlantic and eddy environments). Dotted and dashed lines show linear regression lines for 2015 and 2017, respectively, along with correlation coefficients.

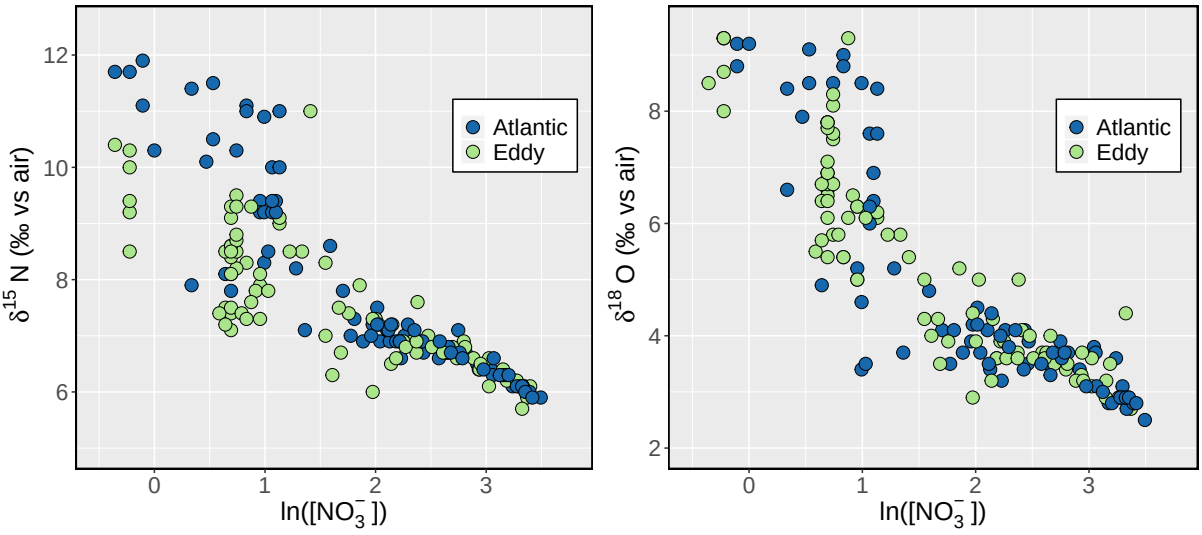

Figure S.2: Nitrogen and oxygen isotopes of seawater nitrate ($\delta^{15}N_{NO_3}$ and $\delta^{18}O_{NO_3}$, respectively) plotted *versus* ln([NO_3^-]) (i.e., in "Rayleigh space") for samples collected in 2015 and 2017. Blue circles indicate Atlantic stations (including leading edge) and green circles represent the Agulhas eddy stations (including trailing edge). The data show how at lower nitrate concentrations (i.e., ln([NO_3^-]) < 1.5; mixed layer), the $\delta^{15}N_{NO_3}$ at the eddy stations is lower than that at the Atlantic stations. By contrast, there is no difference in the $\delta^{18}O_{NO_3}$ between the eddy and Atlantic stations, including at low nitrate concentrations.

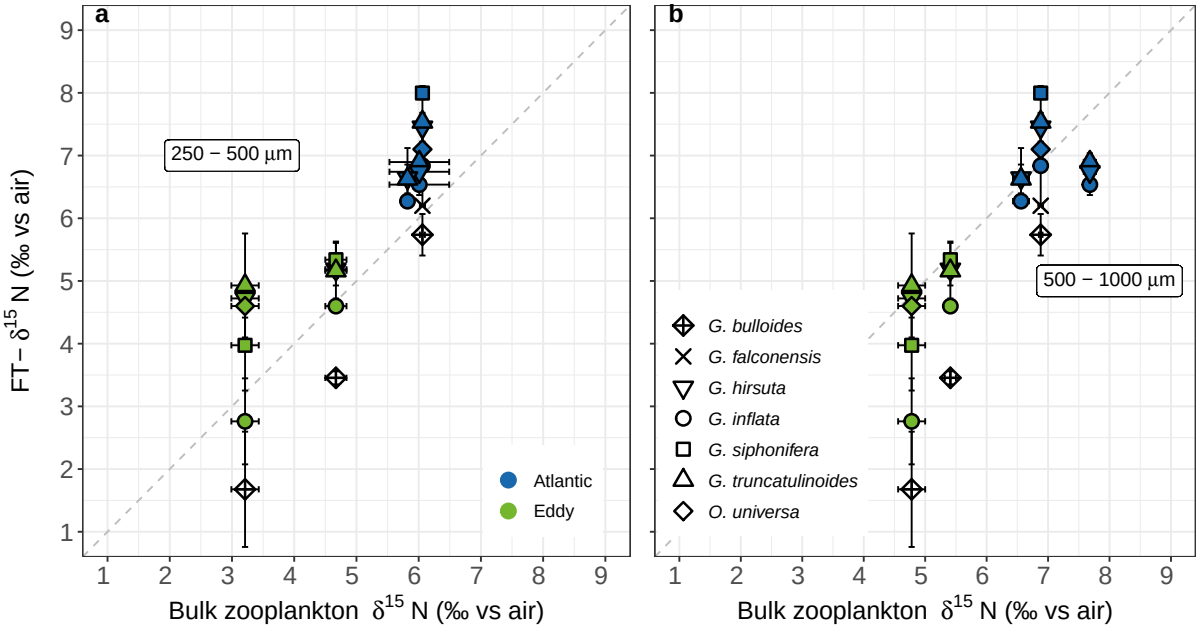

Figure S.3: Foraminifera δ^{15}N *versus* bulk zooplankton δ^{15}N at specific stations (4, 5, 10, 13, 14), where zooplankton size classes are a) 250-500 μm; and b) 500-1000 μm. Species are indicated by shape and are shaded according to station (Atlantic = blue, eddy = green), with error bars denoting $\pm$1 standard deviation from triplicate (foraminifera) and duplicate (bulk zooplankton) measurements.

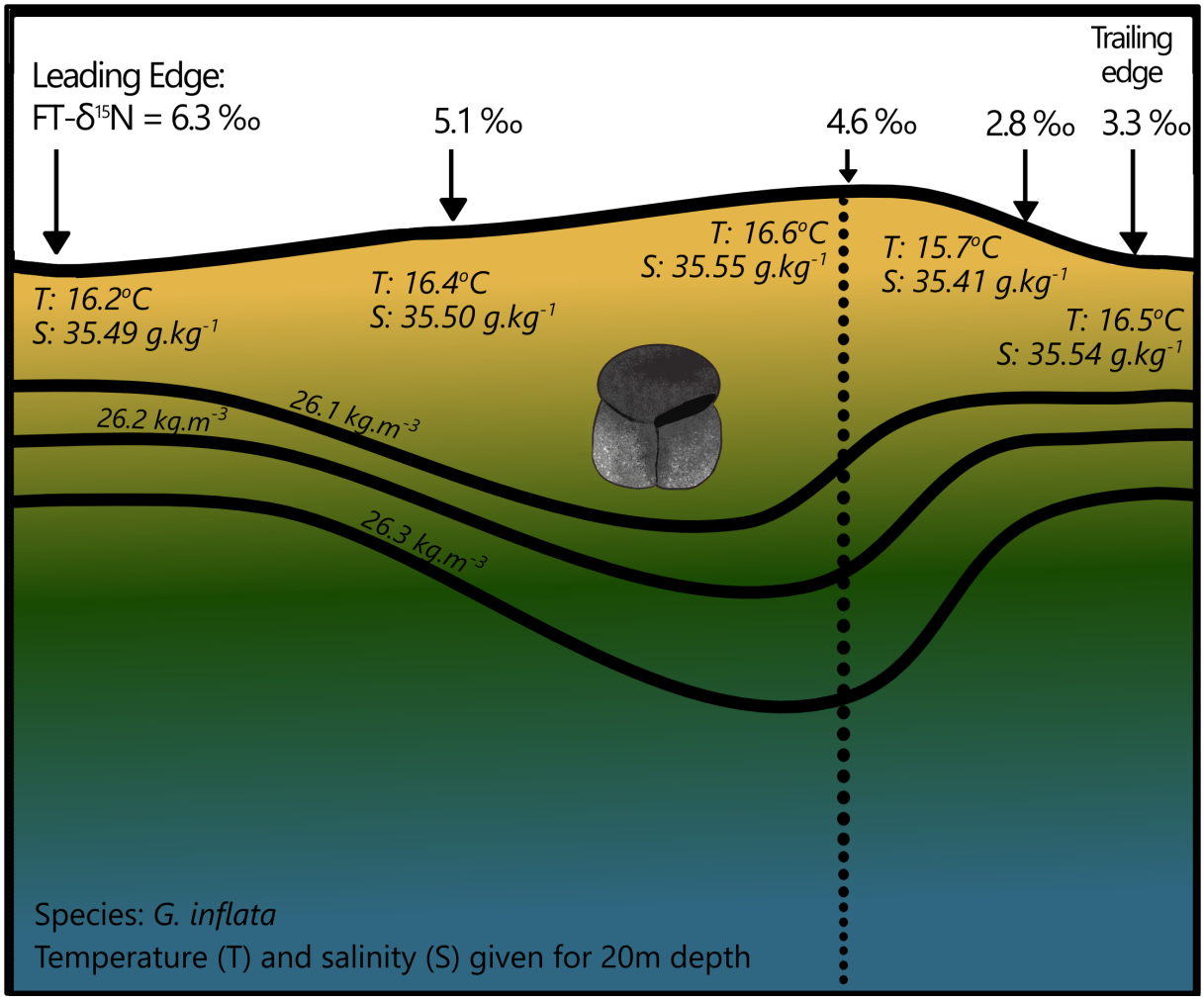

Figure S.4: Schematic demonstrating foraminifera δ^{15}N variation across eddy E1's physical structure (west-to-east). Eddy stations (left to right: stations 10, 9, 5, 4 and 3) are denoted by black arrows. FT-δ^{15}N of *G. inflata* (common to all stations) is shown above the arrows, whilst temperature and salinity at 20 m are written below them. Solid black lines represent density, and the vertical dotted line represents the eddy centre (highest sea surface height anomaly).

References

Altabet, M. A. (1988). Variations in nitrogen isotopic composition between sinking and suspended particles: implications for nitrogen cycling and particle transformation in the open ocean. *Deep Sea Research Part A, Oceanographic Research Papers*, 35(4):535–554.

Altabet, M. A. and Francois, R. (1994). Sedimentary nitrogen isotopic ratio as a recorder for surface ocean nitrate utilization. *Global Biogeochemical Cycles*, 8(1):103–116.

Altabet, M. A. and Francois, R. (2001). Nitrogen isotope biogeochemistry of the Antarctic polar frontal zone at 170°W. *Deep-Sea Research Part II: Topical Studies in Oceanography*, 48(19-20):4247–4273.

Altabet, M. A. and McCarthy, J. J. (1985). Temporal and spatial variations in the natural abundance of 15N in PON from a warm-core ring. *Deep Sea Research Part A, Oceanographic Research Papers*, 32(7):755–772.

Anand, P., Elderfield, H., and Conte, M. H. (2003). Calibration of Mg/Ca thermometry in planktonic foraminifera from a sediment trap time series. *Paleoceanography*, 18(2).

Arhan, M., Mercier, H., and Lutjeharms, J. R. (1999). The disparate evolution of three Agulhas rings in the South Atlantic Ocean. *Journal of Geophysical Research: Oceans*, 104(C9):20987–21005.

Auderset, A., Moretti, S., Taphorn, B., Ebner, P. R., Kast, E., Wang, X. T., Schiebel, R., Sigman, D. M., Haug, G. H., and Martínez-García, A. (2022). Enhanced ocean oxygenation during Cenozoic warm periods. *Nature*, 609(7925):77–82.

Aumont, O., Ethé, C., Tagliabue, A., Bopp, L., and Gehlen, M. (2015). PISCES-v2: An ocean biogeochemical model for carbon and ecosystem studies. *Geoscientific Model Development*, 8(8):2465–2513.

Ballalai, J. M., Santos, T. P., Lessa, D. O., Venancio, I. M., Chiessi, C. M., Johnstone, H. J., Kuhnert, H., Claudio, M. R., Toledo, F., Costa, K. B., and Albuquerque, A. L. S. (2019). Tracking Spread of the Agulhas Leakage Into the Western South Atlantic and Its Northward Transmission During the Last Interglacial. *Paleoceanography and Paleoclimatology*, 34(11):1744–1760.

Bé, A. W. H., Hemleben, C., Anderson, O. R., and Spindler, M. (1979). Chamber Formation in Planktonic Foraminifera. *Micropaleontology*, 25(3):294.

Bé, A. W. H. and Hutson, W. H. (1977). Ecology of Planktonic Foraminifera and Biogeographic Patterns of Life and Fossil Assemblages in the Indian Ocean. *Micropaleontology*, 23(4):369.

Bé, A. W. H. and Tolderlund, D. S. (1971). Distribution and ecology of living planktonic foraminifera in surface waters of the Atlantic and Indian Oceans.

Beal, L., De Ruijter, W. P., Biastoch, A., Zahn, R., Cronin, M., Hermes, J., Lutjeharms, J. R., Quartly, G., Tozuka, T., Baker-Yeboah, S., Bornman, T., Cipollini, P., Dijkstra, H., Hall, I., Park, W., Peeters, F. J., Penven, P., Ridderinkhof, H., and Zinke, J. (2011). On the role of the Agulhas system in ocean circulation and climate. *Nature*, 472(7344):429–436.

Berger, W. H. and Wefer, G. (2002). On the reconstruction of upwelling history: Namibia upwelling in context. *Marine Geology*, 180(1-4):3–28.

Bijma, J., Faber, W. W., and Hemleben, C. (1990). Temperature and salinity limits for growth and survival of some planktonic foraminifers in laboratory cultures. *Journal of Foraminiferal Research*, 20(2):95–116.

Bird, C., LeKieffre, C., Jauffrais, T., Meibom, A., Geslin, E., Filipsson, H. L., Maire, O., Russell, A. D., and Fehrenbacher, J. S. (2020). Heterotrophic Foraminifera Capable of Inorganic Nitrogen Assimilation. *Frontiers in Microbiology*, 11(December):3076.

Böhlke, J. K., Mroczkowski, S. J., and Coplen, T. B. (2003). Oxygen isotopes in nitrate: New reference materials for 18O:17O:16O measurements and observations on nitrate-water equilibration. *Rapid Communications in Mass Spectrometry*, 17(16):1835–1846.

Boltovskoy, D. (1994). The sedimentary record of pelagic biogeography. *Progress in Oceanography*, 34(2-3):135–160.

Boshers, D. S., Granger, J., Tobias, C. R., Böhlke, J. K., and Smith, R. L. (2019). Constraining the Oxygen Isotopic Composition of Nitrate Produced by Nitrification. *Environmental Science and Technology*, 53(3):1206–1216.

Braman, R. S. and Hendrix, S. A. (1989). Nanogram Nitrite and Nitrate Determination in Environmental and Biological Materials by Vanadium(III) Reduction with Chemiluminescence Detection. *Analytical Chemistry*, 61(24):2715–2718.

Browning, T. J., Achterberg, E. P., Rapp, I., Engel, A., Bertrand, E. M., Tagliabue, A., and Moore, C. M. (2017). Nutrient co-limitation at the boundary of an oceanic gyre. *Nature*, 551(7679):242–246.

Buchwald, C. and Casciotti, K. L. (2010). Oxygen isotopic fractionation and exchange during bacterial nitrite oxidation. *Limnology and Oceanography*, 55(3):1064–1074.

Buchwald, C. and Casciotti, K. L. (2013). Isotopic ratios of nitrite as tracers of the sources and age of oceanic nitrite. *Nature Publishing Group*, 6(4):1–6.

Caley, T., Giraudeau, J., Malaizé, B., Rossignol, L., and Pierre, C. (2012). Agulhas leakage as a key process in the modes of Quaternary climate changes. *PNAS*, 109(18):6835–6839.

Caley, T., Kim, J. H., Malaizé, B., Giraudeau, J., Laepple, T., Caillon, N., Charlier, K., Rebaubier, H., Rossignol, L., Castañeda, I. S., Schouten, S., and Sinninghe Damsté, J. S. (2011). High-latitude obliquity as a dominant forcing in the Agulhas current system. *Climate of the Past*, 7(4):1285–1296.

Caley, T., Peeters, F. J., Biastoch, A., Rossignol, L., and Sebille, E. V. (2014). Quantitative estimate of the paleo-Agulhas leakage. *Geophysical Research Letters*, 41:1238–1246.

Campbell, E. (2016). *Where Three Oceans Meet: Nitrate Isotope Measurements From the South Atlantic Along 34.5° S*. PhD thesis, Princeton University.

Capone, D. G., Bronk, D. A., Mulholland, M. R., and Carpenter, E. J. (2008). *Nitrogen in the Marine Environment*. Elsevier, 2nd editio edition.

Carpenter, E. J., Harvey, H. R., Brian, F., and Capone, D. G. (1997). Biogeochemical tracers of the marine cyanobacterium Trichodesmium. *Deep-Sea Research Part I: Oceanographic Research Papers*, 44(1):27–38.

Casciotti, K. L. and McIlvin, M. R. (2007). Isotopic analyses of nitrate and nitrite from reference mixtures and application to Eastern Tropical North Pacific waters. *Marine Chemistry*, 107(2):184–201.

Casciotti, K. L., Sigman, D. M., Hastings, M. G., Bohlke, J. K., and Hilkert, a. (2002). Measurement of the oxygen isotopic composition of nitrate seawater and freshwater using the dentirifier method. *Anal. Chem.*, 74(19):4905–4912.

Cetina-Heredia, P., Roughan, M., Van Sebille, E., Shane, K., Gary, B., Keating, S., and Brassington, G. B. (2019). Retention and leakage of water by mesoscale eddies in the East Australian Current system. *Journal of Geophysical Research: Oceans*, 124(4):2485–2500.

Chapman, M. R. (2010). Seasonal production patterns of planktonic foraminifera in the NE Atlantic Ocean: Implications for paleotemperature and hydrographic reconstructions. *Paleoceanography*, 25(1).

Checkley, D. M. and Miller, C. A. (1989). Nitrogen isotope fractionation by oceanic zooplankton. *Deep Sea Research Part A, Oceanographic Research Papers*, 36(10):1449–1456.

Chelton, D. B., Schlax, M. G., and Samelson, R. M. (2011). Global observations of nonlinear mesoscale eddies. *Progress in Oceanography*, 91(2):167–216.

Chen, G., Yang, J., and Han, G. (2021). Remote Sensing of Environment Eddy morphology : Egg-like shape, overall spinning, and oceanographic implications. *Remote Sensing of Environment*, 257(March 2020):112348.

Condie, S. and Condie, R. (2016). Retention of plankton within ocean eddies. *Global Ecology and Biogeography*, 25(10):1264–1277.

Conway, T. M., John, S. G., and Lacan, F. (2016). Intercomparison of dissolved iron isotope profiles from reoccupation of three GEOTRACES stations in the Atlantic Ocean. *Marine Chemistry*, 183:50–61.

De Ruijter, W. P., Biastoch, A., Drijfhout, S. S., Lutjeharms, J. R., Matano, R. P., Pichevin, T., van Leeuwen, P. J., and Weijer, W. (1999). Indian-Atlantic interocean exchange: Dynamics, estimation and impact. *Journal of Geophysical Research*, 104(C9):20885–20910.

Deman, F., Fonseca-Batista, D., Roukaerts, A., García-Ibáñez, M. I., Le Roy, E., Thilakarathne, E. P., Elskens, M., Dehairs, F., and Fripiat, F. (2021). Nitrate Supply Routes and Impact of Internal Cycling in the North Atlantic Ocean Inferred From Nitrate Isotopic Composition. *Global Biogeochemical Cycles*, 35(4):1–15.

Deuser, W. G., Ross, E., Hemleben, C., and Spindler, M. (1981). Seasonal changes in species composition, numbers, mass, size, and isotopic composition of planktonic foraminifera settling into the deep Sargasso Sea. *Palaeogeography Palaeoclimatology Palaeoecology*, 33:103–127.

Deutsch, C., Sarmiento, J. L., Sigman, D. M., Gruber, N., and Dunne, J. P. (2007). Spatial coupling of nitrogen inputs and losses in the ocean. *Nature*, 445(7124):163–167.

Diamond, D. (1994). Lachat Instruments Inc. *QuikChem method*, pages 31–115.

Dickson, A. J., Leng, M. J., Maslin, M. A., Sloane, H. J., Green, J., Bendle, J. A., McClymont, E. L., and Pancost, R. D. (2010). Atlantic overturning circulation and Agulhas leakage influences on southeast Atlantic upper ocean hydrography during marine isotope stage 11. *Paleoceanography*, 25(3):1–14.

Donners, J., Drijfhout, S. S., and Hazeleger, W. (2005). Water mass transformation and subduction in the South Atlantic. *Journal of Physical Oceanography*, 35(10):1841–1860.

Dortch, Q. (1990). The interaction between ammonium and nitrate uptake in phytoplankton. *Marine ecology progress series*, 61(1):183 – 201.

d'Ovidio, F., De Monte, S., Alvain, S., Dandonneau, Y., and Levy, M. (2010). Fluid dynamical niches of phytoplankton types. *Proceedings of the National Academy of Sciences*, 107(43):18366–18370.

Dufois, F., Hardman-Mountford, N. J., Greenwood, J., Richardson, A. J., Feng, M., and Matear, R. J. (2016). Anticyclonic eddies are more productive than cyclonic eddies in subtropical gyres because of winter mixing. *Science Advances*, 2(5):1–6.

Duncombe Rae, C. M. (1991). Agulhas retroflection rings in the South Atlantic Ocean: An overview. *South African Journal of Marine Science*, 11(1):327–344.

Eguchi, N. O., Ujiié, H., Kawahata, H., and Taira, A. (2003). Seasonal variations in planktonic foraminifera at three sediment traps in the Subarctic, Transition and Subtropical zones of the central North Pacific Ocean. *Marine Micropaleontology*, 48(1-2):149–163.

Eppley, R. W., Renger, E. H., and Betzer, P. R. (1983). The residence time of particulate organic carbon in the surface layer of the ocean. *Deep Sea Research Part A, Oceanographic Research Papers*, 30(3):311–323.

Faber, W. W., Anderson, O. R., Lindsey, J. L., and Caron, D. A. (1988). Algal-foraminiferal symbiosis in the planktonic foraminifer Globigerinella aequilateralia; I, Occurrence and stability of two mutually exclusive chrysophyte endosymbionts and their ultrastructure. *Journal of Foraminiferal Research*, 18(4):334–343.

Fasham, M. J., Ducklow, H. W., and McKelvie, S. M. (1990). A nitrogen-based model of plankton dynamics in the oceanic mixed layer. *Journal of Marine Research*, 48(3):591–639.

Fawcett, S. E., Lomas, M. W., Casey, J. R., Ward, B. B., and Sigman, D. M. (2011). Assimilation of upwelled nitrate by small eukaryotes in the Sargasso Sea. *Nature Geoscience*, 4(10):717–722.

Fawcett, S. E., Lomas, M. W., Ward, B. B., and Sigman, D. M. (2014). The counterintuitive effect of summer-to-fall mixed layer deepening on eukaryotic new production in the Sargasso Sea. *Global Biogeochemical Cycles*, 28:86–102.

Fawcett, S. E., Ward, B. B., Lomas, M. W., and Sigman, D. M. (2015). Vertical decoupling of nitrate assimilation and nitrification in the Sargasso Sea. *Deep-Sea Research Part I: Oceanographic Research Papers*, 103:64–72.

Feldmeijer, W., Metcalfe, B., Brummer, G. J., and Ganssen, G. M. (2015). Reconstructing the depth of the permanent thermocline through the morphology and geochemistry of the deep dwelling planktonic foraminifer Globorotalia truncatulinoides. *Paleoceanography*, 30(1):1–22.

Ferreira, M. L. d. C. and Kerr, R. (2017). Source water distribution and quantification of North Atlantic Deep Water and Antarctic Bottom Water in the Atlantic Ocean. *Progress in Oceanography*, 153:66–83.

Flynn, R. F., Granger, J., Veitch, J. A., Siedlecki, S., Burger, J. M., Pillay, K., and Fawcett, S. E. (2020). On-Shelf Nutrient Trapping Enhances the Fertility of the Southern Benguela Upwelling System. *Journal of Geophysical Research: Oceans*, 125(6):1–24.

Fong, A. A., Karl, D. M., Lukas, R., Letelier, R. M., Zehr, J. P., and Church, M. J. (2008). Nitrogen fixation in an anticyclonic eddy in the oligotrophic North Pacific Ocean. *ISME Journal*, 2(6):663–676.

Franzese, A. M., Hemming, S. R., Goldstein, S. L., and Anderson, R. F. (2006). Reduced Agulhas Leakage during the Last Glacial Maximum inferred from an integrated provenance and flux study. *Earth and Planetary Science Letters*, 250:72–88.

Friedrich, O., Schiebel, R., Wilson, P. A., Weldeab, S., Beer, C. J., Cooper, M. J., and Fiebig, J. (2012). Influence of test size, water depth, and ecology on Mg/Ca, Sr/Ca, δ18O and δ13C in nine modern species of planktic foraminifers. *Earth and Planetary Science Letters*, 319-320:133–145.

Froyland, G., Horenkamp, C., Rossi, V., and van Sebille, E. (2015). Studying an Agulhas ring's long-term pathway and decay with finite-time coherent sets. *Chaos*, 25(8):083119.

Garcia, H. E., Weathers, K., Paver, C. R., Smolyar, I., Boyer, T., Locarnini, R. A., Zweng, M. M., Mishonov, A. V., Baranova, O. K., Seidov, D., and Reagan, J. R. (2019). World Ocean Atlas 2018, Volume 4: Dissolved Inorganic Nutrients (phosphate, nitrate and nitrate+nitrite, silicate). In Mishnov Technical Editor, A., editor, *NOAA Atlas NESDIS 84*, page 35pp.

Garzoli, S. L. and Gordon, A. L. (1996). Origins and variablity of the Benguela Current. *Journal of Geophysical Research*, 101(95):897–906.

Garzoli, S. L. and Matano, R. P. (2011). The South Atlantic and the Atlantic Meridional Overturning Circulation. *Deep-Sea Research Part II: Topical Studies in Oceanography*, 58(17-18):1837–1847.

Gastrich, M. (1987). Ultrastructure of a new intracellular symbiotic alga found within planktonic foraminifera. *Journal of Phycology*, 25:623–632.

Gonfiantini, R., Stichler, W., and Rozanski, K. (1993). Standards and intercomparison materials distributed by the International Atomic Energy Agency for stable isotope measurements. *Standards and intercomparison materials distributed by the International Atomic Energy Agency for stable isotope measurements*, (No. IAEA-TECDOC–825).

Goni, G. J., Garzoli, S. L., Roubicek, A. J., Olson, D. B., and Brown, O. B. (1997). Agulhas ring dynamics from TOPEX/POSEIDON satellite altimeter data. *Journal of Marine Research*, 55(5):861–883.

Gordon, A. L. (1986). Interocean exchange of thermocline water. *Journal of Geophysical Research*, 91(C4):5037.

Gordon, A. L. and Haxby, W. F. (1990). Agulhas eddies invade the south Atlantic: Evidence From Geosat altimeter and shipboard conductivity-temperature-depth survey. *Journal of Geophysical Research*, 95(C3):3117.

Gordon, A. L. and Huber, B. A. (1990). Southern ocean winter mixed layer. *Journal of Geophysical Research*, 95(C7):11655.

Gordon, A. L., Lutjeharms, J. R., and Gründlingh, M. L. (1987). Stratification and circulation at the Agulhas Retroflection. *Deep Sea Research Part A, Oceanographic Research Papers*, 34(4):565–599.

Gordon, A. L., Weiss, R., Smethie, W. M., and Warner, M. J. (1992). Thermocline and Intermediate Water Communication Between the South Atlantic and Indian Oceans. *Journal of Geophysical ...*, 97:7223–7240.

Granger, J. and Sigman, D. M. (2009). Removal of nitrite with sulfamic acid for nitrate N and O isotope analysis with the denitrifier method. *Rapid Communications in Mass Spectrometry*, 23:3753–3762.

Granger, J., Sigman, D. M., Needoba, J. A., and Harrison, P. J. (2004). Coupled nitrogen and oxygen isotope fractionation of nitrate during assimilation by cultures of marine phytoplankton. *Limnology and Oceanography*, 49(5):1763–1773.

Granger, J., Sigman, D. M., Rohde, M. M., Maldonado, M. T., and Tortell, P. D. (2010). N and O isotope effects during nitrate assimilation by unicellular prokaryotic and eukaryotic plankton cultures. *Geochimica et Cosmochimica Acta*, 74(3):1030–1040.

Grasshoff, K. (1976). *Methods of Seawater Analysis*. Verlag Chemie, 2nd edition.

Harms, N. C., Lahajnar, N., Gaye, B., Rixen, T., Dähnke, K., Ankele, M., Schwarz-Schampera, U., and Emeis, K. C. (2019). Nutrient distribution and nitrogen and oxygen isotopic composition of nitrate in water masses of the subtropical southern Indian Ocean. *Biogeosciences*, 16(13):2715–2732.

Hecht, A. D. (1976). An ecologic model for test size variation in Recent planktonic foraminifera; applications to the fossil record. *The Journal of Foraminiferal Research*, 6(4):295–311.

Hemleben, C., Bé, A. W. H., Anderson, O. R., and Tunitivate, S. (1977). Test morphology, organic layers and chamber formation of the planktonic foraminifer Globorotalia menardii (D'Orbigny). *Journal of Foraminiferal Research*, 7(1):1–25.

Hemleben, C., Spindler, M., and Anderson, O. R. (1989). *Modern Planktonic Foraminifera.* Springer-Verlag, New York, 1 edition.

Hemleben, C., Spindler, M., Breitinger, I., and Deuser, W. G. (1985). Field and laboratory studies on the ontogeny and ecology of some globorotaliid species from the Sargasso Sea off Bermuda. *Journal of Foraminiferal Research*, 15(4):254–272.

Henehan, M. J., Rae, J. W., Foster, G. L., Erez, J., Prentice, K. C., Kucera, M., Bostock, H. C., Martínez-Botí, M. A., Milton, J. A., Wilson, P. A., Marshall, B. J., and Elliott, T. (2013). Calibration of the boron isotope proxy in the planktonic foraminifera Globigerinoides ruber for use in palaeo-CO2 reconstruction. *Earth and Planetary Science Letters*, 364:111–122.

Hermes, J., Reason, C. J., and Lutjeharms, J. R. (2007). Modeling the variability of the greater Agulhas Current system. *Journal of Climate*, 20(13):3131–3146.

Hoering, T. C. and Ford, H. T. (1960). The Isotope Effect in the Fixation of Nitrogen by Azotobacter. *J. Am Chem Soc.*, 82:376–378.

Holl, C., Waite, A. M., Pesant, S., Thompson, P. A., and Montoya, J. (2007). Unicellular diazotrophy as a source of nitrogen to Leeuwin Current coastal eddies. *Deep-Sea Research Part II: Topical Studies in Oceanography*, 54(8-10):1045–1054.

Holmes, E., Lavik, G., Fischer, G., Segl, M., Ruhland, G., and Wefer, G. (2002). Seasonal variability of delta δ15N in sinking particles in the Benguela Upwelling region. *Deep-Sea Res.(I Oceanogr.Res.Pap.)*, 49(2):377–394.

Hönisch, B., Fish, C. R., Phelps, S. R., Haynes, L. L., Dyez, K. A., Holland, K., Fehrenbacher, J. S., Allen, K. A., Eggins, S. M., and Goes, J. I. (2021). Symbiont Photosynthesis and Its Effect on Boron Proxies in Planktic Foraminifera. *Paleoceanography and Paleoclimatology*, 36(10):1–22.

Hönisch, B. and Hemming, N. G. (2004). Ground-truthing the boron isotope-paleo-pH proxy in planktonic foraminifera shells: Partial dissolution and shell size effects. *Paleoceanography*, 19(4):1–13.

Jonkers, L. and Kučera, M. (2015). Global analysis of seasonality in the shell flux of extant planktonic Foraminifera. *Biogeosciences*, 12(7):2207–2226.

Jonkers, L. and Kučera, M. (2017). Quantifying the effect of seasonal and vertical habitat tracking on planktonic foraminifera proxies. *Climate of the Past*, 13(6):573–586.

Kast, E. R., Stolper, D. A., Auderset, A., Higgins, J. A., Ren, H., Wang, X. T., Martínez-García, A., Haug, G. H., Sigman, D. M., and Stopler, D. (2019). Nitrogen isotope evidence for expanded ocean suboxia in the early Cenozoic. *Science*, 364(6438):386–389.

King, K. and Hare, P. E. (1972). Amino Acid Composition of the Test as a Taxonomic Character for Living and Fossil Planktonic Foraminifera. *Micropaleontology*, 18(3):285.

Knapp, A. N., DiFiore, P. J., Deutsch, C., Sigman, D. M., and Lipschultz, F. (2008). Nitrate isotopic composition between Bermuda and Puerto Rico: Implications for N2 fixation in the Atlantic Ocean. *Global Biogeochemical Cycles*, 22(3):1–14.

Knapp, A. N., Sigman, D. M., and Lipschultz, F. (2005). N isotopic composition of dissolved organic nitrogen and nitrate at the Bermuda Atlantic Time-series study site. *Global Biogeochemical Cycles*, 19(1):1–15.

Knorr, G. and Lohmann, G. (2003). Southern Ocean origin for the resumption of Atlantic thermohaline circulation during deglaciation. *Letters to Nature*, 424(July):532–536.

Kretschmer, K., Jonkers, L., Kucera, M., and Schulz, M. (2018). Modeling seasonal and vertical habitats of planktonic foraminifera on a global scale. *Biogeosciences*, 15(14):4405–4429.

Landolfi, A., Kähler, P., Koeve, W., and Oschlies, A. (2018). Global marine N2 fixation estimates: From observations to models. *Frontiers in Microbiology*, 9(SEP):1–8.

Lea, D. J., Mirouze, I., Martin, M. J., King, R. R., Hines, A., Walters, D., and Thurlow, M. (2018). GLOBAL_ANALYSISFORECAST_PHY_CPL_001_015.

Lekieffre, C., Spero, H. J., Fehrenbacher, J. S., Russell, A. D., Ren, H., Geslin, E., and Meibom, A. (2020). Ammonium is the preferred source of nitrogen for planktonic foraminifer and their dinoflagellate symbionts: N recycling in a symbiotic foraminifer. *Proceedings of the Royal Society B: Biological Sciences*, 287(1929):1–10.

Lessa, D., Morard, R., Jonkers, L., Venancio, I. M., Reuter, R., Baumeister, A., Albuquerque, A. L., and Kucera, M. (2020). Distribution of planktonic foraminifera in the subtropical South Atlantic: depth hierarchy of controlling factors. *Biogeosciences*, 17(16):4313–4342.

Li, D. W., Xiang, R., Wu, Q., and Kao, S. J. (2019). Planktic foraminifera-bound organic nitrogen isotopic composition in contemporary water column and sediment trap. *Deep-Sea Research Part I*, 143:28–34.

Liu, J., Zhou, L., Li, J., Lin, Y., Ke, Z., Zhao, C., Liu, H., Jiang, X., He, Y., and Tan, Y. (2020). Effect of mesoscale eddies on diazotroph community structure and nitrogen fixation rates in the South China Sea. *Regional Studies in Marine Science*, 35:1–14.

Locarini, R. A., Mishonov, A. V., Antonov, J. I., Boyer, T., Garcia, H. E., Baranova, O. K., Zweng, M. M., Paver, C. R., Reagan, J. R., Johnson, D. R., Hamilton, M., and Seidov, D. (2013). *World Ocean Atlas 2013, Volume 1: Temperature*. NOAA Atlas NESDIS 73.

Lohmann, G. P. and Schweitzer, P. N. (1989). Globorotalia truncatulinoides' growth and chemistry as probes of the past thermocline: 1. Shell size. *Palaeoceanography*, 5(1):55–75.

Loick-Wilde, N., Weber, S. C., Conroy, B. J., Capone, D. G., Coles, V. J., Medeiros, P. M., Steinberg, D. K., and Montoya, J. (2016). Nitrogen sources and net growth efficiency of zooplankton in three Amazon River plume food webs. *Limnology and Oceanography*, 61(2):460–481.

Lombard, F., Labeyrie, L., Michel, E., Bopp, L., Cortijo, E., Retailleau, S., Howa, H., and Jorissen, F. (2011). Modelling planktic foraminifer growth and distribution using an ecophysiological multi-species approach. *Biogeosciences*, 8(4):853–873.

Lončarić, N. (2006). Planktic foraminiferal content in a mature Agulhas eddy from the SE Atlantic: Any influence on foraminiferal export fluxes? *Geologia Croatica*, 59(1):41–50.

Löscher, C. R., Bourbonnais, A., Dekaezemacker, J., Charoenpong, C. N., Altabet, M. A., Bange, H. W., Czeschel, R., Hoffmann, C., and Schmitz, R. (2016). N2 fixation in eddies of the eastern tropical South Pacific Ocean. *Biogeosciences*, 13(10):2889–2899.

Luo, Y. W., Doney, S. C., Anderson, L. A., Benavides, M., Berman-Frank, I., Bode, A., Bonnet, S., Boström, K. H., Böttjer, D., Capone, D. G., Carpenter, E. J., Chen, Y. L., Church, M. J., Dore, J. E., Falcón, L. I., Fernández, A., Foster, R. A., Furuya, K., Gómez, F., Gundersen, K., Hynes, A. M., Karl, D. M., Kitajima, S., Langlois, R. J., Laroche, J., Letelier, R. M., Maranõn, E., McGillicuddy, D. J., Moisander, P. H., Moore, C. M., Mourinõ-Carballido, B., Mulholland, M. R., Needoba, J. A., Orcutt, K. M., Poulton, A. J., Rahav, E., Raimbault, P., Rees, A. P., Riemann, L., Shiozaki, T., Subramaniam, A., Tyrrell, T., Turk-Kubo, K. A., Varela, M., Villareal, T. A., Webb, E. A., White, A. E., Wu, J., and Zehr, J. P. (2012). Database of diazotrophs in global ocean: Abundance, biomass and nitrogen fixation rates. *Earth System Science Data*, 4(1):47–73.

Lutjeharms, J. R. and Stockton, P. L. (1987). Kinematics of the upwelling front off southern Africa. *South African Journal of Marine Science*, 5(1):35–49.

Lutjeharms, J. R. and Valentine, H. R. (1984). Southern ocean thermal fronts south of Africa. *Deep Sea Research Part A. Oceanographic Research Papers*, 31(12):1461–1475.

Marconi, D., Weigand, M. A., and Sigman, D. M. (2019). Nitrate isotopic gradients in the North Atlantic Ocean and the nitrogen isotopic composition of sinking organic matter. *Deep-Sea Research Part I: Oceanographic Research Papers*, 145:109–124.

Marino, G., Zahn, R., Ziegler, M., Purcell, C., Knorr, G., Hall, I. R., Ziveri, P., and Elderfield, H. (2013). Agulhas salt-leakage oscillations during abrupt climate changes of the Late Pleistocene. *Paleoceanography*, 28(3):599–606.

Mariotti, A., A, Germon, J. C., Hubert, P., Kaiser, P., Letolle, R., and Tardieux, A. (1981). Experimental determination of nitrogen kinetic isotope fractionation: some principles: illustration for the denitrification and nitrification processes. *Plant and Soil*, 62(3):413–430.

Marshall, T. A., Sigman, D. M., Beal, L. M., Foreman, A., Martínez-García, A., Blain, S., Campbell, E., Fripiat, F., Granger, R., Harris, E., Haug, G. H., Marconi, D., Oleynik, S., Rafter, P. A., Roman, R., Sinyanya, K., Smart, S. M., and Fawcett, S. E. (2023). The Agulhas Current Transports Signals of Local and Remote Indian Ocean Nitrogen Cycling. *Journal of Geophysical Research: Oceans*, 128:1–29.

Martínez-García, A., Jung, J., Ai, X. E., Sigman, D. M., Auderset, A., Duprey, N. N., Foreman, A., Fripiat, F., Leichliter, J., Lüdecke, T., Moretti, S., and Wald, T. (2022). Laboratory Assessment of the Impact of Chemical Oxidation, Mineral Dissolution, and Heating on the Nitrogen Isotopic Composition of Fossil-Bound Organic Matter. *Geochemistry, Geophysics, Geosystems*, 23(8):1–23.

Martínez-García, A., Sigman, D. M., Ren, H., Anderson, R. F., Straub, M., Hodell, D. A., Jaccard, S. L., Eglinton, T. I., and Haug, G. H. (2014). Iron fertilization of the Subantarctic ocean during the last ice age. *Science (New York, N.Y.)*, 343(6177):1347–50.

Martínez-Méndez, G., Zahn, R., Hall, I. R., Peeters, F. J., Pena, L. D., Cacho, I., Negre, C. C. C. C., and Méndez, G. M. (2010). Contrasting multiproxy reconstructions of surface ocean hydrography in the Agulhas Corridor and implications for the Agulhas Leakage during the last 345,000 years. *Paleoceanography*, 25:1–12.

Meckler, A. N., Ren, H., Sigman, D. M., Gruber, N., Plessen, B., Schubert, C. J., and Haug, G. H. (2011). Deglacial nitrogen isotope changes in the Gulf of Mexico: Evidence from bulk sedimentary and foraminifera-bound nitrogen in Orca Basin sediments. *Paleoceanography*, 26(4):1–13.

Meilland, J., Schiebel, R., Lo Monaco, C., Sanchez, S., and Howa, H. (2018). Abundances and test weights of living planktic foraminifers across the Southwest Indian Ocean: Implications for carbon fluxes. *Deep-Sea Research Part I: Oceanographic Research Papers*, 131:27–40.

Meilland, J., Siccha, M., Weinkauf, M. F., Jonkers, L., Morard, R., Baranowski, U., Baumeister, A., Bertlich, J., Brummer, G. J., Debray, P., Fritz-Endres, T., Groeneveld, J., Magerl, L., Munz, P., Rillo, M. C., Schmidt, C., Takagi, H., Theara, G., and Kucera, M. (2019). Highly replicated sampling reveals no diurnal vertical migration but stable species-specific vertical habitats in planktonic foraminifera. *Journal of Plankton Research*, 41(2):127–141.

Minagawa, M. and Wada, E. (1986). Nitrogen isotope ratios of red tide organisms in the East China Sea: A characterization of biological nitrogen fixation. *Marine Chemistry*, 19(3):245–259.

Mino, Y., Sukigara, C., Honda, M. C., Kawakami, H., Wakita, M., Sasaoka, K., Yoshikawa, C., Abe, O., Kaiser, J., Kimoto, K., Kitamura, M., Fujiki, T., Matsumoto, K., and Saino, T. (2020). Seasonal and Interannual Variations in Nitrogen Availability and Particle Export in the Northwestern North Pacific Subtropical Gyre. *Journal of Geophysical Research: Oceans*, 125(5):1–18.

Mobius, J. (2013). Isotope fractionation during nitrogen remineralization (ammonification): Implications for nitrogen isotope biogeochemistry. *Geochimica et Cosmochimica Acta*, 105:422–432.

Mohtadi, M., Max, L., Hebbeln, D., Baumgart, A., Krück, N., and Jennerjahn, T. (2007). Modern environmental conditions recorded in surface sediment samples off W and SW Indonesia: Planktonic foraminifera and biogenic compounds analyses. *Marine Micropaleontology*, 65(1-2):96–112.

Montoya, J., Carpenter, E. J., and Capone, D. G. (2002). Nitrogen fixation and nitrogen isotope abundance in zooplankton of the oligotrophic North Atlantic. *Limnology & Oceanography*, 47(6):1617–1628.

Moore, M. C., Mills, M. M., Achterberg, E. P., Geider, R. J., Laroche, J., Lucas, M. I., McDonagh, E. L., Pan, X., Poulton, A. J., Rijkenberg, M. J., Suggett, D. J., Ussher, S. J., and Woodward, E. M. S. (2009). Large-scale distribution of Atlantic nitrogen fixation controlled by iron availability. *Nature Geoscience*, 2(12):867–871.

Morris, T., Hermes, J., Beal, L., Du Plessis, M., Rae, C. M. D., Gulekana, M., Lamont, T., Speich, S., Roberts, M., and Ansorge, I. J. (2017). The importance of monitoring the Greater Agulhas Current and its inter-ocean exchanges using large mooring arrays. *South African Journal of Science*, 113(7-8):1–7.

Moutin, T. and Prieur, L. (2012). Influence of anticyclonic eddies on the Biogeochemistry from the Oligotrophic to the Ultraoligotrophic Mediterranean (BOUM cruise). *Biogeosciences*, 9(10):3827–3855.

Nydahl, F. (1978). On the peroxodisulphate oxidation of total nitrogen in waters to nitrate. *Water Research Vol.*, 12:1123–1130.

Olson, D. B., Fine, R. A., and Gordon, A. L. (1992). Convective modifications of water masses in the Agulhas. *Deep Sea Research Part A. Oceanographic Research Papers*, 39(March):S163–S181.

Palter, J. B., Sarmiento, J. L., Gnanadesikan, A., Simeon, J., and Slater, R. D. (2010). Fueling export production: Nutrient return pathways from the deep ocean and their dependence on the Meridional Overturning Circulation. *Biogeosciences*, 7(11):3549–3568.

Pasquero, C. (2005). Differential eddy diffusion of biogeochemical tracers. *Geophysical Research Letters*, 32(17):1–4.

Paul, M., Van De Flierdt, T., Rehkämper, M., Khondoker, R., Weiss, D., Lohan, M. C., and Homoky, W. B. (2015). Tracing the Agulhas leakage with lead isotopes. *Geophysical Research Letters*, 42(20):8515–8521.

Peeters, F. J., Acheson, R., Brummer, G.-J. A., De Ruijter, W. P., Schneider, R., Ganssen, G. M., Ufkes, E., and Kroon, D. (2004). Vigorous exchange between the Indian and Atlantic oceans at the end of the past five glacial periods. *Nature*, 430(7000):661–5.

Peeters, F. J. and Brummer, G. J. A. (2002). The seasonal and vertical distribution of living planktic foraminifera in the NW Arabian Sea. *Geological Society Special Publication*, 195:463–497.

Qi, H., Coplen, T. B., Geilmann, H., Brand, W. A., and Böhlke, J. K. (2003). Two new organic reference materials for δ13C and δ15N measurements and a new value for the δ 13C of NBS 22 oil. *Rapid Communications in Mass Spectrometry*, 17(22):2483–2487.

Raes, E. J., Thompson, P. A., McInnes, A. S., Nguyen, H. M., Hardman-Mountford, N. J., and Waite, A. M. (2015). Sources of new nitrogen in the Indian Ocean. *Global Biogeochemical Cycles*, 29:1283–1297.

Rafter, P. A., Difiore, P. J., and Sigman, D. M. (2013). Coupled nitrate nitrogen and oxygen isotopes and organic matter remineralization in the Southern and Pacific Oceans. *Journal of Geophysical Research: Oceans*, 118(10):4781–4794.

Rebotim, A., Voelker, A. H., Jonkers, L., Waniek, J. J., Meggers, H., Schiebel, R., Fraile, I., Schulz, M., and Kucera, M. (2017). Factors controlling the depth habitat of planktonic foraminifera in the subtropical eastern North Atlantic. *Biogeosciences*, 14(4):827–859.

Ren, H., Sigman, D. M., Meckler, A. N., Plessen, B., Robinson, R., Rosenthal, Y., and Haug, G. H. (2009). Foraminiferal isotope evidence of reduced nitrogen fixation in the ice age Atlantic Ocean. *Science*, 323(5911):244–248.

Ren, H., Sigman, D. M., Thunell, R. C., and Prokopenko, M. G. (2012). Nitrogen isotopic composition of planktonic foraminifera from the modern ocean and recent sediments. *Limnology and Oceanography*, 57(4):1011–1024.

Ren, H., Studer, A. S., Serno, S., Sigman, D. M., Winckler, G., Anderson, R. F., Oleynik, S., Gersonde, R., and Haug, G. H. (2015). Glacial-to-interglacial changes in nitrate supply and consumption in the subarctic North Pacific from microfossil-bound N isotopes at two trophic levels. *Paleoceanography*, 30(9):1217–1232.

Rintoul, S. R. (1991). South Atlantic interbasin exchange. *Journal of Geophysical Research: Oceans*, 96(C2):2675–2692.

Rintoul, S. R. and Trull, W. (2001). Water mass properties along a north-south hydrographic. *Journal of Geophysical Research*, 106(C12):31447–31462.

Robbins, L. L. and Brew, K. (1990). Proteins from the organic matrix of core-top and fossil planktonic foraminifera. *Geochimica et Cosmochimica Acta*, 54(8):2285–2292.

Robinson, R., Kienast, M., Luiza Albuquerque, A., Altabet, M. A., Contreras, S., De Pol-Holz, R., Dubois, N., Francois, R., Galbraith, E. D., Hsu, T. C., Ivanochko, T., Jaccard, S., Kao, S. J., Kiefer, T., Kienast, S., Lehmann, M. F., Martinez, P., McCarthy, M., Möbius, J., Pedersen, T. F., Quan, T. M., Ryabenko, E., Schmittner, A., Schneider, R., Schneider-Mor, A., Shigemitsu, M., Sinclair, D., Somes, C. J., Studer, A. S., Thunell, R. C., and Yang, J. Y. (2012). A review of nitrogen isotopic alteration in marine sediments. *Paleoceanography*, 27(PA4203):1–13.

Robinson, R., Smart, S. M., Cybulski, J. D., McMahon, K. W., Marcks, B., and Nowakowski, C. (2023). Insights from Fossil-Bound Nitrogen Isotopes in Diatoms, Foraminifera, and Corals. *Annual Review of Marine Science*, 15(1):1–24.

Rohde, M. M., Granger, J., Sigman, D. M., and Lehmann, M. F. (2015). Coupled nitrate N and O stable isotope fractionation by a natural marine plankton consortium. *Frontiers in Marine Science*, 2(May).

Rühs, S., Durgadoo, J. V., Behrens, E., and Biastoch, A. (2013). Advective timescales and pathways of Agulhas leakage. *Geophysical Research Letters*, 40:3997–4000.

Saino, T. and Hattori, A. (1980). 15N natural abundance in oceanic suspended particulate matter. *Nature*, 283:752–754.

Salgueiro, E., Voelker, A. H., Martin, P. A., Rodrigues, T., Zúñiga, D., Froján, M., de la Granda, F., Villacieros-Robineau, N., Alonso-Pérez, F., Alberto, A., Rebotim, A., González-Álvarez, R., Castro, C. G., and Abrantes, F. (2020). δ18O and Mg/Ca Thermometry in Planktonic Foraminifera: A Multiproxy Approach Toward Tracing Coastal Upwelling Dynamics. *Paleoceanography and Paleoclimatology*, 35(2):1–27.

Sarmiento, J. L., Gruber, N., Brzezinski, M. A., and Dunne, J. P. (2004). High-latitude controls of thermocline nutrients and low latitude biological productivity. *Nature*, 427(6969):56–60.

Schiebel, R. and Hemleben, C. (2005). Modern planktic foraminifera. *Paläontologische Zeitschrift*, 79(1):135–148.

Schiebel, R. and Hemleben, C. (2017). *Planktic Foraminifers in the Modern Ocean*. Springer-Verlag, Berlin.

Schiebel, R., Smart, S. M., Jentzen, A., Jonkers, L., Morard, R., Meilland, J., Michel, E., Coxall, H. K., Hull, P. M., de Garidel-Thoron, T., Aze, T., Quillévéré, F., Ren, H., Sigman, D. M., Vonhof, H. B., Martínez-García, A., Kučera, M., Bijma, J., Spero, H. J., and Haug, G. H. (2018). Advances in planktonic foraminifer research: New perspectives for paleoceanography. *Revue de Micropaleontologie*, 61(3-4):113–138.

Schmid, C., Boebel, O., Zenk, W., Lutjeharms, J. R., and Garzoli, S. L. (2003). Early evolution of an Agulhas Ring. *Deep Sea Research Part II*, 50:141–166.

Schmitt, R. W. and Olson, D. B. (1985). Wintertime convection in warm-core rings: Thermocline ventilation and the formation of mesoscale lenses. *Journal of Geophysical Research*, 90(C5):8823.

Schouten, M., De Ruijter, W. P., van Leeuwen, P. J., and Lutjeharms, J. R. (2000). Translation, decay and splitting of Agulhas rings in the southeastern Atlantic Ocean. *Journal of Geophysical Research*, 105(9):21913–21925.

Sen Gupta, B. K. (2003). *Modern Foraminifera*, volume 36.

Siegel, D. A., Ohlmann, J. C., Washburn, L., Bidigare, R. R., Nosse, C. T., Fields, E., and Zhou, Y. (1995). Solar radiation, phytoplankton pigments and the radiant heating of the equatorial Pacific warm pool. *Journal of Geophysical Research*, 100(C3):4885–4891.

Sigman, D. M. and Casciotti, K. (2009). Nitrogen Isotopes in the Ocean. *Encyclopedia of Ocean Sciences*, (Ms 632):1884–1894.

Sigman, D. M., Casciotti, K. L., Andreani, M., Barford, C., Galanter, M., and Böhlke, J. K. (2001). A bacterial method for the nitrogen isotopic analysis of nitrate in seawater and freshwater. *Analytical Chemistry*, 73(17):4145–4153.

Sigman, D. M., DiFiore, P. J., Hain, M. P., Deutsch, C., Wang, Y., Karl, D. M., Knapp, A. N., Lehmann, M. F., and Pantoja, S. (2009). The dual isotopes of deep nitrate as a constraint on the cycle and budget of oceanic fixed nitrogen. *Deep-Sea Research Part I: Oceanographic Research Papers*, 56(9):1419–1439.

Sigman, D. M., Granger, J., DiFiore, P. J., Lehmann, M. F., Ho, R., Cane, G., and van Geen, A. (2005). Coupled nitrogen and oxygen isotope measurements of nitrate along the eastern North Pacific margin. *Global Biogeochemical Cycles*, 19(4):1–14.

Sigman, D. M., M. A, A., McCorkle, D. C., Francois, R., and Fischer, G. (1999). The δ15N of nitrate in the Southern Ocean: Nitrate consumption in surface waters. *Global Biogeochemical Cycles*, 13(4):1149–1166.

Simon, M. H., Ziegler, M., Barker, S., van der Meer, M. T. J., Schouten, S., and Hall, I. R. (2020). A late Pleistocene dataset of Agulhas Current variability. *Scientific Data*, 7(1):1–12.

Sinha, A., Balwada, D., Tarshish, N., and Abernathey, R. (2019). Modulation of Lateral Transport by Submesoscale Flows and Inertia-Gravity Waves. *Journal of Advances in Modeling Earth Systems*, 11(4):1039–1065.

Smart, S. M., Fawcett, S. E., Ren, H., Schiebel, R., Tompkins, E. M., García, A. M., Stirnimann, L., Roychoudhury, A., Haug, G. H., and Sigman, D. M. (2020). The Nitrogen Isotopic Composition of Tissue and Shell-Bound Organic Matter of Planktic Foraminifera in Southern Ocean Surface Waters. *Geochemistry, Geophysics, Geosystems*, 21:1–29.

Smart, S. M., Ren, H., Fawcett, S. E., Schiebel, R., Conte, M., Rafter, P. A., Ellis, K. K., Weigand, M. A., Oleynik, S., Haug, G. H., and Sigman, D. M. (2018). Groundtruthing the planktic foraminifer-bound nitrogen isotope paleo-proxy in the Sargasso Sea. *Geochimica et Cosmochimica Acta*, 235:463–482.

Sohm, J. A., Webb, E. A., and Capone, D. G. (2011). Emerging patterns of marine nitrogen fixation. *Nature Reviews Microbiology*, 9(July):499–508.

Somes, C. J., Schmittner, A., Galbraith, E. D., Lehmann, M. F., Altabet, M. A., Montoya, J., Letelier, R. M., Mix, A. C., Bourbonnais, A., and Eby, M. (2010). Simulating the global distribution of nitrogen isotopes in the ocean. *Global Biogeochemical Cycles*, 24(4):1–16.

Sousa, S. H., de Godoi, S. S., Amaral, P. G., Vicente, T. M., Martins, M. V., Sorano, M. R., Gaeta, S. A., Passos, R. F., and Mahiques, M. M. (2014). Distribution of living planktonic foraminifera in relation to oceanic processes on the southeastern continental Brazilian margin (23°S-25°S and 40°W-44°W). *Continental Shelf Research*, 89:76–87.

Spero, H. and Williams, D. (1988). Extracting environmental information planktic foraminiferal d13C data.

Spero, H. J. and Parker, S. L. (1985). Photosynthesis in the symbiotic planktonic foraminifer Orbulina universa, and its potential contribution to oceanic primary productivity. *Journal of Foraminiferal Research*, 15(4):273–281.

Spindler, M., Hemleben, C., Salomons, J. B., and Smit, L. P. (1984). Feeding behavior of some planktonic foraminifers in laboratory cultures. *Journal of Foraminiferal Research*, 14(4):237–249.

Stainbank, S., Kroon, D., Rüggeberg, A., Raddatz, J., de Leau, E. S., Zhang, M., and Spezzaferri, S. (2019). *Controls on planktonic foraminifera apparent calcification depths for the northern equatorial Indian Ocean*, volume 14.

Steinhardt, J., De Nooijer, L. L. J., Brummer, G. J., and Reichart, G. J. (2015). Profiling planktonic foraminiferal crust formation. *Geochemistry, Geophysics, Geosystems*, 16(7):2409–2430.

Stramma, L. and Lutjeharms, J. R. (1997). The flow field of the subtropical gyre of the South Indian Ocean. *Journal of Geophysical Research*, 102:5513–5530.

Stramma, L. and Peterson, R. G. (1989). Geostrophic Transport in the Benguela Current Region.

Strickland, J. and Parsons, T. (1968). *A Practical Handbook of seawater analysis*.

Treibergs, L. A., Fawcett, S. E., Lomas, M. W., and Sigman, D. M. (2014). Nitrogen isotopic response of prokaryotic and eukaryotic phytoplankton to nitrate availability in Sargasso Sea surface waters. *Limnology and Oceanography*, 59(3):972–985.

Tuerena, R. E., Ganeshram, R. S., Geibert, W., Fallick, A. E., Dougans, J., Tait, A., Henley, S. F., and Woodward, E. M. S. (2015). Nutrient cycling in the Atlantic basin: The evolution of nitrate isotope signatures in water masses. *Global Biogeochemical Cycles*, 29:1830–1844.

Uhle, M. E., Macko, S. A., Spero, H. J., David W, L., Ruddiman, W. F., and Engel, M. H. (1999). The fate of nitrogen in the Orbulina universa foraminifera-symbiont system determined by nitrogen isotope analyses of shell-bound organic matter. *Limnology and Oceanography*, 44(8):1968–1977.

Uhle, M. E., Macko, S. A., Spero, H. J., Engel, M. H., and Lea, D. W. (1997). Sources of carbon and nitrogen in modern planktonic foraminifera: The role of algal symbionts as determined by bulk and compound specific stable isotopic analyses. *Organic Geochemistry*, 27(3-4):103–113.

Van Aken, H. M., Van Veldhoven, A. K., Veth, C., De Ruijter, W. P., Van Leeuwen, P. J., Drijfhout, S. S., Whittle, C. P., and Rouault, M. (2003). Observations of a young Agulhas ring, Astrid, during MARE in March 2000. *Deep-Sea Research Part II: Topical Studies in Oceanography*, 50(1):167–195.

van Ballegooyen, R. C., Gründlingh, M. L., and Lutjeharms, J. R. (1994). Eddy fluxes of heat and salt from the southwest Indian Ocean into the southeast Atlantic Ocean: A case study. *Journal of Geophysical Research*, 99(94):14053–14070.

Van Oostende, N., Fawcett, S. E., Marconi, D., Lueders-Dumont, J., Sabadel, A. J., Woodward, E., Jönsson, B. F., Sigman, D. M., and Ward, B. B. (2017). Variation of summer phytoplankton community composition and its relationship to nitrate and regenerated nitrogen assimilation across the North Atlantic Ocean. *Deep-Sea Research Part I: Oceanographic Research Papers*, 121(June 2016):79–94.

Wallschuss, S., Mdutyana, M., Parrott, R. G., Forrer, H. J., Roman, R., Walker, D., Ansorge, I., and Fawcett, S. E. (2022). The Influence of Agulhas Leakage on Primary Production and Nitrogen Cycling in the Southeastern Atlantic Ocean. *Journal of Geophysical Research: Oceans*, 127:1–26.

Wang, L., Huang, B., Laws, E. A., Zhou, K., Liu, X., Xie, Y., and Dai, M. (2018). Anticyclonic Eddy Edge Effects on Phytoplankton Communities and Particle Export in the Northern South China Sea. *Journal of Geophysical Research: Oceans*, 123(11):7632–7650.

Wankel, S. D., Kendall, C., Pennington, J. T., Chavez, F. P., and Paytan, A. (2007). Nitrification in the euphotic zone as evidenced by nitrate dual isotopic composition: Observations from Monterey Bay, California. *Global Biogeochemical Cycles*, 21(2):1–13.

Waterson, A. M., Edgar, K. M., Schmidt, D. N., and Valdes, P. J. (2017). Quantifying the stability of planktic foraminiferal physical niches between the Holocene and Last Glacial Maximum. *Paleoceanography*, 32(1):74–89.

Wefer, G., Berger, W. H., Siedler, G., and Webb, D. J. (1996). Central Themes of South Atlantic Circulation. *The South Atlantic*, pages 1–11.

Weigand, M. A., Foriel, J., Barnett, B., Oleynik, S., and Sigman, D. M. (2016). Updates to instrumentation and protocols for isotopic analysis of nitrate by the denitrifier method. *Rapid Communications in Mass Spectrometry*, 30(12):1365–1383.

Weijer, W., De Ruijter, W. P., Sterl, A., and Drijfhout, S. S. (2002). Response of the Atlantic overturning circulation to South Atlantic sources of buoyancy. *Global and Planetary Change*, 34(3-4):293–311.

Wolff, E. W., Fischer, H., Fundel, F., Ruth, U., Twarloh, B., Littot, G. C., Mulvaney, R., Röthlisberger, R., de Angelis, M., Boutron, C. F., Hansson, M., Jonsell, U., Hutterli, M. A., Lambert, F., Kaufmann, P., Stauffer, B., Stocker, T. F., Steffensen, J. P., Bigler, M., Siggaard-Andersen, M. L., Udisti, R., Becagli, S., Castellano, E., Severi, M., Wagenbach, D., Barbante, C., Gabrielli, P., and Gaspari, V. (2006). Southern Ocean sea-ice extent, productivity and iron flux over the past eight glacial cycles. *Nature*, 440(7083):491–496.

Zarkogiannis, S., Kontakiotis, G., and Antonarakou, A. (2020). Recent planktonic foraminifera population and size response to Eastern Mediterranean hydrography. *Revue de micropaleontologie*, 69(100450):1–10.

Chapter 3

Tracing Agulhas Current System biogeochemistry through the nitrogen isotopes of foraminifera

Abstract

This study presents the first nitrogen isotope (δ^{15}N) measurements from living planktic foraminifera in the Agulhas Current System, a region whose thermocline waters are supplied by both tropical ($\delta^{15}N_{NO_3} = 5.8\,‰$) and subtropical ($\delta^{15}N_{NO_3} = 4.9\,‰$) sources. Foraminifera, bulk zooplankton ($> 250\,\mu$m), and suspended particulate organic nitrogen (PON, $> 0.7\,\mu$m) were collected from a series of net tows across a transect perpendicular to the east coast of South Africa along with seawater nitrate. Foraminifer assemblages responded rapidly to changes in the water column, and showed a progressive offshore decrease in tropical *versus* subtropical species corresponding to the shift from tropical- to subtropical-sourced waters. The tissue-bound (FT-)δ^{15}N of symbiont-hosting foraminifera (Globigerinoides ruber and Trilobatus sacculifer) in the subtropical, N-limited waters offshore of the Agulhas Current was within 0.3 ‰ of thermocline nitrate, in line with what has previously been observed in the Sargasso Sea. Winter δ^{15}N PON and FT-δ^{15}N in the tropical core and inshore of the current were roughly equal to that of subtropical PON and foraminifera, despite the relative elevation of tropical thermocline $\delta^{15}N_{NO_3}$ compared to subtropical thermocline $\delta^{15}N_{NO_3}$. The similarity is attributed to differing degrees of nitrate assimilation occurring between the Agulhas Current and the adjacent subtropical waters. FT-δ^{15}N at the furthest offshore section of the transect was low for most species in comparison to the rest of the transect. This decrease in FT-δ^{15}N was also most likely due to partial assimilation, as a cyclonic intrusion had recently supplied new, low-δ^{15}N nitrate to the euphotic zone through the shoaling of the mixed layer and uplift of subtropical thermocline waters. The resulting FT-δ^{15}N within the cyclonic feature was on average 1.2 ‰ lower than foraminifera offshore of the current outside of the feature. On average, subtropical foraminifer FT-δ^{15}N was higher than what was previously recorded in a mature Agulhas eddy in the southeast Atlantic, despite the waters in the eddy having originated from the Agulhas Current. The isotopic difference between the two regions is

indicative of biogeochemical processes, such as N_2 fixation and recycling of ammonium, acting to lower the N isotopic composition of particulate organic matter during Agulhas leakage transport. Recognizing the importance of these additional mechanisms for yielding FT-δ^{15}N variability within mesoscale eddies is meaningful for the development of an Agulhas leakage FT-δ^{15}N palaeoceanographic proxy, and further research is needed to better understand the influence that rapidly shifting nutrient conditions within Agulhas eddies has on PON and foraminifer δ^{15}N.

3.1 Introduction

The Agulhas Current is one of the strongest western boundary currents in the world, and is an important component in global ocean circulation as it drives an exchange of upper ($\sim$700 m) Indo-Atlantic waters (Bryden and Beal, 2001; Van Aken, 2007; Beal et al., 2015). This exchange, termed "Agulhas leakage", occurs south of the African continent, and transports warm, saline Indian Ocean waters northwestwards into the Cape Basin at the point where the fast-moving inertial jet retroflects to form the eastward-flowing Agulhas Return Current (ARC; Gordon, 1985, 1986). Fluctuations in Agulhas leakage are thought to be closely connected to the strength of the Atlantic Meridional Overturning Circulation (AMOC), with Indian Ocean waters acting as a source of negative buoyancy for Atlantic waters (Weijer et al., 2002; Peeters et al., 2004; Biastoch et al., 2008; Beal et al., 2011; Marino et al., 2013; Weijer and van Sebille, 2014; Biastoch et al., 2015). The majority of leakage is transported by eddies (predominantly anticyclonic), whose dynamics inhibit rapid mixing of leaked Indian Ocean water with that of the surrounding cooler, fresher South Atlantic surface waters (Gordon, 1985; Duncombe Rae, 1991).

Because of its role in moderating the convective stability of AMOC, a system that influences global climate (Weijer et al., 2002; Biastoch et al., 2009), the Agulhas region is of considerable interest for palaeoclimatologists who wish to determine the relationship of long-term glacial-interglacial cycles to changes in (local and global-scale) atmospheric and oceanic circulation. Regarding atmospheric circulation, several models and sediment records suggest that, in addition to latitudinal wind shifts (Peeters et al., 2004; Lamy et al., 2007; Bard and Rickaby, 2009), intensification of Southern Hemisphere westerly winds results in increased leakage, whereas a weaker wind intensity correlates with a reduction in leakage (Graham et al., 2012; Durgadoo et al., 2013; Koutsodendris et al., 2014). Regarding oceanic circulation, evidence suggests that the present-day AMOC is weak in comparison to the past millennium, with warmer climates predicted to increase meltwater and further slow the density-driven circulation system (Beal et al., 2011; Thornalley et al., 2018; Caesar et al., 2021; Marcello et al., 2022). Under such conditions, studies suggest that buoyancy compensation through enhanced Agulhas leakage will play a pivotal role in the reestablishment of a more vigorous AMOC state (Van Sebille et al., 2009; Marino et al., 2013; Dyez et al., 2014). However, the extent to which Agulhas leakage can 'balance-out' observed AMOC weakening remains unknown, in large part due to the difficulty of constraining (sub)mesoscale processes that influence Indo-Atlantic exchange of waters (e.g., the shear associated with mesoscale eddies; Weijer et al. 2002; Biastoch et al. 2008, 2009; Beal et al. 2011; Durgadoo et al. 2013).

Changes in the AMOC and Agulhas leakage also have implications for biogeochemical cycling in the southeast Atlantic and southwest Indian Oceans, as the biological pump (i.e., the export of photosynthetically-produced organic matter into the deep ocean through biological and physical processes; Volk and Hoffert 1985) is tightly coupled to the ocean's physical circulation (Galbraith and Skinner, 2020). One way in which glacial-interglacial

biogeochemical changes in the Indo-Atlantic region might be recorded in the fossil record is in the nitrogen (N) isotopes of organic matter in marine sediments and microfossils. During nitrate assimilation, phytoplankton preferentially consume the lighter ^{14}N isotope, leaving the remaining nitrate pool enriched in ^{15}N (Wada and Hattori, 1978; Sigman et al., 1999). As more nitrate is assimilated, the particulate organic nitrogen (PON) produced also increases in $\delta^{15}N$ ($\delta^{15}N = ([(^{15}N/^{14}N)_{sample}] / [(^{15}N/^{14}N)_{N2\ in\ air}] - 1) \times 1000$, per mil, ‰), eventually converging on that of the original nitrate supply ($\delta^{15}N_{NO_3}$) once all the available nitrate is used up (Wada and Hattori, 1978; Altabet and McCarthy, 1986; Sigman et al., 1999; Sigman and Casciotti, 2009). In this way, the $\delta^{15}N$ of PON and the organisms that consume it can be seen as a reflection of the nitrate (and recycled N) conditions during their lifetime. Palaeoceanographic reconstructions are possible through analysis of bulk sedimentary $\delta^{15}N$ and microfossil-bound $\delta^{15}N$, but the former is more susceptible to post-depositional degradation and diagenetic alteration, which are difficult to correct (Altabet and Francois, 1994; Galbraith et al., 2008).

On the other hand, foraminifera, single-celled protists, are particularly well-suited for isotopic analysis, due to the excellent preservation of their calcite tests after burial in most environments, their abundance throughout the global oceans, and their pervasiveness in the fossil record since the mid-Cretaceous (Schiebel and Hemleben, 2005; Ren et al., 2009; Meckler et al., 2011; Ren et al., 2012b; Robinson et al., 2023). Test chambers contain trace amounts of organic N between and within calcite layers; N is therefore held within the shell matrix and appears to be largely protected from degradation upon burial (Martínez-García et al., 2022) Studies of living and recently deposited foraminifera have shown their $\delta^{15}N$ to be a good reflection of thermocline nitrate in low- to mid-latitude oligotrophic regions where surface-layer nitrate is nearly completely consumed (Chapter 2, Ren et al., 2009, 2012b; Smart et al., 2018), in addition to reflecting the degree of summertime nitrate consumption in areas where N is not a limiting factor for primary production (e.g., the Southern Ocean) (Smart et al., 2020).

Foraminifera are adapted to a wide range of environments, with temperature, food availability and light being the dominant predictors of foraminifera species assemblage (Berger, 1969; Ortiz et al., 1995; Rutherford et al., 1999; Kucera, 2007, and references therein). For simplification, species are often classified according to their habitat preference – tropical, subtropical, transitional or mid-latitude, sub-polar or polar – and occupy varying depths within these zones (Bradshaw, 1959; Bé and Tolderlund, 1971; Bé and Hutson, 1977). Individuals obtain N through their diet, which largely consists of detrital particulate organic nitrogen (PON), although many will supplement this through preying on algae, zooplankton or large phytoplankton (Anderson and Sedell, 1979; Bé et al., 1981; Caron et al., 1982; Spindler et al., 1984; Hemleben et al., 1989; Schiebel et al., 2001). More than half of extant foraminifer species appear to make use of photosymbiosis to some extent, housing algal symbionts that make them functionally mixotrophic rather than heterotrophic (Anderson and Sedell, 1979; Spindler et al., 1984; Hemleben et al.,

1989) Some species (e.g., *Orbulina univera, Globigerina ruber, Trilobus sacculifer*) are dependent upon symbionts to survive (obligatory symbiosis), whilst others appear to utilize them facultatively to different degrees (Hallock, 1981; Hemleben et al., 1989; Stoecker, 1998; Uhle et al., 1999; Takagi et al., 2019). Foraminifera with obligatory symbiosis with dinoflagellates tend to be lower in δ^{15}N due to symbionts recycling of low-δ^{15}N ammonium produced by the host, which offsets some (or all) of the expected increase in δ^{15}N gained through trophic enrichment (Ren et al., 2012b; Smart et al., 2018; Lekieffre et al., 2020). Non-symbiont hosting foraminifera found at deeper average living depths are often higher in δ^{15}N, as they excrete the low-δ^{15}N ammonium produced (Ren et al., 2012b; Smart et al., 2018).

In addition to the absence of symbionts, consumption of partially-degraded PON likely contributes to the higher δ^{15}N typically measured for deep-dwellers such as *Globortalia truncatulinoides*, as bacteria decompose suspended PON as it sinks through the water column, preferentially removing ^{14}N and leaving the remaining particles higher in δ^{15}N (Saino and Hattori, 1980; Altabet and McCarthy, 1986; Altabet et al., 1991; Lehmann et al., 2002; Mobius, 2013). There is also evidence of *Globigerina bulloides*, a non-dinoflagellate-hosting species, directly assimilating low-δ^{15}N ammonium (Bird et al., 2020), which is consistent with several ground-truthing studies that have found its δ^{15}N to be more similar to dinoflagellate-hosting species or between that of the symbiont-hosting foraminifera and asymbiotic intermediate-dwellers (Smart et al., 2018, Chapter 2).

Initial studies indicate that the annually integrated δ^{15}N of certain species of foraminifera accurately reflects that of the local thermocline nitrate (i.e., the immediate nitrate supply to the surface layer; Ren et al. 2009; Li et al. 2019; Smart et al. 2018). Dinoflagellate-hosting foraminifera appear to most closely match thermocline nitrate δ^{15}N in the Sargasso Sea, whilst non-symbiotic species appear to be a better approximation in the South Atlantic (Chapter 2). The similarity of foraminifer δ^{15}N to thermocline nitrate is a key point of interest in terms of reconstructing past climate, as thermocline nitrate is the main source of N to the euphotic zone, and changes in its δ^{15}N are indicative of a change in source waters or net gains and losses in bioavailable N (Altabet, 1988; Knapp et al., 2005).

3.2 Study region and aims

The Agulhas Current transports both tropical and subtropical water masses, which are isotopically distinct from one another (Marshall et al., 2023). Instead of mixing together to form a homogenous poleward-flowing current, the tropically- and subtropically-sourced water masses remain largely separate, generating steep isopycnal gradients (shear) within the current itself (Beal et al., 2006, Fig. S.1). The δ^{15}N of foraminifera in the Agulhas Current System (ACS) should, to some extent, reflect the variable sources and processes acting on the $\delta^{15}N_{NO_3}$ of these water masses. The most significant (with an

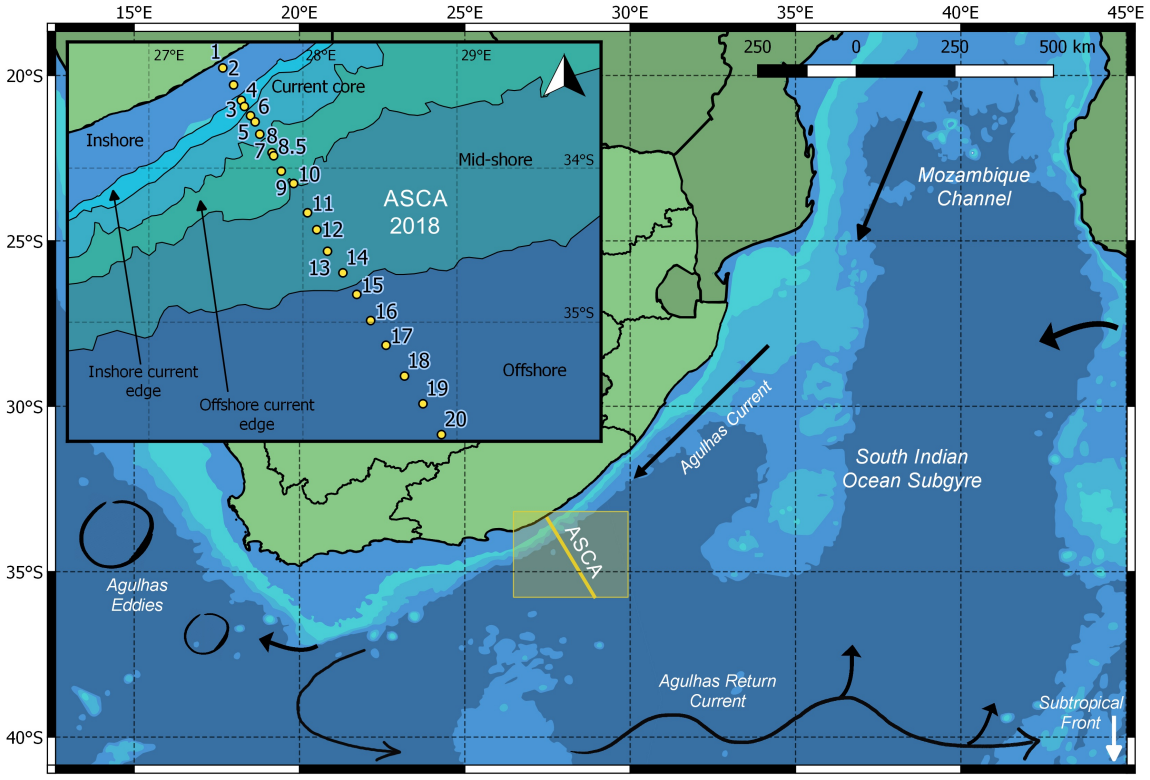

Figure 3.1: Map of the study area, showing the Agulhas System Climate Array (ASCA) (yellow box and map inset) and surrounding southwest Indian Ocean. The large map shows bathymetry (coloured contours) at 200 m, 1000 m and at 1000 m intervals thereafter. Coloured sections in the map inset represent zones mentioned in text. Note that station 6 has a repeat sample (labelled in text as station 6.5), and station 8.5 is an addition (non-ASCA line) station sampled on the inward journey. Black arrows indicate the direction of upper ocean transport.

estimated volume contribution of $\sim 54\%$ to the Agulhas Current; Ridderinkhof et al. 2010; Beal et al. 2015; Ponsoni et al. 2016; Marshall et al. 2023) contributor to the current is subtropical waters from the South Indian Ocean subgyre (referred to as the subgyre hereafter). The subgyre, which is defined as the region of anticyclonic circulation that occurs between 30 and 40°S, and whose eastern boundary lies at roughly 70°E (Fig. 3.1), is primarily made up of recirculation of its own waters (Gordon et al., 1987; Valentine et al., 1993; Stramma and Lutjeharms, 1997; Biastoch et al., 1999; De Ruijter et al., 1999; Palastanga et al., 2007). Initial measurements of subtropical thermocline waters (STTW, $25.5\,\mathrm{kg.m^{-3}} < \sigma_\theta < 26.4\,\mathrm{kg.m^{-3}}$, where σ_θ is potential density) indicate its $\delta^{15}N_{NO_3}$ to be $\sim 4.9\,‰$, lower than that of Subantarctic Mode Water (SAMW, $26.4\,\mathrm{kg.m^{-3}} < \sigma_\theta < 27.0\,\mathrm{kg.m^{-3}}$, $\delta^{15}N_{NO_3} \sim 6.9\,‰$), the water mass below it and the ultimate source of nitrate to the thermocline and euphotic zone (Marshall et al., 2023). SAMW forms in the winter mixed layers north of the Subantarctic Front in the Southern Ocean, and is the source of nutrients to Pacific, Atlantic and Indian Ocean thermocline waters as it flows northwards (McCartney and Woodgate-Jones, 1991; Sloyan and Rintoul, 2001; Sarmiento et al., 2004; Herraiz-Borreguero and Rintoul, 2011); the comparatively

low $\delta^{15}N_{NO_3}$ of STTW relative to SAMW indicates remineralization of low-$\delta^{15}N$ organic matter (the product of N_2 fixation; Hoering and Ford 1960) in the local thermocline (Marshall et al., 2023).

The second source region to the Agulhas Current is the Mozambique Channel, which supplies (via eddies) a smaller volume (contributing an estimated 22% to the total Agulhas Current volume; De Ruijter et al. 2002; Ridderinkhof et al. 2010; Beal et al. 2015; Marshall et al. 2023) of warmer, fresher tropical waters to the inshore of the Agulhas Current (Gordon et al., 1987; Stramma and Lutjeharms, 1997; Donohue and Toole, 2003; Beal et al., 2006). The $\delta^{15}N_{NO_3}$ of nitrate in tropical thermocline waters (TTW) is also lower than the $\delta^{15}N_{NO_3}$ of SAMW, but higher than that of the subtropical thermocline, at $\sim$5.8 ‰ (Marshall et al., 2023) The third source to the Agulhas Current includes waters transported by the South East Madagascar Current ($\sim$ 24% of the total Agulhas Current volume), where the majority of thermocline waters are subtropical (Gordon, 1986; Stramma and Lutjeharms, 1997; Karstensen and Quadfasel, 2002; De Ruijter et al., 2004; Beal et al., 2015).

Since the thermocline nitrate $\delta^{15}N$ in the Agulhas region (4.9 ‰-5.8 ‰, Marshall et al. 2023) is lower than what was measured in the southeast Atlantic in Chapter 2 (6.9 ‰), should foraminifera in the Indo-Atlantic region (i.e., the ocean region encapsulating the southeast Atlantic and southwest Indian Oceans, and the gateway area through which Agulhas leakage occurs) approximate thermocline nitrate $\delta^{15}N$, then foraminifera may "track" the leakage of Agulhas waters, through the sinking of (relatively low-$\delta^{15}N$) leakage-inhabiting foraminifera to the sea floor. Initial results from Chapter 2 are encouraging, with the mixed-layer $\delta^{15}N_{NO_3}$ of an Agulhas eddy and its residing foraminifera community found to be low relative to background South Atlantic waters. Agulhas leakage consists of both tropical and subtropical waters, but the latter is thought to contribute a larger volume (Durgadoo et al., 2017; Marshall et al., 2023), and the isotopic difference in leakage and non-leakage foraminifera ($\sim$2.4 ‰, Chapter 2) was roughly similar to the $\delta^{15}N_{NO_3}$ difference observed between the South Atlantic thermocline and Subtropical thermocline nitrate sources ($\sim$2 ‰). However, the FT-$\delta^{15}N$ of foraminifera living in the Agulhas Current and adjacent subgyre have not yet been measured. A comparison between FT-$\delta^{15}N$ from the South Atlantic and Agulhas Current is necessary to understand whether the leakage signal is a true reflection of southeast Indian Ocean N-cycling, and whether foraminifera in both regions have a similar relationship to thermocline or mixed layer nitrate with regards to nitrogen isotopes.

This study primarily aims to (1) investigate the relationship between foraminifera $\delta^{15}N$ and thermocline $\delta^{15}N_{NO_3}$ in the greater ACS; (2) discuss the impact of having distinct tropical and subtropical habitats within the ACS region on foraminifera assemblages and FT-$\delta^{15}N$; and (3) determine whether the low FT-$\delta^{15}N$ previously observed in a mature Agulhas anticyclonic eddy is an accurate reflection of Agulhas Current conditions, or whether there are additional biogeochemical processes that act to modify FT-$\delta^{15}N$ down-

stream of the transect sampling region (west of 27°E) or post ring-shedding. In answering these questions, this research contributes to the broader objective to assess the potential viability of using foraminifera (shell)-bound (FB-)δ^{15}N as a palaeoceanographic proxy for past Agulhas leakage variability.

3.3 Methods

Samples used in this study were collected along the Agulhas System Climate Array (ASCA) transect line offshore of South Africa in July 2018 on board the R/V *S.A. Agulhas II*. The ASCA line consists of 20 moored stations (Fig. 3.1), all of which were sampled for nitrate isotopes during the cruise on the outgoing journey. An additional two stations were sampled during the return trip, one of which was positioned between stations 8 and 9 (at the current's offshore edge), whilst the other was located in the same location of station 6 (in the current's core). The station closest to the coast was located at 33.35°S 27.48°E; the furthest offshore station was at 35.73°S 28.90°E. The CTD rosette was equipped with a Sea-Bird Electronics CTD, fluoresence sensors, and Niskin bottles, which collected water samples at targeted depths during the cast. Inorganic nutrient nitrate concentrations were determined on board while samples for nitrate isotope analysis were collected in Nalgene HDPE tubes and stored at −20°C until processing.

Between six and eight bulk PON samples were taken at each station across the depth range of 5-200 m. Four litres of seawater per sample (total n = 146 samples) were filtered through 0.3 μm glass fibre filters (either 47 mm or 25 mm in diameter) that were frozen at −20°C. Bongo net oblique tows were performed at 12 stations using a double 1 m2 (250 μm) plankton net. Nets were lowered to a depth of 200 m and then brought up for a total deployment time of around 20 minutes. After rinsing everything from the nets into a bottle, 10% of the sample was removed and size fractionated with sieves (2000 μm, 1000 μm, 500 μm, 250 μm, 150 μm) and filtered onto pre-combusted glass fibre filters for bulk zooplankton isotope analysis. Size-fractionated samples were stored at −20°C. pH-buffered formalin (10% of the sample volume) was added to the remaining 90% of the sample, which was then refrigerated until processing.

3.3.1 Processing and isotope analyses

Bulk zooplankton and PON isotope analyses were conducted at the Stable Light Isotope Laboratory at the University of Cape Town. Size-fractionated zooplankton filters were freeze dried, before between 0.1 and 0.8 mg of material from each size-fractionated zooplankton filter was transferred to a tin cup for δ^{15}N analysis. Empty tin cups were run as blanks. Bulk zooplankton samples (mostly small size fractions) that could not be removed from the filter were quartered, transferred to tin cups, and run separately, with unused pre-combusted filters included as blanks. For PON, a 15.4 mm diameter corer was used to obtain two filter cores per sample, which were then also placed in tin cups for N content

measurements and isotopic analysis. The δ^{15}N analysis for both sets of samples were subsequently carried out using a Delta V Plus isotope ratio mass spectrometer (IRMS) coupled to a Flash elemental analyzer 112 series with a detection limit of 1 μg N. In-house standards (Choc, Merck Gel and Valine) calibrated to international reference materials were used to calibrate sample δ^{15}N measurements to atmospheric N_2.

Seawater samples from a 2016 occupation of the ASCA transect undertaken in the same month (July) were also used in this study (Marshall et al., 2023). These samples had already been measured for the δ^{15}N and δ^{18}O of nitrate (where $\delta^{18}O = \delta^{18}O/^{16}O$) and this data can be found at `https://doi.org/10.5281/zenodo.7628608`. Several seawater profiles from the 2018 cruise were processed in the same way for comparison. Frozen samples collected in 2018 were defrosted and filtered to remove particles before being shipped to the Max Planck Institute for Chemistry, where the remainder of the processing and analysis took place. For nitrate-only δ^{15}N and δ^{18}O analysis, nitrite was removed through the addition of sulfamic acid (Granger and Sigman, 2009). After allowing at least 10 minutes for the reaction to take place, the pH was raised to 6-8 using NaOH. Nitrate was then converted to N_2O gas using the denitrifier method (Sigman et al., 2001) before being measured by a Thermo MAT253 gas chromotography-isotope ratio mass spectrometer (GC-IRMS) with custom-built inline N_2O extraction and purification system (Weigand et al., 2016). Measurements were calibrated to the international reference scales using USGS-34 and IAEA-NO-3 nitrate reference materials (Gonfiantini et al., 1995; Böhlke et al., 2003) as well as an in-house nitrate standard, and are reported relative to atmospheric N_2. The pooled standard deviation of replicates was 0.2 ± 0.3 ‰ δ^{15}N, and 0.5 ± 0.5 ‰ for δ^{18}O.

Foraminifera from the formalin-preserved samples were rinsed through a 1000 μm-mesh sieve with deionized water before undergoing a density separation with 200 g.L^{-1} NaCl solution using 40 mL Falcon tubes (Ren et al., 2012b; Smart et al., 2020). The remaining material was allowed to dry in petri dishes for 1-2 days under a fume hood. Once dry, foraminifera were picked under a microscope and individual species were separated and counted. Triplicates of between 3 and 9 individuals of each species were selected per measurement (where specimen numbers were low, duplicate measurements were made). Specimens were cleaned and weighed according to the protocol outlined in Chapter 2. After weighing, cleaning and crushing samples, 1 mL of persulfate oxidising reagent (POR, see Smart et al. (2020) and Chapter 2 for recipe) was added to each vial to convert organic N in the foraminifera tissue to nitrate, including 10 POR-only (blank) vials per run and a dilution sequence of amino acid standards (USGS-40, USGS-41 and USGS-65). Samples were autoclaved for 65 minutes on a slow vent setting and pH-adjusted with HCl to between 5 and 7 (Ren et al., 2012b). Nitrate concentrations for each sample were measured using chemiluminescence (Braman and Hendrix, 1989), after which the nitrate was converted to N_2O via the denitrifier method and measured for δ^{15}N as described above. The foraminifera tissue δ^{15}N measurements were corrected for POR oxidation blanks,

which on average contributed 7.6% to the total N (sample+blank) N content. Duplicates (different specimens of the same species from the same station) were oxidised in separate batches and measured during separate GC-IRMS runs. Pooled standard deviation of all duplicate samples of 0.46 ‰ (n = 248).

3.4 Results

3.4.1 Station classification and physical oceanography

Each of the 22 stations sampled across the ASCA line were classified into oceanographic zones for the purposes of this study (Fig. 3.1). Physical oceanographic properties (e.g., velocity, density and salinity) were used to characterize water masses and to delineate zones with different water column structures in the ACS. Waters at stations 1 and 2 were tropically-sourced, and are inshore of the current. Stations 3 and 4 comprised the inshore edge of the current core; stations 5, 6, 22 (the repeat sampling at station 6's coordinates) and 7 were positioned within the current's core. Stations 8 and 9 were located at the current's offshore flank (subtropically-sourced), where the isopycnal gradient is less steep than that observed at the inshore edge (stations 3 and 4). The waters offshore of the Agulhas Current were further divided into mid-shore (stations 10 - 15) and offshore (stations 16-20) due to a noticeable uplift of thermocline waters evident in stations 16 to 20. From satellite sea-surface height anomaly and SST data (Global Reanalysis Multi-Model Ensemble Product GREP, not shown), this feature appears to be a two-week old cyclonic eddy that was cut off from the Agulhas Return Current-Subtropical Convergence, and subsequently moved northeastwards through the South Indian Ocean subgyre towards the coast. In this study, we use the term "cyclonic eddy" or "cyclonic intrusion" when referring to this eddy and its effect on the transect region. The 2016 nitrate isotope dataset was similarly classified (see Marshall et al. 2023), with the omission of a mid-shore classification, since the aforementioned cyclonic intrusion was not present in 2016.

During the 2016 transect, the core of the Agulhas Current lay roughly 30 km offshore, and contained clear evidence of low density Tropical Surface Water (TSW, $< 24.5\,\mathrm{kg.m^{-3}}$, Beal et al. 2006) in the upper 100 m (Marshall et al., 2023). In 2018, the current was further offshore ($\sim$45 km), and was composed of higher density waters at the surface ($> 24.5\,\mathrm{kg.m^{-3}}$; Fig. 3.2), which indicate more thorough mixing of TSW with the thermocline waters below (Tropical Thermocline Water, TTW, 24.5-26.4 $\mathrm{kg.m^{-3}}$). SAMW ($> 26.4\,\mathrm{kg.m^{-3}}$) was present inshore of the current during both years, but shoaled to the surface in 2016 whilst remaining below 150 m in 2018. We use the 25.5 $\mathrm{kg.m^{-3}}$ isopycnal as an indication of the base of the mixed layer offshore of the current, as the the isopycnal largely coincides with the mixed layer depth (MLD, although strong vertical advection inshore decouples this relationship; Marshall et al. 2023). Whereas the deepest mixed layers (> 200 m) in 2016 were found furthest offshore, the 25.5 $\mathrm{kg.m^{-3}}$ isopycnal shoaled east of

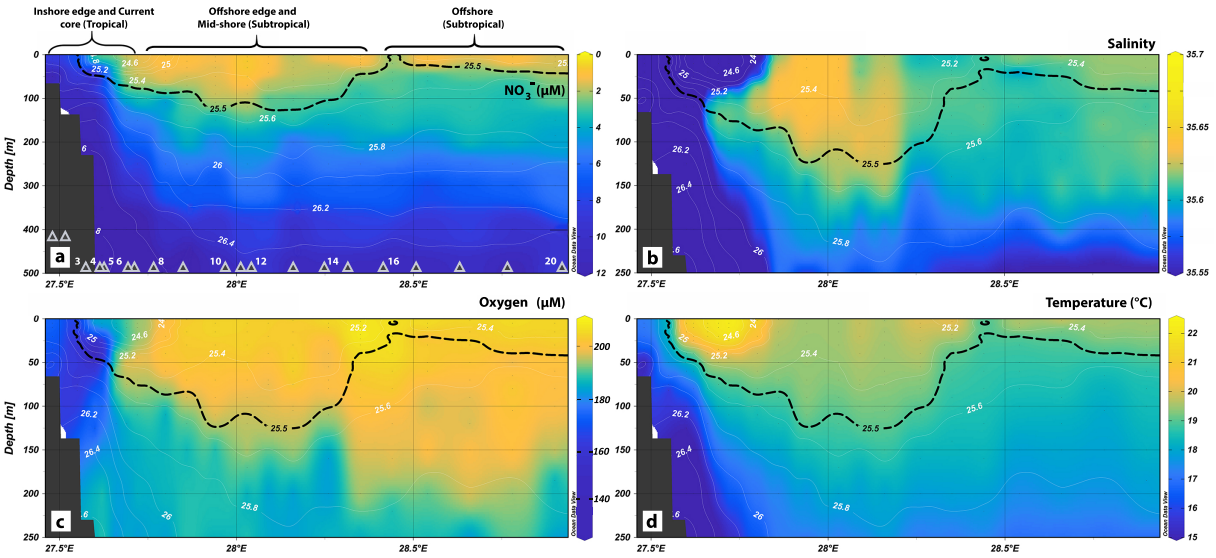

Figure 3.2: Depth sections of the Agulhas System Climate Array (ASCA) transect (from west to east), showing (a) nitrate concentrations (note the difference in depth relative to b, c and d). (b) salinity, (c) oxygen concentration, and (d) temperature. White lines denote contours of potential density, with the 25.5 kg.m^{-3} line (taken as mixed layer depth) emphasized in black. Stations are indicated by grey triangles in (a), and stations where net tows occurred are numbered. Zones mentioned in text are shown at the top of (a).

28.4°E to the surface (< 20 m) in 2018. The shoaling was caused by the 400 m-thick layer of cooler, denser subtropical thermocline waters uplifted by the cyclonic intrusion, which brought nutrients closer to the surface east of station 16 (34.99°S; 28.44◦E). A further distinction between the two transects was the position of the low-oxygen (140 μm) water mass, TTW, which lay below the current (50-200 m) in 2016 but extended inshore closer to the surface (0-150 m) in 2018 (Fig. 3.2c).

3.4.2 Nitrate concentrations and isotope ratios

Nitrate concentrations and isotopes for 2018 were similar to those reported for 2016 (Table 3.1, Fig. 3.3, Fig. 3.4; Marshall et al. 2023). For both years, thermocline calculations excluded waters that were within the appropriate density range but exhibited an assimilation signal (rising $\delta^{15}N_{NO_3}$ with decreasing concentration for a given profile), to better approximate the original nitrate supply to the mixed layer (i.e., before assimilation). The thermocline nitrate concentrations in 2018 decreased with increasing distance from shore (Fig. 3.2a); mean TTW nitrate was 8.5 ± 1.1 μm across the four stations closest to the coast, and mean STTW nitrate concentration for all the mid- and offshore stations was 5.6 ± 0.6 μm. Average $\delta^{15}N_{NO_3}$, $\delta^{18}O_{NO_3}$, and Δ(15-18) for TTW was 6.0 ± 0.3 ‰, 2.8 ± 0.3 ‰, and 3.2 ± 0.1 ‰, respectively, while STTW averages were 5.5 ± 0.2 ‰, 3.4 ± 0.7 ‰, and 2.0 ± 0.6 ‰, respectively. Δ(15-18), defined as the difference between the nitrogen and oxygen isotopes of nitrate, is used in studies to highlight where N-cycling processes decouple the near 1:1 relationship that exists between $\delta^{15}N_{NO_3}$ and $\delta^{18}O_{NO_3}$ during assimilation (e.g., the introduction of low $\delta^{15}N_{NO_3}$ due to N_2 fixation

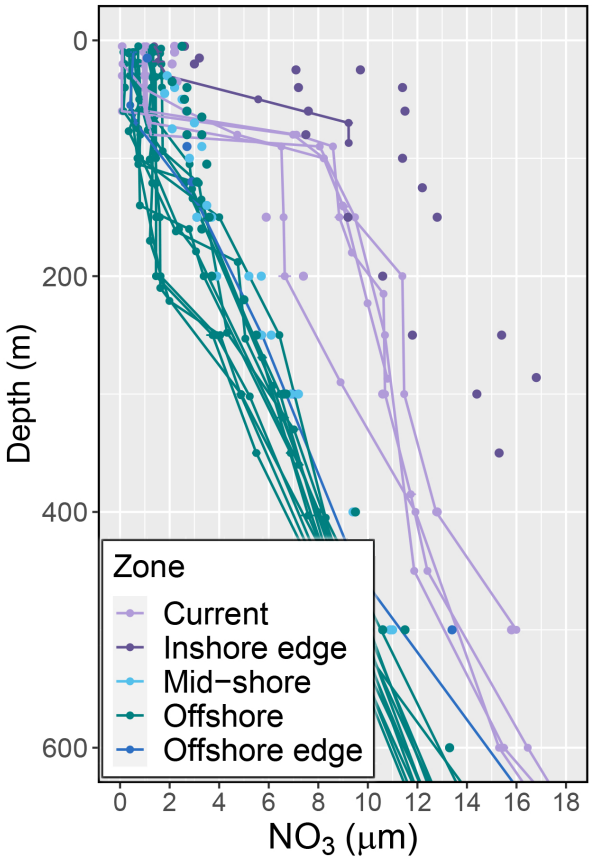

Figure 3.3: Vertical profiles showing nitrate concentration for seawater nitrate samples collected from the Agulhas System Climate Array (ASCA). Lines represent data from 2016 and non-joined points represent 2018 data. Colours correspond to zones mentioned in-text.

lowers $\delta^{15}N_{NO_3}$ relative to $\delta^{18}O_{NO_3}$, lowering the Δ(15-18), Sigman et al. 2005; Rafter et al. 2013). Mixed layer nitrate concentrations also decreased from offshore ($7.1 \pm 3.8\,\mu$m at station 3 to a low of $1.1 \pm 0.0\,\mu$m at station 17 in 2018). Average tropically-sourced, mixed layer nitrate for current core stations (3 - 5) was $6.0 \pm 1.4\,\mu$m compared to $1.6 \pm 0.4\,\mu$m for mid- and offshore stations combined. In the mixed layer, $\delta^{15}N_{NO_3}$ was higher offshore; in the current core it was $5.8 \pm 0.6\,‰$, while for mid- and offshore stations combined it was $6.7 \pm 1.9\,‰$. Mixed layer $\delta^{18}O_{NO_3}$ increased across the transect, from $2.6 \pm 0.5\,‰$ in the current core to $5.8 \pm 0.5\,‰$ offshore of station 9 (resulting in a Δ(15-18) of 3.2 ‰ and 0.9 ‰, respectively).

The similarity of the 2018 data to those acquired on the 2016 cruise (Table 3.1) indicates interannual stability of nitrogen isotopes in the thermocline at least across the two sampling years. We therefore use the mean water mass values from Marshall et al. (2023) when discussing broad trends in ACS N-cycling due to that study presenting a fuller dataset, unless otherwise stated (e.g., when comparing different pools of N at a specific station).

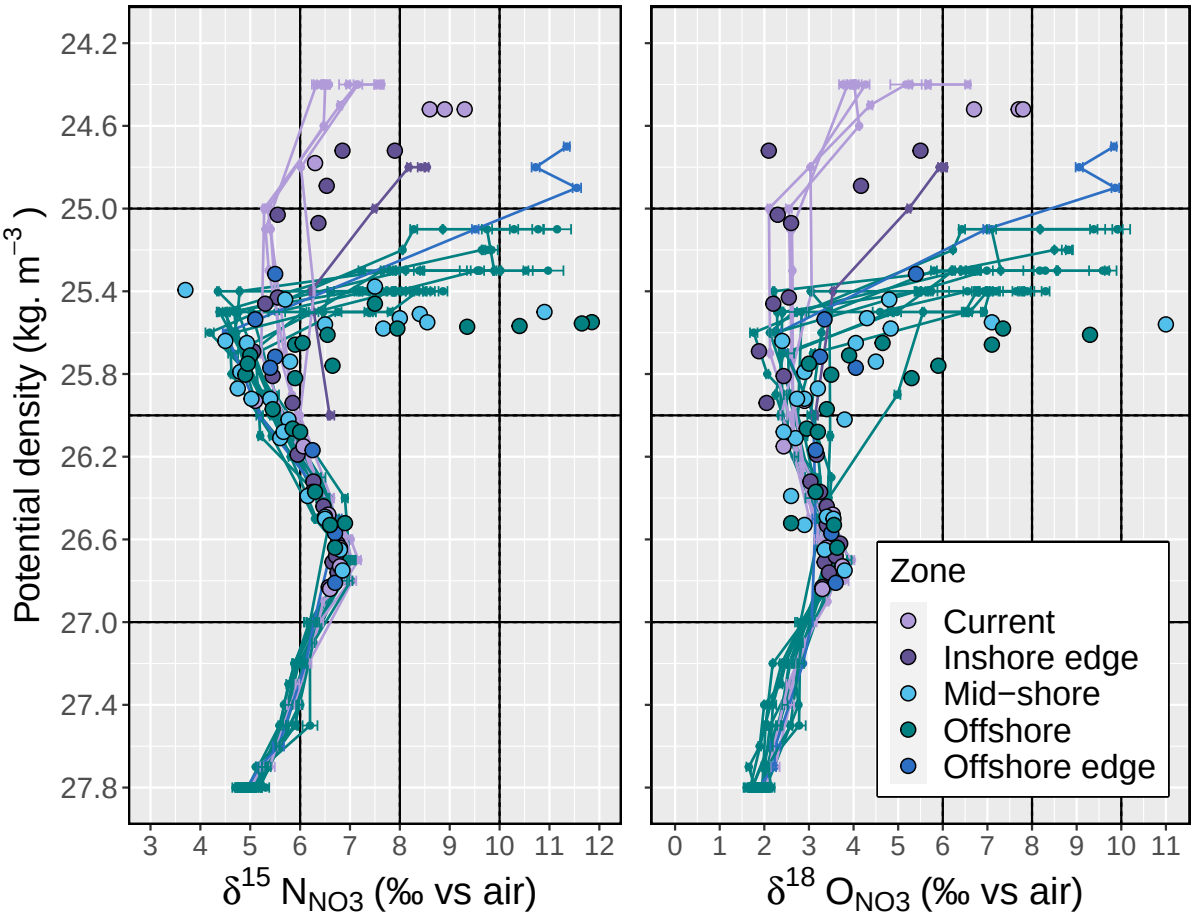

Figure 3.4: Potential density profiles showing (a) $\delta^{15}N_{NO_3}$; and (b) $\delta^{18}O_{NO_3}$ for seawater nitrate samples collected from ASCA. Lines represent data from 2016 and non-joined points represent 2018 data. Colours correspond to zones mentioned in-text.

3.4.3 Organic N: PON and Bulk Zooplankton

There was no significant change in particulate organic nitrogen ($\delta^{15}N_{PON}$) between 0 and 200 m water depth, such that the measurements were averaged for each station. Average $\delta^{15}N_{PON}$ ranged from 0.9 ± 0.1 ‰ at station 16 to 3.9 ± 0.1 ‰ at station 13 (Fig. 3.5, small black circles). $\delta^{15}N_{PON}$ in the current core (TSW, n = 4 stations) averaged 2.4 ± 0.2 ‰. The stations at the current edges and inshore of the current were similar, at 2.4 ± 0.2 ‰ (n = 5) and 2.2 ± 0.1 ‰ (n=2) respectively. Mid-shore stations (STSW) were higher in comparison (3.2 ± 0.2 ‰, n = 6) and offshore stations (STSW) were lower (1.3 ± 0.1 ‰, n = 4).

Three out of twelve stations sampled for bulk zooplankton were located in the current core (stations 5, 6, and 6.5), and were measured for $\delta^{15}N$ of bulk size-fractionated zooplankton ($\delta^{15}N_{zoo}$) (Fig. 3.5, black symbols). Combining size classes of 250-500 μm and 500-1000 μm together gave an average of 5.9 ± 0.1 ‰. As with PON, stations at the current's edges had similar $\delta^{15}N_{zoo}$ values to the current core, although higher $\delta^{15}N$ zoo was measured at the inshore (tropical) edge relative to the offshore (subtropical) boundary (6.3 ± 0.2 ‰, n = 2, vs 5.7 ± 0.1 ‰, n = 3, respectively). Mid-shore $\delta^{15}N_{zoo}$ was also

Table 3.1: Comparison of the nitrate isotope and concentration data for water masses along the Agulhas System Climate Array (ASCA) in 2016 and 2018. Water masses include Tropical Thermocline Water (TTW), Subtropical Thermocline Water (STTW), Subantarctic Mode Water (SAMW), Tropical Surface Water (TSW) and Subtropical Surface Water (STSW). Values followed by * indicate a small sample set (n = 6)

	2016				**2018**			
	$\delta^{15}N_{NO_3}$ (‰)	$\delta^{18}O_{NO_3}$ (‰)	$[NO_3^-]$ (μM)	Δ(15-18) (‰)	$\delta^{15}N_{NO_3}$ (‰)	$\delta^{18}O_{NO_3}$ (‰)	$[NO_3^-]$ (μM)	Δ(15-18) (‰)
TTW	5.8 ± 0.7	2.7 ± 0.3	7.5 ± 1.9	3.0 ± 0.4	6.0 ± 0.3	2.8 ± 0.3	8.5 ± 1.1	3.2 ± 0.1
STTW	4.9 ± 0.4	2.9 ± 0.7	4.8 ± 1.2	2.2 ± 0.8	5.5 ± 0.2	3.4 ± 0.7	5.6 ± 0.6	2.0 ± 0.6
SAMW	6.9 ± 0.2	3.4 ± 0.2	13.7 ± 3.2	3.4 ± 0.1	6.6 ± 0.1	3.4 ± 0.4	13.6 ± 2.7	3.3 ± 0.4
TSW	6.0 ± 1.6	3.2 ± 2.0	3.0 ± 2.7	2.5 ± 0.4	5.9 ± 0.4 *	2.5 ± 0.4 *	6.0 ± 1.4 *	3.1 ± 0.0 *
STSW	7.2 ± 1.3	6.0 ± 1.4	1.3 ± 0.6	1.2 ± 0.6	6.6 ± 1.8	4.9 ± 1.0	1.6 ± 0.4	0.9 ± 2.2

similar to that of the core, at 5.8 ± 0.1 ‰ (n = 3), but offshore stations once again had a noticeably lower $\delta^{15}N_{zoo}$ of 3.8 ± 0.1 ‰ (n = 2).

The calculated difference between bulk zooplankton (combined size classes) and PON $\delta^{15}N$ at each station ranged from 2.6 ‰ (station 5) to 4.3 ‰ (station 3) and averaged 3.4 ± 0.6 ‰. The difference between the averages among the classified zones steadily decreased with distance from shore, from 4.0 ‰ at the inshore current boundary to 2.6 ‰ at the offshore stations. Pearson correlation coefficient and paired t-tests of $\delta^{15}N$ for size classes 250-500 μm and 500-1000 μm against the weighted average PON $\delta^{15}N$ indicate a significant ($p << 0.05$) strong positive ($R^2 > 0.5$ in both cases) correlation between the $\delta^{15}N$ of PON and bulk zooplankton.

3.4.4 Foraminifera

3.4.4.1 Species and abundance

The species observed in the ACS consisted of a mix between tropical and subtropical species. Tropical species included *Trilobus* (previously classified as *Globigerinoides*) *sacculifer*, *Pulleniatina obliquiloculata, Globorotalia menardii, Globigerinoides ruber* and *Globigerinella siphonifera*. Note that although classified here as a tropical species, cryptic forms of *G. siphonifera* have also been found in subtropical regions, and this species occupies a broad range of environmental conditions (Bijma et al., 1998; De Vargas et al., 2002; Lombard et al., 2011; Seears et al., 2012). Likewise, *G. bulloides* is an opportunistic species that has been found near-ubiquitously throughout the world's oceans (Bé and Hutson, 1977; Prell and Curry, 1981; Ufkes et al., 1998; Morard et al., 2013); here, we classify *G. bulloides* as subtropical due to its optimum growth temperature being low in comparison to Agulhas Current SST ($\sim$13°C *versus* $\sim$20°C (Fig. 3.2d), Prasanna et al. 2016). Other species classified as subtropical included *Globorotalia truncatulinoides, Globoro-*

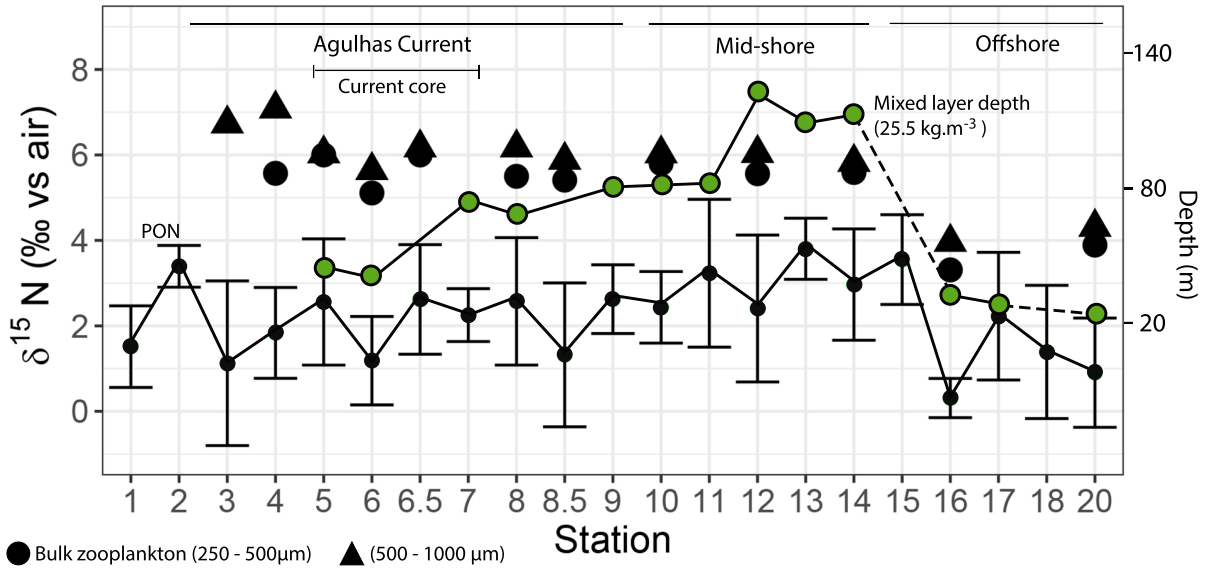

Figure 3.5: Agulhas System Climate Array (ASCA) station δ^{15}N data for PON (weighted average for 0-150 m depth) and bulk, size-fractionated zooplankton (black circles = 1250˘500 μm size class; triangles = 500-100 μm size class), compared to mixed layer depth (secondary y axis, 25.5 kg.m^{-3}, green circles). Stations are positioned west to east. Zones are labelled at the top of the plot; the Agulhas Current label includes both the in- and offshore edges, with the core current labelled below. Error bars for PON show standard deviation.

talia hirsuta, and *Globorotalia inflata*. Other species present along the ASCA line that occur across a wide range of water temperatures included *Orbulina universa, Globigerinita glutinata, Neogloboquadrina dutertrei*, and *Globigerinella calida*.

There was a shift from tropical foraminifera dominance inshore of the current to subtropical dominance offshore (Fig. 3.6). Tropical species *G. siphonifera, Trilobatus sacculifer* and *Globigerinoides ruber* together made up more than 50% of the total assemblage at stations 3 - 5. The relative abundance of subtropical *G. inflata* increased steadily from west to east, peaking at 80% at station 16. Despite being a shoreward-bound repeat of station 6, the species composition of station 6.5 was quite different. Station 6.5 consisted of a larger proportion of *G. inflata* and *G. bulloides* (34% combined at station 6.5 *versus* 6% at station 6), whereas on the outward-bound sampling of station 6, the tropical component was much greater (> 80% of the total assemblage).

G. inflata was found to consistently make up the largest percentage of the subtropical species. Overall, there was a larger diversity of tropical species, and the relative dominance of each varied by station. However, of the stations where tropical foraminifera dominated the assemblages, station 3 is unique in that *T. sacculifer* was almost non-existent, to the point where the species was better represented at some of the subtropical stations (e.g., stations 14 and 20). While we do not know the absolute abundances of foraminifera at each station, the similar towing time (∼20 minutes) at all stations likely means that our highest and lowest counts reflect environmental signals (rather than sampling bias). Thus, foraminifera were likely most abundant at stations 5 (current core) and 10 (mid-shore), and least abundant at stations 3 (inshore), 16 and 20 (offshore).

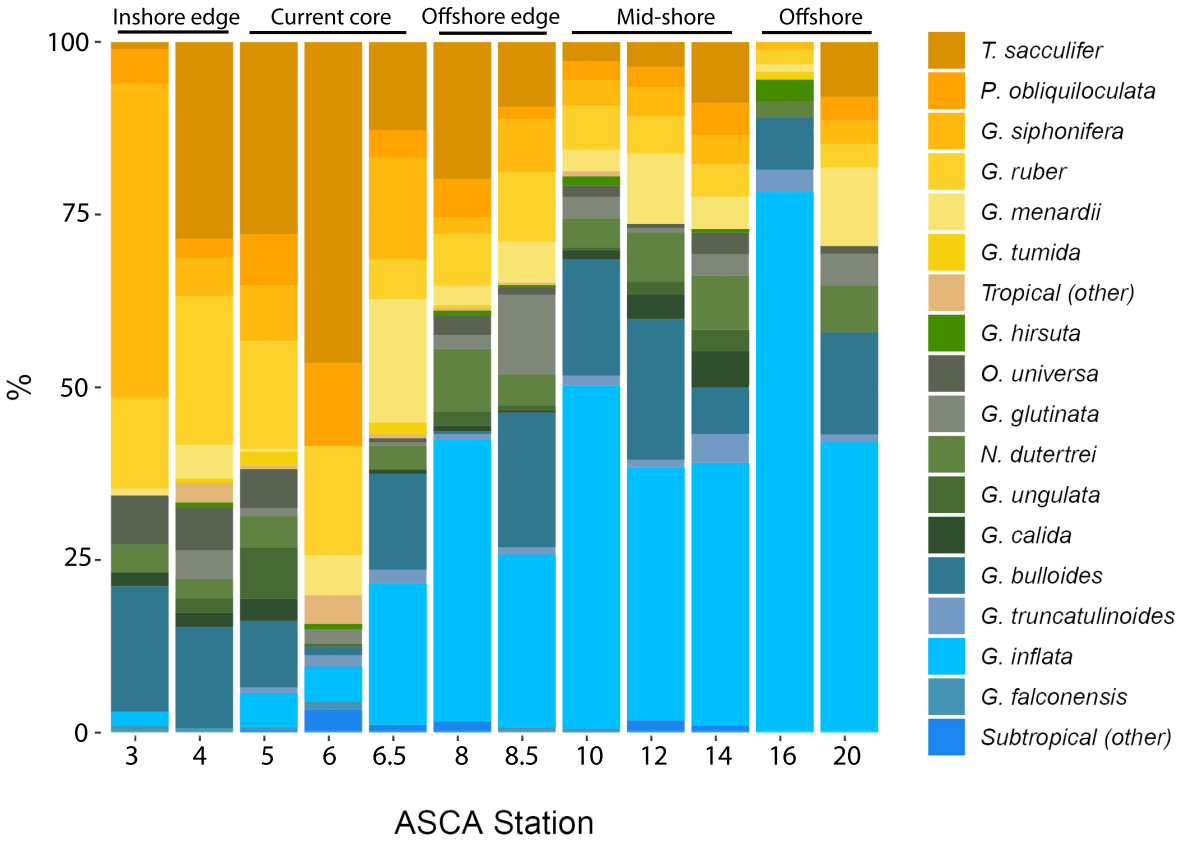

Figure 3.6: Foraminifera assemblages collected from net tows along the Agulhas System Climate Array (ASCA) 2018. Yellow bars represent species previously associated with warm, tropical waters. Blue bars represent species found in cooler, subtropical regions. Green bars represent cosmopolitan species. Rare species in our study were classified as 'other'. 'Tropical (other)' species include *G. pelagica*, *G. radians*, *G. rubescens*, *G. hexagonus* and *G. conglobatus*; 'Subtropical (other)' consists of *N. incompta*, *G. uvula* and *G. scitula*.

3.4.5 N isotopes

3.4.5.1 General trends

For data analysis, foraminifera were divided into groups according to physiology (spinose and non-spinose), primary habitat (shallow, intermediate, deep), and symbiotic status. The resultant six groups were based on the literature (Malmgren et al., 1983; Coulbourn et al., 1980; Hemleben et al., 1989; Takagi et al., 2019) and are referred to by their most distinguishing characteristics: (1) Spinose & symbionts (*Trilobus, Orbulina* and *Globigerinoides*; active dinoflagellate symbionts), (2) Spinose & no symbionts (*Globigerina*), (3) Non-spinose & intermediate (*Globorotalia* (globular), *Globigerinita, Neogloboquadrina, Pulleniatina*; facultative symbiosis), (4) Tropical & intermediate (*Globorotalia* (keeled rim); facultative symbiosis), (5) Subtropical & deep (*Globorotalia*; symbiont-barren), and (6) Other (*Globigerinella*). This final group (Other) consists of *G. siphonifera* and *G. calida*. Several studies have shown the tissue- and shell-bound δ^{15}N of *G. siphonifera* to be consistently high in comparison to both dinoflagellate-bearing and non-symbiont hosting species (Smart et al., 2018; Li et al., 2019, Chapter 2); of the species present in our as-

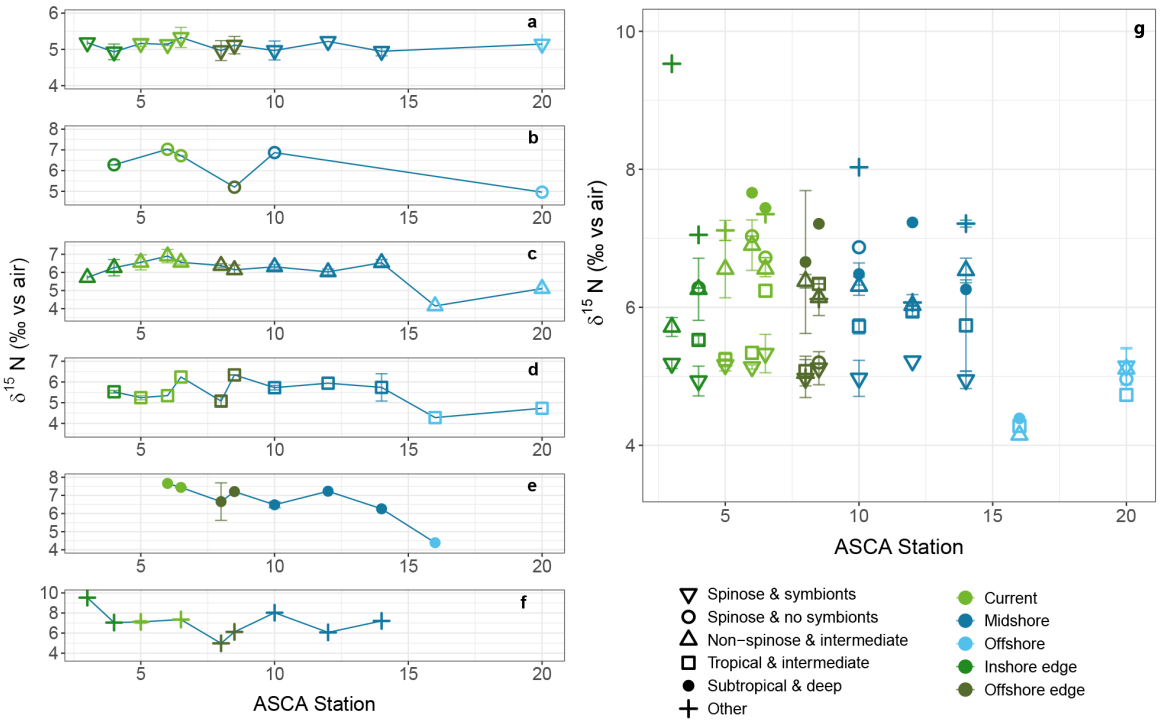

Figure 3.7: Mean FT-δ^{15}N of foraminifera groups at each station. Groups include (a) spinose & symbionts (*G. ruber*, *T. sacculifer*, *O. universa*); (b); spinose & no symbionts (*G. bulloides*) (c) non-spinose & intermediate (*G. inflata*, *N. dutertrei*, *P. obliquiloculata*, *G. crassaformis*, *G. glutinata*); (d) tropical & intermediate (*G. menardii*, *G. tumida*, *G. ungulata*); (e) subtropical & deep (*G. hirsuta*, *G. truncatulinoides*); (f) other (*G. siphonifera, G. calida*); (g) plots (a) to (f) combined, showing standard deviation for duplicate measurements of a species at a tow. Colours indicate zones mentioned in text.

semblage, *G. calida* is the most morphologically and genetically similar to *G. siphonifera*, although recent studies suggest that inter-genus (*Globigerinella*) genetic variability may be higher than in other genera (Seears et al., 2012; Weiner et al., 2014; Morard et al., 2015; Weiner et al., 2015). The two species are also thought to have similarly low degrees of photoysmbiosis (i.e., a low reliance on symbionts for survival; Takagi et al. 2019).

FT-δ^{15}N for all species ranged from 3.4 ‰ to 10.2 ‰ (Fig. 3.7). The lowest FT-δ^{15}N was observed offshore in *G. ruber*, and the highest was found in *G. siphonifera* in the Agulhas Current. *G. siphonifera* and *G. truncatulinoides* (Other and Subtropical and deep, respectively) were consistently higher in FT-δ^{15}N relative to other species at a given station, whereas *G. ruber* and *T. sacculifer* (Spinose & symbionts) typically displayed the lowest FT-δ^{15}N (Fig. 3.8). Across all zones, FT-δ^{15}N was lowest for the Spinose & symbionts group at 5.2 ± 0.6 ‰ (Fig. 3.7a). As with the PON and bulk zooplankton isotopes, the groups Spinose & No symbionts (with the exception of station 8, Fig. 3.7b), Non-spinose & intermediate (Fig. 3.7c, offshore stations dominated by *G. inflata*), Tropical & intermediate (Fig. 3.7d), Subtropical & deep (Fig. 3.7e), and Other (Fig. 3.7f) showed marked offshore decreases in FT-δ^{15}N. Non-spinose & intermediate FT-δ^{15}N decreased from a maximum of 6.8 ± 0.9 ‰ (n = 9) at station 6 to 4.2 ± 0.4 ‰ (n = 4) at station 16, Subtropical & deep FT-δ^{15}N ranged from 7.7 ± 0.5 ‰ (n = 3) at station 6 to

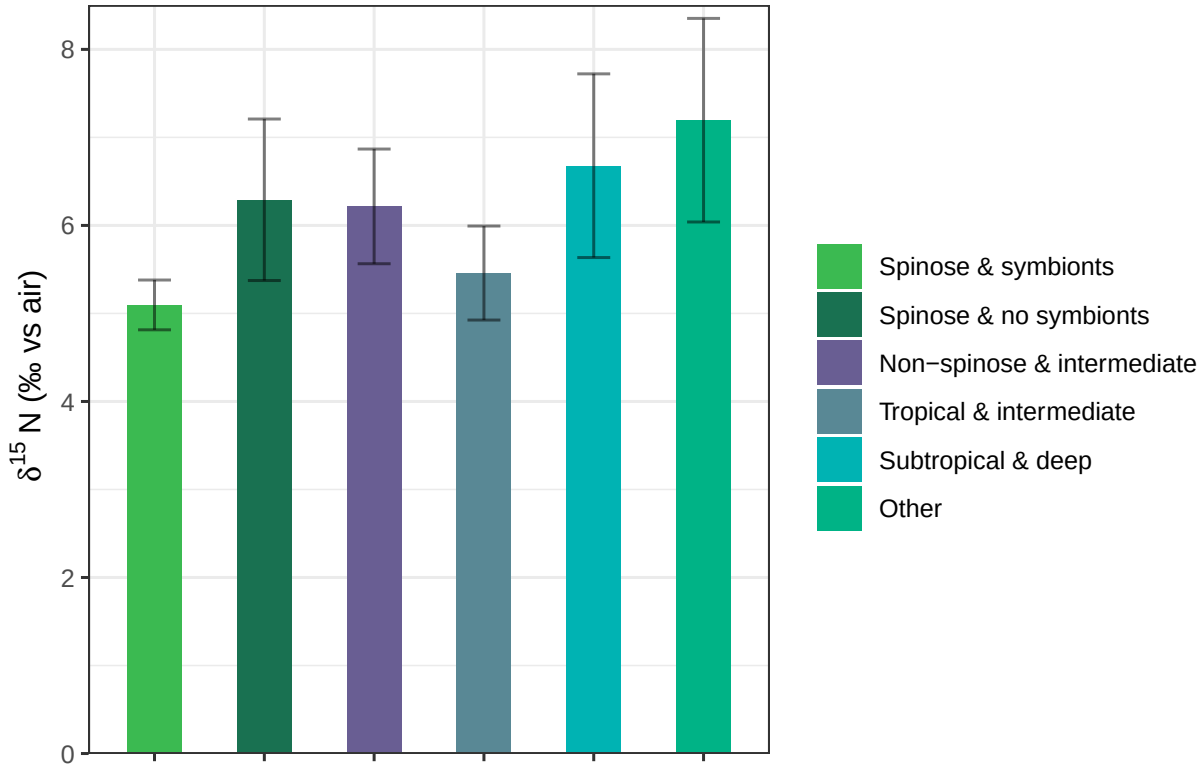

Figure 3.8: Transect mean δ^{15}N for all foraminifera groups (see Fig. 3.7 for species in each group). Error bars show standard deviation of measurements taken across all stations for each group.

4.4 ‰ (n = 1) at station 16, Tropical & intermediate FT-δ^{15}N decreased from 6.2 ± 1.4 ‰ (n = 3) at station 4 to 4.3 ± 0.2 ‰ (n = 2) at station 16, and Other FT-δ^{15}N decreased from 10.2 ‰ at station 3 (n = 1) to 5.2 ‰ at station 8 (n = 1).

3.4.5.2 Agulhas Current Core and Inshore edge: Stations 3 - 7 (Tropical nitrate supply)

Average FT-δ^{15}N for the five core and inshore edge stations was 6.1 ± 1.2 ‰ (n = 108 samples, Fig. S.2). The highest values were observed in Subtropical & deep (non-spinose) species (*G. truncatulinoides, G. hirsuta*), where average FT-δ^{15}N was 7.6 ± 0.4 ‰ (n = 5). Lowest FT-δ^{15}N was measured in spinose, symbiont-hosting foraminifera (*G. ruber, G. sacculifer* and *O. universa*, average 5.2 ± 0.6 ‰, n = 40), all of which are in obligate symbiotic relationships with dinoflagellate algae. The facultatively photosymbiotic group, Non-spinose & intermediate (*G. inflata, P. obliquiloculata, N. dutertrei, G. glutinata*), and Spinose & no symbionts (*G. bulloides*) had averages of 6.4 ± 0.7 ‰ (n = 33) and 6.8 ± 2.1 ‰ (n = 6), respectively, both of which were more than 1 ‰ higher than the spinose, symbiont-hosting group. In comparison to these foraminifera, FT-δ^{15}N for the intermediate-dwelling tropical species was relatively low at 5.6 ± 0.8 ‰ (n = 15).

3.4.5.3 Offshore current edge & Agulhas mid-shore: Stations 8 - 15 (Subtropical nitrate supply)

Average FT-δ^{15}N for the five offshore edge and mid-shore stations was 6.1 ± 0.8 ‰ (n = 94, Fig. S.2), similar to FT-δ^{15}N measured within the Agulhas Current, and all species groups were within 0.5 ‰ of their current value. The FT-δ^{15}N of deep-dwelling subtropical foraminifera remained high in the mid-shore region (6.6 ± 0.6 ‰, n = 10), whilst the FT-δ^{15}N of Spinose & no symbionts (*G. bulloides*) was 6.1 ± 1.1 ‰ (n = 4). As with the Agulhas Current (core and edge) zone, the lowest FT-δ^{15}N was found in the Spinose & symbiont (dinoflagellate-hosting) species (*G. ruber, T. sacculifer* and *O. universa*), where the average FT-δ^{15}N was 5.1 ± 0.6 ‰ (n = 23). The average FT-δ^{15}N for the group Non-spinose & intermediate was 6.3 ± 0.5 ‰ (n = 36).

3.4.5.4 Agulhas Offshore: Stations 16 - 20 (Subtropical nitrate supply)

Average FT-δ^{15}N for the two offshore stations was 4.7 ± 0.6 ‰ (n = 17), 1.4 ‰ lower than in the Agulhas Current zone. Although there were fewer specimens in this more oligotrophic region, several of the inter-species trends remained apparent. The lowest FT-δ^{15}N was measured for the Spinose & symbionts, euphotic-dwelling foraminifera, at 4.2 ± 0.9 ‰ (n = 2). Unlike in the Agulhas Current and mid-shore zones, however, Tropical & intermediate species showed the highest FT-δ^{15}N (4.9 ± 0.5 ‰, n = 5). There were very few specimens available for the Subtropical & deep and the Spinose & no symbionts groups, which averaged 4.4 ‰ (n = 1) and 5.0 ‰(n = 1), respectively; their FT-δ^{15}N relative to other species in this zone are therefore not discussed further.

3.5 Discussion

3.5.1 Interannual variability of ACS water masses

Both the 2016 and 2018 nitrate isotope datasets portray the Agulhas Current and adjacent subgyre as a system composed of several isotopically distinct water masses sourced from tropical and subtropical regions. However, several differences were observed in the vertical displacement of the density-defined water masses between the 2016 and 2018 transects, some of which were noted in Braby et al. (2022), which published the observations of the physical oceanography for the 2018 transect. First, there was a clearer presence of TSW in 2016, as evidenced by the lower density ($< 24.5\,\mathrm{kg.m^{-3}}$, Fig. S.3) waters in the Agulhas Current (to avoid confusion, note that Braby et al. (2022) does not distinguish between surface and thermocline waters, and identifies TSW as $< 25.5\,\mathrm{kg.m^{-3}}$). This telltale low density signal of TSW was much more diluted in 2018, suggesting strong vertical mixing with thermocline waters prior to our sampling. Second, SAMW upwelled close to the coast in 2016, adding nitrate with a higher $\delta^{15}N_{NO_3}$ (6.9 ‰) than the tropical thermocline to the euphotic zone in the inshore zone of the transect (Marshall et al., 2023). In 2018, SAMW

was situated below the thermocline, and there was no strong coastal upwelling event at the time of sampling. Third, a more deeply penetrating pool ($\sim$100-200 m) of TTW was present in 2016 (Fig. S.3), revealed by the mass of low oxygen concentration waters below the current core. Finally, in 2016 the mixed layer deepened with distance offshore from the Agulhas Current, as evidenced by the isopycnals sloping offshore (Fig. S.1, Marshall et al. 2023). In 2018, on the other hand, mixed layers offshore of station 15 (34.8°S 28.4°E) shallowed, as an incursion of subtropical thermocline waters was advected from the east. As previously mentioned, the MLD was decoupled from the 25.5 $kg.m^{-3}$ isopycnal, and waters below the mixed layer were low in nitrate concentration (Fig. 3.2a). Mesoscale variability in the form of eddies is a frequent and integral part of southwest Indian Ocean circulation (Gründlingh et al., 1991; Biastoch et al., 1999; Schouten et al., 2003; Raj et al., 2010; Kolasinski et al., 2012; Lamont et al., 2014; Noyon et al., 2019; Vinayachandran et al., 2021), affecting both stratification and biological activity throughout the year. The cyclonic intrusion observed here demonstrates how mesoscale dynamics can drive variability in the ACS; not only did the intrusion result in a local increase in nitrate availability within the euphotic zone, but it is also suspected to have impacted the Agulhas Current's width, with the raised isopycnals (which brought cooler, fresher and less oxygenated waters closer to the surface) associated with the cyclone's leading edge effectively narrowing the stream (Braby et al., 2022).

Despite the differences in water column structure between the two years, nitrate concentrations and isotopes for the surface and thermocline water masses of the ACS in 2018 were similar to those reported for 2016 (Table 3.1, Fig. 3.3, Fig. 3.4; Marshall et al. 2023). This inter-annual consistency was expected, as the subgyre - from which more than 50% of the Agulhas Current's volume derives - retains recirculated thermocline ($25.7 - 26.2\,kg.m^{-3}$) waters for an estimated four years (Karstensen and Tomczak, 1997; Fine et al., 2008). Therefore, the supply of nitrate entering the mixed layer across the transect was expected to have roughly the same properties ($\delta^{15}N$, $\delta^{18}O$ and concentration) in 2018 as in 2016. The available data support this, with $\delta^{15}N_{NO_3}$ of each water mass in 2018 falling for the most part within one standard deviation of the $\delta^{15}N_{NO_3}$ for 2016 (Table 3.1). The fact that in 2018, the nitrate isotopes of the water masses adhered so closely to the 2016 values, in spite of the physical differences (e.g., stratification, upwelling), is a reflection of how strongly along-isopycnal mixing between tropical and subtropical waters is inhibited across the Agulhas Current (Beal et al., 2006).

3.5.2 Physical changes in water masses reflected in foraminifer assemblages

The offshore shift to a more subtropical foraminifer assemblage coincides with the transition from coastal TTW to STTW (Fig. 3.2 and 6). Temperature has been shown to be the strongest predictor of foraminifer community composition, followed by salinity and turbulence (Meilland et al., 2016; Rebotim et al., 2017; Kontakiotis et al., 2021), and the

ASCA gradients in species composition chiefly aligned with these expectations. Offshore of station 16, the upward mixing of thermocline waters towards the surface was reflected in an increase in intermediate- to deep-dwelling species (e.g., *G. truncatulinoides* and *G. menardii*) relative to the other species at stations 16 and 20. With regards to overall abundance, these offshore stations hosted roughly five- to ten-times fewer individuals than stations sampled in the core of the current. The lower abundances at these stations underlines the oligotrophic nature of the subgyre (although some communities may have also been present below the range of our net tows (200 m), and upward mixing of thermocline waters may have dispersed some species). Subtropical gyres (including the subgyre) are nutrient-poor regions of the ocean characterized by stratified water columns and low productivity for much of the year (Hayward, 1987; Karl, 1999; Jena et al., 2012), which should favour *G. ruber* and *G. sacculifer*, foraminifer species that have traditionally been found to be well-adapted to these conditions (Bijma and Hemleben, 1994; Watkins et al., 1996; Fraile et al., 2008; Lessa et al., 2020; Scott, 2020). Our assemblage data does not show this trend; rather, these two species were most dominant in the higher nutrient current core as opposed to the oligotrophic mid-shore zone. However, the offshore decrease in these two species is not unexpected, as foraminifera can, and do, inhabit waters characterized by non-ideal nutrient conditions, and the Agulhas Current's warm surface temperatures are optimal for the shallow-dwelling *G. ruber* and *G. sacculifer* in terms of reproduction (Bé and Hutson, 1977; Fraile et al., 2008; Rebotim et al., 2017). Interestingly, we do see an increase in *G. inflata*, a species often associated with cool conditions (Boltovskoy, 1969; Pujol and Grazzini, 1995; Lončarić, 2006; Rigual-Hernández et al., 2012; Lessa et al., 2020), offshore where subtropical thermocline waters were uplifted (station 16).

Tropical species associated with warm waters persisted inshore of the Agulhas Current core, despite the upwelling of cool thermocline waters in the section between the current and shelf edge (stations 3 and 4). Foraminifera in this region had likely been advected inshore from the current, as vertical and horizontal shears are at a maximum at the inshore edge of western boundary currents (Beal, 2009; Imawaki et al., 2013; Hood et al., 2017). The absence of strong coastal upwelling in 2018 supports this idea, as upwelling would have brought species better adapted to cooler, more turbulent conditions (e.g., the opportunistic *G. bulloides*; Ortiz et al. 1995; Ufkes et al. 1998; Peeters and Brummer 2002). Further, shallow-dwelling symbiont-bearing species like *G. ruber* and *G. sacculifer* are more likely than other species to be dispersed by horizontal advection. The large, more spherical spinose chambers of these species make their tests more buoyant than non-spinose species, allowing for greater dispersion distances and slower sinking times (Hayward, 1986). The morphology of *G. siphonifera* is similar (i.e., large, spherical chambers), which could also explain the high percentage of *G. siphonifera* at station 3 (both in comparison to other species at the same station, and across all stations), as despite its deeper average living depth, *G. siphonifera* tends to have large tests with spherical chambers. However, *G. siphonifera* is a cosmopolitan species with at least two

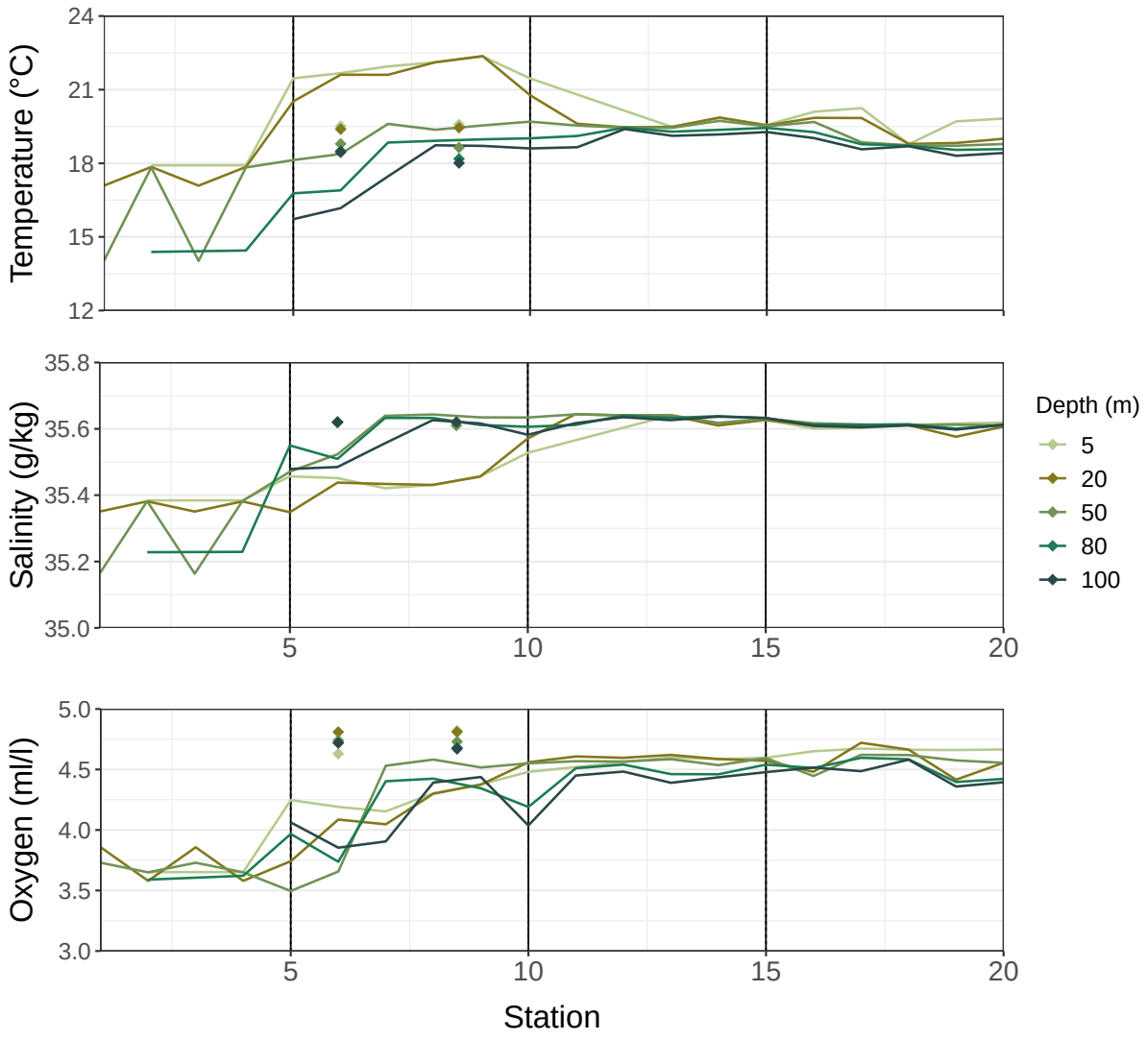

Figure 3.9: Agulhas System Climate Array (ASCA) 2018 physical characteristics of the upper 100 m across transect. Lines represent the outward journey, whilst diamonds indicate properties of the stations sampled on the return journey (stations 6.5 and 8.5 in text). Colours indicate CTD measurements at depth.

morphotypes, one of which appears to have a preference for cool conditions (Bijma et al., 1998; Darling and Wade, 2008), and its disproportionate abundance may instead indicate a stronger presence of TTW than STW at the surface. The same could be true for *G. bulloides*, an intermediate-dweller that has been used as an upwelling indicator in palaeoreconstructions due to its preference for cool, high productivity waters (Hemleben et al., 1989; Ufkes et al., 1998; Mollenhauer et al., 2003).

Another station where *G. bulloides* was prominent was during the repeat sampling of station 6 (referred to as station 6.5); although not high in abundance relative to most stations across the transect, the increase in the species is noticeable when considering its absence at station 6 (sampled four days prior). Other intermediate- (*G. inflata*) and deep-dwelling (*G. menardii*) species also increased relative to the initial sampling at this location. The increase can be attributed to intensification of upwelling between sam-

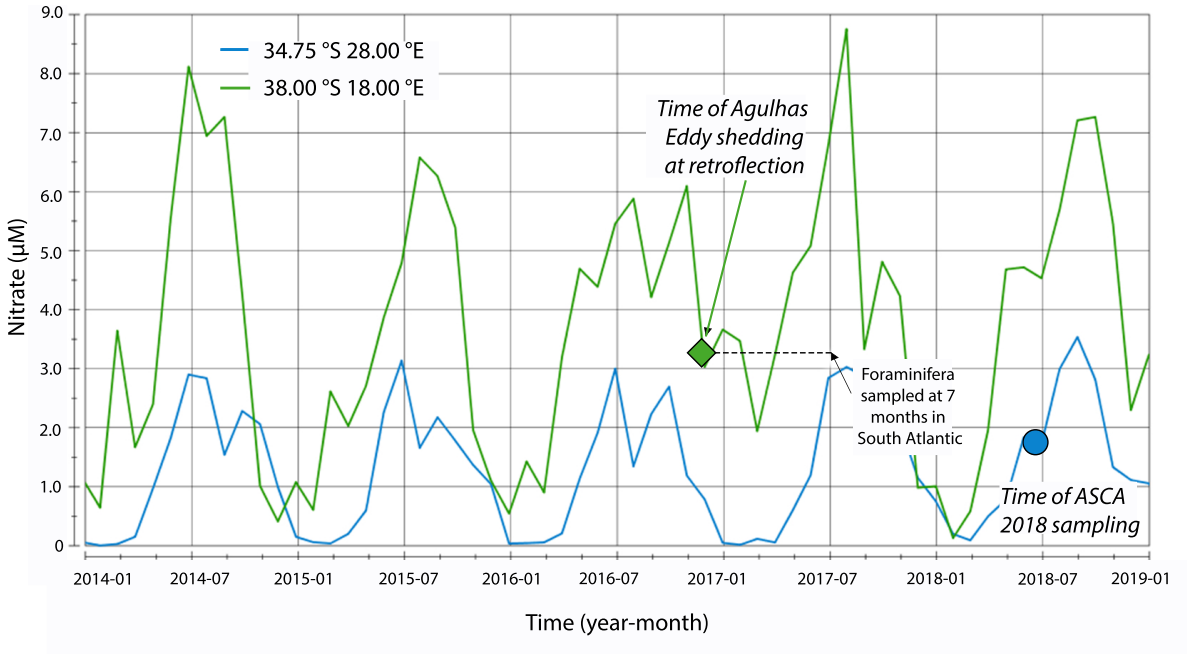

Figure 3.10: Time series data of nitrate concentration in the Agulhas Current. The blue line shows a point in the offshore edge of the Agulhas Current, whilst the green line shows seasonality at a point further downstream in the area of retroflection, where a mature Agulhas eddy (Chapter 2) was shed at the end of 2016.

plings, causing the mixed layer to shallow and cool by 2°C (Fig. 3.9). The sudden change led to a noticeably larger proportion of intermediate-dwellers, which were likely vertically transported along with STTW. Conditions were no longer favourable to the shallowest-dwelling (and highly buoyant) foraminfera, *G. ruber* and *T. sacculifer*, causing them to become displaced to another location. This shift in population may provide an analogue for longer-term seasonal or inter-annual variability, showing the response of foraminifer populations in this region to changing environmental conditions resulting from underlying physical and biogeochemical processes (Schiebel and Hemleben, 2000; Barlow et al., 2020). Upwelling conditions in the Agulhas Current and subgyre region are largely controlled by seasonal winds and topographic forcing (Hood et al., 2017); therefore, if wind intensity/wind stress curl were to increase during glacial periods as has been suggested (Huang et al., 2007; Rampen et al., 2008; Marlow et al., 2000), glacial foraminifer assemblages recovered from Agulhas sediments might be more strongly dominated by subtropical or deeper-dwelling species better adapted to turbulent conditions (Simon et al., 2013).

3.5.3 Controls on FT-δ^{15}N

3.5.3.1 Relationship of FT-δ^{15}N to PON and bulk zooplankton δ^{15}N

Across the ASCA transect, $\delta^{15}N_{PON}$ was significantly (weakly) correlated with mean FT-δ^{15}N ($R^2 = 0.35$; not shown). The positive relationship was particularly evident when isolating specific species, including *G. inflata* (non-spinose with symbionts, $R^2 = 0.58$, not

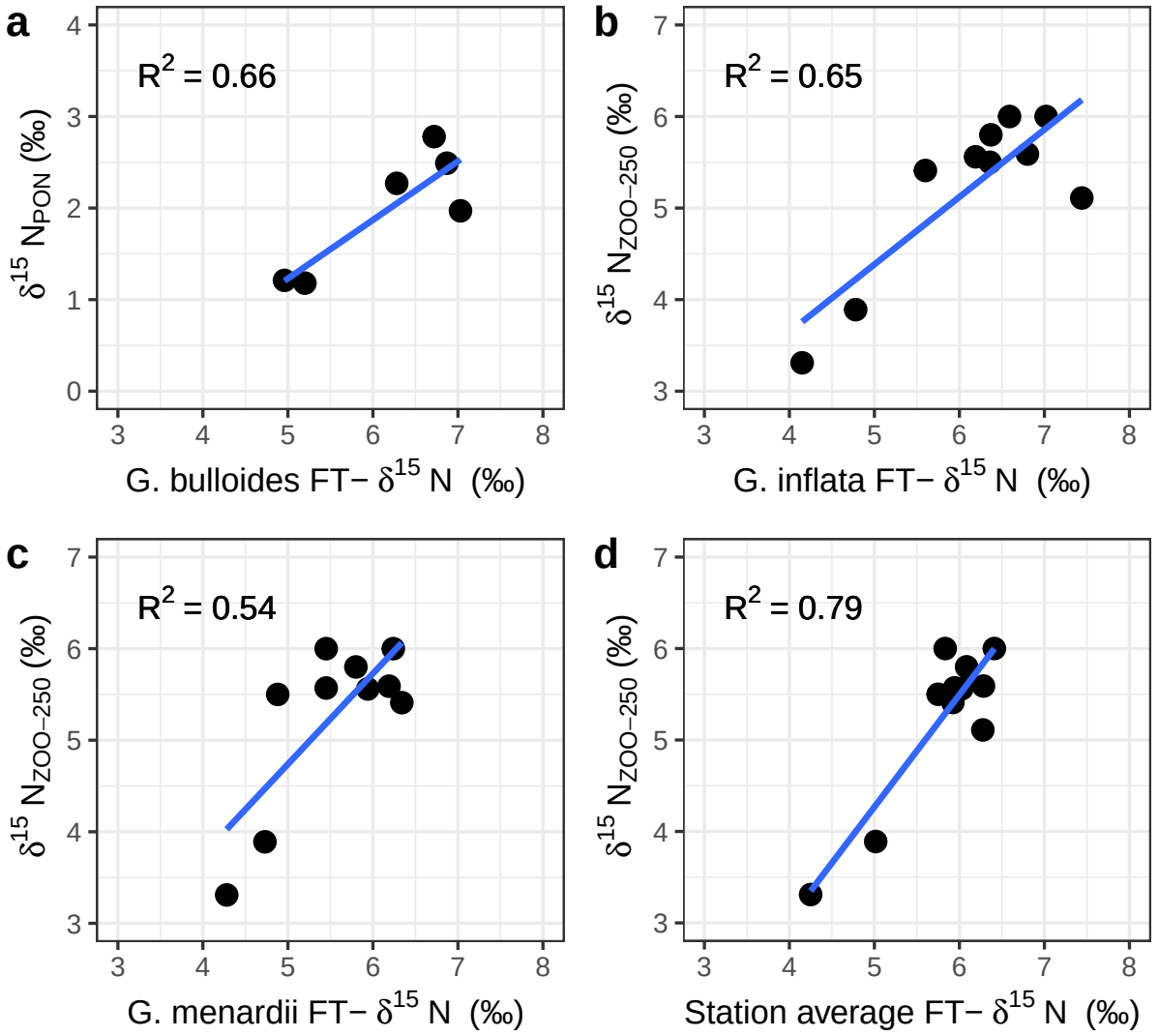

Figure 3.11: Correlation plots of station data, showing (a) FT-δ^{15}N of *G. bulloides* vs δ^{15}N-PON (weighted average of 0-200 m), (b) FT-δ^{15}N of *G. inflata* vs bulk zooplankton δ^{15}N, (c) FT-δ^{15}N of *G. menardii* vs bulk zooplankton δ^{15}N, (d) mean FT-δ^{15}N (all species) vs bulk zooplankton δ^{15}N (size class 250-500 μm).

shown) and *G. bulloides* (spinose without symbionts, $R^2 = 0.66$, Fig. 3.11a). Both species also showed a strong correlation with bulk zooplankton δ^{15}N (size classes 250-500 μm and 500-1000 μm, the size range that includes foraminifera and their potential prey, along with other microzooplankton (Fig. 3.11b), as did *G. menardii* (tropical deep dweller, $R^2 = 0.54$ (*versus* 250-500 μm bulk zooplankton, $p < 0.01$, Fig. 3.11c)). When pooling all species together, bulk zooplankton measurements were even more strongly correlated with FT-δ^{15}N ($R^2 = 0.79$ ($p < 0.01$) for size class 250-500 μm and $R^2 = 0.65$ ($p < 0.01$) for size class 500-1000 μm, Figs. 11a-d). A similarly close relationship between foraminifera and PON (the primary food source for foraminifera) δ^{15}N was previously observed in the Subantarctic and Polar Frontal Zones (Smart et al., 2020). Upper-ocean nitrate in these more southerly locations did not co-vary with FT-δ^{15}N in winter (unlike in the South Atlantic (Chapter 2) and Sargasso Sea; Smart et al. 2018), in part due to lower

productivity and higher bacterial decomposition of PON during winter, while FT-δ^{15}N and $\delta^{15}N_{PON}$ remained coupled throughout the year (Smart et al., 2020). In the southeast Atlantic, the relationship of foraminifera to PON appeared to be disrupted by Agulhas leakage waters overlying South Atlantic thermocline waters (Chapter 2).

The species that were least correlated with PON and/or bulk zooplankton are spinose, dinoflagellate symbiont-hosting species (*T. sacculifer, O. universa, G. ruber*). All three species are thought to be carnivorous, having eaten zooplankton like copepods under laboratory conditions, in addition to phytoplankton (Bé and Hutson, 1977; Bé et al., 1981; Caron et al., 1982; Caron and Bé, 1984; Hemleben et al., 1989), but their obligatory photosymbiosis means that these species are arguably less reliant on PON for nutrition than other foraminifera. Although chrysophyte algae have on occasion been observed to be in symbiosis with *G. inflata*, this species is predominantly heterotrophic, unlike the aforementioned dinoflagellate-hosting foraminifera (Hemleben et al., 1989; Takagi et al., 2019). Its average living depth and herbivorous diet indicates that it should be more isotopically similar to the deeper-dwelling, symbiont-barren species, which is what we observed in our study (and has also been observed in other regions (Chapter 2; Smart et al. 2018, 2020)).

The mean difference between FT-δ^{15}N and $\delta^{15}N_{PON}$ was similar in the ACS to what was observed in the South Atlantic (3.7 ± 0.6 ‰ vs 3.8 ± 1.3 ‰, respectively, Chapter 2), which is roughly equivalent to the nitrogen isotopic enrichment expected for a one trophic level difference (Minagawa and Wada, 1984; Peterson and Fry, 1987). Further south (in the region of the subtropical and subantarctic fronts), this trophic difference was similar, averaging 3.2 ± 0.2 ‰ across all species despite seasonal variation in both FT-δ^{15}N and $\delta^{15}N_{PON}$, and was $\sim$3.3 ‰ at the Agulhas Retroflection (40.9°S, 26.8°E, Smart et al. 2020). The relatively small deviation of the FT-δ^{15}N— $\delta^{15}N_{PON}$ offset across the ASCA stations (0.6 ‰) suggests that the isotopic relationship between foraminifera and PON is fairly consistent in the region, whilst the intra-annual consistency of the offset further south (Smart et al., 2020) is a promising indicator that FT-δ^{15}N may be a good reflection of $\delta^{15}N_{PON}$ variability in the region throughout the year.

3.5.3.2 Species-specific controls on FT-δ^{15}N

The broad inter-species trends in the Agulhas region are similar to those previously measured in the Subantarctic Zone and Polar Frontal Zone, Sargasso Sea, South China Sea, and Southeast Atlantic (Ren et al. 2009; Li et al. 2019; Smart et al. 2018, 2020 Chapter 2), and are mostly consistent across the transect (Fig. 3.7, Fig. 3.8). Species-specific differences in FT-δ^{15}N are thought to arise predominantly from diversity in diets, depth habitats, and metabolic pathways (Hemleben et al., 1989; Schiebel and Hemleben, 2005; Ren et al., 2012b; Bird et al., 2020). Foraminfera-algal symbiosis has regularly been associated with low FT-δ^{15}N in comparison to heterotrophic species (with offsets of 0.5-3 ‰ in the Sargasso Sea (Smart et al., 2018) and $\sim$1.5 ‰ in the ACS). Exceptions to this trend

have in the past included *G. bulloides* (symbiont-barren) and *G. siphonifera* (symbiont-hosting, referred to as *Globigerinella aequilateralis* in Ren et al. 2012b), which were found to have unexpectedly low and high FT-δ^{15}N, respectively, in all the aforementioned regions (Smart et al. 2018, 2020, Chapter 2, Li et al. 2019). Although our measurements of *G. siphonifera* were, for the majority of stations, consistent with a high FT-δ^{15}N for *G. siphonifera, G. bulloides* FT-δ^{15}N was surprisingly high in both the tropical and subtropical sectors of the ARC.

Research has shown that the FT-δ^{15}N of the symbiont-barren, heterotrophic *G. bulloides* can be lowered through direct consumption of low-δ^{15}N ammonium or raised during periods of increased ammonium availability where increased protein production and storage results in ^{1}5N enrichment (Lee et al., 1965; Bird et al., 2020). However, ammonium was not present in the range of concentrations needed to bring about this increase ($> 10\,\mu$m, Bird et al. 2020). *G. bulloides* appears to have occupied a broad trophic range, with a diet that consists of bacteria and phytoplankton (Bird et al. 2017; Chronopoulou et al. 2019). We posit that the persistently higher-than-expected *G. bulloides* FT-δ^{15}N measured in this study was due to a low reliance on ammonium as an N source relative to other food sources in this environment, or an average living depth similar to intermediate or deep-dwellers, since the trophic difference of *G. bulloides* FT-δ^{15}N from PON is similar to that of *G. inflata* and *G. truncatulinoides* ($\sim$4 ‰). In particular, *G. bulloides*' strong correlation to PON δ^{15}N (Fig. 3.11a, $R^2 = 0.66$) suggests that in this case, the majority of the species' diet was organic matter (PON and/or bacteria).

The reason for the consistently high FT-δ^{15}N measured for *G. siphonifera* across multiple environments is uncertain. One underlying reason could be due to cryptic speciation producing several morphotypes of *G. siphonifera*, which complicates the understanding of its physiology and its relationship to its environment. Morphotypes of *G. siphonifera* include Type I, Type IIa and Type IIb (Darling et al., 1997; Huber et al., 1997; Darling et al., 1999); it is possible that the type that has been sampled for δ^{15}N (in this and also in existing studies) has a similar diet to deep-dwelling foraminifera, or that its host/symbiont interactions or growth characteristics (e.g., time of chamber formation) produce a signal different from that of other foraminifer species (Huber et al., 1997; Bijma et al., 1998; De Vargas et al., 2002). A further distinction is that the dominant algal symbionts for *G. siphonifera* are chrysophytes and/or prymnesiophytes, as opposed to the dinoflagellates associated with *G. ruber, T. sacculifer* and *O. universa* (Gastrich, 1987; Faber et al., 1988). Under laboratory conditions where water temperatures deviated from the optimal temperature (24°C) *G. siphonifera* experienced a decrease in the rate of symbiont photosynthesis, which was attributed to the partial inactivation of symbiont photosynthetic enzymes (Lombard et al., 2009). That the maximum SST across the ASCA transect was 23°C, with the majority of the 0-200 m depth interval characterized by a temperature between 17 and 20°C, could explain the non-symbiont-like FT-δ^{15}N of *G. siphonifera* in this region, but not necessarily in other basins where temperatures are warmer (Bermuda)

and yet the FT-δ^{15}N of the species remained high.

Previous studies have linked the high FT-δ^{15}N of deep-dwelling species such as *G. truncatulinoides* to their reliance on partially-degraded PON and lack of algal symbionts (Ren et al., 2012b; Smart et al., 2018). Bacteria preferentially remove ^{14}N from PON over time as it ages and/sinks in the water column, leading to the PON in sub-euphotic waters being more enriched in 15N than at the surface (Saino and Hattori, 1980; Altabet and McCarthy, 1986; Altabet et al., 1991; Lehmann et al., 2002). In our study, $\delta^{15}N_{PON}$ at depth (150 m) was not obviously higher than was measured at the surface, but the deep-dwelling species in our assemblage likely spent time below this depth, as evidenced by the FT-δ^{15}N of *G. truncatulinoides* remaining consistently high across the transect (> 6.3 ‰ in current (core and edge) zones). Reliance on symbionts may explain the small but consistent difference in FT-δ^{15}N that was observed between Non-spinose & intermediate and Tropical & intermediate groups, where the latter was on average 0.7 ‰ lower than the former. Both groups host algal symbionts and tend to subsist at roughly the same depths (50-100 m, Rebotim et al. 2017; Venancio et al. 2017; Stainbank et al. 2019), but photosymbiotic activity in the *G. menardii*-like species (i.e., Tropical & Intermediate) is higher (Takagi et al., 2019).

3.5.3.3 FT-δ^{15}N *versus* thermocline nitrate

FT-δ^{15}N was stable across much of the transect (mean $= 6.0 \pm 1.1$ ‰, n = 219 at 12 stations, Fig. 3.7g) despite the roughly 1 ‰ difference in $\delta^{15}N_{NO_3}$ observed between the tropical and subtropical thermocline. Existing studies of foraminifera biomass and shell δ^{15}N in low-to-mid-latitude regions where N is limiting have shown that N isotopes in foraminifera tend to reflect variations in thermocline nitrate on an annual basis (Ren et al. 2009, 2012a; Smart et al. 2018, Chapter 2); if this were the case in the ACS, we might expect a clearer distinction between FT-δ^{15}N inshore of (and including) station 7 (with tropical thermocline water underlying the mixed layer) and those collected offshore of station 8 (which are supplied by subtropical thermocline waters). However, we observed little to no distinction in FT-δ^{15}N between stations 7 and 8, and instead noted a decrease between stations 14 and 16 (i.e., between mid-shore and offshore zones) where there was no accompanying thermocline $\delta^{15}N_{NO_3}$ change. This contrast indicates that FT-δ^{15}N may not be a straightforward reflection of thermocline $\delta^{15}N_{NO_3}$ variation in the region.

First, we discuss the possible reasons for the observed difference in FT-δ^{15}N between the mid-shore and offshore zones. Since both zones are ultimately supplied by the same nitrate source (STTW, mean $\delta^{15}N_{NO_3}$ of 4.9 ‰), complete consumption of the available nitrate would result in a net fractionation of zero, with no isotopic difference between the PON (and FT-δ^{15}N) produced at the mid-shore and offshore stations (Wada and Hattori, 1978; Altabet and McCarthy, 1985; Montoya et al., 1992). Since the δ^{15}N of foraminifera is set by their diet, the discrepancy between their species-specific FT-δ^{15}N values must therefore ultimately result from a difference in the relative consumption of

available nitrate by phytoplankton, the consumption of an additional nitrate source with a different N-isotopic composition, and/or changes in feeding strategies of foraminifera under different habitat conditions. Phytoplankton assimilating an additional source of nitrate can be dismissed as 1) the physical and biogeochemical properties of the water masses agree with what has previously been observed in the region (Valentine et al., 1993; Beal et al., 2006; Marshall et al., 2023) and 2) the $\delta^{15}N_{NO_3}$ profiles for both zones were very similar (Figure 4a), with thermocline $\delta^{15}N_{NO_3}$ values between stations 10 and 19 that were within 0.5 ‰ of one another.

We therefore look to partial nitrate consumption to explain the discrepancy between the mid-shore and offshore, an explanation that is supported by the hydrographic and nutrient data. The shoaling of the mixed layer coincided with the presence of the cyclonic intrusion at the offshore section of the transect (station 16), and thermocline waters were uplifted towards the surface (Figure 3). Mixing STTW with surface waters supplied new nitrate to the euphotic zone, observable in cross-section plots of the ASCA transect as the decoupling of oxygen and salinity from the mixed layer (25.5 $kg.m^{-3}$, Fig. 3.2). Consumption of the new supply of nitrate (which is lower in $\delta^{15}N_{NO_3}$ than STSW) from below would result in PON that is relatively depleted in ^{15}N, and foraminifera with a similarly low $\delta^{15}N$ signal. On average, $\delta^{15}N_{PON}$ is set over the course of several hours to days (Waser et al., 1998; Treibergs et al., 2014), whereas FT-$\delta^{15}N$ likely integrates over days to weeks (Smart et al., 2018; Robinson et al., 2023). Given that (1) the offshore nitrate concentrations between 100 and 200 m were lower than the average STTW nitrate concentrations, indicating that some of the nitrate had already been assimilated by the time of sampling, and (2) satellite (sea level anomaly and velocity vector) data showed that the cyclonic feature had been present in the region for at least 2 weeks prior to sampling, it is likely that the low offshore FT-$\delta^{15}N$ is a consequence of foraminifera incorporating the low $\delta^{15}N_{PON}$ signal derived from partial consumption of newly-supplied (i.e., uplifted) thermocline water nitrate.

With regards to changing feeding strategies of foraminifera, it is possible that being located closer to the oligotrophic subgyre and further from the tropically-influenced waters of the Agulhas Current might influence the diet of some species, resulting in an altered FT-$\delta^{15}N$ signal. However, considering the evidence for increased nitrate availability in the offshore euphotic layer, combined with the duration of the cyclonic feature ($>$ 2 weeks) and the relatively short distance (40 km) between stations 14 (mid-shore) and 16 (offshore), it is unlikely that the lower FT-$\delta^{15}N$ in the offshore zone was the result of the subgyre affecting diet preferences.

The conclusion that a lower degree of nitrate consumption is responsible for the observed decrease in offshore FT-$\delta^{15}N$ has implications for Agulhas leakage, as the offshore FT-$\delta^{15}N$ signal presented here should increase as phytoplankton continue to assimilate the available nitrate. Assuming nitrate is mostly consumed in ACS surface waters, mid-shore foraminifera may be a better indication of the average relationship between FT-$\delta^{15}N$ and

thermocline (source) $\delta^{15}N_{NO_3}$ than what was observed at the offshore stations. In order for FB-δ^{15}N to work as an Agulhas leakage proxy, the foraminifera within the leakage need to be isotopically distinct from their surroundings (i.e., the south Atlantic). In Chapter 2, FT-δ^{15}N was measured for foraminifera living in the southeast Atlantic, as well as for specimens inhabiting a mature Agulhas eddy (roughly 7 months old, Chapter 2, Wallschuss et al. 2022). Comparing mid-shore FT-δ^{15}N with the background Atlantic dataset (species common to both include *G. truncatulinoides, G. inflata, G. bulloides, G. hirsuta*, and *G. siphonifera*) shows that the Agulhas mid-shore foraminifera were lower in FT-δ^{15}N for all species except *G. hirsuta*. This is to be expected due to STTW having a lower $\delta^{15}N_{NO_3}$ than South Atlantic Subtropical Mode Water (SASTMW), the nitrate supply to the mixed layer in the southeast Atlantic (SASTMW, $\delta^{15}N_{NO_3} = 6.9$ ‰, Chapter 2). However, the difference in FT-δ^{15}N between the two regions (Fig. S.2) was smaller than the difference between the δ^{15}N of the nitrate source to the southeast Atlantic (δ^{15}N SASTMW) and that of the subtropical subgyre nitrate source (δ^{15}N STTW) (0.5 ‰ difference in FT-δ^{15}N *versus* 2 ‰ difference in thermocline $\delta^{15}N_{NO_3}$). In addition, the mid-shore ACS FT-δ^{15}N was significantly higher than the average measurements from the mature eddy in the Cape Basin ($p < 0.01$; higher by an average of 2.2 ‰), indicating that the eddy is not a simple reflection of Agulhas conditions; instead, we observed that Agulhas offshore FT-δ^{15}N was more similar to the FT-δ^{15}N within the mature eddy.

3.5.3.4 Comparison to southeast Atlantic FT-δ^{15}N

Agulhas Current (core and edge) FT-δ^{15}N values are similar to those recorded in the South Atlantic during the winter of the previous year (Fig. S.2), with South Atlantic FT-δ^{15}N on average 0.4 ± 0.8 ‰ greater than that of the same species in the Agulhas Current. Of the six overlapping species, only three were present offshore in the ACS in suitable quantities for FT-δ^{15}N measurements (*G. truncatulinoides, G. inflata and G. bulloides*). Offshore FT-δ^{15}N was on average 2.2 ‰ lower than South Atlantic values for the same species, and were more isotopically similar to their counterparts from within the anticyclonic eddy (Chapter 2). Offshore ACS FT-δ^{15}N for *G. truncatulinoides* and *G. inflata* were 1.0 ‰ lower and 0.9 ‰ higher than in the South Atlantic eddy, respectively. On the other hand, *G. bulloides* was 2.2 ‰ higher offshore than in the eddy; however, as noted above, the FT-δ^{15}N of this species within the ACS was unexpectedly high in comparison to other studies (Ren et al., 2012b; Smart et al., 2018, 2020).

In the South Atlantic, FT-δ^{15}N of deep-dwelling foraminifera was a good indicator for local thermocline $\delta^{15}N_{NO_3}$ ($\sim$6.7 ‰; Chapter 2). If the same were true within the ACS, we would expect these species to be lower in δ^{15}N than in the South Atlantic, since the tropical and subtropical thermocline $\delta^{15}N_{NO_3}$ in 2016 was 5.8 ‰ and 4.9 ‰, respectively. Instead, the FT-δ^{15}N of deep and intermediate-dwelling foraminifera was consistently higher than that of thermocline nitrate (with the exception of the low FT-δ^{15}N associated with the cyclonic intrusion), whilst the FT-δ^{15}N of spinose, symbiont-hosting foraminifera

was a closer match to thermocline $\delta^{15}N_{NO_3}$. This is more in line with what was observed in the Sargasso, where *O. universa, G. ruber* and *T. sacculifer* were consistently within 0.5 ‰ of thermocline nitrate (Ren et al., 2012b; Smart et al., 2018).

N_2 fixation and ammonium assimilation could lower the FT-$\delta^{15}N$ within an Agulhas eddy during leakage transport. Since the isotope effect associated with N_2 fixation is small (−2-0 ‰, Hoering and Ford 1960; Delwiche et al. 1979; Carpenter et al. 1997), N_2 fixation produces organic N that is low in $\delta^{15}N$, the remineralization of which results in low $\delta^{15}N$ nitrate. Anticyclonic eddies are becoming increasingly recognized as hotspots for N_2 fixation, and may contribute to a lower FT-$\delta^{15}N$ relative to eddy surroundings (Holl et al., 2007; Fong et al., 2008; Li et al., 2020; Liu et al., 2020; Chen et al., 2021; Dugenne and Gradoville, 2022). The recycling and assimilation by phytoplankton of low $\delta^{15}N$ ammonium produced through organic matter decomposition (Altabet, 1988; Mino et al., 2002; Fawcett et al., 2011) and via zooplankton excretion (Checkley and Miller, 1989) also has the potential to lower the $\delta^{15}N_{PON}$ over time, creating a low $\delta^{15}N$ food source for foraminifera. The ACS data presented here support a scenario in which one or both of these processes are active in-situ during the transport of Agulhas leakage, as either of these processes could yield a 2.2 ‰ decrease in the leakage FT-$\delta^{15}N$ relative to the pre-leakage signal (when considering Agulhas mid-shore FT- $\delta^{15}N$ as the pre-leakage end-member).

It is also possible that the comparatively low Agulhas leakage eddy FT-$\delta^{15}N$ could be a result of seasonal variability in $\delta^{15}N_{PON}$. Species-specific FT-$\delta^{15}N$ seasonal changes of 2 ‰ have been observed in the mid-latitude Sargasso Sea, where an increased reliance on ammonium relative to nitrate during mid- to late summer is thought to be responsible for observed decreases in $\delta^{15}N_{PON}$ and FT-$\delta^{15}N$ (Smart et al., 2018). Although there are differences in the nutrient sources and biogeochemical cycling of the two basins, the Sargasso Sea dataset arguably provides the best available seasonal comparison for the subtropical portion of the ACS, in that nitrate is supplied via winter mixing to an oligotrophic surface layer (Lomas et al., 2013; Treibergs et al., 2014) and is subsequently taken up to completion (Lipschultz, 2001; Fawcett et al., 2015). The Agulhas eddy from which foraminifera were sampled in 2017 was formed and migrated into the South Atlantic in early summer (Wallschuss et al. 2022, Chapter 2). Whilst some amount of N had likely undergone recycling by this time (Menzel and Ryther, 1959; Lipschultz, 2001), time-series satellite model data of the Agulhas Retroflection indicate that surface nitrate was not used up at this time (3.10), and it is uncertain how much greater the reliance on ammonium was during early summer than during our sampling period (winter). It is difficult to draw any definitive conclusions regarding the seasonal variations in FT-$\delta^{15}N$ without data collected during other months; however, the region in which FT-$\delta^{15}N$ decreased becomes less of an issue when focusing on reconstructing Agulhas leakage. An increase in ammonium consumption would have the same impact on FT-$\delta^{15}N$, whether the signal resulted from seasonal variation in the ACS nitrate supply or from the retention

of nitrate-deplete waters in the eddy during the transport of leakage.

Therefore, although uncertainty remains regarding the processes affecting FT-δ^{15}N downstream of the Agulhas Current region and during the transport of leakage, we are confident that Agulhas leakage foraminifera are noticeably lower in δ^{15}N (both in tissue and shell) than the foraminifera inhabiting the surrounding Atlantic (Chapter 2). The utility of the foraminifer-bound nitrogen isotopes as a proxy for Agulhas leakage is determined by being able to identify this low FB-δ^{15}N in the sediment, not by quantifying the degree to which each process contributed to the final isotopic composition. Although definitively identifying such processes will greatly improve our understanding of local mesoscale controls on biology and stratification in the ACS, as well as providing further insight into the role of eddies in biogeochemical cycling and carbon export, the findings of our initial work are encouraging for research aimed at reconstructing past leakage.

3.5.3.5 Influence of recent changes to water column structure on FT-δ^{15}N

Along the ASCA transect, we next examine the unexpected similarity in FT-δ^{15}N between tropical and subtropical FT-δ^{15}N found across stations 3 - 14, despite their being supplied by two separate, isotopically different nitrate sources (mean $\delta^{15}N_{NO_3}$ of 5.8 ‰ *versus* 4.9 ‰ for TTW and STTW, respectively). Partial assimilation offered a potential reason for the FT-δ^{15}N differences observed between the mid- and offshore zones, and may also explain the similarity of FT-δ^{15}N between the tropical current and subtropical mid-shore zones. Nitrate concentrations in the upper 100 m were low at $\sim$1-2 μM (Fig. 3.2a) at the current's offshore edge and mid-shore stations (stations 8 - 14), and the water column became increasingly stratified with distance from the coast (Fig. 3.2a). In contrast, TTW shoaled to the surface inshore of the Agulhas Current (evident in the sloped isopycnals and low oxygen concentration characteristic of TTW at stations 3 - 5; Fig. 3.2c), bringing subsurface nitrate with a δ^{15}N of 5.8 ‰ and concentration $> 10\,\mu$M to the surface to supply stations 3 - 7 (Fig. 3.2a, c).

In comparison to thermocline nitrate, both the current and mid-shore zones showed a nitrate utilization of roughly 50% at the surface. Applying a Rayleigh (for the subtropical section) and steady state (for the tropical section) framework to our data, where the δ^{15}N of both the reactant (nitrate) and product (PON) increase as nitrate consumption proceeds, indicates that the same degree of consumption of TTW and STTW would result in the production of a higher TTW-supplied $\delta^{15}N_{PON}$ (and foraminifera) than PON derived from STTW by around 1 ‰. However, neither model is particularly appropriate for the tropical current zone, due to high velocities and large flow variability inshore and within the core of the Agulhas Current (Beal et al., 2015), which violates the models' assumptions. The vertical transport of water is an order of magnitude lower than its downstream surface velocity ($\sim$0.2 m.s^{-1} *versus* $\sim$2 m.s^{-1}, Figure S.1; Bryden et al. 2005; Beal et al. 2015). Rapid downstream (advective) transport of nutrients combined with diapycnal mixing and entrainment of thermocline waters into the surface means the upper layers of

the current will be characterized by higher nitrate concentrations than would be possible through vertical supply alone. This makes the fraction of nitrate utilization difficult to quantify (Pelegrí and Csanady, 1991). The extremely low apparent isotope effects for nitrate assimilation calculated by applying the Rayleigh model to the 2018 data, ($\varepsilon < 1\,‰$, $\varepsilon = (\delta^{15}N_{NO3\text{-initial}} - \delta^{15}N_{NO3\text{-reactant}})/(\ln[f])$, where f is the fraction of nitrate remaining ($[NO_3^-]_{measured}]/[NO_3^-]_{initial}$)) confirm a high degree of mixing or uplift of tropical thermocline waters (i.e., violating Rayleigh model conditions). The constant mixing and import of low $\delta^{15}N$ nitrate for assimilation would yield a low $\delta^{15}N_{PON}$ source of food for foraminifera. We also note that the difference between TTW and STTW is less than 1 ‰, and that only a small amount of mixing of additional nitrate would be necessary to lower the tropical $\delta^{15}N_{PON}$ to a value similar to that observed in the mid-shore, which was driven solely by the consumption of subtropical thermocline-supplied nitrate.

The Agulhas Current consists of a mixture of tropical and subtropical waters, but the majority of its volume (and likely the majority of leakage volume) is sourced from subtropical regions (Stramma and Lutjeharms, 1997; Durgadoo et al., 2017). Considering that the average difference between the background Atlantic and Agulhas eddy FT-$\delta^{15}N$ (Chapter 2) was more than double that of the difference between TTW and STTW $\delta^{15}N_{NO_3}$, logic suggests that even if a large portion of leakage was derived from TTW, the additional processes responsible for lowering $\delta^{15}N_{PON}$ of Agulhas leakage would still create a lower FT-$\delta^{15}N$ than that of the background Atlantic. If this is true, then Agulhas leakage would manifest as a low FB-$\delta^{15}N$ signal in the southeast Atlantic sediment, regardless of whether the dominant portion of leakage was derived from tropical or subtropical thermocline waters.

3.6 Conclusions

In this study, nitrate isotopes across the ACS were found to be consistent with previous measurements, suggesting isotopic inter-annual stability in the region. Northern-sourced tropical thermocline waters appear to be consistently higher in $\delta^{15}N_{NO_3}$ than the oligotrophic subtropical thermocline waters (Marshall et al., 2023). The sharp frontal boundaries created by the meeting of these water masses over a relatively short distance across the Agulhas Current System provide an excellent window through which to view how physical properties of the marine environment govern foraminifera assemblages; a clear shift was visible from $> 80\%$ dominance by tropical species in the warm core of the Agulhas Current to a similar level of dominance by subtropical species offshore, over a distance of 50 km (station 6 to station 10). This work builds on existing ground-truthing efforts (Ren et al. 2009, 2012b; Li et al. 2019; Smart et al. 2018, 2020; Chapter 2) aiming to understand the link between ocean biogeochemistry and foraminifera-bound $\delta^{15}N$ preserved in the fossil record. As in the aforementioned studies, we find FT-$\delta^{15}N$ to be consistently lower in spinose, dinoflagellate-hosting species in the ACS (e.g., *G. ruber, T. sacculifer*)

relative to non-symbiont hosting or facultatively symbiont-reliant species. Furthermore, dinoflagellate-hosting species appear to best approximate thermocline nitrate δ^{15}N in the ACS, which is consistent with data from the Sargasso and South China Seas (Li et al., 2019; Smart et al., 2018), but divergent from the southeast Atlantic, where the isotopic composition of deep-dwellers in winter was more comparable to that of thermocline nitrate (Chapter 2).

The positive correlation between foraminifera and PON (and zooplankton (250-1000 μm)) is consistent with knowledge of foraminifera's reliance on particulates and zooplankton to subsist (Bé et al., 1981; Hemleben et al., 1989), and suggests that foraminifera are reliable isotopic indicators of particulate N in the ACS. Species-specific subtropical FT-δ^{15}N under nitrate-deplete conditions in the ACS appears similar to that of the southeast Atlantic, despite the lower thermocline $\delta^{15}N_{NO_3}$ in the ACS. The data therefore suggest that additional processes, like in-situ N_2 fixation and recycling and consumption of ammonium act to lower the $\delta^{15}N_{NO_3}$ (and FT-δ^{15}N) of leakage in transit, yielding the low FT-δ^{15}N measured in the Agulhas eddy in the southeast Atlantic (Chapter 2). Should these processes regularly lower the δ^{15}N of PON in leaked eddies in this manner, a significant increase in leakage from the Agulhas Current could significantly lower the δ^{15}N of the foraminifer flux to the seafloor, along the Southeast Atlantic leakage pathway.

The data from several pools of marine N demonstrate the importance of mesoscale dynamics in the ACS on biological assemblage and nitrogen isotope composition. Examples of this include (1) fluctuations in inshore upwelling (lowering mixed layer δ^{15}N through resupply and partial consumption of new nitrate from below), (2) lateral advection of organisms from the current (buoyant euphotic-dwelling foraminifera carrying their current-derived FT-δ^{15}N signal inshore/shorewards) and (3) cyclonic intrusions disrupting offshore stratification and bringing low $\delta^{15}N_{NO_3}$ thermocline waters closer to the surface.

Finally, we note the fast responses of foraminifera assemblages and FT-δ^{15}N to mesoscale processes (i.e., the shoaling of thermocline waters). A noticeable change in the upper (200 m) water column assemblage occurred over the course of four days, exhibited by the repeat sampling of a station within the current's core, and a change in FT-δ^{15}N developed as a result of a transient cyclonic feature roughly 2 - 3 weeks old. These shifts further illustrate the importance of understanding mesoscale and seasonal processes that influence regional biogeochemistry, as seasons where shell export from the mixed layer is high may not be representative of average (or even predictable) conditions. However, despite the nonlinear controls and intrinsic variability of the ACS environment, FT-δ^{15}N has a similar relationship to thermocline nitrate as has been observed in other basins (Sargasso and South China Sea). This consistency is promising with regards to developing an N isotope-based proxy for Agulhas leakage, but also in terms of local palaeoceanographic reconstructions that seek to better understand past Agulhas Current dynamics, as intra- and interannual variability become less important over longer time scales.

Supplementary Figures

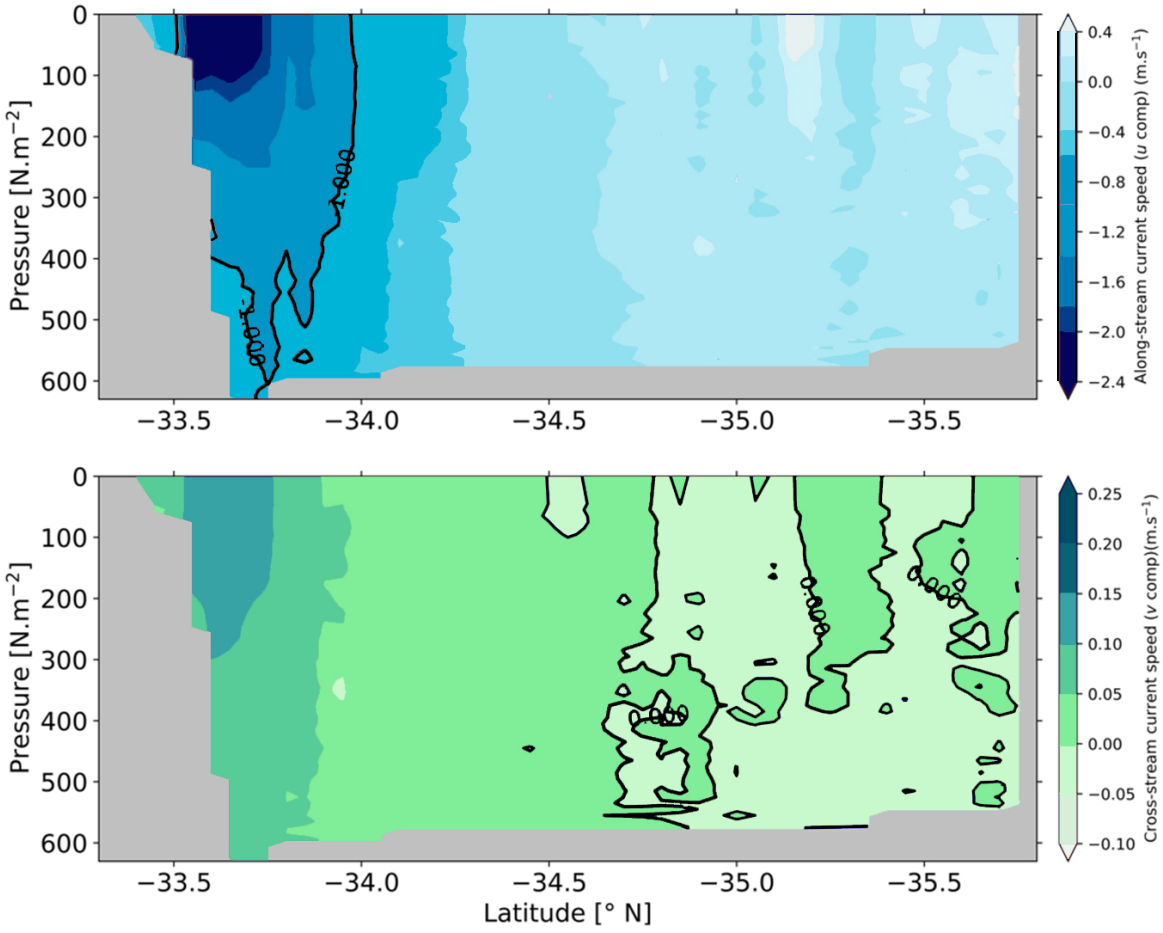

Figure S.1: Velocity plot of the Agulhas System Climate Array (ASCA) 2018 transect (adapted from an original image created by T. Marshall), showing the structure of the Agulhas Current using (a) along-stream and (b) cross-stream velocity (m.s^{-1}). Negative values indicate southward flow in (a) and westward flow in (b). Black lines show the 0 and -1 m.s^{-1} contours.

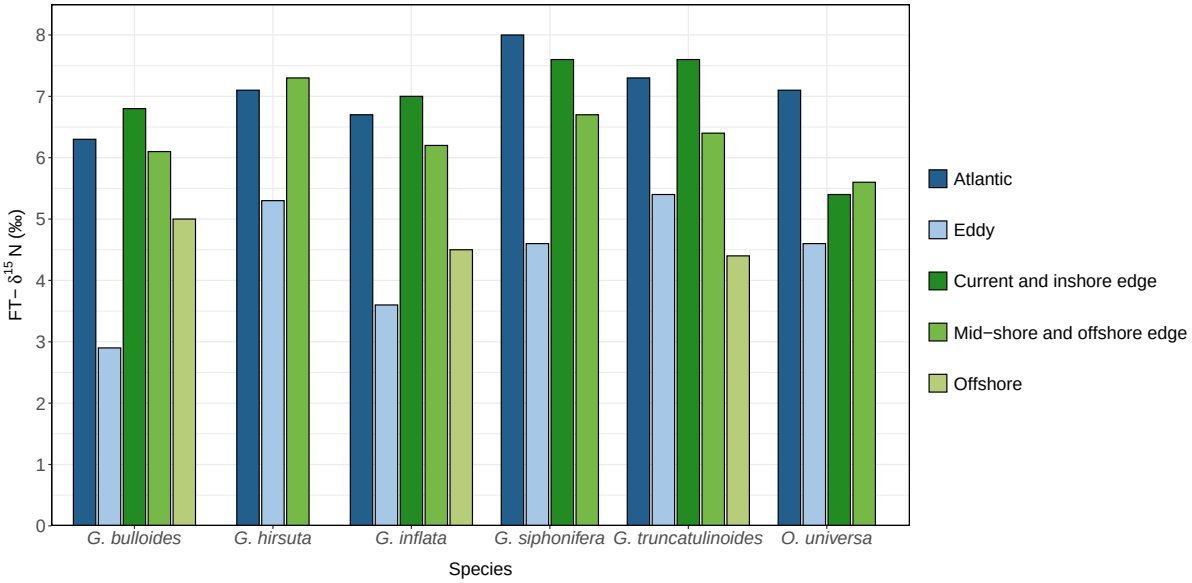

Figure S.2: Comparison of FT-δ^{15}N data from 6 species common in net tows from the southeast Atlantic and southwest Indian Ocean. Mean FT-δ^{15}N refers to all the average of all individuals of that species from within a zone, which included five Atlantic stations, four Eddy stations (Chapter 2), six Agulhas System Climate Array (ASCA) current & inshore edge stations, four ASCA mid-shore and offshore edge stations, and two ASCA offshore stations. Missing bars indicate stations where there were not enough (or any) individuals present for FT-δ^{15}N measurements.

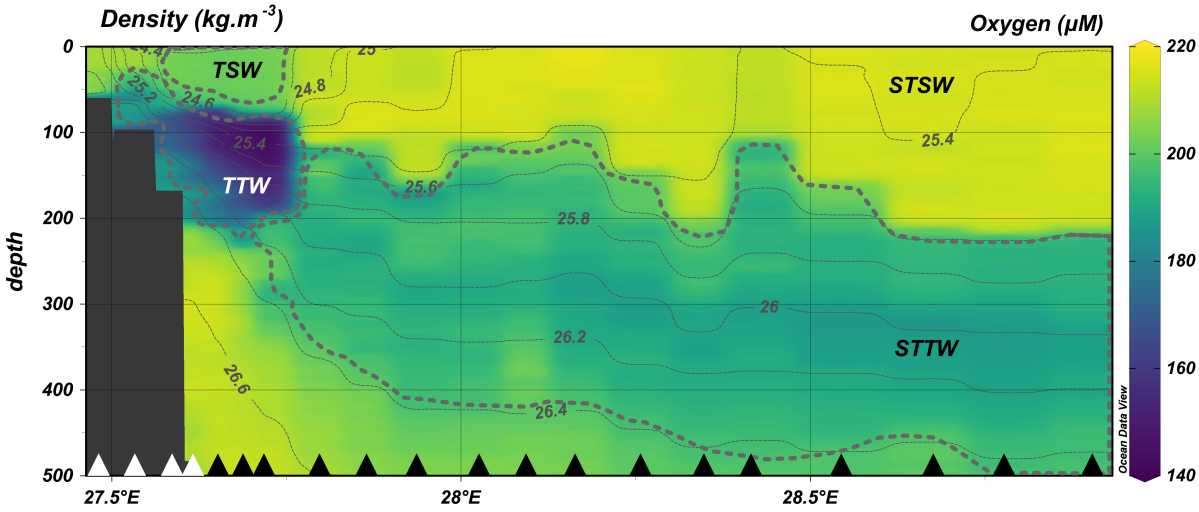

Figure S.3: Section plot showing oxygen concentrations from ASCA 2016. Contours lines refer to density, and dashed lines denote the boundaries of water masses (Tropical Surface Water (TSW), Tropical Thermocline Water (TTW), Subtropical Surface Water (STSW) and Subtropical Thermocline Water (STTW)). Triangles on the x axis (degrees longitude) indicate station positions along the transect.

References

Altabet, M. A. (1988). Variations in nitrogen isotopic composition between sinking and suspended particles: implications for nitrogen cycling and particle transformation in the open ocean. *Deep Sea Research Part A, Oceanographic Research Papers*, 35(4):535–554.

Altabet, M. A., Deuser, W. G., Honjo, S., Stienen, C., and Stienent, C. (1991). Seasonal and depth-related changes in the source of sinking particles in the North Atlantic. *Nature*, 354(November):136–139.

Altabet, M. A. and Francois, R. (1994). Sedimentary nitrogen isotopic ratio as a recorder for surface ocean nitrate utilization. *Global Biogeochemical Cycles*, 8(1):103–116.

Altabet, M. A. and McCarthy, J. J. (1985). Temporal and spatial variations in the natural abundance of 15N in PON from a warm-core ring. *Deep Sea Research Part A, Oceanographic Research Papers*, 32(7):755–772.

Altabet, M. A. and McCarthy, J. J. (1986). Vertical patterns in 15N natural abundance in PON from the surface waters of warm-core rings. *Journal of Marine Research*, 44(1):185–201.

Anderson, N. and Sedell, J. (1979). Detritus processing by macroinvertebrates in stream ecosystems. *Ann. Rev. Entomol.*, (24):351–357.

Bard, E. and Rickaby, R. E. (2009). Migration of the subtropical front as a modulator of glacial climate. *Nature*, 460(7253):380–383.

Barlow, R., Lamont, T., Gibberd, M. J., Russo, C., Airs, R., Tutt, G., Britz, K., and van den Berg, M. (2020). Phytoplankton adaptation and absorption properties in an Agulhas Current ecosystem. *Deep-Sea Research Part I: Oceanographic Research Papers*, 157(December 2019):103209.

Bé, A. W. H., Caron, D. A., and Anderson, O. R. (1981). Effects of feeding frequency on life processes of the planktonic foraminifer globigerinoides sacculifer in laboratory culture. *Journal of the Marine Biological Association of the United Kingdom*, 61(1):257–277.

Bé, A. W. H. and Hutson, W. H. (1977). Ecology of Planktonic Foraminifera and Biogeographic Patterns of Life and Fossil Assemblages in the Indian Ocean. *Micropaleontology*, 23(4):369.

Bé, A. W. H. and Tolderlund, D. S. (1971). Distribution and ecology of living planktonic foraminifera in surface waters of the Atlantic and Indian Oceans.

Beal, L. (2009). A time series of agulhas undercurrent transport. *Journal of Physical Oceanography*, 39(10):2436–2450.

Beal, L., Chereskin, T. K., Lenn, Y. D., and Elipot, S. (2006). The sources and mixing characteristics of the Agulhas Current. *Journal of Physical Oceanography*, 36(11):2060–2074.

Beal, L., De Ruijter, W. P., Biastoch, A., Zahn, R., Cronin, M., Hermes, J., Lutjeharms, J. R., Quartly, G., Tozuka, T., Baker-Yeboah, S., Bornman, T., Cipollini, P., Dijkstra, H., Hall, I., Park, W., Peeters, F. J., Penven, P., Ridderinkhof, H., and Zinke, J. (2011). On the role of the Agulhas system in ocean circulation and climate. *Nature*, 472(7344):429–436.

Beal, L., Elipot, S., Houk, A., and Leber, G. M. (2015). Capturing the transport variability of a western boundary jet: Results from the Agulhas Current time-series experiment (ACT). *Journal of Physical Oceanography*, 45(5):1302–1324.

Berger, W. H. (1969). Ecologic patterns of living planktonic Foraminifera. *Deep-Sea Research and Oceanographic Abstracts*, 16(1):1–24.

Biastoch, A., Boening, C. W., and Lutjeharms, J. R. (2008). Agulhas leakage dynamics affects decadal variability in Atlantic overturning circulation. *Nature*, 456(November):489–492.

Biastoch, A., Boening, C. W., Schwarzkopf, F. U., and Lutjeharms, J. R. (2009). Increase in Agulhas leakage due to poleward shift of Southern Hemisphere westerlies. *Nature*, 462(November):495–499.

Biastoch, A., Durgadoo, J. V., Morrison, A. K., Van Sebille, E., Weijer, W., and Griffies, S. M. (2015). Atlantic multi-decadal oscillation covaries with Agulhas leakage. *Nature Communications*, 6:1–7.

Biastoch, A., Reason, C. J., Lutjeharms, J. R., and Boebel, O. (1999). The importance of flow in the Mozambique Channel to seasonality in the greater Agulhas Current system. *Geophysical Research Letters*, 26(21):3321–3324.

Bijma, J. and Hemleben, C. (1994). Population dynamics of the planktic foraminifer Globigerinoides sacculifer (Brady) from the central Red Sea. *Deep Sea Research Part I: Oceanographic Research Papers*, 41(3):485–510.

Bijma, J., Hemleben, C., Huber, B. T., Erlenkeuser, H., and Kroon, D. (1998). Experimental determination of the ontogenetic stable isotope variability in two morphotypes of Globigerinella siphonifera (d'Orbigny). *Marine Micropaleontology*, 35(3-4):141–160.

Bird, C., Darling, K. F., Russell, A. D., Davis, C. V., Fehrenbacher, J., Free, A., Wyman, M., and Ngwenya, B. T. (2017). Cyanobacterial endobionts within a major marine planktonic calcifier (Globigerina bulloides, Foraminifera) revealed by 16S rRNA metabarcoding. *Biogeosciences*, 14(4):901–920.

Bird, C., LeKieffre, C., Jauffrais, T., Meibom, A., Geslin, E., Filipsson, H. L., Maire, O., Russell, A. D., and Fehrenbacher, J. S. (2020). Heterotrophic Foraminifera Capable of Inorganic Nitrogen Assimilation. *Frontiers in Microbiology*, 11(December):3076.

Böhlke, J. K., Mroczkowski, S. J., and Coplen, T. B. (2003). Oxygen isotopes in nitrate: New reference materials for 18O:17O:16O measurements and observations on nitrate-water equilibration. *Rapid Communications in Mass Spectrometry*, 17(16):1835–1846.

Boltovskoy, E. (1969). Living Planktonic Foraminifera at the 90 E Meridian from the Equator to the Antarctic. *The Micropaleontolgy Project Inc.*, 15(2):237–255.

Braby, L., Deshayes, J., Beal, L., Morris, T., Novelli, G., Maitland, J., Ansorge, I., and Hermes, J. (2022). First Observations of Seasonal Variability in Water Mass Properties Across the Agulhas Current. *Journal of Geophysical Research: Oceans*, 127(9):1–20.

Bradshaw, J. (1959). Ecology of living planktonic foraminifera in the north and equatorial Pacific Ocean. *Contribution from the Cushman Foundation for Foraminiferal Research*, 10:25–64.

Braman, R. S. and Hendrix, S. A. (1989). Nanogram Nitrite and Nitrate Determination in Environmental and Biological Materials by Vanadium(III) Reduction with Chemiluminescence Detection. *Analytical Chemistry*, 61(24):2715–2718.

Bryden, H. L. and Beal, L. (2001). Role of the Agulhas Current in Indian Ocean circulation and associated heat and freshwater fluxes. *Deep-Sea Research Part I: Oceanographic Research Papers*, 48(8):1821–1845.

Bryden, H. L., Beal, L., and Duncan, L. M. (2005). Structure and Transport of the Agulhas Current and Its Temporal Variability. *Journal of Oceanography*, 61:479–492.

Caesar, L., McCarthy, G. D., Thornalley, D., Cahill, N., and Rahmstorf, S. (2021). Current Atlantic Meridional Overturning Circulation weakest in last millennium. *Nature Geoscience*, 14(3):118–120.

Caron, D., Bé, A. W. H., and Anderson, O. R. (1982). Effects of variations in light intensity on life processes of the planktonic foraminifer Globigerinoides sacculifer in laboratory culture. *Journal of the Marine Biological Association of the United Kingdom*, 62(2):435–451.

Caron, D. A. and Bé, A. W. H. (1984). PREDICTED AND OBSERVED FEEDING RATES OF THE GLOBIGERINOIDES SACCULIFER. *Bulletin of Marine Science*, 35(1):1–10.

Carpenter, E. J., Harvey, H. R., Brian, F., and Capone, D. G. (1997). Biogeochemical tracers of the marine cyanobacterium Trichodesmium. *Deep-Sea Research Part I: Oceanographic Research Papers*, 44(1):27–38.

Checkley, D. M. and Miller, C. A. (1989). Nitrogen isotope fractionation by oceanic zooplankton. *Deep Sea Research Part A, Oceanographic Research Papers*, 36(10):1449–1456.

Chen, G., Yang, J., and Han, G. (2021). Remote Sensing of Environment Eddy morphology : Egg-like shape, overall spinning, and oceanographic implications. *Remote Sensing of Environment*, 257(March 2020):112348.

Chronopoulou, P.-M., Salonen, I., Bird, C., Reichart, G. J., and Koho, K. A. (2019). Metabarcoding insights into the trophic behavior and identity of intertidal benthic foraminifera. *Frontiers in Microbiology*, 10(MAY):1–16.

Coulbourn, W., Parker, F., and Berger, W. (1980). Faunal and Solution Patterns of Planktonic Foraminifera in Surface Sediments of the North Pacific. *Marine Micropaleontology*, 5:329 – 399.

Darling, K., Wade, C. M., Kroon, D., and Leigh, A. J. (1997). Planktic foraminiferal molecular evolution and their polyphyletic origins from benthic taxa. *Marine Micropaleontology*, 30:251–266.

Darling, K. F. and Wade, C. M. (2008). The genetic diversity of planktic foraminifera and the global distribution of ribosomal RNA genotypes. *Marine Micropaleontology*, 67(3-4):216–238.

Darling, K. F., Wade, M., Kroon, D., Brown, A. J. L., and Bijma, J. (1999). The diversity and distribution of modern planktic foraminiferal small subunit ribosomal RNA genotypes and their potential as tracers of present and past ocean circulations. *Palaeoceanography*, 14(1):3–12.

De Ruijter, W. P., Biastoch, A., Drijfhout, S. S., Lutjeharms, J. R., Matano, R. P., Pichevin, T., van Leeuwen, P. J., and Weijer, W. (1999). Indian-Atlantic interocean exchange: Dynamics, estimation and impact. *Journal of Geophysical Research*, 104(C9):20885–20910.

De Ruijter, W. P., Ridderinkhof, H., Lutjeharms, J. R., Schouten, M. W., and Veth, C. (2002). Observations of the flow in the Mozambique Channel. *Geophysical Research Letters*, 29(10):140–1.

De Ruijter, W. P., Ridderinkhof, H., and Schouten, M. W. (2004). Variability of the southwest Indian Ocean. *Philosophical Transactions of the Royal Society A: Mathematical, Physical and Engineering Sciences*, 363(1826):63–76.

De Vargas, C., Bonzon, M., Rees, N. W., Pawlowski, J., and Zaninetti, L. (2002). A molecular approach to biodiversity and biogeography in the planktonic foraminifer Globigerinella siphonifera (d'Orbigny). *Marine Micropaleontology*, 45(2):101–116.

Delwiche, C. C., Zinke, P. J., Johnson, C. M., and Virginia, R. A. (1979). Nitrogen isotope distribution as a presumptive indicator of nitrogen fixation. *Botanical Gazette*, 140:65–69.

Donohue, K. A. and Toole, J. M. (2003). A near-synoptic survey of the Southwest Indian Ocean. *Deep-Sea Research Part II: Topical Studies in Oceanography*, 50(12-13):1893–1931.

Dugenne, M. and Gradoville, M. R. (2022). Nitrogen fixation in mesoscale eddies of the North Pacific Subtropical Gyre : patterns and mechanisms.

Duncombe Rae, C. M. (1991). Agulhas retroflection rings in the South Atlantic Ocean: An overview. *South African Journal of Marine Science*, 11(1):327–344.

Durgadoo, J. V., Loveday, B., Reason, C., Penven, P., and Biastoch, A. (2013). Agulhas Leakage Predominantly Responds to the Southern Hemisphere Westerlies. *Journal of Physical Oceanography*, 43:2113–2131.

Durgadoo, J. V., Rühs, S., Biastoch, A., and Böning, C. W. (2017). Indian Ocean sources of Agulhas leakage. *Journal of Geophysical Research: Oceans*, 122(4):3481–3499.

Dyez, K. A., Zahn, R., and Hall, I. R. (2014). Multicentennial Agulhas leakage variability and links to North Atlantic climate during the past 80,000-years. *Paleoceanography*, 29(12):1238–1248.

Faber, W. W., Anderson, O. R., Lindsey, J. L., and Caron, D. A. (1988). Algal-foraminiferal symbiosis in the planktonic foraminifer Globigerinella aequilateralia; I, Occurrence and stability of two mutually exclusive chrysophyte endosymbionts and their ultrastructure. *Journal of Foraminiferal Research*, 18(4):334–343.

Fawcett, S. E., Lomas, M. W., Casey, J. R., Ward, B. B., and Sigman, D. M. (2011). Assimilation of upwelled nitrate by small eukaryotes in the Sargasso Sea. *Nature Geoscience*, 4(10):717–722.

Fawcett, S. E., Ward, B. B., Lomas, M. W., and Sigman, D. M. (2015). Vertical decoupling of nitrate assimilation and nitrification in the Sargasso Sea. *Deep-Sea Research Part I: Oceanographic Research Papers*, 103:64–72.

Fine, R. A., Smethie, W. M., Bullister, J. L., Rhein, M., Min, D. H., Warner, M. J., Poisson, A., and Weiss, R. F. (2008). Decadal ventilation and mixing of Indian Ocean waters. *Deep-Sea Research Part I: Oceanographic Research Papers*, 55(1):20–37.

Fong, A. A., Karl, D. M., Lukas, R., Letelier, R. M., Zehr, J. P., and Church, M. J. (2008). Nitrogen fixation in an anticyclonic eddy in the oligotrophic North Pacific Ocean. *ISME Journal*, 2(6):663–676.

Fraile, I., Schulz, M., Mulitza, S., and Kucera, M. (2008). Predicting the global distribution of planktonic foraminifera using a dynamic ecosystem model. *Biogeosciences*, 5(3):891–911.

Galbraith, E. D., Sigman, D. M., Robinson, R., and Pedersen, T. F. (2008). *Nitrogen in Past Marine Environments*.

Galbraith, E. D. and Skinner, L. C. (2020). The Biological Pump during the Last Glacial Maximum. *Annual Review of Marine Science*, 12:559–586.

Gastrich, M. (1987). Ultrastructure of a new intracellular symbiotic alga found within planktonic foraminifera. *Journal of Phycology*, 25:623–632.

Gonfiantini, R., Stichler, W., and Rozanski, K. (1995). Standards and intercomparison materials distributed by the international atomic energy agency for stable isotope measurements. In *Proceedings of a consultants meeting held in Vienna, 1 - 3 December 1993*, pages 13–29.

Gordon, A. L. (1985). Indian-Atlantic Transfer of Thermocine Water at the Agulhas Retroflection. *Science*, 227:1030–1033.

Gordon, A. L. (1986). Interocean exchange of thermocline water. *Journal of Geophysical Research*, 91(C4):5037.

Gordon, A. L., Lutjeharms, J. R., and Gründlingh, M. L. (1987). Stratification and circulation at the Agulhas Retroflection. *Deep Sea Research Part A, Oceanographic Research Papers*, 34(4):565–599.

Graham, R. M., De Boer, A. M., Heywood, K. J., Chapman, M. R., and Stevens, D. P. (2012). Southern Ocean fronts: Controlled by wind or topography? *Journal of Geophysical Research: Oceans*, 117(8):1–14.

Granger, J. and Sigman, D. M. (2009). Removal of nitrite with sulfamic acid for nitrate N and O isotope analysis with the denitrifier method. *Rapid Communications in Mass Spectrometry*, 23:3753–3762.

Gründlingh, M. L., Carter, R. A., and Stanton, R. C. (1991). Circulation and water properties of the southwest Indian Ocean, Spring 1987. *Progress in Oceanography*, 28(4):305–342.

Hallock, P. (1981). Algal symbiosis: A mathematical analysis. *Marine Biology*, 62(4):249–255.

Hayward, T. L. (1987). The nutrient distribution and primary production in the central North Pacific. *Deep Sea Research Part A, Oceanographic Research Papers*, 34(9):1593–1627.

Hemleben, C., Spindler, M., and Anderson, O. R. (1989). *Modern Planktonic Foraminifera.* Springer-Verlag, New York, 1 edition.

Herraiz-Borreguero, L. and Rintoul, S. R. (2011). Subantarctic mode water: Distribution and circulation. *Ocean Dynamics*, 61(1):103–126.

Hoering, T. C. and Ford, H. T. (1960). The Isotope Effect in the Fixation of Nitrogen by Azotobacter. *J. Am Chem Soc.*, 82:376–378.

Holl, C., Waite, A. M., Pesant, S., Thompson, P. A., and Montoya, J. (2007). Unicellular diazotrophy as a source of nitrogen to Leeuwin Current coastal eddies. *Deep-Sea Research Part II: Topical Studies in Oceanography*, 54(8-10):1045–1054.

Hood, R. R., Beckley, L. E., and Wiggert, J. D. (2017). Biogeochemical and Ecological Impacts of Boundary Currents in the Indian Ocean. *Progress in Oceanography*, 156:290–325.

Huang, B., Jian, Z., Cheng, X., and Wang, P. (2007). Foraminiferal responses to upwelling variations in the South China Sea over the last 220 000 years. *Marine Micropaleontology*, 47:1–15.

Huber, B. T., Bijma, J., and Darling, K. (1997). Cryptic Speciation in the Living Planktonic Foraminifer Globigerinella siphonifera (d'Orbigny). *Paleobiology*, 23(1):33–62.

Imawaki, S., Bower, A. S., Beal, L., and Qiu, B. (2013). *Western boundary currents*, volume 103. Elsevier Ltd., 2 edition.

Jena, B., Swain, D., and Avinash, K. (2012). Investigation of the biophysical processes over the oligotrophic waters of south indian ocean subtropical gyre, triggered by cyclone edzani. *International Journal of Applied Earth Observation and Geoinformation*, 18(1):49–56.

Karl, D. M. (1999). A sea of change: Biogeochemical variability in the North Pacific Subtropical Gyre. *Ecosystems*, 2(3):181–214.

Karstensen, J. and Quadfasel, D. (2002). Water subducted into the Indian Ocean subtropical gyre. *Deep Sea Research Part II*, 49:1441–1457.

Karstensen, J. and Tomczak, M. (1997). Ventilation processes and water mass ages in the thermocline of the southeast Indian Ocean. *Geophys. Res. Lett.*, 24(22):2777–2780.

Knapp, A. N., Sigman, D. M., and Lipschultz, F. (2005). N isotopic composition of dissolved organic nitrogen and nitrate at the Bermuda Atlantic Time-series study site. *Global Biogeochemical Cycles*, 19(1):1–15.

Kolasinski, J., Kaehler, S., and Jaquemet, S. (2012). Distribution and sources of particulate organic matter in a mesoscale eddy dipole in the Mozambique Channel (southwestern Indian Ocean): Insight from C and N stable isotopes. *Journal of Marine Systems*, 96-97:122–131.

Kontakiotis, G., Efstathiou, E., Zarkogiannis, S., Besiou, E., and Antonarakou, A. (2021). Latitudinal Differentiation among Modern Planktonic Foraminiferal Populations of Central Mediterranean : Species – Specific Distribution Patterns and Size Variability. *Journal of Marine Science and Engineering*, 9(551):1–23.

Koutsodendris, A., Pross, J., and Zahn, R. (2014). Exceptional Agulhas leakage prolonged interglacial warmth during MIS 11c in Europe. *Palaeoceanography*, 29:1062–1071.

Kucera, M. (2007). Chapter Six Planktonic Foraminifera as Tracers of Past Oceanic Environments. *Developments in Marine Geology*, 1(November 2017):213–262.

Lamont, T., Barlow, R. G., Morris, T., and van den Berg, M. A. (2014). Characterisation of mesoscale features and phytoplankton variability in the Mozambique Channel. *Deep-Sea Research Part II: Topical Studies in Oceanography*, 100:94–105.

Lamy, F., Kaiser, J., Arz, H., Hebbeln, D., Ninnemann, U., Timm, O., Timmerman, A., and Toggweiler, J. (2007). Modulation of the bipolar seesaw in the Southeast Pacific during Termination 1. *Earth and Planetary Science Letters*, 259:400–413.

Lee, J. J., Freudenthal, H., Kossoy, V., and Bé, A. W. H. (1965). Cytological Observations on Two Planktonic Foraminifera, Globigerina bulloides and Globigerinoides ruber. *J. Protozool.*, 12:531–542.

Lehmann, M. F., Bernasconi, S. M., Barbieri, A., and McKenzie, J. A. (2002). Preservation of organic matter and alteration of its carbon and nitrogen isotope composition during simulated and in situ early sedimentary diagenesis. *Geochimica et Cosmochimica Acta*, 66(20):3573–3584.

Lekieffre, C., Spero, H. J., Fehrenbacher, J. S., Russell, A. D., Ren, H., Geslin, E., and Meibom, A. (2020). Ammonium is the preferred source of nitrogen for planktonic foraminifer and their dinoflagellate symbionts: N recycling in a symbiotic foraminifer. *Proceedings of the Royal Society B: Biological Sciences*, 287(1929):1–10.

Lessa, D., Morard, R., Jonkers, L., Venancio, I. M., Reuter, R., Baumeister, A., Albuquerque, A. L., and Kucera, M. (2020). Distribution of planktonic foraminifera in the subtropical South Atlantic: depth hierarchy of controlling factors. *Biogeosciences*, 17(16):4313–4342.

Li, C., Sonke, J. E., Le Roux, G., Van der Putten, N., Piotrowska, N., Jeandel, C., Mattielli, N., Benoit, M., Wiggs, G. F., and De Vleeschouwer, F. (2020). Holocene

dynamics of the southern westerly winds over the Indian Ocean inferred from a peat dust deposition record. *Quaternary Science Reviews*, 231:1–13.

Li, D. W., Xiang, R., Wu, Q., and Kao, S. J. (2019). Planktic foraminifera-bound organic nitrogen isotopic composition in contemporary water column and sediment trap. *Deep-Sea Research Part I*, 143:28–34.

Lipschultz, F. (2001). A time-series assessment of the nitrogen cycle at BATS. *Deep-Sea Research Part II: Topical Studies in Oceanography*, 48(8-9):1897–1924.

Liu, H., Zhu, M., Guo, S., Zhao, X., and Sun, X. (2020). Effects of an anticyclonic eddy on the distribution and community structure of zooplankton in the South China Sea northern slope. *Journal of Marine Systems*, 205(January):103311.

Lomas, M. W., Bates, N. R., Johnson, R. J., Knap, A. H., Steinberg, D. K., and Carlson, C. A. (2013). Two decades and counting: 24-years of sustained open ocean biogeochemical measurements in the Sargasso Sea. *Deep-Sea Research Part II: Topical Studies in Oceanography*, 93:16–32.

Lombard, F., Erez, J., Michel, E., and Labeyrie, L. (2009). Temperature effect on respiration and photosynthesis of the symbiont-bearing planktonic foraminifera Globigerinoides ruber, Orbulina universa, and Globigerinella siphonifera. *Limnology and Oceanography*, 54(1):210–218.

Lombard, F., Labeyrie, L., Michel, E., Bopp, L., Cortijo, E., Retailleau, S., Howa, H., and Jorissen, F. (2011). Modelling planktic foraminifer growth and distribution using an ecophysiological multi-species approach. *Biogeosciences*, 8(4):853–873.

Lončarić, N. (2006). Planktic foraminiferal content in a mature Agulhas eddy from the SE Atlantic: Any influence on foraminiferal export fluxes? *Geologia Croatica*, 59(1):41–50.

Malmgren, B., Berggren, W., and Lohmann, G. (1983). Evidence for punctuated gradualism in the Late Neogene Globorotalia tumida lineage of planktonic foraminifera. *Paleobiology*, 9(4):377–389.

Marcello, F., Tonelli, M., Ferrero, B., Marcello, F., Tonelli, M., Ferrero, B., and Wainer, I. (2022). Weakened AMOC upper limb compensated by strengthened South Atlantic subtropical gyre circulation in CESM1-LE simulations Weakened AMOC upper limb compensated by strengthened South Atlantic subtropical gyre circulation in CESM1-LE simulations. *Research Square*, Preprint:0–20.

Marino, G., Zahn, R., Ziegler, M., Purcell, C., Knorr, G., Hall, I. R., Ziveri, P., and Elderfield, H. (2013). Agulhas salt-leakage oscillations during abrupt climate changes of the Late Pleistocene. *Paleoceanography*, 28(3):599–606.

Marlow, J. R., Lange, C. B., Wefer, G., and Rosell-Melé, A. (2000). Upwelling Intensification As Part of the Pliocene-Pleistocene Climate Transition. *Science*, 290:2288–2291.

Marshall, T. A., Sigman, D. M., Beal, L. M., Foreman, A., Martínez-García, A., Blain, S., Campbell, E., Fripiat, F., Granger, R., Harris, E., Haug, G. H., Marconi, D., Oleynik, S., Rafter, P. A., Roman, R., Sinyanya, K., Smart, S. M., and Fawcett, S. E. (2023). The Agulhas Current Transports Signals of Local and Remote Indian Ocean Nitrogen Cycling. *Journal of Geophysical Research: Oceans*, 128:1–29.

Martínez-García, A., Jung, J., Ai, X. E., Sigman, D. M., Auderset, A., Duprey, N. N., Foreman, A., Fripiat, F., Leichliter, J., Lüdecke, T., Moretti, S., and Wald, T. (2022). Laboratory Assessment of the Impact of Chemical Oxidation, Mineral Dissolution, and Heating on the Nitrogen Isotopic Composition of Fossil-Bound Organic Matter. *Geochemistry, Geophysics, Geosystems*, 23(8):1–23.

McCartney, M. S. and Woodgate-Jones, M. E. (1991). A deep-reaching anticyclonic eddy in the subtropical gyre of the eastern South Atlantic. *Deep Sea Research*, 38:S411–S443.

Meckler, A. N., Ren, H., Sigman, D. M., Gruber, N., Plessen, B., Schubert, C. J., and Haug, G. H. (2011). Deglacial nitrogen isotope changes in the Gulf of Mexico: Evidence from bulk sedimentary and foraminifera-bound nitrogen in Orca Basin sediments. *Paleoceanography*, 26(4):1–13.

Meilland, J., Fabri-Ruiz, S., Koubbi, P., Monaco, C. L., Cotte, C., Hosie, G. W., Sanchez, S., and Howa, H. (2016). Planktonic foraminiferal biogeography in the Indian sector of the Southern Ocean: Contribution from CPR data. *Deep-Sea Research Part I: Oceanographic Research Papers*, 110:75–89.

Menzel, D. W. and Ryther, J. H. (1959). The annual cycle of primary production in the Sargasso Sea off Bermuda. *Deep Sea Research (1953)*, 6:351–367.

Minagawa, M. and Wada, E. (1984). Stepwise enrichment of 15N along food chains: Further evidence and the relation between 15N and animal age. *Geochimica et Cosmochimica Acta*, 48(5):1135–1140.

Mino, Y., Saino, T., Suzuki, K., and Marañón, E. (2002). Isotopic composition of suspended particulate nitrogen (δ 15 N sus) in surface waters of the Atlantic Ocean from 50°N to 50°S . *Global Biogeochemical Cycles*, 16(4):7–1.

Mobius, J. (2013). Isotope fractionation during nitrogen remineralization (ammonification): Implications for nitrogen isotope biogeochemistry. *Geochimica et Cosmochimica Acta*, 105:422–432.

Mollenhauer, G., Eglinton, T. ., Ohkouchi, N., Schneider, R., Müller, P., Grootes, P., and Rullkotter, J. (2003). Asynchronous alkenone and foraminifera records from the Benguela Upwelling System. *Geochemica et Cosmochimica Acta*, 67(12):2157–2171.

Montoya, J., Wiebe, P., and McCarthy, J. J. (1992). Natural abundance of 15N in particulate nitrogen and zooplankton in the Gulf Stream region and warm-core ring 86A. *Deep Sea Research*, 39:S636–S391.

Morard, R., Darling, K. F., Mahé, F., Audic, S., Ujiié, Y., Weiner, A. K., André, A., Seears, H. A., Wade, C. M., Quillévéré, F., Douady, C. J., Escarguel, G., de Garidel-Thoron, T., Siccha, M., Kucera, M., and de Vargas, C. (2015). PFR2: A curated database of planktonic foraminifera 18S ribosomal DNA as a resource for studies of plankton ecology, biogeography and evolution. *Molecular Ecology Resources*, 15(6):1472–1485.

Morard, R., Quillévéré, F., Escarguel, G., de Garidel-Thoron, T., de Vargas, C., and Kucera, M. (2013). Ecological modeling of the temperature dependence of cryptic species of planktonic Foraminifera in the Southern Hemisphere. *Palaeogeography, Palaeoclimatology, Palaeoecology*, 391:13–33.

Noyon, M., Morris, T., Walker, D., and Huggett, J. (2019). Plankton distribution within a young cyclonic eddy off south-western Madagascar. *Deep-Sea Research Part II: Topical Studies in Oceanography*, 166(August 2018):141–150.

Ortiz, J. D., Mix, A. C., and Collier, R. W. (1995). Environmental control of living symbiotic and asymbiotic foraminifera of the California Current. *Paleoceanography*, 10(6):987–1009.

Palastanga, V., van Leeuwen, P. J., Schouten, M., and De Ruijter, W. P. (2007). Flow structure and variability in the subtropical Indian Ocean: Instability of the South Indian Ocean countercurrent. *Journal of Geophysical Research: Oceans*, 112(1):1–11.

Peeters, F. J., Acheson, R., Brummer, G.-J. A., De Ruijter, W. P., Schneider, R., Ganssen, G. M., Ufkes, E., and Kroon, D. (2004). Vigorous exchange between the Indian and Atlantic oceans at the end of the past five glacial periods. *Nature*, 430(7000):661–5.

Peeters, F. J. and Brummer, G. J. A. (2002). The seasonal and vertical distribution of living planktic foraminifera in the NW Arabian Sea. *Geological Society Special Publication*, 195:463–497.

Pelegrí, J. L. and Csanady, G. T. (1991). Nutrient transport and mixing in the Gulf Stream. *Journal of Geophysical Research*, 96(C2):2577–2583.

Peterson, B. J. and Fry, B. (1987). Stable isotopes in ecosystem studies. *Annual review of ecology and systematics. Vol. 18*, 18:293–320.

Ponsoni, L., Aguiar-González, B., Ridderinkhof, H., and Maas, L. R. (2016). The East Madagascar Current: Volume transport and variability based on long-term observations. *Journal of Physical Oceanography*, 46(4):1045–1065.

Prasanna, K., Ghosh, P., Bhattacharya, S. K., Mohan, K., and Anilkumar, N. (2016). Isotopic disequilibrium in Globigerina bulloides and carbon isotope response to productivity increase in Southern Ocean. *Scientific Reports*, 6(October 2015):1–12.

Prell, W. L. and Curry, W. B. (1981). Western Arabian Sea. *Oceanologica Acta*, 4(1):91–98.

Pujol, C. and Grazzini, C. V. (1995). Distribution patterns of live planktic foraminifers as related to regional hydrography and productive systems of the Mediterranean Sea. *Marine Micropaleontology*, 25:187–217.

Rafter, P. A., Difiore, P. J., and Sigman, D. M. (2013). Coupled nitrate nitrogen and oxygen isotopes and organic matter remineralization in the Southern and Pacific Oceans. *Journal of Geophysical Research: Oceans*, 118(10):4781–4794.

Raj, R. P., Peter, B. N., and Pushpadas, D. (2010). Oceanic and atmospheric influences on the variability of phytoplankton bloom in the Southwestern Indian Ocean. *Journal of Marine Systems*, 82(4):217–229.

Rampen, S. W., Schouten, S., Koning, E., Brummer, G. J. A., and Sinninghe Damsté, J. (2008). A 90 kyr upwelling record from the northwestern Indian Ocean using a novel long-chain diol index. *Earth and Planetary Science Letters*, 276(1-2):207–213.

Rebotim, A., Voelker, A. H., Jonkers, L., Waniek, J. J., Meggers, H., Schiebel, R., Fraile, I., Schulz, M., and Kucera, M. (2017). Factors controlling the depth habitat of planktonic foraminifera in the subtropical eastern North Atlantic. *Biogeosciences*, 14(4):827–859.

Ren, H., Sigman, D. M., Chen, M. T., and Kao, S. J. (2012a). Elevated foraminifera-bound nitrogen isotopic composition during the last ice age in the South China Sea and its global and regional implications. *Global Biogeochemical Cycles*, 26(1):1–13.

Ren, H., Sigman, D. M., Meckler, A. N., Plessen, B., Robinson, R., Rosenthal, Y., and Haug, G. H. (2009). Foraminiferal isotope evidence of reduced nitrogen fixation in the ice age Atlantic Ocean. *Science*, 323(5911):244–248.

Ren, H., Sigman, D. M., Thunell, R. C., and Prokopenko, M. G. (2012b). Nitrogen isotopic composition of planktonic foraminifera from the modern ocean and recent sediments. *Limnology and Oceanography*, 57(4):1011–1024.

Ridderinkhof, H., Van Der Werf, P. M., Ullgren, J. E., Van Aken, H. M., Van Leeuwen, P. J., and De Ruijter, W. P. (2010). Seasonal and interannual variability in the Mozambique Channel from moored current observations. *Journal of Geophysical Research*, 115:1–18.

Rigual-Hernández, A. S., Sierro, F. J., Bárcena, M. A., Flores, J. A., and Heussner, S. (2012). Seasonal and interannual changes of planktic foraminiferal fluxes in the Gulf of Lions (NW Mediterranean) and their implications for paleoceanographic studies: Two 12-year sediment trap records. *Deep-Sea Research Part I: Oceanographic Research Papers*, 66:26–40.

Robinson, R., Smart, S. M., Cybulski, J. D., McMahon, K. W., Marcks, B., and Nowakowski, C. (2023). Insights from Fossil-Bound Nitrogen Isotopes in Diatoms, Foraminifera, and Corals. *Annual Review of Marine Science*, 15(1):1–24.

Rutherford, S., D'Hondt, S., and Prell, W. (1999). Environmental controls on the geographic distribution of zooplankton diversity. *Nature*, 400(6746):749–753.

Saino, T. and Hattori, A. (1980). 15N natural abundance in oceanic suspended particulate matter. *Nature*, 283:752–754.

Sarmiento, J. L., Gruber, N., Brzezinski, M. A., and Dunne, J. P. (2004). High-latitude controls of thermocline nutrients and low latitude biological productivity. *Nature*, 427(6969):56–60.

Schiebel, R. and Hemleben, C. (2000). Interannual variability of planktic foraminiferal populations and test flux in the eastern North Atlantic Ocean (JGOFS). *Deep-Sea Research Part II: Topical Studies in Oceanography*, 47(9-11):1809–1852.

Schiebel, R. and Hemleben, C. (2005). Modern planktic foraminifera. *Paläontologische Zeitschrift*, 79(1):135–148.

Schiebel, R., Waniek, J., Bork, M., and Hemleben, C. (2001). Planktic foraminiferal production stimulated by chlorophyll redistribution and entrainment of nutrients. *Deep-Sea Research Part I: Oceanographic Research Papers*, 48(3):721–740.

Schouten, M. W., De Ruijter, W. P., Van Leeuwen, P. J., and Ridderinkhof, H. (2003). Eddies and variability in the Mozambique Channel. *Deep-Sea Research Part II: Topical Studies in Oceanography*, 50(12-13):1987–2003.

Scott, G. H. (2020). Zooplankters in an oligotrophic ocean: Contrasts in the niches of Globigerinoides ruber and Trilobatus sacculifer (Foraminifera: Globigerinida) in the South Pacific. *Ecoscience*, 27(4):269–278.

Seears, H. A., Darling, K. F., and Wade, C. M. (2012). Ecological partitioning and diversity in tropical planktonic foraminifera. *BMC Evolutionary Biology*, 12(1):54.

Sigman, D. M. and Casciotti, K. (2009). Nitrogen Isotopes in the Ocean. *Encyclopedia of Ocean Sciences*, (Ms 632):1884–1894.

Sigman, D. M., Casciotti, K. L., Andreani, M., Barford, C., Galanter, M., and Böhlke, J. K. (2001). A bacterial method for the nitrogen isotopic analysis of nitrate in seawater and freshwater. *Analytical Chemistry*, 73(17):4145–4153.

Sigman, D. M., Granger, J., DiFiore, P. J., Lehmann, M. F., Ho, R., Cane, G., and van Geen, A. (2005). Coupled nitrogen and oxygen isotope measurements of nitrate along the eastern North Pacific margin. *Global Biogeochemical Cycles*, 19(4):1–14.

Sigman, D. M., M. A, A., McCorkle, D. C., Francois, R., and Fischer, G. (1999). The δ15N of nitrate in the Southern Ocean: Nitrate consumption in surface waters. *Global Biogeochemical Cycles*, 13(4):1149–1166.

Simon, M., Arthur, K., Hall, I. R., Peeters, F. J., Loveday, B. R., Barker, S., Ziegler, M., and Zahn, R. (2013). Millennial-scale Agulhas Current variability and its implications for salt-leakage through the Indian–Atlantic Ocean Gateway. *Earth and Planetary Science Letters*, 383:101–112.

Sloyan, B. M. and Rintoul, S. R. (2001). Circulation, renewal, and modification of antarctic mode and intermediate water. *Journal of Physical Oceanography*, 31(4):1005–1030.

Smart, S. M., Fawcett, S. E., Ren, H., Schiebel, R., Tompkins, E. M., García, A. M., Stirnimann, L., Roychoudhury, A., Haug, G. H., and Sigman, D. M. (2020). The Nitrogen Isotopic Composition of Tissue and Shell-Bound Organic Matter of Planktic Foraminifera in Southern Ocean Surface Waters. *Geochemistry, Geophysics, Geosystems*, 21:1–29.

Smart, S. M., Ren, H., Fawcett, S. E., Schiebel, R., Conte, M., Rafter, P. A., Ellis, K. K., Weigand, M. A., Oleynik, S., Haug, G. H., and Sigman, D. M. (2018). Groundtruthing the planktic foraminifer-bound nitrogen isotope paleo-proxy in the Sargasso Sea. *Geochimica et Cosmochimica Acta*, 235:463–482.

Spindler, M., Hemleben, C., Salomons, J. B., and Smit, L. P. (1984). Feeding behavior of some planktonic foraminifers in laboratory cultures. *Journal of Foraminiferal Research*, 14(4):237–249.

Stainbank, S., Kroon, D., Rüggeberg, A., Raddatz, J., de Leau, E. S., Zhang, M., and Spezzaferri, S. (2019). *Controls on planktonic foraminifera apparent calcification depths for the northern equatorial Indian Ocean*, volume 14.

Stoecker, D. K. (1998). Conceptual models of mixotrophy in planktonic protists and some ecological and evolutionary implications. *European Journal of Protistology*, 34(3):281–290.

Stramma, L. and Lutjeharms, J. R. (1997). The flow field of the subtropical gyre of the South Indian Ocean. *Journal of Geophysical Research*, 102:5513–5530.

Takagi, H., Kimoto, K., Fujiki, T., Saito, H., Schmidt, C., Kucera, M., and Moriya, K. (2019). Characterizing photosymbiosis in modern planktonic foraminifera. *Biogeosciences*, 16(17):3377–3396.

Thornalley, D., Delia, W., Ortega, P., Robson, J. I., Brierley, C. M., Davis, R., Hall, I. R., Moffa-sanchez, P., Rose, N. L., Spooner, P. T., Yashayaev, I., and Keigwin, L. D. (2018). Atlantic overturning during the past 150 years. *Nature*, 556(7700):227–230.

Treibergs, L. A., Fawcett, S. E., Lomas, M. W., and Sigman, D. M. (2014). Nitrogen isotopic response of prokaryotic and eukaryotic phytoplankton to nitrate availability in Sargasso Sea surface waters. *Limnology and Oceanography*, 59(3):972–985.

Ufkes, E., Jansen, J. H., and Brummer, G. J. A. (1998). Living planktonic foraminifera in the eastern South Atlantic during spring: Indicators of water masses, upwelling and the Congo (Zaire) river plume. *Marine Micropaleontology*, 33(1-2):27–53.

Uhle, M. E., Macko, S. A., Spero, H. J., David W, L., Ruddiman, W. F., and Engel, M. H. (1999). The fate of nitrogen in the Orbulina universa foraminifera-symbiont system determined by nitrogen isotope analyses of shell-bound organic matter. *Limnology and Oceanography*, 44(8):1968–1977.

Valentine, H. R., Lutjeharms, J. R., and Brundrit, G. B. (1993). The water masses and volumetry of the southern Agulhas Current region. *Deep-Sea Research Part I*, 40(6):1285–1305.

Van Aken, H. (2007). *The oceanic thermohaline circulation: an introduction*, volume 39. Springer Science+Business Media LLC.

Van Sebille, E., Biastoch, A., Van Leeuwen, P. J., and De Ruijter, W. P. (2009). A weaker Agulhas current leads to more Agulhas leakage. *Geophysical Research Letters*, 36(3):10–13.

Venancio, I. M., Belem, A. L., Santos, T. P., Lessa, D., Albuquerque, A. L., Mulitza, S., Schulz, M., and Kucera, M. (2017). Calcification depths of planktonic foraminifera from the southwestern Atlantic derived from oxygen isotope analyses of sediment trap material. *Marine Micropaleontology*, 136(January):37–50.

Vinayachandran, P. N. M., Masumoto, Y., Roberts, M. J., Huggett, J. A., Halo, I., Chatterjee, A., Amol, P., Gupta, G. V., Singh, A., Mukherjee, A., Prakash, S., Beckley, L. E., Raes, E. J., and Hood, R. R. (2021). Reviews and syntheses: Physical and biogeochemical processes associated with upwelling in the Indian Ocean. *Biogeosciences*, 18:5967–6029.

Volk, T. and Hoffert, M. I. (1985). Ocean carbon pumps: analysis of relative strengths and efficiencies in ocean-driven atmospheric CO2 changes. In Sundquist, E. and Broecker,

W., editors, *The Carbon Cycle and Atmospheric CO2: Natural Variations Archaean to Present*, volume 32, pages 99–110. DC: Am. Geophys. Union, Washington.

Wada, E. and Hattori, A. (1978). Nitrogen isotope effects in the assimilation of inorganic nitrogenous compounds by marine diatoms. *Geomicrobiology Journal*, 1:85–101.

Wallschuss, S., Mdutyana, M., Parrott, R. G., Forrer, H. J., Roman, R., Walker, D., Ansorge, I., and Fawcett, S. E. (2022). The Influence of Agulhas Leakage on Primary Production and Nitrogen Cycling in the Southeastern Atlantic Ocean. *Journal of Geophysical Research: Oceans*, 127:1–26.

Waser, N. A., Yin, K., Yu, Z., Tada, K., Harrison, P. J., Turpin, D. H., and Calvert, S. E. (1998). Nitrogen isotope fractionation during nitrate, ammonium and urea uptake by marine diatoms and coccolithophores under various conditions of N availability. *Marine Ecology Progress Series*, 169:29–41.

Watkins, J. M., Mix, A. C., and Wilson, J. (1996). Living planktic foraminifera: Tracers of circulation and productivity regimes in the central equatorial Pacific. *Deep-Sea Research Part II: Topical Studies in Oceanography*, 43(4-6):1257–1282.

Weigand, M. A., Foriel, J., Barnett, B., Oleynik, S., and Sigman, D. M. (2016). Updates to instrumentation and protocols for isotopic analysis of nitrate by the denitrifier method. *Rapid Communications in Mass Spectrometry*, 30(12):1365–1383.

Weijer, W., De Ruijter, W. P., Sterl, A., and Drijfhout, S. S. (2002). Response of the Atlantic overturning circulation to South Atlantic sources of buoyancy. *Global and Planetary Change*, 34(3-4):293–311.

Weijer, W. and van Sebille, E. (2014). Impact of Agulhas leakage on the Atlantic overturning circulation in the CCSM4. *Journal of Climate*, 27(1):101–110.

Weiner, A. K., Weinkauf, M. F., Kurasawa, A., Darling, K. F., and Kucera, M. (2015). Genetic and morphometric evidence for parallel evolution of the Globigerinella calida morphotype. *Marine Micropaleontology*, 114:19–35.

Weiner, A. K., Weinkauf, M. F., Kurasawa, A., Darling, K. F., Kucera, M., and Grimm, G. W. (2014). Phylogeography of the tropical planktonic foraminifera lineage Globigerinella reveals isolation inconsistent with passive dispersal by ocean currents. *PLoS ONE*, 9(3):1–12.

Chapter 4

Nitrogen isotopic composition of modern ocean and core-top planktic foraminifera in the South Atlantic

Abstract

The isotope ratio of organic nitrogen in fossil foraminifera (FB-δ^{15}N) has the potential to help reconstruct changes in upper ocean biogeochemistry and circulation. However, the drivers of isotopic variation affecting FB-δ^{15}N are not well constrained in the South Atlantic due to the complex interplay between Atlantic, Indian and Southern Ocean waters. This study reports modern (net tow) and recent fossil (core-top) foraminifera ^{15}N measurements from the Cape Basin in order to assess the viability of the method in this region. We find positive species-specific correlations between modern foraminifer tissue- (biomass) and shell-bound δ^{15}N (regression slope = 0.57), as well as between modern and fossil FB-δ^{15}N (regression slope = 0.54). However, we also observe a consistent offset of 1.4 ‰ between the tissue and modern shell data, and 2.8 ‰ between modern and fossil FB-δ^{15}N, indicating that additional influences acted to alter FB-δ^{15}N prior to deposition. We propose that the tissue-shell offsets are due to recent change in environmental conditions prior to net tow sampling whilst modern-fossil shell offsets are generated through some combination of (1) deposition of transported foraminifera from the continental shelf; (2) foraminifer consumption of high-^{15}N particulate organic nitrogen (PON) at greater depths during gametogenesis; (3) selective dissolution of low-δ^{15}N foraminifer test chambers upon export from the photic zone, and/or selective dissolution of smaller individuals; (4) FB-δ^{15}N reflecting the integration of different environmental conditions over several thousand years; and (5) a change in the growth period of foraminifera relative to seasonal biogeochemical cycles over the mid- to late Holocene. Nevertheless, the consistency of the modern and fossil FB-δ^{15}N offset across multiple species and the strong relationship between tissue and modern shell-bound δ^{15}N are promising with regards to use of the palaeoceanographic proxy in this region, and suggest that variations in the fossil record can likely be attributed to changes in upper ocean biogeochemical cycling.

4.1 Introduction

The Southeast Atlantic is a complex region that is influenced by the interplay of oceanic and atmospheric processes of Atlantic, Indian and Southern Ocean origin. The interplay between the Benguela Upwelling System, South Atlantic Subtropical Gyre, the Agulhas Current and Southern Ocean fronts result in a region controlled by nonlinear mesoscale dynamics that is subject to large amounts of turbulence (Lutjeharms, 1981; De Ruijter and Boudra, 1985; Duncombe Rae et al., 1992; Gordon et al., 1992; De Ruijter et al., 1999; Dencausse et al., 2010). Variability in this region is particularly relevant for global ocean circulation, as it is a gateway for the transport of upper ocean Indian Ocean waters to the Atlantic, where they ultimately contribute to deepwater formation via convective overturning (Gordon, 1985; Broecker, 1991; Gordon et al., 1992; Biastoch et al., 2008; Van Sebille et al., 2010). This transfer of Indian Ocean waters, known as Agulhas leakage, occurs predominantly through the generation of anticyclonic eddies and filaments at the point of Agulhas Current retroflection, south of South Africa (De Ruijter et al., 1999; Lutjeharms, 2006; Van Sebille et al., 2009). Water mass properties and oceanic variability in the southeast Atlantic have been linked to glacial-interglacial ocean-atmospheric changes, in particular with the large scale, density-driven overturning system known as the Atlantic Meridional Overturning Circulation (AMOC) (Lutjeharms, 2006; Beal et al., 2011). Understanding the variability of southeast Atlantic ocean dynamics and Agulhas leakage is therefore crucial for predicting future impacts of global climate change (Weijer et al., 2002; Biastoch et al., 2008; Caley et al., 2012).

Various proxy methods have been used to reconstruct centennial- and millennial- scale climate variability in the region of Agulhas leakage, including radiogenic isotope composition (e.g., Franzese et al. 2006), trace element ratios (Martínez-Méndez et al., 2008), oxygen and hydrogen isotopes (e.g., Flores et al. 1999; Kasper et al. 2014), grain size analyses (e.g., Stuut et al. 2002; Granger et al. 2018), and the relative abundance of foraminifera (e.g., Peeters et al. 2004; Caley et al. 2014). However, the complexity of its oceanographic setting makes straightforward interpretation of the region's paleoclimate records challenging, and new proxies are necessary to help disentangle the competing processes that may be confounding our interpretation of past climate dynamics.

4.1.1 Nitrogen isotopes as a proxy for southeast Atlantic variability

One promising avenue by which progress could be made in this regard involves reconstructing how the N isotope composition (δ^{15}N) of organic matter exported to the seafloor may have changed over time. This organic matter contains information about ocean productivity and nutrient-cycling processes that acted upon it prior to and during its sinking and burial (Hoering and Ford, 1960; Cline and Kaplan, 1975; Altabet and Francois, 1994; Carpenter et al., 1997; Sigman et al., 1999). This is because the biological processes of

creating, removing and converting between forms of bioavailable N are all associated with fractionation of N isotopes (Wellman et al., 1968; Altabet and Francois, 1994; Montoya, 1994). Given that N is an essential and often limiting element for phytoplankton productivity, the reconstruction of N isotopes has thus long been a focus of the paleoceanographic community (Sigman et al., 2009).

Globally, downcore reconstruction efforts initially focused on measuring bulk sedimentary δ^{15}N over millennial (e.g., Kienast, 2000; Freudenthal et al., 2002; Deutsch et al., 2004; Tesdal et al., 2013, and references therein) and even longer (e.g. Etourneau et al., 2009) timescales, with several records even having been produced in the southeast Atlantic region (Rau et al., 2002; Pichevin et al., 2005; Etourneau et al., 2009). However, alteration of the original δ^{15}N in bulk sedimentary organic matter can occur through microbial degradation during sinking and after burial (Freudenthal et al., 2001; Gaye-Haake et al., 2005; Gaye et al., 2013), as bacteria preferentially consume the lighter ^{14}N isotope, raising the δ^{15}N of the remaining original matter (i.e., in bulk sediment) (Möbius et al., 2010). There are also processes that add extraneous material post deposition (Schubert and Calvert, 2001; Robinson et al., 2012), confounding interpretation of bulk sediment δ^{15}N records. In an effort to eliminate this uncertainty in the bulk sediment record, the δ^{15}N of organic matter bound in fossils has been proposed as a reliable alternative for reconstructing past N cycling, since organic N 'trapped' in a calcite shell matrix appears to be largely protected from diagenesis (Sigman et al., 1999; Ren et al., 2009; Straub et al., 2013; Martínez-García et al., 2014; Studer et al., 2015; Smart et al., 2018; Martínez-García et al., 2022), with downcore records of foraminifera showing minimal changes in amino acid composition and N content over time (King and Hare, 1972; Robbins and Brew, 1990; Ren et al., 2009). Reconstructions extending back as far as the Cenozoic suggest that microfossils have the potential to protect organic matter on time scales of millions of years (Kast et al., 2019; Auderset et al., 2022).

Spurred by initial promising ground-truthing research (Ren et al., 2009), which showed a strong correlation between the shell-bound (FB-)δ^{15}N of foraminifera and thermocline nitrate δ^{15}N, reconstructions of FB-δ^{15}N have been applied on multiple timescales to reconstruct biogeochemical cycling (Ren et al., 2009; Meckler et al., 2011; Ren et al., 2012a; Straub et al., 2013; Martínez-García et al., 2014; Ren et al., 2015; Studer et al., 2015; Kast et al., 2019; Studer et al., 2021; Auderset et al., 2022). Broadly, these studies have found that nutrient dynamics at a local scale are demonstrably affected by global-scale climate forcing at multiple timescales, and that local responses to climate fluctuations have significant implications for the partitioning of carbon within the ocean-atmosphere system.

Beyond their implication for global climate, however, these studies have also highlighted the need for detailed ground-truthing of FB-δ^{15}N. For instance, downcore FB-δ^{15}N records from multiple species at the same core site have revealed that species' patterns of isotopic variation can alternate between aligning with and diverging from one another

during glacial-interglacial fluctuations (Ren et al., 2009; Meckler et al., 2011). This phenomenon, which suggests habitat-related or biological control, can affect foraminifera living at different depths (or those with different diets) to varying extents. Similar variation can result from changes in the season of peak productivity and foraminifer growth cycles (Fraile et al., 2009; Jonkers and Kučera, 2015). Given that our understanding of foraminifer physiology and biogeographic distribution are continually being updated, and that ground-truthing data on which the FB-δ^{15}N method is based is spatially-limited, there is a strong need to better understand the relationship between local biogeochemistry and FB-δ^{15}N in the modern ocean, particularly for areas with complex circulation like the SE Atlantic.

4.1.2 Existing ground-truthing studies of FB-δ^{15}N

Ground-truthing efforts into identifying the biogeochemical controls on FB-δ^{15}N involve comparisons between the δ^{15}N of modern (water column, tow-collected) foraminifer tissue and shells, sinking (trap-collected) shells, core top (i.e., recent sediment) fossils, present-day seawater nitrate, particulate organic nitrogen (PON) and larger particulates (bulk zooplankton) (Ren et al., 2012b; Smart et al., 2018, 2020, Chapter 2, Chapter 3). Physical oceanographic data (e.g., temperature, salinity and density) are used to supplement isotopic measurements, and can provide context regarding water column structure, source regions of nutrients, and seasonality. These data help to establish a comprehensive view of the local marine environment and relevant biogeochemical processes that might affect FB-δ^{15}N.

Thus far, ground-truthing FB-δ^{15}N data has predominantly focused on two subtropical locations (the Sargasso Sea and the South China Sea) and two Southern Ocean latitudinal transects, which include the Subantarctic Zone (SAZ) and Polar Frontal Zone (PFZ), south of South Africa (the two zones hereafter referred to together as the Subantarctic) (Ren et al., 2012b; Li et al., 2019; Smart et al., 2018, 2020). Both subtropical regions are N-limited (Dugdale and Goering, 1967; Chen et al., 2004; Lipschultz, 2001; Knapp et al., 2005; Zhang et al., 2020), whereas the Subantarctic is predominantly limited by iron and light (Martin, 1990; Mitchell et al., 1991; Sunda and Huntaman, 1997; DiFiore et al., 2006). In the former, changing degrees of nitrate consumption can be ruled out as a primary driver for upper ocean δ^{15}N variation on an annual (or longer) timescale (Knapp et al., 2005; Fawcett et al., 2015), whereas for the latter, the extent to which nitrate is consumed has been observed to influence FB-δ^{15}N in the SAZ (Lourey and Trull, 2001; Smart et al., 2020).

FB-δ^{15}N in low latitude regions appears to closely resemble the δ^{15}N of thermocline nitrate (Ren et al., 2009, 2012b; Li et al., 2019; Smart et al., 2018), whereas FB-δ^{15}N in the Subantarctic tracks ambient nitrate only when PON is positively correlated with thermocline nitrate (i.e., late spring to late summer, Smart et al. 2020). However, several common trends exist at all locations studied so far (as well as in the southeast Atlantic

and southwest Indian regions discussed in Chapters 2 and 3 of this thesis). Despite relatively large differences in the actual values of FB-δ^{15}N between regions, there are roughly consistent inter-species isotopic differences between dinoflagellate (obligatory) photosymbiotic-, facultatively photosymbiotic-, and symbiont-barren foraminifera species in the modern ocean, although this is not always the case in sediment records (Ren et al., 2012b; Li et al., 2019; Smart et al., 2018, 2020; Auderset et al., 2022). Symbiont-barren species (e.g., *Globorotalia truncatulinoides*) are typically high in δ^{15}N compared to facultatively photosymbiotic species (e.g., *Neogloboquadrina dutertrei* and *Globorotalia menardii*), which are in turn higher in δ^{15}N than species that rely upon dinoflagellate symbionts for their survival (e.g., *Globigerinoides ruber*, *Trilobus sacculifer* and *Orbulina universa*) (Bé and Hutson, 1977; Schiebel et al., 2017; Takagi et al., 2019). Furthermore, in all regions where it is present, the chrysophyte-hosting species *Globigerinella siphonifera* possesses an anomalously high tissue- and modern shell-bound δ^{15}N, often surpassing that of the symbiont-barren species (Chapter 2; Chapter 3; Ren et al., 2012b; Li et al., 2019; Smart et al., 2018). The average FB-δ^{15}N difference between symbiont-barren and -obligatory species in both tissue and modern shell data appears to be around 1-2 ‰ (Ren et al., 2012b; Smart et al., 2018, Chapter 2, Chapter 3), a difference roughly equivalent to half a trophic level (Post, 2002; Caut et al., 2009). The lower FB-δ^{15}N evident in dinoflagellate-hosting foraminifera species is thought to be due to the symbionts' recycling and retention of low δ^{15}N ammonium within the hosts that would otherwise be excreted (Ren et al., 2012b; Smart et al., 2018). Photosymbiosis in foraminifera therefore minimizes the trophic level effect, which usually raises a consumer's δ^{15}N by approximately 2-4 ‰ (Minagawa and Wada, 1984; Deniro, 1987; Post, 2002).

The positive linear relationship exhibited between species-specific tissue- and shell-bound δ^{15}N is also consistent in the two regions where tissue δ^{15}N was measured along with FB-δ^{15}N from living shells (Sargasso Sea and Subantarctic, Ren et al. 2012b; Smart et al. 2020, 2018; Robinson et al. 2023), as well as in the southeast Atlantic (Chapter 2). In the Sargasso Sea, there was no noticeable offset between the δ^{15}N of the foraminifer's tissue and what was incorporated into its shell matrix (Smart et al., 2018), on average, this lack of difference was also apparent in the Subantarctic, although larger standard deviations were associated with inter-species and intra-species differences in the offsets between shell- and tissue-bound δ^{15}N during the same season (Smart et al., 2020).

An small increase ($\sim$0.5-1.3 ‰) in FB-δ^{15}N has been observed between the net tow and sediment trap foraminifera in both the Sargasso Sea and South China Sea (Li et al., 2019; Smart et al., 2018). Although the organic matter found between calcite layers of shells is largely protected, an increase in FB-δ^{15}N has been observed to occur in the Sargasso during the initial export of foraminifera from the photic zone upon their death (Smart et al., 2018). There appears to be little to no isotopic deviation after this point, with the FB-δ^{15}N of recent core-top foraminifera roughly equivalent to that of recently dead, sinking organisms (Smart et al., 2018). One explanation is that the tow-to-trap δ^{15}N

increase is the consequence of preferential dissolution of thin-walled juveniles during post-death sinking (Peeters et al., 1999), where younger foraminifera (which may have formed a part of the net tow assemblage measured for living shells δ^{15}N) are removed through dissolution before burial (Smart et al., 2018). Smart et al. (2018) reasoned that younger foraminifera may subsist on a diet that is biased towards smaller, lower δ^{15}N prey (e.g., phytoplankton rather than larger copepods that are higher in δ^{15}N), meaning that the dissolution of these individuals would remove foraminifera with a low (relative to mature foraminifera) FB-δ^{15}N. An alternative explanation is that weight loss of shells before burial might have an effect on FB-δ^{15}N, as thinning of shells has been documented to occur between 100 and 1000 m (Schiebel et al., 2007). The weight loss could come from dissolution and/or breakage of the outermost chambers during sinking; the outermost chambers of mature symbiont-hosting foraminifera may be lower in δ^{15}N than the inner chambers due to larger individuals housing more symbionts (i.e., stronger ammonium retention) when the more recent chambers were produced (Smart et al., 2018). If these thin, low δ^{15}N outer chambers are preferentially degraded or lost to dissolution (and/or breakage) during sinking, they would not be integrated into the fossil FB-δ^{15}N. An alternative reason for weight loss of shells is the dissolution of the innermost chambers; bacterial degradation of the organic tissue within the foraminifer's shell can create an acidic microenvironment capable of dissolving the inner layers in contact with the tissue (Schiebel et al., 2007; Smart et al., 2018).

4.1.3 Study region and aims

This study builds on existing ground-truthing efforts, and aims to characterize the efficiency with which the complex southeast Atlantic Ocean circulation and productivity fluctuations are recorded in the sediment. Surface nitrate concentrations in the region are similarly low to those observed in the Sargasso Sea (Andrews and Hutchings 1980; Browning et al. 2017; Chapter 2), but our region is also influenced by both Southern Ocean water masses and the highly productive Benguela Upwelling System (BUS). North of $\sim$27°S, upwelling is perennial, whilst mid-latitude westerly winds act to suppress upwelling in the southern BUS during austral winter (Nelson, 1992; Shannon and Nelson, 1996; Hutchings et al., 2009). Offshore of the BUS, nitrate is predominantly supplied to the mixed layer through winter mixing (Donners et al., 2005), but offshore advection from upwelling cells (in particular those in the northern region) may supplement areas close to the continental shelf (Shillington et al., 1992; Shannon and Nelson, 1996). Eddies transporting waters north-westwards from the Agulhas Current System (ACS) may also introduce small amounts of newly fixed nitrogen to the southern region, given that recent experiments conducted in other regions have found increased rates of nitrogen fixation inside anticyclonic eddies (Fong et al., 2008; Löscher et al., 2016; Li et al., 2020).

The purpose of this study is twofold: (1) to ground-truth the use of FB-δ^{15}N in the Southeast Atlantic Ocean; and (2) to assess the consistency of the FB-δ^{15}N drivers and

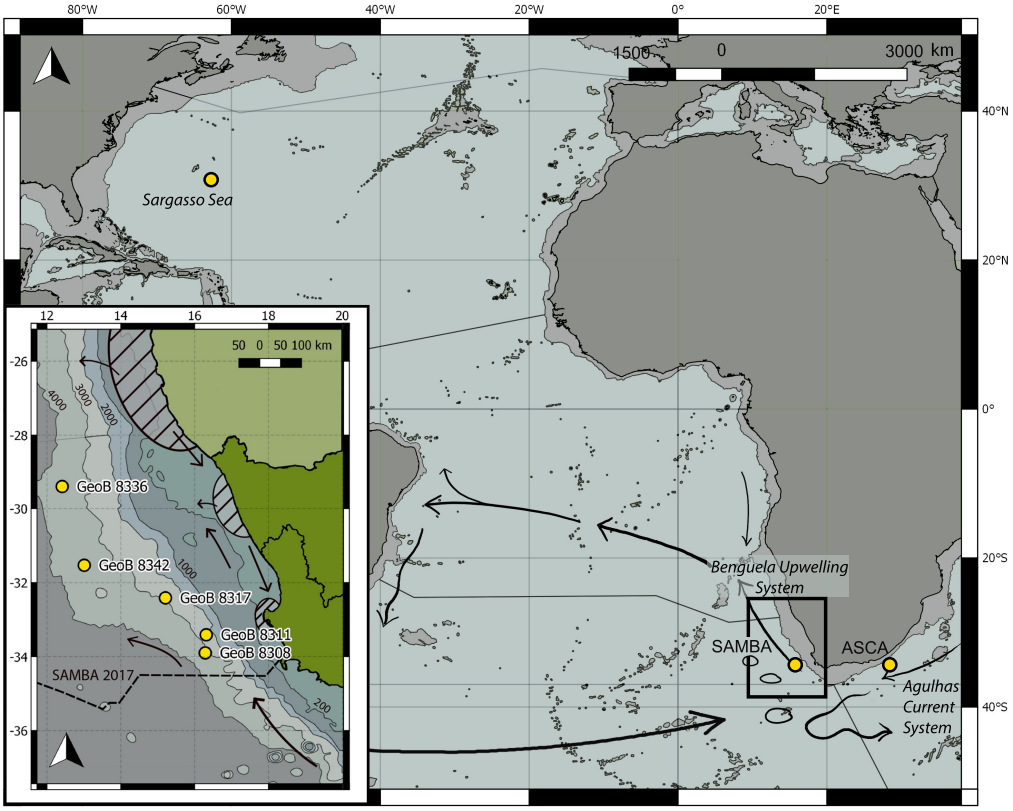

Figure 4.1: Locations of multicores (MUCs) used in this study relative to the SAMBA 2017 line. Bathymetry contours (from the southern African west coast outwards) are 200 m, 1000 m, and at 1000 m intervals thereafter. Major upwelling cells are indicated by diagonal lines, and arrows illustrate directions of surface transport.

relationships across vastly different nutrient regimes of the world's ocean. To achieve these objectives, we compare δ^{15}N measurements from recent (core-top) fossil foraminifer shells with modern foraminifer tissue and shell samples collected via net tows in the Indo-Atlantic region, and then compare these finding with existing data from ground-truthing studies conducted in the Sargasso and Subantarctic regions. We discuss the extent to which offsets in δ^{15}N between modern (tissue and shells) and fossil shells can be attributed to environmental or physiological controls. In this way, we seek to contribute to a more robust interpretation of FB-δ^{15}N variability in the fossil record.

4.2 Methods

4.2.1 Collection of living and fossil foraminifera

Living foraminifera were collected from the southeast Atlantic and southwest Indian Oceans using a double 1 m^2 opening, 200 m-mesh plankton net during two austral winter cruises in 2017 (SAMBA line, Atlantic) and 2018 (ASCA line, Indian) (Fig. 4.1). The SAMBA line extends westwards from South Africa along 34.5°S, whilst the ASCA line stretches to the southeast from 33.5°S up to 300 km offshore. Details regarding stations

and background hydrography for each cruise can be found in Wallschuss et al. (2022) (SAMBA), Marshall et al. (2023) (ASCA), and Chapter 2, Chapter 3 (SAMBA, ASCA). Nine and twelve net tows were performed during the SAMBA and ASCA cruises, respectively; of the nine SAMBA stations, four were sampled inside a roughly 7-month old Agulhas eddy, and five were sampled outside of the eddy in ambient (background) Atlantic conditions. ASCA stations were classified into four zones (central current, current shear, mid-shore, and offshore) depending on their water mass composition and distance from the Agulhas Current's core. Nets were towed for an average of 40 minutes (2017) and 20 minutes (2018) to a maximum depth of 200 m, after which the tow material was preserved in a pH buffered 5-10% formalin solution and refrigerated at 4°C until processing (Ren et al., 2012b).

Surface sediments were collected in the Cape Basin and larger Benguela Upwelling System during the M57/1 R/V *Meteor* cruise in 2003 using a multicorer (Schneider, 2003). Sub-samples of sedimentary material were stored at the University of Cape Town until processing, whereupon five core tops (0-2 cm) were selected for foraminifera-bound δ^{15}N analysis based on location relative to the modern tows and preservation state of foraminifer shells (Fig. 4.1), as no δ^{15}N (nitrate or foraminifera-bound) data exist for the exact location of available core tops. Sediment rates for GeoB 8336 and GeoB 8342 range between 0.3 and 1.3 cm/1000 years (Bergh et al., 2021), whilst some studies suggest that the region of GeoB 8308 has a higher sedimentation rate of $\sim$4 cm/1000 years (Herbert and Compton, 2007). The two most northern core tops (GeoB 8336 and GeoB 8342) were classified in the original cruise report (Zabel et al., 2005) as "northern deepwater" cores (i.e., deepwater referring to cores offshore of the shallow Benguela mudbelt; Birch 1977; Meadows and Baxter 2001; Compton et al. 2009), whereas the remaining three (GeoB 8308, GeoB 8311, and GeoB 8317) were classified as "southern deepwater" cores. Foraminifera (*Globorotalia inflata*) from four of the samples were submitted for AMS radiocarbon analysis (Beta Analytic Inc, Miami) and were calibrated using the BetaCal4.20 software and the MARINE20 calibration curve, and a local reservoir age of 29 $\pm$ 88 years was applied (Heaton et al., 2020).

4.2.2 Cleaning and oxidation of living and fossil foraminifera

Living foraminifera were processed for tissue- and shell-bound δ^{15}N as outlined in Chapters 2 and 3. In addition to the data reported in these chapters, between 18 and 67 individuals of each species were selected from picked Agulhas Current specimens (net-tow collected) for shell-bound δ^{15}N analysis, resulting in 19 measurements from this region.

The protocol for fossil foraminifera δ^{15}N followed that of (Ren et al., 2009) and was performed at the Max Planck Institute for Chemistry (MPIC). Individuals were picked manually from the 500 μm - 1000 μm size fraction under a Zeiss Stemi 508 Stereo microscope (within a given species, individuals of roughly similar size were collected), and between 2.6 and 16.6 mg of foraminifera tests were collected for each sample.

Table 4.1: Locations, water depth, sample depth and radiocarbon age (1950 = 0 years before present (BP)) of multicores. The age of GeoB 8311 was not analysed due to its close proximity to GeoB 8308.

Core Site	*Group*	*Lat (S)*	*Lon (E)*	*Water depth (m)*	*Sample depth (m)*	*Age (BP)*
GeoB 8308	north	33° 55.18	16°16.06	3162	0 - 1 cm	5780 ± 30*
GeoB 8311	north	33° 21.90	16° 18.59	2535	0 - 1 cm	-
GeoB 8317	south	32° 19.74	15° 09.80	2930	1 - 2 cm	1340 ± 30
GeoB 8342	south	31° 29.99	13° 00.00	3521	1 - 2 cm	3600 ± 30
GeoB 8336	south	29° 12.58	12° 20.64	3626	0 - 1 cm	3680 ± 30

*Reported reservoir ages from this region vary, but although adjustment of the reservoir age would result in changes to individual ages, the differences between the core sites themselves would be the same.

Specimens were gently crushed and transferred to 15 mL polypropylene centrifuge tubes. Clay particles were removed by adding 10 mL of a 2% polyphosphate solution and sonicating them in an ultrasonic bath for ~ 10 seconds. After rinsing three times with Milli-Q, 7 mL of dithionite-citric-acid (pH $\sim$ 8) was added to each vial. Samples were placed in a water bath at 80°C for 40 minutes to remove Fe-Mn oxides before again rinsing three times with Milli-Q. The remainder of each sample was transferred into a muffled 4 mL vial for oxidative cleaning in order to remove non-shell-bound organic matter. A potassium persulfate/sodium hydroxide solution was prepared using 2 g potassium persulfate that had been recrystallized three times, 2 g NaOH pellets and 100 mL Milli-Q, with 3 mL of the resulting solution being added to all vials. Samples were then autoclaved for 65 minutes at 125°C, rinsed four times with Milli-Q, and left to oven dry overnight at 50°C. Between 0.6 and 5.1 mg of cleaned shell fragments were weighed out for oxidation of shell-bound N. Dissolution of $CaCO_3$ was facilitated through the addition of 45 μL of 4N HCl, which released the organic matter from the shell matrix. Sample N was then oxidized to nitrate using 1 mL of a basic potassium persulfate solution (1 g NaOH, 100 mL Milli-Q, 0.7 g recrystallized persulfate) and autoclaved for 65 minutes. The resultant N concentrations were measured by chemiluminescence detection following the reduction of an aliquot of sample nitrate to nitric oxide using vanadium (III) (Braman and Hendrix, 1989).

4.2.3 N isotope analysis

Sample nitrate was quantitatively converted to N_2O via the denitrifier method (Sigman et al., 2001). Where sample size allowed, for each sample 5 nmoles of nitrate was injected into 3 mL of buffered (pH 6.3) media containing denitrifying bacteria (*P. chlororaphis*), and the resulting N_2O was measured by gas chromatography-isotope ratio mass spectrometry (GC-IRMS) using a Thermo MAT 253 with online N_2O extraction and purification

(Sigman et al., 2001; Casciotti et al., 2002; Weigand et al., 2016). International references IAEA-NO-3 and USGS34 standards were used to calibrate the isotopic composition of the samples to air.

The contribution of the oxidation reaction (the oxidation blank) was measured by combining five individual 1 mL aliquots of oxidation solution into a single aliquot, which was then injected into a bacterial vial. The oxidation blank was on average 8.3% of the total N concentration (nmol.mL^{-1}). Standard deviation of duplicate oxidations (samples of the same species from the same core) was 0.8 ‰ (n = 2).

Three in-house MPIC coral standards (CF1, CF2, PO-2) were measured in duplicate, and a mixed foram standard (FB-1) was measured in triplicate, which was on average within 0.4 ± 0.1 ‰ (n = 3) of the laboratory's long-term average (5.8 ‰).

4.2.4 Correcting for low concentration samples

There were fewer specimens per species collected from the ASCA tows in comparison to SAMBA (average of 40 for each measurement, with an average of 1.8 shell measurements per net tow, vs 45 at an average of 3.6 shell measurements per tow). In addition, the most abundant species in the Agulhas Current System (e.g., *G. ruber*, *T. sacculifer*, *G. inflata*, *Globigerina bulloides*) were smaller and shallower-dwelling than *G. truncatulinoides* and *Globorotalia hirsuta*, two of the main species measured for FB-δ^{15}N in the Atlantic. These large deep-dwelling species had visibly thick calcite crusts, whereas the tests of foraminifera in the ACS were thinner, thus providing less material for analysis. This resulted in lower- than-expected concentration samples being measured via GC-IRMS, and it was necessary to perform additional corrections to these data. In order to obtain Agulhas FB-δ^{15}N, we performed three different correction methods and compared them to an expected value calculated using the difference between tissue- and shell-bound δ^{15}N in the South Atlantic. These calibrations therefore served as an exercise to examine the effect that different correction methods have on low N samples. The bracketing amino acid standards used in this specific run (referred to as 'U41' and 'U65') were higher in δ^{15}N than the samples (USGS41 = +47.6 ‰, USGS65 = +20.68 ‰), and were therefore dismissed as a suitable correction method (other runs have previously also included 'U40' (USGS40 = −4.52 ‰), which is more appropriate).

Method I used the calibration curve (of area vs δ^{15}N) from low amounts of IAEA-NO-3 standards and method II used the calibration curve from USGS34. Although standards below 3 nmol were not used during the Agulhas GC-IRMS run due to unexpectedly low Agulhas shell concentrations, 1 nmol and 0.5 nmol standards were included in the previous two runs, which had likely produced similar measurement errors to the Agulhas run on the machine. Linear regression functions using both IAEA-NO-3 (method I) and USGS34 (method II) standards were produced by comparing the peak area and δ^{15}N anomaly from the known value of each (4.7 ‰ and −1.8 ‰). Both IAEA-NO-3 and USGS34 displayed negative trends for areas < 3.5 Vs (< 1 nM) as well as for areas between 3 - 9 Vs (1-3 nM)

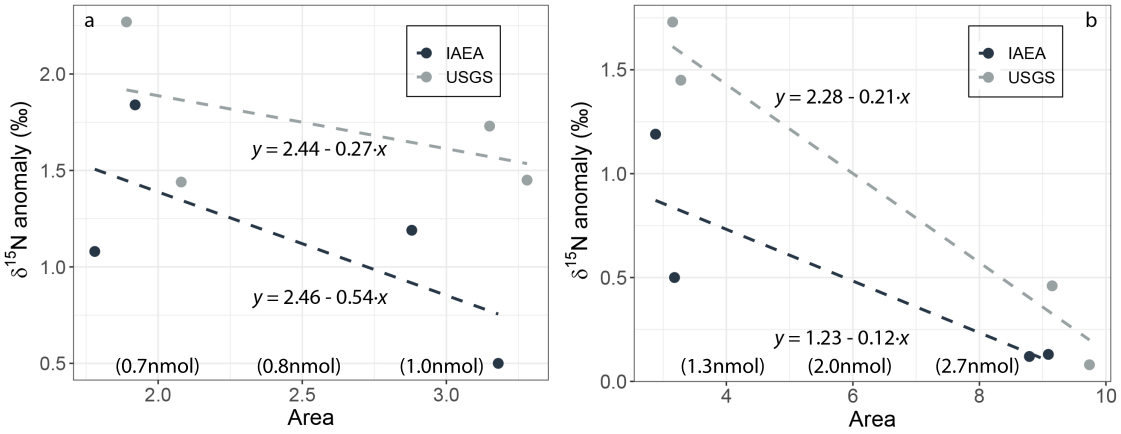

Figure 4.2: IAEA-NO-3 ('IAEA') and USGS34 ('USGS') calibration curves for low N samples. Linear regressions calculated for (a) < 1 nM (area = 0 - 3) and (b) 1-3 nM (area 3 - 9) using two previous GC-IRMS runs.

(Fig. 4.2). Samples less than 1 nmol resulted in regression equations $y = 2.46 - 0.54x$ and $y = 2.44 - 0.27x$ for IAEA-NO-3 and USGS34 respectively, where x is sample area, and y is the FB-δ^{15}N anomaly. Linear regression for samples between 1 and 3nmol produced equations of $y = 1.23 - 0.12x$ (IAEA-NO-3) and $y = 2.28 - 0.21x$ (USGS34).

Method III involved calculating the difference between two identical ACS tissue GC-IRMS runs (n = 9 samples from 6 species) where samples were injected at different concentrations, due to unexpectedly low concentrations in the initial run (Replicate method). Based on concentrations back-calculated from the first GC-IRMS run, replicate samples (same species, same tows) were rerun using their correct concentrations, targeting 5nmol of N for all samples. Calculating the difference in tissue-bound δ^{15}N between the replicates, a linear regression was plotted *versus* peak area, resulting in $y = 1.25 - 0.26x$ (Fig. 4.3).

Corrected values for Agulhas FB-δ^{15}N were calculated using all methods, with linear regression functions for IAEA-NO-3 and USGS34 being assigned to samples based on the original peak area (i.e., < 1 nmol or 1-3 nmol). Expected values were estimated based on the average difference between southeast Atlantic tissue and shell δ^{15}N from the same species at the same tow; USGS34- and IAEA-NO-3-corrected FB-δ^{15}N were on average 0.8 ‰ lower and 1.0 ‰ higher than the expected sample value, whereas replicate-corrected FB-δ^{15}N was 0.1 higher. There were four cases (out of a potential 19) where the corrected data were noticeably different from the expected FB-δ^{15}N (*G. bulloides* 1, *G. bulloides* 2, *G. menardii*, and *T. sacculifer* 4 (Fig. 4.4). Of these, *G. menardii* was the only sample to produce a higher-than-expected FB-δ^{15}N. For all plots and further analysis, we use the 'replicate- corrected' data with these four outlier data points removed.

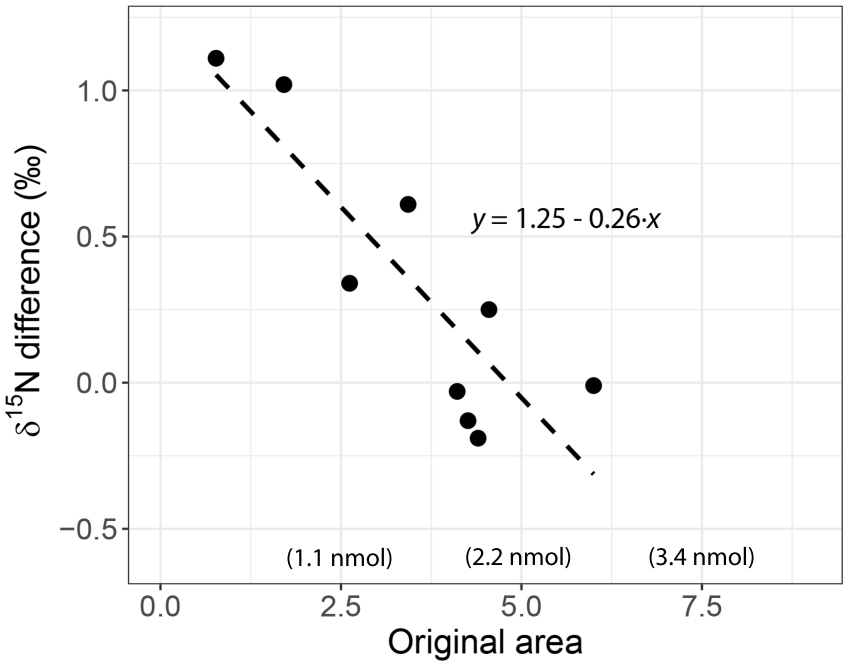

Figure 4.3: Replicate method (method III) calibration curve comparing low concentration (< 2.7 nmol, area < 6) and 5 nmol FB-δ^{15}N samples. δ^{15}N difference (y axis) is equal to the FB-δ^{15}N of the low concentration sample minus the FB-δ^{15}N of the 5 nmol sample.

4.2.5 Additional repository data

Foraminifera δ^{15}N data from existing publications were accessed from the Biological & Chemical Oceanography Data Management Office (`https://www.bco-dmo.org/dataset/` 747394, 747341, 747248, 805653). These datasets contain (1) modern (net tow) tissue- and shell-bound δ^{15}N, shell-bound sediment trap shell-bound δ^{15}N, and core-top fossil shell-bound δ^{15}N from the Sargasso Sea (Smart et al., 2018); and (2) modern (net tow) tissue- and shell-bound δ^{15}N from the Southern Ocean (SAZ) (Smart et al., 2020).

4.2.6 Terminology

Two types of foraminifera shell are used in this study: those sampled used net tows, and fossil foraminifera from sediment multicores. To distinguish between the two, we refer to them as 'modern shell' and 'fossil shell' data, respectively. The notation FB-δ^{15}N is used to refer to both modern and fossil shells, whereas tissue-bound δ^{15}N refers to the δ^{15}N of foraminifera tissue (mostly cytoplasm) measured from living (net tow) specimens. Tissue-bound δ^{15}N was referred to in Chapters 2 and 3 as FT-δ^{15}N, due to minimal references to shell-bound data, but is written in full for this chapter to avoid confusion regarding the similarity of the terms FB and FT.

With regards to location, we have chosen to refer to the two sampling locations as 'Atlantic' and 'Indian' when referring to the regions as a whole (e.g., when comparing data from these regions to published Sargasso Sea or Subantarctic data). These regions

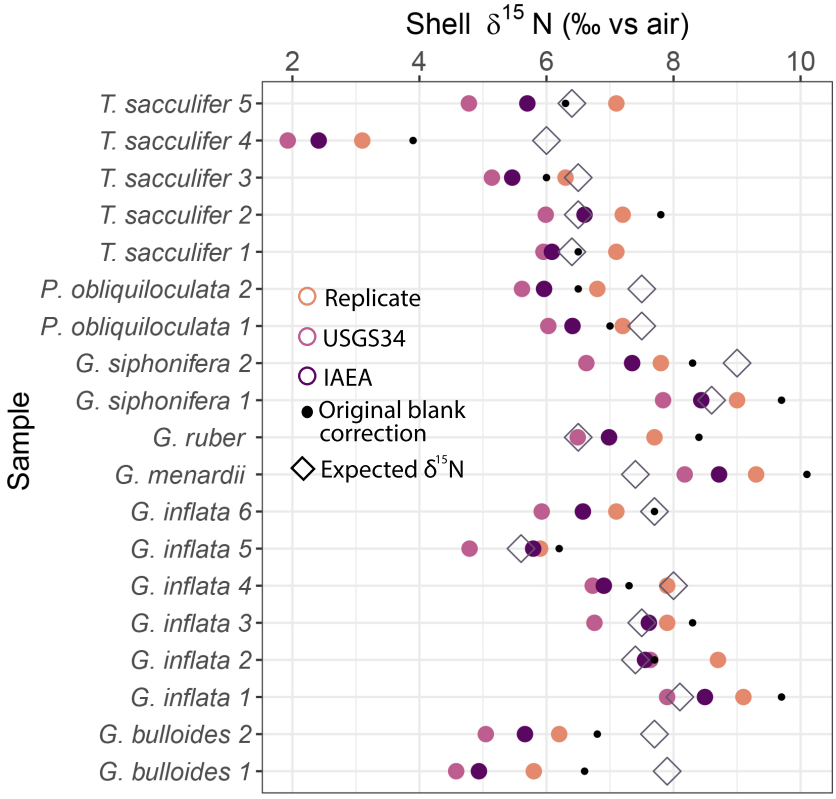

Figure 4.4: A comparison of the original blank-corrected FB-δ^{15}N of ASCA shell samples to the results acquired using methods I - III. Expected δ^{15}N is an estimate of FB-δ^{15}N based on the addition of the difference between southeast Atlantic tissue and shell samples (1.3 ‰) to average Agulhas zone-and-species-specific tissue δ^{15}N.

can be further subdivided to examine variability within a basin, or to compare local and meso-scale dynamics between neighbouring southeast Atlantic and southwest Indian areas. In the Atlantic, these subdivisions are 'background Atlantic' and 'eddy' environments (Chapter 2); with Indian data, we divide the sampled area into 'current δ^{15}N inshore edge' (sometimes abbreviated to 'current'), 'mid-shore and offshore edge' (abbreviated to 'mid-shore') and 'offshore' (Chapter 3).

4.3 Results

4.3.1 Modern foraminifera tissue *versus* shell δ^{15}N

Compiling modern foraminifera δ^{15}N from the southeast Atlantic and ACS, we observe a significant ($R^2 = 0.57$, $p < 0.01$) positive linear correlation between tissue and shells (using the average species δ^{15}N per tow (station); i.e., shell measurements are compared with tissue measurements from the same station and same net tow). Regression analysis produced a near 1:1 slope (gradient = 0.87) with an average δ^{15}N offset of 1.5 ± 1.0 ‰ (shell δ^{15}N > tissue δ^{15}N) (Fig. 4.5a); the offset in each region was similar, with the Agulhas offset slightly higher than the offset calculated for the southeast Atlantic (1.8 ‰

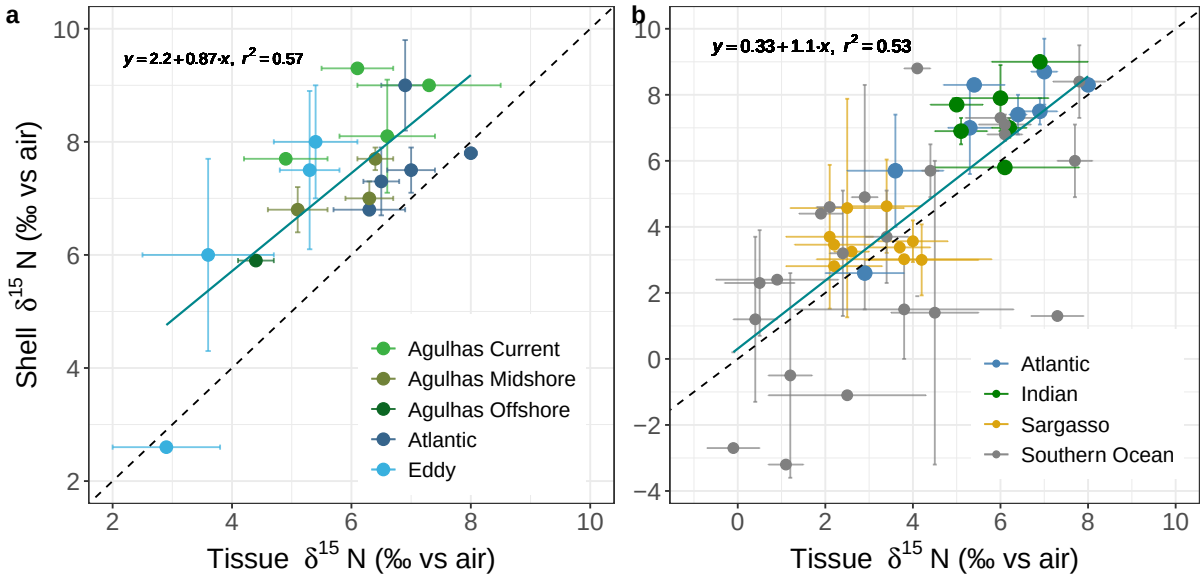

Figure 4.5: Comparison between (a) all Atlantic and Agulhas tissue- and modern shell-bound δ^{15}N from this study, specific to each station and coloured by zone; and (b) data from this study compared to existing tissue and shell data from Sargasso Sea (Smart et al., 2018) and Subantarctic/Southern Ocean (Smart et al., 2020). "Indian" refers to all Agulhas zones, and "Atlantic" refers to both background Atlantic and eddy data pairs. Data points for both (a) and (b) reflect the species-averaged δ^{15}N per station, and standard deviation refers to the deviation between duplicate samples at from the same net tow. The dotted line represents the 1:1 line.

and 1.2 ‰, respectively). We note that excluding the samples with low concentrations (< 3 nmol N) from the analysis makes no significant difference to the relationship, where $R^2 = 0.58$, $p < 0.01$ and a linear function of $y = 2.2 + 0.86x$. We therefore choose to include the low concentration, replicate-corrected, samples during the analyses presented here. In the southeast Atlantic, average offsets were variable, but were larger for the eddy samples than for the same species collected from stations characterized by background Atlantic conditions (Table 4.2), with *G. truncatulinoides* displaying the largest offsets in both regions. Two species (*G. siphonifera*, background Atlantic, and *G. bulloides*, eddy) displayed negative offsets (i.e., greater tissue-bound δ^{15}N than modern shell FB-δ^{15}N; *G. siphonifera* = −0.2 ‰, *G. bulloides* = −0.3 ‰), whereas a larger FB-δ^{15}N than tissue-bound δ^{15}N was measured for the remainder of southeast Atlantic data. All Agulhas offsets were positive (Table 4.3), the largest being a difference of 3.2 ‰ between shell and tissue δ^{15}N (*G. menardii*), and the lowest being observed for *Pulleniatina obliquiloculata* at 0.7 ‰.

A similar slope of ∼1 (1.1) is observed when the Sargasso Sea and Southern Ocean (SAZ) data are included in the regression, with the former providing a composite of low-δ^{15}N samples (mean shell δ^{15}N = 3.5 ± 0.6 ‰ for spring; n = 72 samples, 10 species) relative to the data from this study (mean δ^{15}N of 7.6 ± 0.9 ‰ (not including eddy shell δ^{15}N, n = 38 samples, 8 species), Fig. 4.5b). In contrast, the Southern Ocean data span a much larger range than the data presented here or for the Sargasso Sea, despite comparatively few measurements (FB-δ^{15}N range > 10 ‰; mean δ^{15}N = 2.7 ± 4.2 ‰; n = 69

Table 4.2: Tissue and modern shell δ^{15}N of South Atlantic foraminifera under background and eddy (leakage) conditions. $\Delta\delta^{15}$N = Shell δ^{15}N- Tissue δ^{15}N (italicized). Species-specific offsets in tissue and shell δ^{15}N were calculated at each station, and the $\Delta\delta^{15}$N reported here refers to the average of each station- and species-specific offset within a zone.

Species	Background Atlantic			Eddy		
	Tissue δ^{15}N (‰)	Shell δ^{15}N (‰)	Δ δ^{15}N (‰)	Tissue δ^{15}N (‰)	Shell δ^{15}N (‰)	Δ δ^{15}N (‰)
G. bulloides				2.9	2.6	*-0.4*
G. falconensis	6.2					
G. glutinata	7.0					
G. hirsuta	7.0	7.5	*0.5*	5.3	7.5	*2.3*
G. inflata	6.5	7.3	*0.8*	3.6	6.0	*2.4*
G. siphonifera	8.0	7.8	*-0.2*	4.6		
G. truncatulinoides	6.9	9.0	*2.1*	5.4	8.0	*2.6*
O. universa	7.1			4.6		

samples, 5 species). Most (80%) of the species measured for FB-δ^{15}N in the Sargasso Sea and Subarctic studies were common to those measured here in the Atlantic and Agulhas (the exceptions being *G. falconensis*, *O. universa*, and *G. glutinata*, species whose tissue-bound δ^{15}N in the southeast Atlantic was in-line with other facultatively photosymbiotic or symbiont-barren species. Although tissue data were measured for these species in both regions, there were not enough specimens for shell measurements).

4.3.2 Fossil shell δ^{15}N from multicores in the southeast Atlantic

Fossil FB-δ^{15}N ranged from 7.7 ‰ to 12.0 ‰ (Fig. 4.6a). At all locations, symbiont- bearing species *G. ruber* and *T. sacculifer* showed the lowest FB-δ^{15}N, whilst *G. siphonifera* was consistently high and displayed little variation (11.3 ± 0.1 ‰). *O. universa* and *G. truncatulinoides* showed variable FB-δ^{15}N, low relative to other species at some sites (GeoB 8308 and GeoB 8317, both southern) but high at others (northern GeoB 8336 and southern GeoB 8311). A small yet significant difference ($p < 0.01$, Fig. 4.6b) was apparent between the mean fossil FB-δ^{15}N of the northern and southern cores (10.8 ± 1.2 ‰ *versus* 9.9 ± 1.0 ‰, respectively, yielding a difference of 0.8 ‰). The high *G. bulloides* FB-δ^{15}N value (11.9 ‰) was excluded from this comparison, since there was only one fossil measurement of this species in the dataset, and this measurement was an integrated 'northern site' signal, containing specimens from both GeoB 8336 and GeoB 8342. A further difference between the southern and northern cores (excluding in-between site, GeoB 8317) is the range in FB-δ^{15}N between the four species common to each site (*G. truncatulinoides*, *G.*

Table 4.3: Tissue and modern shell δ^{15}N of southwest Indian (Agulhas Current System) foraminifera across three "zones" defined in Chapter 3. $\Delta\delta^{15}$N = Shell δ^{15}N- Tissue δ^{15}N (italicized). Species-specific offsets in tissue and shell δ^{15}N were calculated at each station, and the $\Delta\delta^{15}$N reported here refers to the average of each station- and species-specific offset within a zone.

Species	Current + Inshore Shear			Mid-shore + Offshore Shear			Offshore		
	Tissue δ^{15}N (‰)	Shell δ^{15}N (‰)	$\Delta\ \delta^{15}$N (‰)	Tissue δ^{15}N (‰)	Shell δ^{15}N (‰)	$\Delta\ \delta^{15}$N (‰)	Tissue δ^{15}N (‰)	Shell δ^{15}N (‰)	$\Delta\ \delta^{15}$N (‰)
G. bulloides	6.4			6.9			5.0		
G. calida	6.9						7.3		
G. crassaformis	6.7								
G. glutinata	6.4			5.9					
G. inflata	6.6	8.1	*1.6*	6.4	7.7	*1.3*	4.4	6.0	*1.6*
G. menardii	6.1	9.3	*3.2*	6.0			4.7		
G. ruber	4.9	7.7	*2.7*	4.8			4.8		
G. siphonifera	7.3	9.0	*1.7*	6.9					
G. truncatulinoides	7.5			6.5			4.4		
G. tumida	4.8								
G. ungulata	5.3			5.3					
O. universa	5.5			4.6					
P. obliquiloculata	6.3	7.0	*0.7*	6.2			5.8		
T. sacculifer	5.1	6.4	*1.3*	5.2			3.5		

hirsuta, *G.inflata* and *O. universa*). At northern sites, the range between these species was 1.1 ± 0.1 ‰, whereas measurements from southern sites found the spread between species at a site to be more than twice this amount (average = 2.8 ± 0.4 ‰).

4.3.3 Modern *versus* fossil shell δ^{15}N

Eddy (i.e., Agulhas leakage) data were not included when comparing fossil and shell data, as fossil FB-δ^{15}N records the long-term flux; a 'pure' eddy FB-δ^{15}N would not be represented in fossil FB-δ^{15}N, as leakage of low δ^{15}N nitrate would result in the integration of leakage foraminifera with background Atlantic foraminifera (i.e., fossil FB-δ^{15}N variation may be caused by the changes in the amount of leakage foraminifera proportional to background foraminifera, but an integrated FB-δ^{15}N is likely to show a more muted contrast than evident in the modern data shown in Chapter 2). However, FB-δ^{15}N from the Agulhas Current was not removed, as our study serves to provide baseline fossil FB-δ^{15}N measurements for the region. Modern foraminifera tissue and shell δ^{15}N in the background Atlantic was similar to foraminifera from in-current/mid-shore ACS (Chapter 3; the single offshore shell measurement was also excluded from core top comparisons as it (like the

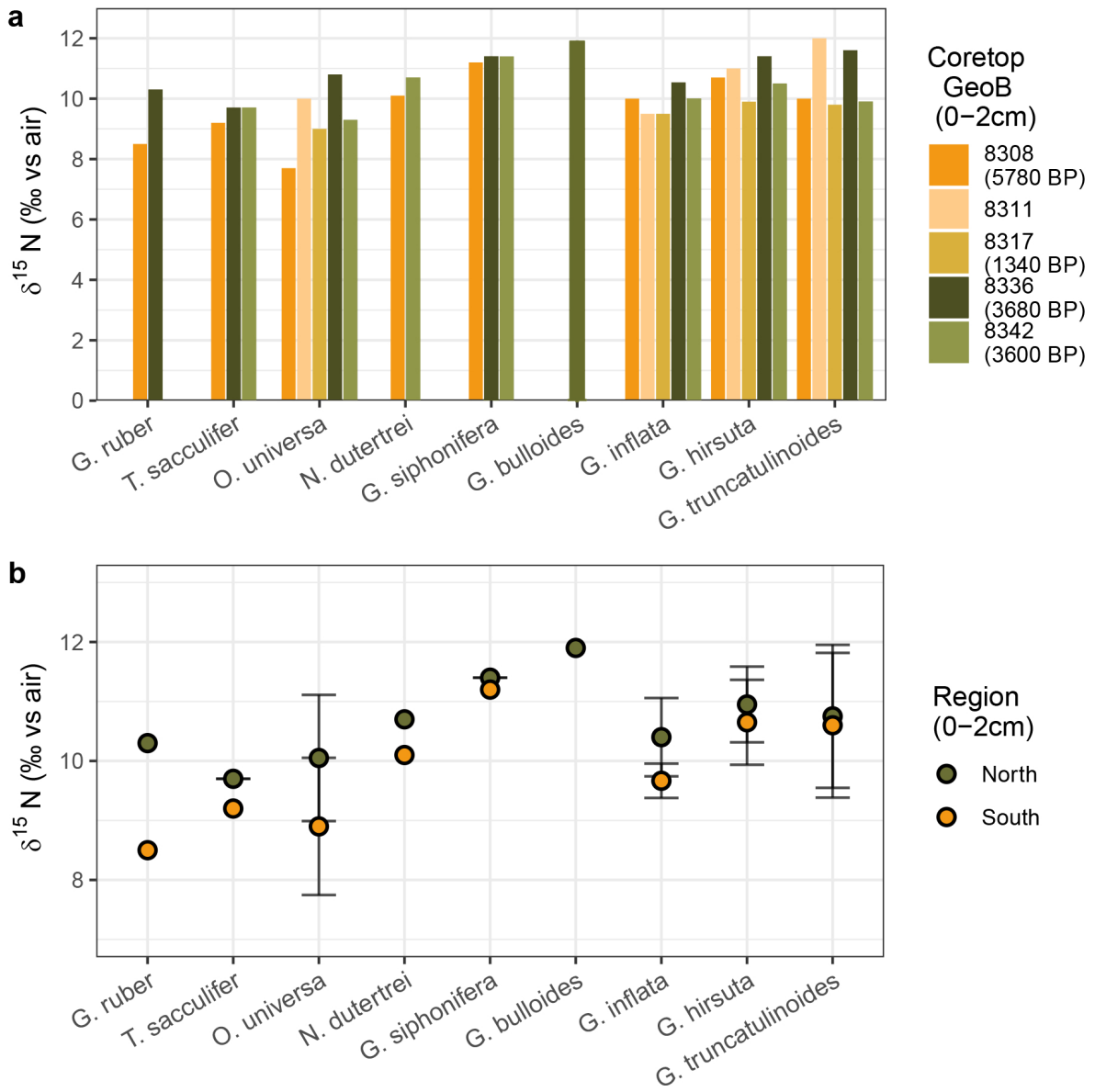

Figure 4.6: FB-δ^{15}N of all core top samples in this study. In text, core locations are divided into southern (GeoB 8308, GeoB 8311 and GeoB 8317) and northern (GeoB 8336 and GeoB 8342) locations. Core ages are indicated by brackets below the core name in the legend. Figure (a) presents the average FB-δ^{15}N per species, where *G. bulloides* specimens from GeoB 8342 were added to GeoB 8336 to bulk up sample size for an accurate measurement, and FB-δ^{15}N of *T. sacculifer* from GeoB 8336 included specimens added from GeoB 8317 and GeoB 8311. Figure (b) displays the average FB-δ^{15}N for northern (green) and southern (yellow) sites.

eddy) reflects a more transient feature, rather than an average condition), and inclusion of ASCA data allowed for the addition of *N. dutertrei*, *G. ruber* and *T. sacculifer*, three species that were not present during the winter Atlantic tow but were abundant in the Atlantic multicores. We also chose to exclude *G. bulloides* from any linear regression calculations in this section (although the data are plotted in Fig. 4.7), as a single, anomalously high, FB-δ^{15}N fossil measurement was made from northern core material, whilst all modern data were collected from a location closer to the southern sites. At least two measurements were obtained for all other species.

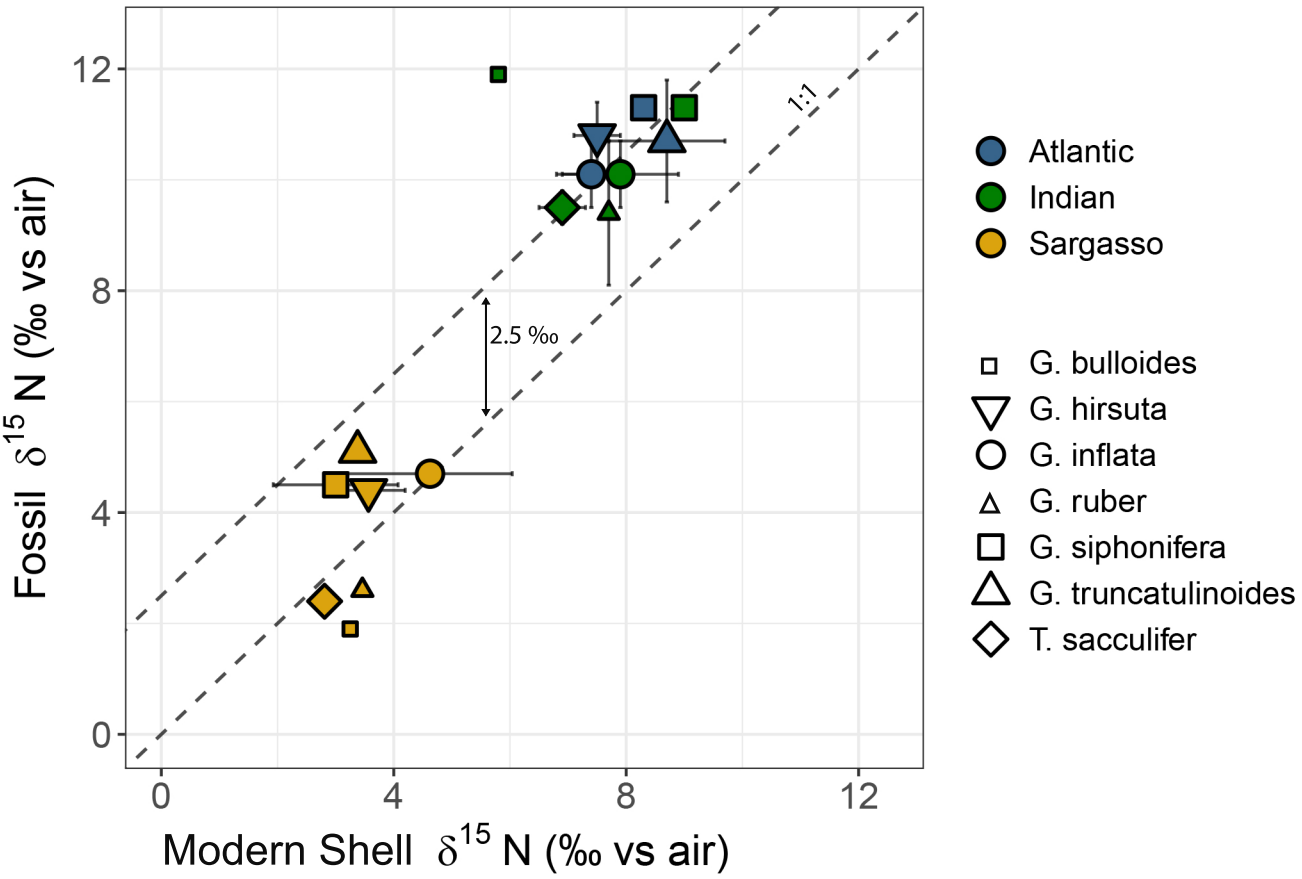

Figure 4.7: Comparison between modern shell FB-δ^{15}N and fossil shell FB-δ^{15}N (MUCs). Fossil δ^{15}N is calculated as the mean δ^{15}N for a given species across all five core sites (standard deviation refers to the deviation per species across all sites). Species' averages of Sargasso Sea data from Smart et al. (2018) are plotted in yellow in both figures, where a) shows a 2.5 ‰ offset from the 1:1 line with a y intercept of 0.

As is the case for tissue *versus* shell δ^{15}N (Fig. 4.5), there is a significant (R^2 = 0.54, $p < 0.05$) positive correlation between modern shell and fossil FB-δ^{15}N. The symbiont-bearing, shallow-dwelling species, *T. sacculifer* displayed the lowest FB-δ^{15}N in both datasets, and *G. siphonifera* and *G. truncatulinoides* were consistently the highest (Fig. 4.7). Overall, the data have a regression slope of 0.78 and an intercept of 2.1 ‰ using species-specific measurements (on average, fossils were 2.8 ‰ higher than modern shells, and 4.1 ‰ higher than modern tissue δ^{15}N). Considered separately, the northern and southern core tops yield similar trends, with southern species displaying a slightly steeper gradient (0.93 in southern *versus* 0.65 in northern core tops) and lower y intercept (Fig. 4.8). If we include existing data from the Sargasso Sea (where there was only a minor difference between modern shells (from tows and traps) and core-top fossil δ^{15}N), the correlation remains strong ($R^2 = 0.89$, $p << 0.01$) and the slope increases to 1.6.

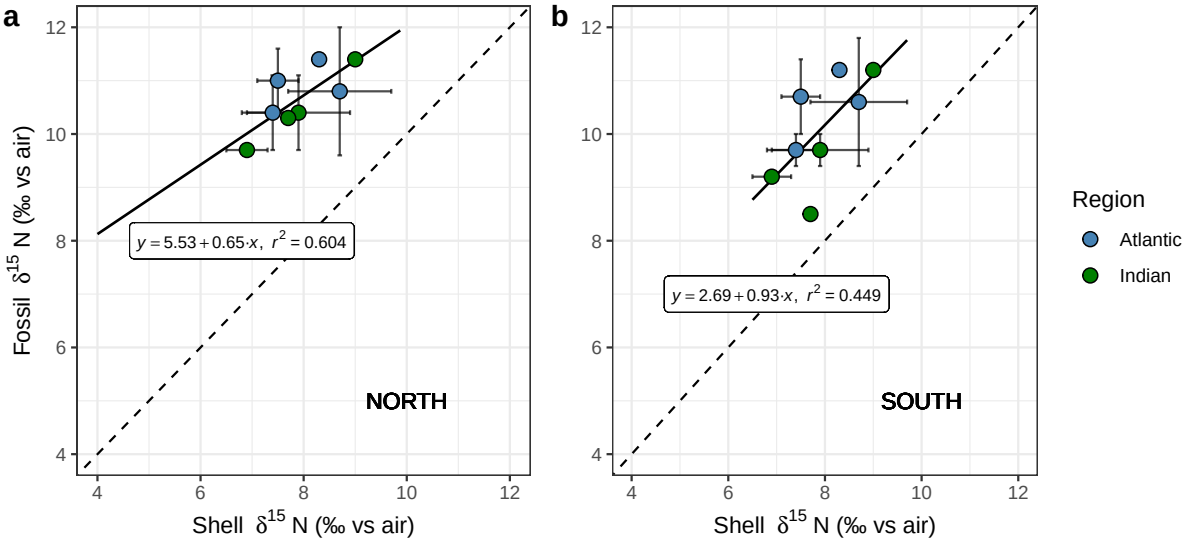

Figure 4.8: Comparison between average species- and location-specific modern shell-bound δ^{15}N and average fossil shell-bound δ^{15}N from (a) the northern coretops (north of 32°S, GeoB 8336 and GeoB 8342); and (b) the southern coretops (south of 32°S, GeoB 8308, GeoB 8311 and GeoB 8317). Blue points indicate data from the modern southeast Atlantic, whilst green points indicate where data from the modern southwest Indian Ocean was used. The 1:1 line is shown as a dashed grey line in both figures.

4.4 Discussion

4.4.1 Modern foraminifera: tissue *versus* shell δ^{15}N

4.4.1.1 Global patterns in FB-δ^{15}N

The assumption that modern shell-bound δ^{15}N in foraminifera is a reliable reflection of tissue δ^{15}N is one of the underlying principles of the fossil FB-δ^{15}N proxy (Ren et al., 2009; Robinson et al., 2023). The slight offset observed between tissue and shell δ^{15}N in our data (average = 1.4 ± 1.0 ‰ using paired tissue-shell data from the same species and same tow) at first glance appears to contradict findings from the Sargasso Sea, where no offset was observed in samples collected from net tows (Smart et al., 2018). However, when plotted together with previously published Sargasso Sea and Southern Ocean data over a broader δ^{15}N range (Smart et al., 2018, 2020; Robinson et al., 2023), the 1.4 ‰ offset observed in our study appears less consequential (Fig. 4.4b). The data presented here provide a 'high end- member' ($\delta^{15}N_{NO_3} \sim 6.9$ ‰, Chapter 2) setting, whereas the Sargasso Sea foraminifera represent a 'low end-member' setting ($\delta^{15}N_{NO_3} \sim 2.6$ ‰, Knapp et al. 2005; Fawcett et al. 2015; Smart et al. 2018), whilst the majority of the data from the Subantarctic Zone (Smart et al., 2020) are located between the two ($\delta^{15}N_{NO_3}$ = 7.9-12.2 ‰; DiFiore et al. 2006).

The high R^2 (0.53) value (from the combined dataset) indicates a strong relationship between tissue- and shell-bound δ^{15}N; a strong relationship for each individual dataset (R^2 = 0.57 for Atlantic and Indian measurements, with the R^2 of Sargasso species ranging from 0.35 - 0.97 (excluding *G. truncatulinoides* (R^2 = 0.07) and *G. siphonifera*, (R^2 =

0.05); Smart et al. 2018) suggests the relationship may be independent of region. In the combined tissue *versus* shell dataset, the near 1:1 gradient combined with a small y-intercept (0.33) hints that the N used in biomineralization during chamber formation is not isotopically distinct from that used in everyday cell functioning. This is consistent with the Sargasso data of Smart et al. (2018) who noted that the majority of the bound N that is measured in foraminifera tests is found in amino acids, which are also a significant component of the organic tissue. In this way, foraminifera appear similar to symbiotic corals (Muscatine et al., 2005), and different from diatoms, where N is present in several compounds in frustules (Sigman et al., 1999; Horn et al., 2011; Morales et al., 2013; Robinson et al., 2023). The gradient of the Atlantic and Indian dataset (< 1) is also consistent with Smart et al. (2018)'s observation of greater variability in tissue δ^{15}N relative to modern shell δ^{15}N, the latter of which integrates over a longer time, smoothing out shorter-term variability.

4.4.1.2 Potential reasons for the local offset between tissue- and shell-bound δ^{15}N

Below, we outline several mechanisms that could have potentially raised the shell- bound δ^{15}N relative to tissue δ^{15}N. The lack of offset observed in the Sargasso Sea (Smart et al., 2018) for the same species as were present in our study suggests that we can rule out fractionation (during biomineral formation) or a systematic difference in N sources used in cell functioning *versus* those involved in the shell building process (Muscatine et al., 2005). One contributor to the 1.4 ‰ offset could simply be related to the small sample size of our shell dataset, which resulted in a larger standard deviation between duplicates from the same net tow than was observed in the tissue samples. Average standard deviation for *G. inflata*, *G. truncatulinoides*, and *G. hirsuta* shell δ^{15}N in the Atlantic was 0.6 ‰, whilst in the eddy it was 1.4 ‰ (Table 4.1). If this deviation is subtracted from the original offset, we are left with a shell- to tissue-bound δ^{15}N offset of 0-0.8 ‰, revealing that more than half of the offset could potentially be attributed to high variability within an eddy environment throughout a foraminifer's lifetime resulting in a larger discrepancy between tissue- and shell-bound δ^{15}N than is observed under background Atlantic conditions.

A second possibility is that the δ^{15}N increase in the shells relative to the tissue may be a result of foraminifera having experienced a recent change in their habitat, either via drifting or a change in ocean nutrient conditions and/or stratification. These environmental changes may have occurred in the period between the latest chamber formation and the sampling of specimens by net tow, but more likely reflect a proportionately larger amount of shell sample recording the earlier conditions (since shells integrate over a longer period than tissue). Sampling occurred in austral winter, which is a period of increased turbulence and deepening mixed layers in both the southeast Atlantic and southwest Indian regions (Shannon and Nelson, 1996; Lutjeharms, 2006; Lamont et al., 2016; Braby et al., 2022). Wintertime convection resupplies the euphotic zone with relatively low-δ^{15}N

nitrate (Holmes et al., 2002; Marshall et al., 2023), in which case the PON consumed by foraminifera in the days-weeks prior to sampling may have been lower in δ^{15}N than the longer-term (i.e., life-long) average represented by the shells. This explanation is consistent with the large interannual and seasonal variability in productivity and water column stratification observed in the Indo-Atlantic region (Matano et al., 1999; Weeks et al., 2006; Hutchings et al., 2012); seasonal changes in sinking particulate δ^{15}N along the Walvis Ridge, for example, can result in changes of several per mille (Holmes et al., 2002), and δ^{15}N PON in the Southern Benguela Upwelling System has shown large variations (up to 9 ‰) even within a single season (Flynn et al., 2020). This reasoning could also explain the larger (on average) tissue-shell δ^{15}N offset seen in the eddy relative to the background Atlantic foraminifera; eddy dynamics are inherently turbulent, and organisms transported within them are subjected to spatial changes affecting δ^{15}N of particulate N, as well as changes in δ^{15}N that occur due to the longer retention time of the particulates (Heywood and Priddle, 1987; Mackas et al., 2005; Condie and Condie, 2016; Vortmeyer-Kley et al., 2018; Cetina-Heredia et al., 2019).

However, δ^{15}N variations between chambers in a single foraminifera are likely to be minor in comparison to centennial- or millennial-scale changes in FB-δ^{15}N. FB-δ^{15}N over the late Quaternary (0 - 30,000 years BP) appears to range from 3 to 5 ‰, depending on the species and basin (Ren et al., 2009; Meckler et al., 2011; Martínez-García et al., 2014; Studer et al., 2015, 2021), which is larger than the entire offset observed between the tissue- and modern shell-bound δ^{15}N in this study.

4.4.2 Fossil shell δ^{15}N *versus* Modern shell δ^{15}N

4.4.2.1 Variability in core top fossil shell-bound δ^{15}N

We are cautious to interpret fossil shell δ^{15}N variation between sites, due both to the differences in radiocarbon age (samples range from 1370 BP to 5780 BP, [Table 4.1]) and the relatively minor inter-site δ^{15}N differences in comparison to the measurement standard deviations [Fig. 4.6]. However, foraminifera from northern sites showed smaller inter-species ranges, and were on average slightly higher in δ^{15}N than those at southern sites (by 0.9 ‰), with the largest difference in FB-δ^{15}N observed between the northernmost GeoB 8336 (29°12.58′ S) and the southernmost GeoB 8308 (33°55.18′ S) for most species (mean difference in FB-δ^{15}N = 1.3 ± 1.1 ‰ for 6 species).

The comparatively large inter-species FB-δ^{15}N range observed at the southern sites (2.8 ‰ *versus* 1.1 ‰ at northern core sites, [Figs 4.6, 4.8]) is likely driven by the high seasonal (as well as decadal and millennial) variability of the southern section of the Benguela Upwelling System (Meadows and Baxter, 2001; Tyson et al., 2002; Hutchings et al., 2009). Stronger seasonality is apt to produce larger intra-annual changes in δ^{15}N PON than in regions where seasonal changes in winds, mixed layer depths, and productivity, are minor (Altabet and McCarthy, 1985; Holmes et al., 2002; Lourey et al., 2003;

Bănaru et al., 2014). Since the dominant species of foraminifer in the southeast Atlantic varies throughout the year, depending on habitat suitability (e.g., water column temperature and stratification; Lončarić 2006, Chapter 2), the inter-species FB-δ^{15}N range is likely to be greater. There is less seasonality in wind strength north of 31°S, where the Lüderitz cell (centred at ∼27°S) hosts perennial upwelling (Shannon and Nelson, 1996). In contrast, mid-latitude westerly winds heavily influence the dynamics of the area south of 31°S, with northward migration of the wind system in winter acting to suppress upwelling and long-term hemispheric-scale changes in westerly wind intensity driving inter-annual variability (Cohen and Tyson, 1995; Shannon and Nelson, 1996; Stuut et al., 2002).

With regards to spatial variability, it is possible that Agulhas leakage contributed to lowering the average FB-δ^{15}N in the southern core-tops relative to the two northern sites. All five core locations have the potential to be affected by Agulhas eddies, but GeoB 8311 and GeoB 8308 are located at the inshore edge of the leakage corridor (where the majority of Agulhas eddies propagate, Garzoli and Gordon 1996; Garzoli et al. 1996; Dencausse et al. 2010) and are thus more likely to be affected by a less-diluted leakage transportation signal, which brings nitrate (and particulate N) with a characteristically low δ^{15}N into the southern Benguela region (Marshall et al., 2023, Chapter 2).

Although additional data are needed to more confidently identify trends, the slightly higher FB-δ^{15}N for foraminifera in the northern cores could potentially be a result of closer proximity to strong perennial upwelling. Highly productive upwelling systems are typically also regions of subsurface denitrification; high levels of primary productivity at the surface and organic matter decomposition below and on the shelf result in oxygen deficient zones (ODZs), conducive to the removal of fixed N from the water column (Dugdale et al., 1977; Ganeshram et al., 2000; Tyrrell and Lucas, 2002; Kuypers et al., 2005). Water column denitrification has a large isotope effect (∼ 13-25 ‰; Cline and Kaplan 1975; Brandes et al. 1998; Sigman et al. 2005; Kritee et al. 2012; Marconi et al. 2017), which raises the δ^{15}N of the resulting organic matter (and, subsequently, foraminifera). Moreover, studies from the west coasts of South Africa and Namibia suggest that, similar to other eastern boundary currents, the Benguela Upwelling System hosts intermittent water column denitrification, inshore of the current (Tyrrell and Lucas, 2002; Kuypers et al., 2005; Flynn et al., 2020). Although GeoB 8336 and GeoB 8342 are not located within the upwelling cells themselves, low oxygen conditions extend westwards off the continental shelf (Chapman and Shannon, 1987; Bailey, 1991; Monteiro and van der Plas, 2006), and changes in upwelling and productivity have previously been inferred from downcore records at both of these sites (Bergh et al., 2021). The higher FB-δ^{15}N observed for the foraminifera from GeoB 8336 and GeoB 8342 therefore raises the possibility of a denitrification signal (which elevates remaining nitrate in δ^{15}N) at these sites relative to those further south.

4.4.3 Comparing modern *versus* fossil shell δ^{15}N

Overall, fossil FB-δ^{15}N measurements exhibited similar inter-species trends to both tissue- and modern shell-bound δ^{15}N [Fig. 4.7]. The lowest fossil shell FB-δ^{15}N were found for dinoflagellate-hosting species, *G. ruber*, *O. universa* and *T. sacculifer*. *G. siphonifera* was consistently high, which is in agreement with existing modern and global fossil data (Smart et al., 2018; Lekieffre et al., 2020; Li et al., 2020). Given the moderately high δ^{15}N of the asymbiotic deep-dwelling *G. truncatulinoides* in modern tissue and shell data, we expected this species to yield high FB-δ^{15}N values at all core sites. Surprisingly, FB-δ^{15}N was high at only two stations (GeoB 8311, south, GeoB 8336, north), with *G. truncatulinoides* at the other three stations displaying a lower FB-δ^{15}N, similar to that of *G. inflata*, an intermediate-dwelling and facultatively photosymbiotic species [Fig. 4.6]. However, there is large variability in the depth habitat of *G. truncatulinoides*, both in different regions (Reynolds et al., 2018; Lessa et al., 2020) and throughout a single foraminifer's life cycle (Bé and Hutson, 1977; Hemleben et al., 1989; Lohmann and Schweitzer, 1989), which is roughly one year (Hemleben et al., 1989; Steinhardt et al., 2015; Reynolds et al., 2018). Variability in the species' fossil FB-δ^{15}N may thus be a result of changing water column conditions over time leading to shifts in *G. truncatulinoides*' seasonal habits and vertical migrations. One point in favour of this argument is that a variable offset (-5 ‰ to 2.2 ‰) between the deep dweller and the dinoflagellate-hosting *O. universa* has previously been noted in the region (Foreman, unpublished), with the FB-δ^{15}N of the two species converging for several thousand years during the last glacial-interglacial cycle.

When comparing modern and fossil shell-bound δ^{15}N, we have included several south Indian Ocean modern shell measurements, despite the sediment cores being located in the Cape Basin. This decision is based on the fact that two species (*G. ruber* and *T. sacculifer*) were not present during the winter SAMBA sampling (Cape Basin; Chapter 2), but were abundant in the core-tops and the modern ASCA collection (Agulhas region; Chapter 3), so the (winter) ASCA data allow a preliminary comparison. *G. ruber* and *T. sacculifer* have previously been identified in the water column in the Cape Basin using a sediment trap that integrated populations over a 6-month (February - July) interval (Lončarić, 2006), so the absence of these species from our SAMBA net tow was almost certainly due to their reduced abundance in winter. The best analogue available to compare modern and fossil shell δ^{15}N from these species is therefore to use the values of their Agulhas Current ("current & midshore"; Chapter 3) counterparts, where they do occur in winter. The caveats to this approach include the assumption that these species of foraminifera have a similar tissue- and shell-bound δ^{15}N in the Cape Basin as in the ACS. The assumption was based on the fact that similar δ^{15}N values had been observed in the species common to both regions (*G. inflata*, *G. truncatulinoides*, *G. siphonifera* and *G. bulloides*) in the modern net tow data (Chapter 2, Chapter 3). However, since *G. ruber* and *T. sacculifer* appear to occur in the Cape Basin predominantly in summer (Lončarić, 2006; Lončarić et al., 2006), there is the possibility that seasonal shifts in FB-δ^{15}N would

cause a discrepancy between the signal used here to approximate modern FB-δ^{15}N *versus* the signal recorded in the fossil record (which reflects the period of highest foraminifer flux to the seafloor).

In complement to the assumption that modern shell-bound δ^{15}N reflects tissue δ^{15}N, equally important is the premise that the isotopic composition of a specimen's shell is not altered post-mortem, i.e., there should be negligible or quantifiable (ideally constant) change in δ^{15}N after death. Our data show a pervasive 2.5 ‰ offset in fossil shell δ^{15}N relative to our modern shell δ^{15}N (Fig. 4.7). In the following section, we consider at what point this change occurs, and whether it is driven by sampling bias, assemblage differences between modern winter net tows and the sediment, or real physical and/or biological processes.

4.4.3.1 Reasons for higher FB-δ^{15}N in fossils relative to living foraminifera

We suggest three potential explanations for the isotopic difference observed between modern and fossil shells within the Cape Basin. First, it is possible that the FB-δ^{15}N is an accurate reflection of living shells, but in the past. The core tops range in age from 1,340 to 5,780 years BP [Table 4.1], with an estimated sedimentation rate of 4 cm / 1,000 years in the region (Herbert and Compton, 2007). Several studies from other regions have shown noticeable decreases in FB-δ^{15}N during this time period due to increases in N_2 fixation in the North Atlantic basin (Ren et al., 2012b; Straub et al., 2013; Studer et al., 2021). The southeast Atlantic Ocean is highly dynamic owing to the complex interactions between Atlantic, Indian and Southern Oceans (Lutjeharms and Meeuwis, 1987; Boebel et al., 1999, 2003; Lutjeharms and Ansorge, 2001; Garzoli and Matano, 2011; Weldeab et al., 2013) and could have experienced a similar degree of FB-δ^{15}N fluctuations, thus explaining the offset seen here between modern and fossil FB- δ^{15}N.

Although a baseline shift of 2.5 ‰ in the span of 3,000 years would be large (existing foraminifera records show species-specific changes of this magnitude over 8,000 - 20,000 years (Ren et al., 2009; Straub et al., 2013; Martínez-García et al., 2014)), an *O. universa* record from the same region (Core U1479, 35°03′ S, 17°24′ E) shows a 2.5 ‰ change over a similar time period (between the core top and 6,000 years BP; Foreman, unpublished). In addition, coral records from the Mozambique Channel show a similar range over a much shorter timescale (∼200 years; Foreman, unpublished), indicating that the dynamic Indo-Atlantic system can experience large δ^{15}N fluctuations and noticeable long-term trends over hundreds of years, particularly at sites near the coast. Given the close interactions between the Agulhas and southeast Atlantic regions, it is likely that at least some of the offset observed between living and fossil shell δ^{15}N is due to late Holocene changes in N-cycling. Indeed, other studies in this region have shown a broad trend towards cooler waters during the late Holocene (∼5,000 - 0 years BP), interspersed with significant decadal and centennial variability (Farmer et al., 2005; Kim et al., 2003; Leduc et al., 2010; Meisel et al., 2011; Granger et al., 2018).

Second, the fossil foraminifera specimens may have been transported to the core sites from another location. The sites are located just offshore of the continental slope [Fig. 1]; both terrigenous and marine organic material is frequently transported from the shelf and deposited at intermediate depths on the slope and potentially further offshore (Herbert and Compton, 2007; Compton and Wiltshire, 2009; Compton et al., 2009). It is therefore possible that a portion of the material sampled for our study originated in a shallower, more coastal setting. On the Southern Benguela shelf, nutrient trapping leads to low oxygen conditions that are potentially suitable for denitrification, and subsurface nitrate δ^{15}N has been shown to be slightly higher on-shelf than in the off-shelf water column (Flynn et al., 2020); a rise in nitrate δ^{15}N would likely act to raise the δ^{15}N of foraminifera on the shelf relative to those living further offshore. However, the influence of transported material can be difficult to account for in coastal settings, and one might argue that inshore denitrification would result in a deviation from inter-species FB-δ^{15}N variation (in comparison to the modern shells, Chapter 2), rather than a roughly consistent offset across most species, as shallow shelf conditions (responsible for higher subsurface δ^{15}N nitrate) inshore of the Benguela Current would likely not be equally suitable for all species.

A third potential reason for the increase in FB-δ^{15}N could be that the modern winter samples are not representative of the time of greatest flux to the seafloor. FB-δ^{15}N is largely set by the isotopic composition of PON (Smart et al., 2020, Chapter 2), which varies seasonally due to changes in the degree of nitrate consumption (Altabet et al., 1991) and N cycling processes like ammonium-based phytoplankton growth and particle reworking by bacteria (Cifuentes et al., 1988, 1989; Altabet et al., 1991; Montoya, 1994; Altabet and Francois, 2001; Lourey et al., 2003). It is therefore reasonable to assume that FB-δ^{15}N should be biased towards the period of greatest flux, which is dependent on factors such as primary productivity and mixed layer deepening (nutrient supply), as well as when environmental conditions (including temperature, nutrient availability and water column stratification) are best suited to individual species (Bé and Tolderlund, 1971; Deuser et al., 1981; Ladigbolu et al., 2020). Some species (e.g., *G. truncatulinoides*) prefer winter conditions, whilst *G. ruber*, *T. sacculifer* and N. dutertrei tend to prefer spring or early summer conditions (Schiebel and Hemleben, 2000; Rebotim, 2018). In general, the largest export flux occurs during, or directly after, periods of peak productivity. In the Cape Basin/Benguela region, productivity is highest during austral spring and summer (September - February) (Shannon and Nelson, 1996; Holmes et al., 2002; Weeks et al., 2006; Hutchings et al., 2009), whereas net tow samples for the present study were collected in mid-winter (July), which might be representative of the start of the nutrient resupply period. Winter-summer shell δ^{15}N differences in the Subantarctic Zone have been observed to be as large as 3.6 ‰, with maximum tissue and modern shell-bound δ^{15}N tending to occur during winter for most species (Smart et al., 2020). If the sediments are recording an early springtime signal, then one would expect fossil shell-bound δ^{15}N to be lower than that of the net-tow specimens, which is not the case. However, the δ^{15}N of PON and

some species of foraminifera peak during early summer in the Sargasso Sea, just after the spring bloom (Smart et al., 2018); a similar environment in the Southeast Atlantic would result in sinking shells being higher in δ^{15}N than living foraminifera in winter, especially if there had been some initial drawdown of nitrate due to recent winter mixing at the time of sampling, or if there was an increase in ammonium uptake relative to nitrate, which has been shown to be the case on the Southern Benguela Upwelling System shelf (Flynn et al., 2018). Seasonal bias is therefore not ruled out as a contributor to the observed isotopic offset between our modern and fossil foraminifera.

A further point in regards to seasonality is that some of the offset could potentially be explained by a change in the growth season of foraminifera during the mid to late Holocene, thereby changing the δ^{15}N of species' diets. One point in favour of this argument is the late Holocene (2,000 - 0 BP) divergence observed between $U^{K'}_{37}$ and TEX_{86} temperature proxies in this region (Granger, 2016). Both proxies have been shown to record sea surface temperature but involve biomarkers synthesized by different groups of microbes (i.e., *Emiliana huxleyi versus* Thaumarcheota; Brassell et al. 1986; Schouten et al. 2002). Divergence between the two proxies may reflect a change in growth seasons, a trend that could be echoed in foraminifera over the same time period (Barker et al., 2009; Huguet et al., 2011; Lopes Dos Santos et al., 2013). However, a change in the growth season of a species would likely have resulted in more intra-site FB-δ^{15}N variability between the younger (GeoB 8317) and older (GeoB 8308) sediments, whereas all sites show a similar FB-δ^{15}N species hierarchy (Fig. 4.6).

4.4.3.2 Potential biological processes affecting foraminifer (shell)-bound δ^{15}N

Biological mechanisms for the isotopic difference between modern and fossil shells include a (1) change of diet prior to gametogenesis; and (2) the loss of calcite after death. Additional calcite tends to be added to foraminiferal tests during gametogenesis (reproduction) (Hemleben et al., 1985, 1989; Caron et al., 1990; Steinhardt et al., 2015), and this may amount to a significant percentage of total shell weight depending on the species (e.g., 28% on average of the total shell weight of *T. sacculifer*; Bé et al. 1981). During this stage in their life cycle, several species descend deeper in the water column before releasing gametes (Emiliani, 1971; Erez et al., 1991; Lohmann, 1995; Schiebel and Hemleben, 2005; Steinhardt et al., 2015). Since bacteria preferentially consume ^{14}N, bacterially-mediated diagenesis raises particulate δ^{15}N over time, and deeper particles tend to have a higher δ^{15}N (Altabet, 1988; Altabet et al., 1991; Casciotti et al., 2008). Mature foraminifera may ingest this high-δ^{15}N PON when they migrate out of the mixed layer, raising their tissue-δ^{15}N just prior to gametogenesis (and the FB-δ^{15}N thereafter). Modern specimens sampled in this study were all adults that had been captured within 200 m of the surface, but had not descended yet, and would thus not shown this final, high FB-δ^{15}N. However, another argument suggests that foraminifera feed less just prior to gametogenesis as symbionts appear to be digested or discarded and spines are shed, decreasing the ability

of foraminifera to feed and thus arguing against a significant change in the δ^{15}N of final chambers (Bé et al., 1981; Hemleben et al., 1989). Should feeding not take place after descending, the δ^{15}N of the final chamber would not be raised, and would therefore not explain the increase in fossil FB-δ^{15}N relative to modern shells.

Regarding the loss of calcite post-mortem, although FB-δ^{15}N is largely protected from diagenetic alteration, a portion of the shell is 'lost' as foraminifera sink out of the mixed layer (Lohmann, 1995; Broecker, 2001). In the case of juvenile foraminifera, some are entirely dissolved before reaching the seafloor. The fossil record preferentially records mature foraminifera, whilst younger (smaller) individuals are removed during sinking due to their slower descent (increasing the time and extent of dissolution), as well as due to the lack of a 'protective' thicker gametogenic layer (Adelseck and Berger, 1975; Hemleben et al., 1989; Fehrenbacher et al., 2017; Smart et al., 2018). Of the shells that do reach the seafloor, research suggests that an average of 19% of total shell weight is lost during sinking between 100 and 1000 m due to dissolution in the twilight zone (Schiebel et al., 2007). The idea of invoking partial shell loss as a mechanism for raising FB-δ^{15}N was suggested by Smart et al. (2018) who observed a 0.5 ‰ increase in sediment trap foraminifera shells in the Sargasso Sea relative to shell measurements from net tows (surface ocean). Smart et al. (2018) put forward two explanations for this increase. First, they raise the possibility that breakage of the largest (outer) chambers of dinoflagellate-hosting species during sinking or burial (Constandache et al., 2013) may also remove low FB-δ^{15}N due to an increased reliance on (or larger abundance of) symbionts towards the end of the organism's life. This scenario is likely not the case here, as the fossil-modern shell offset appears consistent in both symbiont-barren (offset $= 2.5 \pm 1.1$ ‰, *G. truncatulinoides* and *G. hirsuta*) and dinoflagellate-hosting species (offset $= 2.2 \pm 0.7$ ‰, *G. ruber* and *T. sacculifer*). Second, Smart et al. (2018) suggest that if one assumes lower δ^{15}N diet for juveniles than for adults, where young foraminifera rely less on carnivory and more on surface and subsurface PON, the removal of the inner chambers (or the complete dissolution of juveniles upon sinking) would result in sea-floor, fossil foraminifera being higher in FB-δ^{15}N than living foraminifera dwelling in the mixed layer. Dissolution of the inner chambers may have occurred as a result of their being in contact with a foraminifer's organic tissue, which is decomposed by bacteria after death, forming an acidic microenvironment through the release of weak organic acids (Schiebel et al., 2007; Smart et al., 2018). Dissolution of juveniles and/or juvenile chambers is a more likely scenario than the removal of low-δ^{15}N outer chambers in dinoflagellate-hosting species, but is difficult to prove without more data. It is also unclear whether dissolution would affect all species to similar degrees, as some (e.g., *G. truncatulinoides*) are less carnivorous (Anderson and Sedell, 1979; Spindler et al., 1984), which might result in a smaller fossil-to-modern shell δ^{15}N offset relative to euphotic dwellers like *G. ruber*.

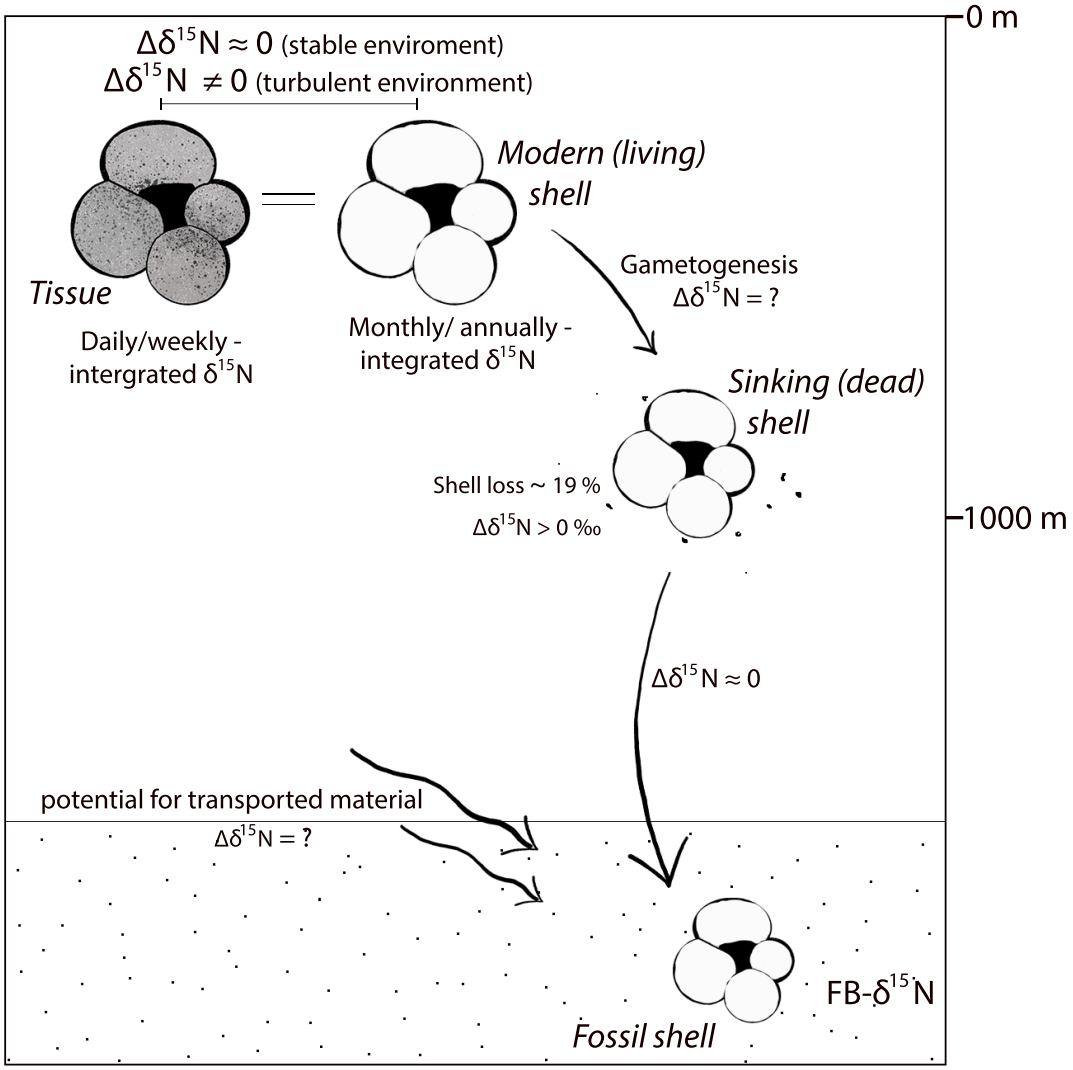

Figure 4.9: Schematic illustrating some of the potential processes influencing FB-δ^{15}N prior to measurement. (1) Differences between tissue and modern-shell δ^{15}N can arise due to changing environmental conditions during a foraminifer's lifetime, with larger discrepancies occurring in more turbulent environments; (2) Descent in the water column has the potential to alter the δ^{15}N of foraminifer diet prior to gametogenesis; (3) Sinking foraminifera may experience dissolution of thin-walled, low δ^{15}N juvenile chambers; and (4) Specimens used in analysis may have been transported from elsewhere via bottom currents or movement off the continental shelf.

4.5 Conclusions

This study adds to global ground-truthing efforts of the FB-δ^{15}N palaeoceanographic proxy by comparing modern foraminifera tissue and shell measurements with measurements of fossil foraminifera from coretops in the South Atlantic region. The results of these comparisons reveal that fossil foraminifera FB-δ^{15}N is strongly linked in this region to the original organic tissue of living foraminifera, which is in turn a reflection of habitat (mixed layer and thermocline) nutrient conditions. Further examination of the three distinct datasets allows for the identification of the stages in a foraminfer's life cycle (and

subsequent sinking and deposition) where changes in N isotopic composition can occur, creating apparent offsets from the original living foraminifer tissue [Fig. 4.9]. We discuss the relative importance of these isotopic offsets with regards to palaeoceanographic proxy interpretation, as some changes may have implications for how palaeoceanographic sediment records are interpreted whereas in other instances, changes may have no influence on interpretations. We conclude that rapid changes in water column conditions are likely responsible for the difference between tissue and modern shell-bound δ^{15}N, but that this finding means little for the fossil record. A single measurement of fossil FB-δ^{15}N yields an integrated signal of multiple foraminifera from a span of at least several centuries, whilst a discrepancy between an individual's tissue- and shell-bound δ^{15}N (caused by short-term, intra-seasonal variability) measured at a single point in time will not affect the long-term average.

At the same time, several mechanisms are proposed as potential reasons for the consistently higher FB-δ^{15}N in fossil foraminifera relative to modern foraminifera, including individuals feeding on PON with a higherδ^{15}N prior to gametogenesis, loss of inner chambers during sinking, loss of juvenile shells prior to burial, and the post-depositional transport of foraminifera off the continental shelf. Additionally, the core-top sediment used in this study also does not present a true analogue to modern ocean conditions, as the measured fossil FB-δ^{15}N represents an integrated signal over the age range of 1,340 to 5,380 BP. It is difficult to dismiss any of these processes from the available data; nonetheless, the data presented here appear to validate the assumption that shell-bound δ^{15}N is a good indicator of the δ^{15}N of living foraminifera (Ren et al., 2009), and suggest that modern shell FB-δ^{15}N is a composite of signals acquired throughout an organism's life (Li et al., 2019; Smart et al., 2018, 2020). The positive relationship between tissue- and shell-bound δ^{15}N bodes well for use of the proxy in this region and a larger sample set would likely reduce some of this uncertainty. Indeed, the remaining ambiguity presents an opportunity for future research to focus on clarifying the effect that modern spatial and temporal variability has on the palaeoceanographic record in the southeast Atlantic Ocean.

Our findings suggest that FB-δ^{15}N will work well as a proxy method for establishing changes in local nitrate sources, including supply changes resulting from fluctuations in Agulhas leakage. The close agreement of the relationship between modern and fossil foraminifer δ^{15}N to previous studies (where source nitrate δ^{15}N is lower than in the southeast Atlantic and biogeochemical cycling is different) strengthens the hypothesis that the proxy appears viable in multiple regions with different N-cycling dynamics, and is therefore applicable throughout the global ocean. Our initial fossil FB-δ^{15}N data also raise the idea that downcore records taken from core sites located close to one another in the southeast Atlantic may record very different processes. There are multiple factors that can potentially drive δ^{15}N changes in nitrate in the southeast Atlantic, including proximity to the continental shelf (and the influence of water column denitrification), location

relative to the Agulhas leakage corridor (which introduces low $\delta^{15}N_{NO_3}$ into the system), and the influence of seasonal or perennial upwelling (i.e., more southerly sites experience higher inter-annual variability than northern sites, where upwelling is more perennial). Additionally, centennial or millennial shifts in westerly wind position and intensity might result in periodic fluctuations between the competing drivers of biogeochemical cycling at a single location. Combining FB-δ^{15}N with other palaeoceanographic proxies (e.g., for SST) when reconstructing past climates could help in distinguishing among these drivers, as well as increasing our understanding of how local- and global-scale climate forcings interact in this region. In this way, FB-δ^{15}N is a powerful tool in palaeoceanographic reconstructions of biogeochemical cycling in the southeast Atlantic Ocean.

Supplementary Figures

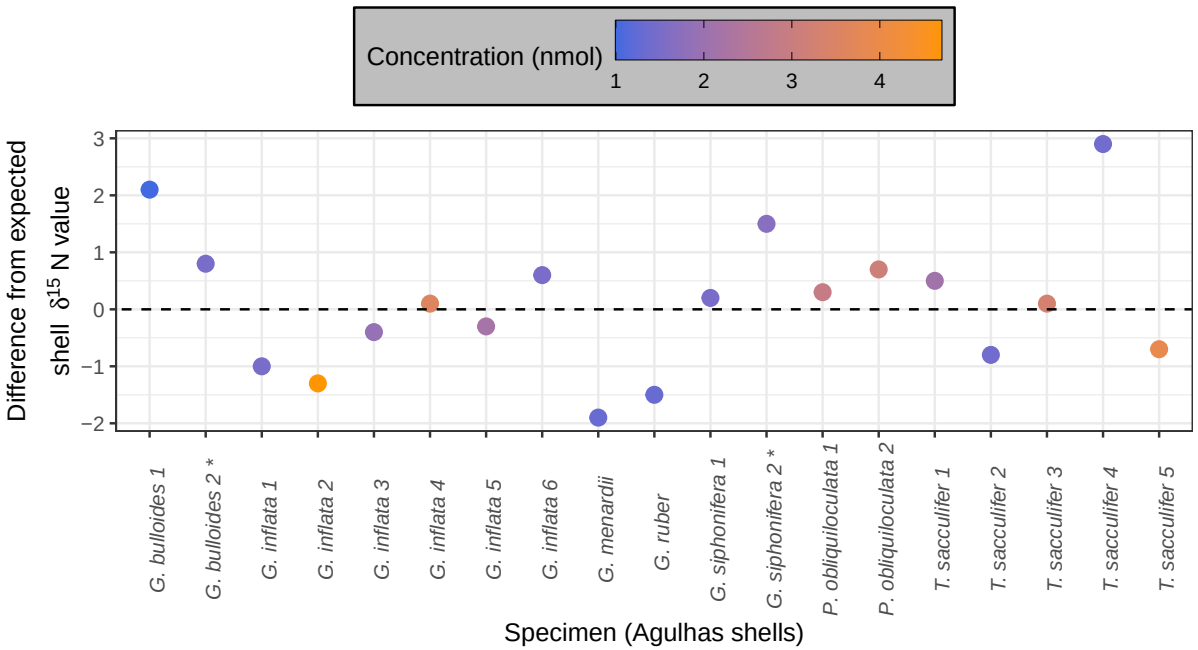

Figure S.1: Difference between corrected and expected FB-δ^{15}N for low concentration ($<$ 4 nmol) samples. All samples are from Agulhas net tows, with the exception of two Atlantic shell samples from station 14 (denoted by a * following the species name). Positive values indicate higher expected FB-δ^{15}N relative to replicate-corrected FB-δ^{15}N.

References

Adelseck, C.G., J. and Berger, W. (1975). On the dissolution of planktonic foraminifera and associated micro-fossils during settling and on the sea floor. *Dissolution of deep-sea carbonates. Cushman Found.*, 13(Foraminiferal Res., Spec. Publ.):70–81.

Altabet, M. A. (1988). Variations in nitrogen isotopic composition between sinking and suspended particles: implications for nitrogen cycling and particle transformation in the open ocean. *Deep Sea Research Part A, Oceanographic Research Papers*, 35(4):535–554.

Altabet, M. A., Deuser, W. G., Honjo, S., Stienen, C., and Stienent, C. (1991). Seasonal and depth-related changes in the source of sinking particles in the North Atlantic. *Nature*, 354(November):136–139.

Altabet, M. A. and Francois, R. (1994). Sedimentary nitrogen isotopic ratio as a recorder for surface ocean nitrate utilization. *Global Biogeochemical Cycles*, 8(1):103–116.

Altabet, M. A. and Francois, R. (2001). Nitrogen isotope biogeochemistry of the Antarctic polar frontal zone at 170°W. *Deep-Sea Research Part II: Topical Studies in Oceanography*, 48(19-20):4247–4273.

Altabet, M. A. and McCarthy, J. J. (1985). Temporal and spatial variations in the natural abundance of 15N in PON from a warm-core ring. *Deep Sea Research Part A, Oceanographic Research Papers*, 32(7):755–772.

Anderson, N. and Sedell, J. (1979). Detritus processing by macroinvertebrates in stream ecosystems. *Ann. Rev. Entomol.*, (24):351–357.

Andrews, W. and Hutchings, L. (1980). Upwelling in the Southern Benguela Current. *Progress in Oceanography*, 9:1–81.

Auderset, A., Moretti, S., Taphorn, B., Ebner, P. R., Kast, E., Wang, X. T., Schiebel, R., Sigman, D. M., Haug, G. H., and Martínez-García, A. (2022). Enhanced ocean oxygenation during Cenozoic warm periods. *Nature*, 609(7925):77–82.

Bailey, G. W. (1991). Organic carbon flux and development of oxygen deficiency on the modern Benguela continential shelf south of 22{degrees}S: spatial and temporal variability. *Modern and Ancient Continental Shelf Anoxia*, 58(1):171–183.

Barker, S., Diz, P., Vautravers, M. J., Pike, J., Knorr, G., Hall, I. R., and Broecker, W. S. (2009). Interhemispheric Atlantic seesaw response during the last deglaciation. *Nature*, 457(7233):1097–1102.

Bé, A. W. H., Caron, D. A., and Anderson, O. R. (1981). Effects of feeding frequency on life processes of the planktonic foraminifer globigerinoides sacculifer in laboratory

culture. *Journal of the Marine Biological Association of the United Kingdom*, 61(1):257–277.

Bé, A. W. H. and Hutson, W. H. (1977). Ecology of Planktonic Foraminifera and Biogeographic Patterns of Life and Fossil Assemblages in the Indian Ocean. *Micropaleontology*, 23(4):369.

Bé, A. W. H. and Tolderlund, D. S. (1971). Distribution and ecology of living planktonic foraminifera in surface waters of the Atlantic and Indian Oceans.

Beal, L., De Ruijter, W. P., Biastoch, A., Zahn, R., Cronin, M., Hermes, J., Lutjeharms, J. R., Quartly, G., Tozuka, T., Baker-Yeboah, S., Bornman, T., Cipollini, P., Dijkstra, H., Hall, I., Park, W., Peeters, F. J., Penven, P., Ridderinkhof, H., and Zinke, J. (2011). On the role of the Agulhas system in ocean circulation and climate. *Nature*, 472(7344):429–436.

Bergh, E. W., von Koslowski, R., and Compton, J. S. (2021). Variations in deep water masses along the western margin of South Africa, spanning the last two glacial terminations. *Palaeogeography, Palaeoclimatology, Palaeoecology*, 562(August 2020):110148.

Biastoch, A., Boening, C. W., and Lutjeharms, J. R. (2008). Agulhas leakage dynamics affects decadal variability in Atlantic overturning circulation. *Nature*, 456(November):489–492.

Birch, G. F. (1977). Surficial sediments on the continental margin off the west coast of South Africa. *Marine Geology*, 23(4):305–337.

Boebel, O., Davis, R. E., Ollitrault, M., Peterson, R. G., Richardson, P. L., Schmid, C., and Zenk, W. (1999). The intermediate depth circulation of the western South Atlantic. *Geophysical Research Letters*, 26(21):3329–3332.

Boebel, O., Rossby, T., Lutjeharms, J. R., Zenk, W., and Barron, C. (2003). Path and variability of the Agulhas Return Current. *Deep Sea Research Part II*, 50:35–56.

Braby, L., Deshayes, J., Beal, L., Morris, T., Novelli, G., Maitland, J., Ansorge, I., and Hermes, J. (2022). First Observations of Seasonal Variability in Water Mass Properties Across the Agulhas Current. *Journal of Geophysical Research: Oceans*, 127(9):1–20.

Braman, R. S. and Hendrix, S. A. (1989). Nanogram Nitrite and Nitrate Determination in Environmental and Biological Materials by Vanadium(III) Reduction with Chemiluminescence Detection. *Analytical Chemistry*, 61(24):2715–2718.

Brandes, J. A., Devol, A. H., Yoshinari, T., Jayakumar, D. A., and Naqvi, S. W. (1998). Isotopic composition of nitrate in the central Arabian Sea and eastern tropical North Pacific: A tracer for mixing and nitrogen cycles. *Limnology and Oceanography*, 43(7):1680–1689.

Brassell, S. C., Eglinton, G., Marlowe, I. T., Pflaumannt, U., and Sarntheint, M. (1986). Molecular stratigraphy: a new tool for climatic assessment. *Nature*, 230:129–133.

Broecker, W. S. (1991). The Great Ocean Conveyor. *Oceanography*, 4(2):79–89.

Broecker, W. S. (2001). PALEOCLIMATE: Was the Medieval Warm Period Global? *Science*, 291(5508):1497–1499.

Browning, T. J., Achterberg, E. P., Rapp, I., Engel, A., Bertrand, E. M., Tagliabue, A., and Moore, C. M. (2017). Nutrient co-limitation at the boundary of an oceanic gyre. *Nature*, 551(7679):242–246.

Bănaru, D., Carlotti, F., Barani, A., Grégori, G., Neffati, N., and Harmelin-Vivien, M. (2014). Seasonal variation of stable isotope ratios of size-fractionated zooplankton in the Bay of Marseille (NW Mediterranean Sea). *Journal of Plankton Research*, 36(1):145–156.

Caley, T., Giraudeau, J., Malaizé, B., Rossignol, L., and Pierre, C. (2012). Agulhas leakage as a key process in the modes of Quaternary climate changes. *PNAS*, 109(18):6835–6839.

Caley, T., Peeters, F. J., Biastoch, A., Rossignol, L., and Sebille, E. V. (2014). Quantitative estimate of the paleo-Agulhas leakage. *Geophysical Research Letters*, 41:1238–1246.

Caron, D. A., Roger Anderson, O., Lindsey, J. L., Faber, W. W., and Lin Lim, E. E. (1990). Effects of gametogenesis on test structure and dissolution of some spinose planktonic foraminifera and implications for test preservation. *Marine Micropaleontology*, 16(1-2):93–116.

Carpenter, E. J., Harvey, H. R., Brian, F., and Capone, D. G. (1997). Biogeochemical tracers of the marine cyanobacterium Trichodesmium. *Deep-Sea Research Part I: Oceanographic Research Papers*, 44(1):27–38.

Casciotti, K. L., Sigman, D. M., Hastings, M. G., Bohlke, J. K., and Hilkert, a. (2002). Measurement of the oxygen isotopic composition of nitrate seawater and freshwater using the dentirifier method. *Anal. Chem.*, 74(19):4905–4912.

Casciotti, K. L., Trull, T. W., Glover, D. M., and Davies, D. (2008). Constraints on nitrogen cycling at the subtropical North Pacific Station ALOHA from isotopic measurements of nitrate and particulate nitrogen. *Deep-Sea Research Part II: Topical Studies in Oceanography*, 55(14-15):1661–1672.

Caut, S., Angulo, E., and Courchamp, F. (2009). Variation in discrimination factors (Δ15N and Δ13C): The effect of diet isotopic values and applications for diet reconstruction. *Journal of Applied Ecology*, 46(2):443–453.

Cetina-Heredia, P., Roughan, M., Van Sebille, E., Shane, K., Gary, B., Keating, S., and Brassington, G. B. (2019). Retention and leakage of water by mesoscale eddies in the East Australian Current system. *Journal of Geophysical Research: Oceans*, 124(4):2485–2500.

Chapman, P. and Shannon, L. V. (1987). Seasonality in the oxygen minimum layers at the extremities of the Benguela system. *South African Journal of Marine Science*, 5(1):85–94.

Chen, Y. L. L., Chen, H. Y., Karl, D. M., and Takahashi, M. (2004). Nitrogen modulates phytoplankton growth in spring in the South China Sea. *Continental Shelf Research*, 24(4-5):527–541.

Cifuentes, L. A., Fogel, M. L., Pennock, J. R., and Sharp, J. H. (1989). Biogeochemical factors that influence the stable nitrogen isotope ratio of dissolved ammonium in the Delaware Estuary. *Geochimica et Cosmochimica Acta*, 53(10):2713–2721.

Cifuentes, L. A., Sharp, J. H., and Fogel, M. L. (1988). Stable carbon and nitrogen isotope biogeochemistry in the Delaware estuary. *Limnology and Oceanography*, 33(5):1102–1115.

Cline, J. D. and Kaplan, I. R. (1975). Isotopic fractionation of dissolved nitrate during denitrification in the eastern tropical north pacific ocean. *Marine Chemistry*, 3(4):271–299.

Cohen, A. L. and Tyson, P. (1995). Sea surface temperature fluctuations during the Holocene off the south coast of Africa: implications for terrestrial climate and rainfall. *The Holocene*, 5(3):304–312.

Compton, J. S., Herbert, C. T., and Schneider, R. (2009). Organic-rich mud on the western margin of southern Africa: Nutrient source to the Southern Ocean? *Global Biogeochemical Cycles*, 23:1–12.

Compton, J. S. and Wiltshire, J. G. (2009). Terrigenous sediment export from the western margin of South Africa on glacial to interglacial cycles. *Marine Geology*, 266(1-4):212–222.

Condie, S. and Condie, R. (2016). Retention of plankton within ocean eddies. *Global Ecology and Biogeography*, 25(10):1264–1277.

Constandache, M., Yerly, F., and Spezzaferri, S. (2013). Internal pore measurements on macroperforate planktonic Foraminifera as an alternative morphometric approach. *Swiss Journal of Geosciences*, 106:179–186.

De Ruijter, W. P., Biastoch, A., Drijfhout, S. S., Lutjeharms, J. R., Matano, R. P., Pichevin, T., van Leeuwen, P. J., and Weijer, W. (1999). Indian-Atlantic interocean exchange: Dynamics, estimation and impact. *Journal of Geophysical Research*, 104(C9):20885–20910.

De Ruijter, W. P. and Boudra, D. B. (1985). The wind-driven circulation in the South Atlantic-Indian Ocean—I. Numerical experiments in a one-layer model. *Deep Sea Research Part A. Oceanographic Research Papers*, 32(5):557–574.

Dencausse, G., Arhan, M., and Speich, S. (2010). Routes of Agulhas rings in the southeastern Cape Basin. *Deep-Sea Research Part I*, 57(11):1406–1421.

Deniro, M. J. (1987). Stable isotopy and archaeology. *American Scientist*, 75(2):182–191.

Deuser, W. G., Ross, E., Hemleben, C., and Spindler, M. (1981). Seasonal changes in species composition, numbers, mass, size, and isotopic composition of planktonic foraminifera settling into the deep Sargasso Sea. *Palaeogeography Palaeoclimatology Palaeoecology*, 33:103–127.

Deutsch, C., Sigman, D. M., Thunell, R. C., Meckler, A. N., and Haug, G. H. (2004). Isotopic constraints on glacial/interglacial changes in the oceanic nitrogen budget. *Global Biogeochemical Cycles*, 18(4):1–22.

DiFiore, P. J., Sigman, D. M., Trull, T. W., Lourey, M. J., Karsh, K. L., Cane, G., and Ho, R. (2006). Nitrogen isotope constraints on subantarctic biogeochemistry. *Journal of Geophysical Research: Oceans*, 111(8):1–19.

Donners, J., Drijfhout, S. S., and Hazeleger, W. (2005). Water mass transformation and subduction in the South Atlantic. *Journal of Physical Oceanography*, 35(10):1841–1860.

Dugdale, R. C. and Goering, J. J. (1967). Uptake of new and regenerated forms of nitrogen in primary productivity. *Limnology & Oceanography*, 12(2):196–206.

Dugdale, R. C., Goering, J. J., Barber, R. T., Smith, R. L., and Packard, T. T. (1977). Denitrification and hydrogen sulfide in the Peru upwelling region during 1976. *Deep-Sea Research*, 24(6):601–608.

Duncombe Rae, C. M., Shillington, F. A., Agenbag, J. J., Taunton-Clark, J., and Gründlingh, M. L. (1992). An agulhas ring in the South Atlantic ocean and its interaction with the Benguela upwelling frontal system. *Deep Sea Research Part A, Oceanographic Research Papers*, 39(11-12):2009–2027.

Emiliani, C. (1971). Depth Habitats of Growth Stages of Pelagic Foraminifera. *Science*, 173:1122–1124.

Erez, J., Almogi-Labin, A., and Avraham, S. (1991). ON THE LIFE HISTORY OF PLANKTONIC FORAMINIFERA: LUNAR REPRODUCTION CYCLE IN GLOBIGERINOIDES SACCULIFER (BRADY). *Palaeoceanography*, 6(3):295–306.

Etourneau, J., Martinez, P., Blanz, T., and Schneider, R. (2009). Pliocene-Pleistocene variability of upwelling activity, productivity, and nutrient cycling in the Benguela region. *Geology*, 37(10):871–874.

Farmer, C., deMenocal, P. B., and Marchitto, T. M. (2005). Holocene and deglacial ocean temperature variability in the Benguela upwelling region: Implications for low-latitude atmospheric circulation. *Paleoceanography*, 20(2):1–16.

Fawcett, S. E., Ward, B. B., Lomas, M. W., and Sigman, D. M. (2015). Vertical decoupling of nitrate assimilation and nitrification in the Sargasso Sea. *Deep-Sea Research Part I: Oceanographic Research Papers*, 103:64–72.

Fehrenbacher, J. S., Russell, A. D., Davis, C. V., Gagnon, A. C., Spero, H. J., Cliff, J. B., Zhu, Z., and Martin, P. (2017). Link between light-triggered Mg-banding and chamber formation in the planktic foraminifera Neogloboquadrina dutertrei. *Nature Communications*, 8(May):1–10.

Flores, J., Gersonde, R., and Sierro, F. J. (1999). Pleistocene fluctuations in the Agulhas Current Retroflection based on the calcareous plankton record. *Marine Micropaleontology*, 37(1):1–22.

Flynn, R. F., Burger, J. M., Pillay, K., and Fawcett, S. E. (2018). Wintertime rates of net primary production and nitrate and ammonium uptake in the southern Benguela upwelling system Wintertime rates of net primary production and nitrate and ammonium. *African Journal of Marine Science*, 40(3):253–266.

Flynn, R. F., Granger, J., Veitch, J. A., Siedlecki, S., Burger, J. M., Pillay, K., and Fawcett, S. E. (2020). On-Shelf Nutrient Trapping Enhances the Fertility of the Southern Benguela Upwelling System. *Journal of Geophysical Research: Oceans*, 125(6):1–24.

Fong, A. A., Karl, D. M., Lukas, R., Letelier, R. M., Zehr, J. P., and Church, M. J. (2008). Nitrogen fixation in an anticyclonic eddy in the oligotrophic North Pacific Ocean. *ISME Journal*, 2(6):663–676.

Fraile, I., Schulz, M., Mulitza, S., Merkel, U., Prange, M., and Paul, A. (2009). Modeling the seasonal distribution of planktonic foraminifera during the last glacial maximum. *Paleoceanography*, 24(2):1–15.

Franzese, A. M., Hemming, S. R., Goldstein, S. L., and Anderson, R. F. (2006). Reduced Agulhas Leakage during the Last Glacial Maximum inferred from an integrated provenance and flux study. *Earth and Planetary Science Letters*, 250:72–88.

Freudenthal, T., Meggers, H., Henderiks, J., Kuhlmann, H., Moreno, A., and Wefer, G. (2002). Upwelling intensity and filament activity off Morocco during the last 250,000 years. *Deep-Sea Research Part II: Topical Studies in Oceanography*, 49(17):3655–3674.

Freudenthal, T., Wagner, T., Wenzhöfer, F., Zabel, M., and Wefer, G. (2001). Early diagenesis of organic matter from sediments of the eastern subtropical Atlantic: Evidence from stable nitrogen and carbon isotopes. *Geochimica et Cosmochimica Acta*, 65(11):1795–1808.

Ganeshram, S., Pedersen, F., Calvert, E., Mcneill, W., and Fontugne, M. R. (2000). Glacial-interglacial variability in denitrification in the world's oceans: Causes and consequence. *Carbon*, 15(4):361–376.

Garzoli, S. L. and Gordon, A. L. (1996). Origins and variablity of the Benguela Current. *Journal of Geophysical Research*, 101(95):897–906.

Garzoli, S. L., Gordon, A. L., Kamenkovich, V., Pillsbury, D., and Duncombe-Rae, C. (1996). Variability and sources of the southeastern Atlantic circulation. *Journal of Marine Research*, 54(6):1039–1071.

Garzoli, S. L. and Matano, R. P. (2011). The South Atlantic and the Atlantic Meridional Overturning Circulation. *Deep-Sea Research Part II: Topical Studies in Oceanography*, 58(17-18):1837–1847.

Gaye, B., Nagel, B., Dähnke, K., Rixen, T., Lahajnar, N., and Emeis, K. C. (2013). Amino acid composition and δ15N of suspended matter in the Arabian Sea: Implications for organic matter sources and degradation. *Biogeosciences*, 10(11):7689–7702.

Gaye-Haake, B., Lahajnar, N., Emeis, K. C., Unger, D., Rixen, T., Suthhof, A., Ramaswamy, V., Schulz, H., Paropkari, A. L., Guptha, M. V., and Ittekkot, V. (2005). Stable nitrogen isotopic ratios of sinking particles and sediments from the northern Indian Ocean. *Marine Chemistry*, 96(3-4):243–255.

Gordon, A. L. (1985). Indian-Atlantic Transfer of Thermocine Water at the Agulhas Retroflection. *Science*, 227:1030–1033.

Gordon, A. L., Weiss, R., Smethie, W. M., and Warner, M. J. (1992). Thermocline and Intermediate Water Communication Between the South Atlantic and Indian Oceans. *Journal of Geophysical ...*, 97:7223–7240.

Granger, R. (2016). Palaeoenvironmental reconstruction of late Holocene climate dynamics in Southwest Africa using a multi-proxy characterization of Namaqualand mudbelt. (January):i–153.

Granger, R., Meadows, M. E., Hahn, A., Zabel, M., Stuut, J.-B., Herrmann, N., and Schefuß, E. (2018). Late-Holocene dynamics of sea-surface temperature and terrestrial hydrology in southwestern Africa. *Holocene*, 28(5).

Heaton, T. J., Köhler, P., Butzin, M., Bard, E., Reimer, R. W., Austin, W. E., Bronk Ramsey, C., Grootes, P. M., Hughen, K. A., Kromer, B., Reimer, P. J., Adkins, J., Burke, A., Cook, M. S., Olsen, J., and Skinner, L. C. (2020). Marine20 - The Marine Radiocarbon Age Calibration Curve (0-55,000 cal BP). *Radiocarbon*, 62(4):779–820.

Hemleben, C., Spindler, M., and Anderson, O. R. (1989). *Modern Planktonic Foraminifera.* Springer-Verlag, New York, 1 edition.

Hemleben, C., Spindler, M., Breitinger, I., and Deuser, W. G. (1985). Field and laboratory studies on the ontogeny and ecology of some globorotaliid species from the Sargasso Sea off Bermuda. *Journal of Foraminiferal Research*, 15(4):254–272.

Herbert, C. T. and Compton, J. S. (2007). Geochronology of Holocene sediments on the western margin of South Africa. *South African Journal of Geology*, 110(2-3):327–338.

Heywood, R. B. and Priddle, J. (1987). Retention of phytoplankton by an eddy. *Continental Shelf Research*, 7(8):937–955.

Hoering, T. C. and Ford, H. T. (1960). The Isotope Effect in the Fixation of Nitrogen by Azotobacter. *J. Am Chem Soc.*, 82:376–378.

Holmes, E., Lavik, G., Fischer, G., Segl, M., Ruhland, G., and Wefer, G. (2002). Seasonal variability of delta δ15N in sinking particles in the Benguela Upwelling region. *Deep-Sea Res.(I Oceanogr.Res.Pap.)*, 49(2):377–394.

Horn, M. G., Robinson, R., Rynearson, T. A., and Sigman, D. M. (2011). Nitrogen isotopic relationship between diatom-bound and bulk organic matter of cultured polar diatoms. *Paleoceanography*, 26:1–12.

Huguet, C., Martrat, B., Grimalt, J. O., Sinninghe Damsté, J. S., and Schouten, S. (2011). Coherent millennial-scale patterns in UK'37 and TEXH86 temperature records during the penultimate interglacial-to-glacial cycle in the western Mediterranean. *Paleoceanography*, 26(PA2218):1–10.

Hutchings, L., Jarre, A., Lamont, T., van den Berg, M., and Kirkman, S. P. (2012). St Helena Bay (southern Benguela) then and now: muted climate signals, large human impact. *African Journal of Marine Science*, 34(4):559–583.

Hutchings, L., van der Lingen, C. D., Shannon, L. J., Crawford, R. J. M., Verheye, H. M. S., Bartholomae, C. H., van der Plas, A. K., Louw, D., Kreiner, A., Ostrowski, M., Fidel, Q., Barlow, R., Lamont, T., Coetzee, J., Shillington, F. A., Veitch, J. A., Currie,

J. C., and Monteiro, P. M. S. (2009). The Benguela Current: An ecosystem of four components. *Progress in Oceanography*, 83(1-4):15–32.

Jonkers, L. and Kučera, M. (2015). Global analysis of seasonality in the shell flux of extant planktonic Foraminifera. *Biogeosciences*, 12(7):2207–2226.

Kasper, S., van der Meer, M. T. J., Mets, A., Zahn, R., Sinninghe Damsté, J. S., and Schouten, S. (2014). Salinity changes in the Agulhas leakage area recorded by stable hydrogen isotopes of C37 alkenones during Termination I and II. *Climate of the Past*, 10:251–260.

Kast, E. R., Stolper, D. A., Auderset, A., Higgins, J. A., Ren, H., Wang, X. T., Martínez-García, A., Haug, G. H., Sigman, D. M., and Stopler, D. (2019). Nitrogen isotope evidence for expanded ocean suboxia in the early Cenozoic. *Science*, 364(6438):386–389.

Kienast, M. (2000). Unchanged nitrogen isotopic composition of organic matter in the South China Sea during the last climatic cycle: Global implications. *Palaeoceanography*, 16(2):244–253.

Kim, J. H., Schneider, R. R., Mulitza, S., and Muller, P. J. (2003). Reconstruction of SE trade-wind intensity based on sea-surface temperature gradients in the Southeast Atlantic over the last 25 kyr. *Geophysical Research Letters*, 30(22):3–6.

King, K. and Hare, P. E. (1972). Amino Acid Composition of the Test as a Taxonomic Character for Living and Fossil Planktonic Foraminifera. *Micropaleontology*, 18(3):285.

Knapp, A. N., Sigman, D. M., and Lipschultz, F. (2005). N isotopic composition of dissolved organic nitrogen and nitrate at the Bermuda Atlantic Time-series study site. *Global Biogeochemical Cycles*, 19(1):1–15.

Kritee, K., Sigman, D. M., Granger, J., Ward, B. B., Jayakumar, A., and Deutsch, C. (2012). Reduced isotope fractionation by denitrification under conditions relevant to the ocean. *Geochimica et Cosmochimica Acta*, 92:243–259.

Kuypers, M., Lavik, G., Woebken, D., Schmid, M. C., Fuchs, B. M., Amann, R., Jorgensen, B. B., and Jetten, M. S. M. (2005). Massive nitrogen loss from the Benguela upwelling system through anaerobic ammonium oxidation. *Proc Natl Acad Sci U S A*, 102(18):6478–6483.

Ladigbolu, I. A., Li, B. H., Li, H. L., Wiesner, M. G., Yu, Z. F., Zhang, J. J., Sun, L., Ran, L. H., Ye, Y., and Chen, J. F. (2020). Fluxes and isotopic composition of planktonic foraminifera off Hainan Island, northern South China Sea: Implications for paleoceanographic studies. *Palaeoworld*, 29(3):636–647.

Lamont, T., Van Den Berg, M. A., and Barlow, R. (2016). Agulhas current influence on the shelf dynamics of the KwaZulu-Natal bight. *Journal of Physical Oceanography*, 46(4):1323–1338.

Leduc, G., Herbert, C. T., Blanz, T., Martinez, P., and Schneider, R. (2010). Contrasting evolution of sea surface temperature in the Benguela upwelling system under natural and anthropogenic climate forcings. *Geophysical Research Letters*, 37(20):1–5.

Lekieffre, C., Spero, H. J., Fehrenbacher, J. S., Russell, A. D., Ren, H., Geslin, E., and Meibom, A. (2020). Ammonium is the preferred source of nitrogen for planktonic foraminifer and their dinoflagellate symbionts: N recycling in a symbiotic foraminifer. *Proceedings of the Royal Society B: Biological Sciences*, 287(1929):1–10.

Lessa, D., Morard, R., Jonkers, L., Venancio, I. M., Reuter, R., Baumeister, A., Albuquerque, A. L., and Kucera, M. (2020). Distribution of planktonic foraminifera in the subtropical South Atlantic: depth hierarchy of controlling factors. *Biogeosciences*, 17(16):4313–4342.

Li, C., Sonke, J. E., Le Roux, G., Van der Putten, N., Piotrowska, N., Jeandel, C., Mattielli, N., Benoit, M., Wiggs, G. F., and De Vleeschouwer, F. (2020). Holocene dynamics of the southern westerly winds over the Indian Ocean inferred from a peat dust deposition record. *Quaternary Science Reviews*, 231:1–13.

Li, D. W., Xiang, R., Wu, Q., and Kao, S. J. (2019). Planktic foraminifera-bound organic nitrogen isotopic composition in contemporary water column and sediment trap. *Deep-Sea Research Part I*, 143:28–34.

Lipschultz, F. (2001). A time-series assessment of the nitrogen cycle at BATS. *Deep-Sea Research Part II: Topical Studies in Oceanography*, 48(8-9):1897–1924.

Lohmann, G. P. (1995). A model for variation in the chemistry of planktonic foraminifera due to secondary calcification and selective dissolution. *Paleoceanography*, 10(3):445–457.

Lohmann, G. P. and Schweitzer, P. N. (1989). Globorotalia truncatulinoides' growth and chemistry as probes of the past thermocline: 1. Shell size. *Palaeoceanography*, 5(1):55–75.

Lončarić, N. (2006). Planktic foraminiferal content in a mature Agulhas eddy from the SE Atlantic: Any influence on foraminiferal export fluxes? *Geologia Croatica*, 59(1):41–50.

Lončarić, N., Peeters, F. J., Kroon, D., and Brummer, G. J. A. (2006). Oxygen isotope ecology of recent planktic foraminifera at the central Walvis Ridge (SE Atlantic). *Paleoceanography*, 21(3):1–18.

Lopes Dos Santos, R. A., Spooner, M. I., Barrows, T. T., De Deckker, P., Sinninghe Damsté, J. S., and Schouten, S. (2013). Comparison of organic (UK'37, TEXH86, LDI) and faunal proxies (foraminiferal assemblages) for reconstruction of late Quaternary sea surface temperature variability from offshore southeastern Australia. *Paleoceanography*, 28(3):377–387.

Löscher, C. R., Bourbonnais, A., Dekaezemacker, J., Charoenpong, C. N., Altabet, M. A., Bange, H. W., Czeschel, R., Hoffmann, C., and Schmitz, R. (2016). N2 fixation in eddies of the eastern tropical South Pacific Ocean. *Biogeosciences*, 13(10):2889–2899.

Lourey, M. J. and Trull, T. W. (2001). Seasonal nutrient depletion and carbon export in the Subantarctic and Polar Frontal Zones of the Southern Ocean south of Australia. *Journal of Geophysical Research*, 106(C12):31463–31487.

Lourey, M. J., Trull, T. W., and Sigman, D. M. (2003). Sensitivity of δ15N of nitrate, surface suspended and deep sinking particulate nitrogen to seasonal nitrate depletion in the Southern Ocean. *Global Biogeochemical Cycles*, 17(3):1–18.

Lutjeharms, J. R. (1981). Features of the southern Agulhas Current circulation from satellite remote sensing. *South African Journal of Science*, 77(May):231–236.

Lutjeharms, J. R. (2006). *The Agulhas Current*. Springer-Verlag, Berlin Heidelberg, 1 edition.

Lutjeharms, J. R. and Ansorge, I. J. (2001). The Agulhas Return Current. *Journal of Marine Systems*, 30(1-2):115–138.

Lutjeharms, J. R. and Meeuwis, J. M. (1987). The extent and variability of South-East Atlantic upwelling. *South African Journal of Marine Science*, 5(1):51–62.

Mackas, D. L. , Tsurumi, M., Galbraith, M. D., and Yelland, D. R. (2005). Zooplankton distribution and dynamics in a North Pacific Eddy of coastal origin: II . Mechanisms of eddy colonization by and retention of offshore species. *Deep-Sea Research II*, 52:1011–1035.

Marconi, D., Sigman, D. M., Casciotti, K. L., Campbell, E., Alexandra Weigand, M., Fawcett, S. E., Knapp, A. N., Rafter, P. A., Ward, B. B., and Haug, G. H. (2017). Tropical Dominance of N2 Fixation in the North Atlantic Ocean. *Global Biogeochemical Cycles*, 31(10):1608–1623.

Marshall, T. A., Sigman, D. M., Beal, L. M., Foreman, A., Martínez-García, A., Blain, S., Campbell, E., Fripiat, F., Granger, R., Harris, E., Haug, G. H., Marconi, D., Oleynik, S., Rafter, P. A., Roman, R., Sinyanya, K., Smart, S. M., and Fawcett, S. E. (2023). The Agulhas Current Transports Signals of Local and Remote Indian Ocean Nitrogen Cycling. *Journal of Geophysical Research: Oceans*, 128:1–29.

Martin, K. (1990). Department of Marine Sciences, University of Puerto Rico, Mayagiiez. (4):479–486.

Martínez-García, A., Jung, J., Ai, X. E., Sigman, D. M., Auderset, A., Duprey, N. N., Foreman, A., Fripiat, F., Leichliter, J., Lüdecke, T., Moretti, S., and Wald, T. (2022). Laboratory Assessment of the Impact of Chemical Oxidation, Mineral Dissolution, and Heating on the Nitrogen Isotopic Composition of Fossil-Bound Organic Matter. *Geochemistry, Geophysics, Geosystems*, 23(8):1–23.

Martínez-García, A., Sigman, D. M., Ren, H., Anderson, R. F., Straub, M., Hodell, D. A., Jaccard, S. L., Eglinton, T. I., and Haug, G. H. (2014). Iron fertilization of the Subantarctic ocean during the last ice age. *Science (New York, N.Y.)*, 343(6177):1347–50.

Martínez-Méndez, G., Zahn, R., Hall, I. R., Pena, L. D., and Cacho, I. (2008). 345 , 000-year-long multi-proxy records off South Africa document variable contributions of Northern versus Southern Component Water to the Deep South Atlantic. *Earth and Planetary Science Letters 267*, 267:309–321.

Matano, R. P., Simionato, C. G., De Ruijter, W. P., Van Leeuween, P. J., Strub, P. T., Chelton, D. B., and Schlax, M. G. (1999). Seasonal variability in the Agulhas Retroflection region. *Geophysical Research Letters*, 25(23):4361–4364.

Meadows, M. E. and Baxter, A. (2001). Holocene vegetation history and palaeoenvironments at Klaarfontein Springs, Western Cape, South Africa. *The Holocene*, 11(6):699–706.

Meckler, A. N., Ren, H., Sigman, D. M., Gruber, N., Plessen, B., Schubert, C. J., and Haug, G. H. (2011). Deglacial nitrogen isotope changes in the Gulf of Mexico: Evidence from bulk sedimentary and foraminifera-bound nitrogen in Orca Basin sediments. *Paleoceanography*, 26(4):1–13.

Meisel, S., Emeis, K.-C., Struck, U., and Kristen, I. (2011). Nutrient regime and upwelling in the northern Benguela since the middle Holocene in a global context - a multi-proxy approach. *Fossil Record*, 14(2):171–193.

Minagawa, M. and Wada, E. (1984). Stepwise enrichment of 15N along food chains: Further evidence and the relation between 15N and animal age. *Geochimica et Cosmochimica Acta*, 48(5):1135–1140.

Mitchell, B. G., Brody, E. A., Holm-Hansen, O., McClain, C., and Bishop, J. (1991). Light limitation of phytoplankton biomass and macronutrient utilization in the Southern Ocean. *Limnology and Oceanography*, 36(8):1662–1677.

Möbius, J., Lahajnar, N., and Emeis, K. C. (2010). Diagenetic control of nitrogen isotope ratios in Holocene sapropels and recent sediments from the Eastern Mediterranean Sea. *Biogeosciences*, 7(11):3901–3914.

Monteiro, P. M. and van der Plas, A. K. (2006). 5 Low oxygen water (LOW) variability in the Benguela system: Key processes and forcing scales relevant to forecasting. *Large Marine Ecosystems*, 14(C):71–90.

Montoya, J. (1994). Nitrogen Isotope Fractionation in the Modern Ocean: Implications for the Sedimentary Record. In Zahn, R., editor, *Carbon Cycling in the Glacial Ocean: Constraints on the Ocean's Role in Global Change*, volume I 17, pages 259–279. Springer-Verlag.

Morales, L. V., Sigman, D. M., Horn, M. G., and Robinson, R. (2013). Cleaning methods for the isotopic determination of diatombound nitrogen in non-fossil diatom frustules. *Limnology and Oceanography: Methods*, 11(FEB):101–112.

Muscatine, L., Goiran, C., Land, L., Jaubert, J., Cuif, J. P., and Allemand, D. (2005). Stable isotopes (δ13C and δ15N) of organic matrix from coral skeleton. *Proceedings of the National Academy of Sciences of the United States of America*, 102(5):1525–1530.

Nelson, G. (1992). Equatorward wind and atmospheric pressure spectra as metrics for primary productivity in the Benguela system. *South African Journal of Marine Science*, 12(March 2015):19–28.

Peeters, F. J., Acheson, R., Brummer, G.-J. A., De Ruijter, W. P., Schneider, R., Ganssen, G. M., Ufkes, E., and Kroon, D. (2004). Vigorous exchange between the Indian and Atlantic oceans at the end of the past five glacial periods. *Nature*, 430(7000):661–5.

Peeters, F. J., Ivanova, E., Conan, S., Brummer, G.-j., Ganssen, G., Troelstra, S., and Hinte, J. V. (1999). A size analysis of planktic foraminifera from the Arabian Sea. *Marine Micropaleontology*, 36:31–63.

Pichevin, L., Martinez, P., Bertrand, P., Schneider, R., Giraudeau, J., and Emeis, K. (2005). Nitrogen cycling on the Namibian shelf and slope over the last two climatic cycles: Local and global forcings. *Paleoceanography*, 20(2):1–13.

Post, D. (2002). Using stable iotopes to estimate trophic position: models, methods and assumptions. *Ecology*, 83(3):703–718.

Rau, A. J., Rogers, J., Lutjeharms, J. R., Giraudeau, J., Lee-thorp, J. A., Chen, M., and Waelbroeck, C. (2002). A 450-kyr record of hydrological conditions on the western Agulhas Bank Slope , south of Africa. *Marine Geology*, 180:183–201.

Rebotim, A. (2018). *Ecology and stable isotope geochemistry of modern planktonic foraminifera in the Northeast Atlantic*. PhD thesis, Universität Bremen.

Ren, H., Sigman, D. M., Chen, M. T., and Kao, S. J. (2012a). Elevated foraminifera-bound nitrogen isotopic composition during the last ice age in the South China Sea and its global and regional implications. *Global Biogeochemical Cycles*, 26(1):1–13.

Ren, H., Sigman, D. M., Meckler, A. N., Plessen, B., Robinson, R., Rosenthal, Y., and Haug, G. H. (2009). Foraminiferal isotope evidence of reduced nitrogen fixation in the ice age Atlantic Ocean. *Science*, 323(5911):244–248.

Ren, H., Sigman, D. M., Thunell, R. C., and Prokopenko, M. G. (2012b). Nitrogen isotopic composition of planktonic foraminifera from the modern ocean and recent sediments. *Limnology and Oceanography*, 57(4):1011–1024.

Ren, H., Studer, A. S., Serno, S., Sigman, D. M., Winckler, G., Anderson, R. F., Oleynik, S., Gersonde, R., and Haug, G. H. (2015). Glacial-to-interglacial changes in nitrate supply and consumption in the subarctic North Pacific from microfossil-bound N isotopes at two trophic levels. *Paleoceanography*, 30(9):1217–1232.

Reynolds, C. E., Richey, J. N., Fehrenbacher, J. S., Rosenheim, B. E., and Spero, H. J. (2018). Environmental controls on the geochemistry of Globorotalia truncatulinoides in the Gulf of Mexico: Implications for paleoceanographic reconstructions. *Marine Micropaleontology*, 142(January):92–104.

Robbins, L. L. and Brew, K. (1990). Proteins from the organic matrix of core-top and fossil planktonic foraminifera. *Geochimica et Cosmochimica Acta*, 54(8):2285–2292.

Robinson, R., Kienast, M., Luiza Albuquerque, A., Altabet, M. A., Contreras, S., De Pol-Holz, R., Dubois, N., Francois, R., Galbraith, E. D., Hsu, T. C., Ivanochko, T., Jaccard, S., Kao, S. J., Kiefer, T., Kienast, S., Lehmann, M. F., Martinez, P., McCarthy, M., Möbius, J., Pedersen, T. F., Quan, T. M., Ryabenko, E., Schmittner, A., Schneider, R., Schneider-Mor, A., Shigemitsu, M., Sinclair, D., Somes, C. J., Studer, A. S., Thunell, R. C., and Yang, J. Y. (2012). A review of nitrogen isotopic alteration in marine sediments. *Paleoceanography*, 27(PA4203):1–13.

Robinson, R., Smart, S. M., Cybulski, J. D., McMahon, K. W., Marcks, B., and Nowakowski, C. (2023). Insights from Fossil-Bound Nitrogen Isotopes in Diatoms, Foraminifera, and Corals. *Annual Review of Marine Science*, 15(1):1–24.

Schiebel, R., Barker, S., Lendt, R., Thomas, H., and Bollman, J. (2007). Planktic foraminiferal dissolution in the twilight zone. *Deep Sea Research Part II*, 54:676–686.

Schiebel, R. and Hemleben, C. (2000). Interannual variability of planktic foraminiferal populations and test flux in the eastern North Atlantic Ocean (JGOFS). *Deep-Sea Research Part II: Topical Studies in Oceanography*, 47(9-11):1809–1852.

Schiebel, R. and Hemleben, C. (2005). Modern planktic foraminifera. *Paläontologische Zeitschrift*, 79(1):135–148.

Schiebel, R., Spielhagen, R. F., Garnier, J., Hagemann, J., Howa, H., Jentzen, A., Martínez-García, A., Meilland, J., Michel, E., Repschläger, J., Salter, I., Yamasaki, M., and Haug, G. H. (2017). Modern planktic foraminifers in the high-latitude ocean. *Marine Micropaleontology*, 136:1–13.

Schneider, R. (2003). Report and Preliminary Results of METEOR Cruise M 57/1, Cape Town - Walvis Bay, 20.01. - 08.02.2003.

Schouten, S., Hopmans, E. C., and M, E. S. (2002). Distributional variations in marine crenarchaeotal membrane lipids : a new tool for reconstructing ancient sea water temperatures. *Earth and Planetary Science Letters*, 204:265–274.

Schubert, C. J. and Calvert, S. E. (2001). Nitrogen and carbon isotopic composition of marine and terrestrial organic matter in Arctic Ocean sediments: implications for nutrient utilization and organic matter composition. *Deep Sea Research Part I: Oceanographic Research Papers*, 48:789–810.

Shannon, L. V. and Nelson, G. (1996). The Benguela: Large Scale Features and Processes and System Variability. In Wefer, G., Berger, W., Siedler, G., and Webb, D., editors, *The South Atlantic*, pages 163–210. Springer, Berlin.

Shillington, F. A., Hutchings, L., Probyn, T. A., Waldron, H. N., and Peterson, W. T. (1992). Filaments and the Benguela frontal zone: Offshore advection or recirculating loops? *South African Journal of Marine Science*, 12(1):207–218.

Sigman, D. M., Casciotti, K. L., Andreani, M., Barford, C., Galanter, M., and Böhlke, J. K. (2001). A bacterial method for the nitrogen isotopic analysis of nitrate in seawater and freshwater. *Analytical Chemistry*, 73(17):4145–4153.

Sigman, D. M., DiFiore, P. J., Hain, M. P., Deutsch, C., Wang, Y., Karl, D. M., Knapp, A. N., Lehmann, M. F., and Pantoja, S. (2009). The dual isotopes of deep nitrate as a constraint on the cycle and budget of oceanic fixed nitrogen. *Deep-Sea Research Part I: Oceanographic Research Papers*, 56(9):1419–1439.

Sigman, D. M., Granger, J., DiFiore, P. J., Lehmann, M. F., Ho, R., Cane, G., and van Geen, A. (2005). Coupled nitrogen and oxygen isotope measurements of nitrate along the eastern North Pacific margin. *Global Biogeochemical Cycles*, 19(4):1–14.

Sigman, D. M., M. A, A., McCorkle, D. C., Francois, R., and Fischer, G. (1999). The δ15N of nitrate in the Southern Ocean: Nitrate consumption in surface waters. *Global Biogeochemical Cycles*, 13(4):1149–1166.

Smart, S. M., Fawcett, S. E., Ren, H., Schiebel, R., Tompkins, E. M., García, A. M., Stirnimann, L., Roychoudhury, A., Haug, G. H., and Sigman, D. M. (2020). The Nitrogen Isotopic Composition of Tissue and Shell-Bound Organic Matter of Planktic Foraminifera in Southern Ocean Surface Waters. *Geochemistry, Geophysics, Geosystems*, 21:1–29.

Smart, S. M., Ren, H., Fawcett, S. E., Schiebel, R., Conte, M., Rafter, P. A., Ellis, K. K., Weigand, M. A., Oleynik, S., Haug, G. H., and Sigman, D. M. (2018). Groundtruthing the planktic foraminifer-bound nitrogen isotope paleo-proxy in the Sargasso Sea. *Geochimica et Cosmochimica Acta*, 235:463–482.

Spindler, M., Hemleben, C., Salomons, J. B., and Smit, L. P. (1984). Feeding behavior of some planktonic foraminifers in laboratory cultures. *Journal of Foraminiferal Research*, 14(4):237–249.

Steinhardt, J., De Nooijer, L. L. J., Brummer, G. J., and Reichart, G. J. (2015). Profiling planktonic foraminiferal crust formation. *Geochemistry, Geophysics, Geosystems*, 16(7):2409–2430.

Straub, M., Sigman, D. M., Ren, H., Martínez-García, A., Meckler, A. N., Hain, M. P., and Haug, G. H. (2013). Changes in North Atlantic nitrogen fixation controlled by ocean circulation. *Nature*, 501:200–204.

Studer, A. S., Mekik, F., Ren, H., Hain, M. P., Oleynik, S., Martínez-García, A., Haug, G. H., and Sigman, D. M. (2021). Ice Age-Holocene Similarity of Foraminifera-Bound Nitrogen Isotope Ratios in the Eastern Equatorial Pacific. *Paleoceanography and Paleoclimatology*, 36(5):1–16.

Studer, A. S., Sigman, D. M., Martínez-García, A., Benz, V., Winckler, G., Kuhn, G., Esper, O., Lamy, F., Jaccard, S. L., Wacker, L., Oleynik, S., Gersonde, R., and Haug, G. H. (2015). Antarctic Zone nutrient conditions during the last two glacial cycles. *Paleoceanography*, 30:845–862.

Stuut, J.-B. W., Prins, M. a., Schneider, R., Weltje, G. J., Jansen, J., and Postma, G. (2002). A 300-kyr record of aridity and wind strength in southwestern Africa: inferences from grain-size distributions of sediments on Walvis Ridge, SE Atlantic. *Marine Geology*, 180(1-4):221–233.

Sunda, W. G. and Huntaman, S. A. (1997). Interrelated influence of iron, light and cell size on marine phytoplankton growth. *Nature*, 390(6658):389–392.

Takagi, H., Kimoto, K., Fujiki, T., Saito, H., Schmidt, C., Kucera, M., and Moriya, K. (2019). Characterizing photosymbiosis in modern planktonic foraminifera. *Biogeosciences*, 16(17):3377–3396.

Tesdal, J. E., Galbraith, E. D., and Kienast, M. (2013). Nitrogen isotopes in bulk marine sediment: Linking seafloor observations with subseafloor records. *Biogeosciences*, 10(1):101–118.

Tyrrell, T. and Lucas, M. I. (2002). Geochemical evidence of denitrification in the Benguela upwelling system. *Continental Shelf Research*, 22(17):2497–2511.

Tyson, P., Cooper, G., and McCarthy, T. (2002). Millennial to multi-decadal variability in the climate of southern Africa. *International Journal of Climatology*, 22(9):1105–1117.

Van Sebille, E., Barron, C. N., Biastoch, A., Van Leeuwen, P. J., Vossepoel, F. C., and De Ruijter, W. P. (2009). Relating Agulhas leakage to the Agulhas Current retroflection location. *Ocean Science*, 5(4):511–521.

Van Sebille, E., Van Leeuwen, P. J., Biastoch, A., and De Ruijter, W. P. (2010). On the fast decay of Agulhas rings. *Journal of Geophysical Research: Oceans*, 115(3):1–15.

Vortmeyer-Kley, R., Lünsmann, B., Berthold, M., Gräwe, U., and Feudel, U. (2018). Eddies: fluid dynamical niches or transporters? - A case study in the Western Baltic Sea. *Frontiers in Marine Science – Physical Oceanography*, 6(March):1–15.

Wallschuss, S., Mdutyana, M., Parrott, R. G., Forrer, H. J., Roman, R., Walker, D., Ansorge, I., and Fawcett, S. E. (2022). The Influence of Agulhas Leakage on Primary Production and Nitrogen Cycling in the Southeastern Atlantic Ocean. *Journal of Geophysical Research: Oceans*, 127:1–26.

Weeks, S., Barlow, R., Roy, C., and Shillington, F. A. (2006). Remotely sensed variability of temperature and chlorophyll in the southern Benguela: upwelling frequency and phytoplankton response. *African Journal of Marine Science*, 28(3-4):493–509.

Weigand, M. A., Foriel, J., Barnett, B., Oleynik, S., and Sigman, D. M. (2016). Updates to instrumentation and protocols for isotopic analysis of nitrate by the denitrifier method. *Rapid Communications in Mass Spectrometry*, 30(12):1365–1383.

Weijer, W., De Ruijter, W. P., Sterl, A., and Drijfhout, S. S. (2002). Response of the Atlantic overturning circulation to South Atlantic sources of buoyancy. *Global and Planetary Change*, 34(3-4):293–311.

Weldeab, S., Stuut, J.-B. W., Schneider, R., and Siebel, W. (2013). Holocene climate variability in the winter rainfall zone of South Africa. *Climate of the Past*, 9(5):2347–2364.

Wellman, R., Cook, F., and Krouse, H. (1968). Nitrogen-15: Microbioloical Alteration of Abundance. *Science*, 161:269–270.

Zabel, M., Schneider, R. R., and Brüchert, V. (2005). METEOR Berichte 05-1 The Benguela Upwelling System 2003. Technical Report 57.

Zhang, R., Wang, X. T., Ren, H., Huang, J., Chen, M., and Sigman, D. M. (2020). Dissolved organic nitrogen cycling in the South China Sea from an isotopic perspective. *Global Biogeochemical Cycles*, 34:1–19.

Chapter 5

Conclusion

The chapters in this thesis provide insights into the relationship between the N isotope composition of planktic foraminifera and that of their environment, in both the southeast Atlantic and southwest Indian Oceans. The broad aim of the project was to determine whether the living, and ultimately fossil, foraminifera-bound (FB-) δ^{15}N signal accurately records changes in upper ocean biogeochemistry, with a particular interest in examining the potential of the proxy as a means to identify past fluctuations in Agulhas leakage. In this final chapter, I summarize the key findings of my research and propose potential ideas for future research that would build upon the work presented here.

5.1 Summary of key findings

Key finding 1: Foraminifera δ^{15}N is correlated to the δ^{15}N of thermocline nitrate and PON in the southeast Atlantic and southwest Indian Oceans.

A major focus of **Chapters 2 and 3** included assessing whether the δ^{15}N in the tissue of living foraminifera varied in conjunction with the δ^{15}N of thermocline nitrate in the southeast Atlantic, a relationship previously observed elsewhere in the low-to-mid latitude ocean (Ren et al., 2009; Smart et al., 2018), and one that has important implications for how FB-δ^{15}N variation is interpreted in downcore records. There was a strong relationship of foraminifera tissue- (FT-) and shell-bound (FB-) δ^{15}N with thermocline nitrate δ^{15}N ($\delta^{15}N_{NO_3}$) under background southeast Atlantic conditions, suggesting that foraminifera in this region do track changes in the δ^{15}N of the nitrate supply to the mixed layer. In the Agulhas Current System (ACS), FT-δ^{15}N variability was more closely tied to δ^{15}N PON (more similar to previous findings from the Subantarctic Zone), although the actual value of $\delta^{15}N_{NO_3}$ remained within similar to the FT-δ^{15}N of several species. The weaker correlation between foraminifera and nitrate δ^{15}N in the ACS was likely an effect of the δ^{15}N of variability in the degree of nitrate consumption (affected by the mixing of new thermocline nitrate into surface waters via a mesoscale cyclonic feature, which led to

a decrease in FT-δ^{15}N and the δ^{15}N of all measured forms of organic N/particulates) than the largely oligotrophic southeast Atlantic. This process of partial consumption demonstrated the rapidity at which the δ^{15}N of foraminifera responds to changes in the δ^{15}N of available nitrate (within $\sim$2 weeks), despite foraminifera being at least one trophic level removed from the nitrate, the source of isotopic change. Nonetheless, although the species whose FT-δ^{15}N best approximated that of thermocline nitrate differed across the ACS, the broad trend of foraminifera reflecting $\delta^{15}N_{NO_3}$ (as has been reported for other regions; Ren et al. 2009, 2012; Smart et al. 2018, 2020) remained, despite the highly nonlinear controls and (sub)mesoscale variability associated with the ACS. This trend is extremely promising for the application of the proxy on a global scale, as it demonstrates consistency among regions and provides evidence that inter-basin comparisons are feasible, despite regional variability.

Also consistent with previous studies' (Ren et al., 2009, 2012, 2015; Smart et al., 2018, 2020) interpretations is the lower FT-δ^{15}N observed in symbiont-hosting species in the ACS, relative to non-symbiont, deeper-dwelling species; symbionts are thought to retain and recycle low δ^{15}N that would otherwise be excreted by the host foraminifer, effectively reducing the δ^{15}N increase associated with trophic level fractionation (Ren et al., 2012; Smart et al., 2018). Furthermore, symbiont-hosting foraminifera best approximated the actual value of thermocline nitrate δ^{15}N in the subtropical and tropical ACS, whilst deeper-dwellers were higher in δ^{15}N. In the southeast Atlantic, however, it was the deep- and intermediate-dwelling species (*G. truncatulinoides*, *G. hirsuta* and *G. inflata*) that appeared to best approximate the actual value of thermocline nitrate (within 0.4 ‰ of the thermocline nitrate δ^{15}N), rather than the shallow, dinoflagellate-hosting species, of which there were relatively few, but whose FT-δ^{15}N was still lower in comparison. It is possible that the relationship between the δ^{15}N of foraminifera and thermocline nitrate could change during warmer conditions, when the symbiont-hosting species become more abundant in the region (Lončarić, 2006), confirmation of this idea would require collection of samples during spring and summer in the region. Nonetheless, initial findings from the southeast Atlantic strongly suggest that there is potential for the use of *G. truncatulinoides* and *G. hirsuta* (as well as *G. inflata*) FB-δ^{15}N as an indicator of long-term (e.g., centennial and longer) changes in winter thermocline conditions, providing that the core site is outside of the main corridor of Agulhas leakage.

Key finding 2: The isotopic signal of nitrate and foraminifera transported in Agulhas leakage remains distinct from that of the background Atlantic.

Chapter 2 compared the δ^{15}N of upper-ocean nitrate and foraminifera under background southeast Atlantic conditions and within a mature anticyclonic eddy (i.e., Agulhas leakage conditions). Even after seven months, the δ^{15}N of the Agulhas eddy remained distinctly

lower than that of its surroundings, although it was higher than offshore ACS subtropical mixed layer and thermocline waters. The low Δ(15-18), the difference between the N and O isotopes of nitrate, was even more reminiscent of Agulhas subtropical waters (Marshall et al., 2023), and implied retention of the Agulhas source waters within the eddy environment. FT- and FB-δ^{15}N in the Agulhas eddy was on average 2.4 ‰ lower than background Atlantic foraminifera of the same species. The similarity of the species assemblage across the transect (i.e., the absence of traditional "leakage fauna") was hypothesized to be due to rapid cooling within eddies, as this would lead to a shift in species dominance to those better adapted for reproduction in cooler waters. Remarkably, the low δ^{15}N signal in leakage foraminifera appears resilient to transitions in foraminifera generations and species, and therefore holds potential for tracking leakage in the Cape Basin beyond where the characteristic warm Agulhas temperature signature is lost and distinctive "leakage fauna" disappear.

Key finding 3: The FT-δ^{15}N of leakage foraminifera is not a straightforward reflection of FT-δ^{15}N in the ACS prior to ring shedding.

Thermocline waters in the ACS are made up of Tropical Thermocline Water (TTW) and Subtropical Thermocline Water (STTW), both of which are lower in nitrate δ^{15}N than South Atlantic thermocline waters, with STTW δ^{15}N lower in comparison to TTW. However, the FT-δ^{15}N of the majority of ACS foraminifera in **Chapter 3** was not low enough to explain the low FT-δ^{15}N observed in the Agulhas eddy in **Chapter 2**. Instead, only the FT-δ^{15}N measured furthest offshore of the Agulhas Current core (and whose low FT-δ^{15}N was likely due in part to the recent injection of new nitrate) resembled that measured within the Agulhas eddy. As mentioned above (*Key finding 1*), thermocline nitrate δ^{15}N across much of the sampled ACS region was best recorded by symbiont-hosting species such as *G. ruber* and *T. sacculifer*, which are relatively low in ^{15}N in comparison to the deep-dwelling, symbiont-barren species (e.g., *G. truncatulinoides* and *G. hirsuta*), which were better approximators of thermocline nitrate δ^{15}N in the southeast Atlantic. Species-specific FT-δ^{15}N was thus similar between the most oligotrophic sections of the southeast Atlantic and ACS environments, leading to the conclusion that additional N-cycling processes must be occurring downstream and/or within the eddy, post-shedding, to produce the low FT-δ^{15}N observed in Agulhas leakage. Two mechanisms that may have yielded the δ^{15}N decrease are N_2 fixation – which would introduce new N with a low δ^{15}N into the system – and the recycling of low-δ^{15}N ammonium generating low-δ^{15}N PON (i.e., foraminifer food sources). To test these hypotheses, in-situ measurements of N_2 fixation and ammonium cycling within an Agulhas eddy are needed, alongside time series FT-δ^{15}N data in the ACS to investigate inter-seasonal signals.

Key finding 4: Ground-truthing the FB-δ^{15}N method in the southeast Atlantic shows that modern tissue- and shell-bound δ^{15}N are strongly correlated to the δ^{15}N of fossil foraminifera in recent sediments, but that biogeochemical processes integrating over different time intervals can result in δ^{15}N offsets

The strong positive relationship between modern tissue and shell-bound δ^{15}N observed in the Southeast Atlantic and Southwest Indian study areas supports the hypothesis that FB-δ^{15}N is a good representation of the isotopic composition of the living organism, even in this dynamic mid-latitude region. This finding, from **Chapters 2 and 4**, is in line with previous ground-truthing research in the Sargasso Sea (Smart et al., 2018) and Southern Ocean regions (Smart et al., 2020). A difference in the integration times between tissue- (days) and shell-bound (weeks) δ^{15}N was likely responsible for shell-bound δ^{15}N being on average 1.4 ‰ higher than tissue δ^{15}N. Both the southeast Atlantic and ACS were sampled at the start of the winter mixing period, thus tissue potentially reflected some of the low-δ^{15}N PON derived from newly supplied (not yet δ^{15}N-elevated) nitrate from below the mixed layer whereas the shells had incorporated N prior to winter mixing.

A strong, positive linear correlation was again evident when comparing (species-specific) fossil foraminifera δ^{15}N to that of modern shells, but with an additional average offset of 2.5 ‰ between them (where fossil shell δ^{15}N > modern shell δ^{15}N). A difference in the integration time of δ^{15}N within samples was again suggested as a potential explanation; given that the δ^{15}N of the fossil shells reflected a signal integrated over several thousand years (somewhere between 1,340 and 5,780 years), it is likely that some of this offset is due to changing ocean conditions during the late Holocene. There are other potential causes of the higher δ^{15}N that cannot at this stage be ruled out. These include (1) the preferential dissolution of low-δ^{15}N juvenile foraminifera during sinking (due to a slower sinking rate or thinner shells); (2) post-mortem decomposition of foraminifera tissue creating an acidic microenvironment that dissolved low-δ^{15}N inner chambers; (3) a higher δ^{15}N PON diet prior to gametogenesis (a stage not captured by the net tows); and (4) a shift in the season of highest productivity between the mid-Holocene and the present day.

More research is needed to determine which of these explanations is the most likely to account for the higher FB-δ^{15}N observed in the fossil shells in the Cape Basin; additional global ground-truthing efforts will help to constrain the isotopic effect of shell loss during sinking, whereas downcore FB-δ^{15}N reconstructions in the region will allow for a better estimation of the magnitude of expected FB-δ^{15}N change over centennial and millennial time scales. Knowledge of the latter would be useful when determining the sensitivity of FB-δ^{15}N to changes in environmental conditions. Regardless of which of these processes are responsible for the δ^{15}N offset, the strong correlation that exists between modern and fossil FB-δ^{15}N is promising for the use of the FB-δ^{15}N proxy method in the Southeast

Atlantic, as the modern *versus* fossil FB-δ^{15}N offset appears to be consistent across species.

Key finding 5: Relatively small distances matter when interpreting FB-δ^{15}N variability in the southeast Atlantic.

Although some of the small but noticeable variability between core sites in **Chapter 4** could be attributed to differences in surface sediment age, the differences also suggest that location may be an important factor in δ^{15}N variability. Dominant biogeochemical processes can vary strongly across relatively small distances in the modern Cape Basin; downcore variability in FB-δ^{15}N may therefore reflect different processes depending on the core location. Water column denitrification, which raises the δ^{15}N of nitrate and the organic matter derived from it (Brandes et al., 1998), may have contributed to the FB-δ^{15}N difference observed between the two coretops located north of 32°S and the three coretops south of this latitude. Sediments located closer to regions of perennial upwelling in the Northern Benguela Upwelling System, where low oxygen conditions are more persistent (Tyrrell and Lucas, 2002; Kuypers et al., 2005), are more likely to be influenced by denitrification. Denitrification could explain the higher average FB-δ^{15}N (by 0.9 ‰) in the northern coretops relative to those further south. On the other hand, the southern cores were located closer to the corridor (most frequent pathway) of Agulhas leakage. Fossil foraminifera sampled from this sediment may therefore show a stronger (low-δ^{15}N) Agulhas leakage signal, explaining the lower FB-δ^{15}N in the southern cores relative to the northern cores, and demonstrating again how small spatial changes might result in substantial isotopic variability.

5.2 Concluding remarks and future research

Ground-truthing the FB-δ^{15}N proxy involves examining and understanding the dominant forcings in a region, investigating how best to distinguish between biogeochemical processes that act to produce similar signals to one another (e.g., N_2 fixation, partial assimilation of nitrate, and ammonium cycling), and developing potential scenarios that could cause the dominant drivers of variability to change over time. The research detailed in this thesis not only provides baseline δ^{15}N values with which to compare downcore records from the region, but also helps to interpret downcore FB-δ^{15}N changes. Given the emphasis on determining average baseline biogeochemical conditions against which palaeo-records can be compared, it might seem counter-intuitive that seasonality or mesoscale features such as eddies could significantly impact the interpretation of sediment records with centennial- or millennial-scale integration times. However, analysis of short-term variability is an important component of ground-truthing any method, as it provides analogues to longer term changes and increases awareness of which processes are best recorded in the sediment. For example, with regards to particles and organic matter,

sediment records are inherently biased in favour of the season where the flux out of the photic zone (and deposition on the seafloor) is greatest.

It is therefore important to know what biogeochemical processes are dominant in particular seasons, in order to correctly interpret FB-δ^{15}N variation in the sediment record. Similarly, when eddies are a frequent and integral component of a region, as is the case in the Indo-Atlantic gateway region, biogeochemical processes specific to these mesoscale features have the potential to significantly affect the sedimentary FB-δ^{15}N signal. The low FB-δ^{15}N signal within an Agulhas eddy is one example where understanding mesoscale dynamics plays a crucial role in how one might interpret FB-δ^{15}N variability within the southeast Atlantic. The consistently low foraminifera tissue and shell-bound δ^{15}N within the Agulhas eddy revealed that not only do these mesoscale features bring low δ^{15}N nitrate and foraminifera into the Atlantic, but the isotopic signal remains distinct from its surroundings (and potentially intensifies) over the course of several months. In this way, the 'average' conditions, whereby FB-δ^{15}N approximates the local thermocline nitrate δ^{15}N, are disrupted. It is therefore important to be able to recognize when and where fossil FB-δ^{15}N variability is a product of a shift in the season of peak productivity, or the result of a change in the frequency and/or intensity of local mesoscale features. Generating multiple FB-δ^{15}N measurements from a variety of foraminifer species, and/or the inclusion of additional proxy methods (e.g., proxies for wind strength or dust flux), when reconstructing past ocean conditions, will be valuable for distinguishing between the two drivers. Furthermore, future research into seasonal signals of modern foraminifera tissue- and shell-bound N from the study region would be invaluable, as has been done in the Sargasso Sea (Smart et al., 2018) and Southern Ocean (Smart et al., 2020).

While challenging, the Cape Basin is a useful region for palaeoceanographers to test the effects of varying biogeochemical processes on FB-δ^{15}N. Different drivers of isotopic variability dominate at different sites, sometimes over relatively short distances, such as multiple nitrate sources to the euphotic zone (South Atlantic Subtropical Mode Water, Tropical Thermocline Water, Subtropical Thermocline Water), perennial and seasonal coastal upwelling, denitrification off the west coast of South Africa and Namibia, oligotrophic gyre conditions, mesoscale eddy environments (altering stratification), and N_2 fixation (both in the offshore Agulhas Current System and potentially within anticyclonic eddies). Each of these processes has an isotopic effect on δ^{15}N-NO_3 and the biological community it supports, and it may be possible to separate out the effects of each process on FB-δ^{15}N, if there is careful consideration of sampling location. For example, coastal sites located close to the Lüderitz upwelling cell could be used to reconstruct cycles of denitrification in the Benguela Upwelling System, whilst a comparison of FB-δ^{15}N just south and north of the Walvis Ridge could reveal changes in the proportion of Agulhas leakage progressing into the North Atlantic.

In summary, continued research into the nuances of foraminifera ecology and the responses of foraminifera to seasonal and longer-term change is needed to address new

research questions involving seasonality and location that have arisen as a result of this study, and to avoid misinterpreting isotopic changes observed in fossil foraminifera. Nonetheless, the key findings of this study strongly support the continued ground-truthing and future use of FB-δ^{15}N in the southeast Atlantic and southwest Indian Oceans, as a means of identifying past changes in thermocline nitrate conditions. In addition, these initial data highlight the potential of the proxy to record past fluctuations in Agulhas leakage. Palaeoceanographic reconstructions making use of FB-δ^{15}N to investigate changes in leakage within these dynamic ocean regions could greatly assist in forecasting the response(s) of the Atlantic Meridional Overturning Circulation to future climate change.

References

Brandes, J. A., Devol, A. H., Yoshinari, T., Jayakumar, D. A., and Naqvi, S. W. (1998). Isotopic composition of nitrate in the central Arabian Sea and eastern tropical North Pacific: A tracer for mixing and nitrogen cycles. *Limnology and Oceanography*, 43(7):1680–1689.

Kuypers, M., Lavik, G., Woebken, D., Schmid, M. C., Fuchs, B. M., Amann, R., Jorgensen, B. B., and Jetten, M. S. M. (2005). Massive nitrogen loss from the Benguela upwelling system through anaerobic ammonium oxidation. *Proc Natl Acad Sci U S A*, 102(18):6478–6483.

Lončarić, N. (2006). Planktic foraminiferal content in a mature Agulhas eddy from the SE Atlantic: Any influence on foraminiferal export fluxes? *Geologia Croatica*, 59(1):41–50.

Marshall, T. A., Sigman, D. M., Beal, L. M., Foreman, A., Martínez-García, A., Blain, S., Campbell, E., Fripiat, F., Granger, R., Harris, E., Haug, G. H., Marconi, D., Oleynik, S., Rafter, P. A., Roman, R., Sinyanya, K., Smart, S. M., and Fawcett, S. E. (2023). The Agulhas Current Transports Signals of Local and Remote Indian Ocean Nitrogen Cycling. *Journal of Geophysical Research: Oceans*, 128:1–29.

Ren, H., Sigman, D. M., Meckler, A. N., Plessen, B., Robinson, R., Rosenthal, Y., and Haug, G. H. (2009). Foraminiferal isotope evidence of reduced nitrogen fixation in the ice age Atlantic Ocean. *Science*, 323(5911):244–248.

Ren, H., Sigman, D. M., Thunell, R. C., and Prokopenko, M. G. (2012). Nitrogen isotopic composition of planktonic foraminifera from the modern ocean and recent sediments. *Limnology and Oceanography*, 57(4):1011–1024.

Ren, H., Studer, A. S., Serno, S., Sigman, D. M., Winckler, G., Anderson, R. F., Oleynik, S., Gersonde, R., and Haug, G. H. (2015). Glacial-to-interglacial changes in nitrate supply and consumption in the subarctic North Pacific from microfossil-bound N isotopes at two trophic levels. *Paleoceanography*, 30(9):1217–1232.

Smart, S. M., Fawcett, S. E., Ren, H., Schiebel, R., Tompkins, E. M., García, A. M., Stirnimann, L., Roychoudhury, A., Haug, G. H., and Sigman, D. M. (2020). The Nitrogen Isotopic Composition of Tissue and Shell-Bound Organic Matter of Planktic Foraminifera in Southern Ocean Surface Waters. *Geochemistry, Geophysics, Geosystems*, 21:1–29.

Smart, S. M., Ren, H., Fawcett, S. E., Schiebel, R., Conte, M., Rafter, P. A., Ellis, K. K., Weigand, M. A., Oleynik, S., Haug, G. H., and Sigman, D. M. (2018). Ground-truthing the planktic foraminifer-bound nitrogen isotope paleo-proxy in the Sargasso Sea. *Geochimica et Cosmochimica Acta*, 235:463–482.

Tyrrell, T. and Lucas, M. I. (2002). Geochemical evidence of denitrification in the Benguela upwelling system. *Continental Shelf Research*, 22(17):2497–2511.

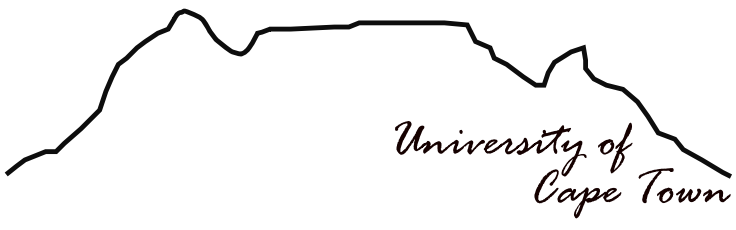

Appendix A

Additional Data Tables

Table A.1: Abundance of foraminifera at Southeast Atlantic (SAMBA) stations.

	Eddy			Atlantic				
Station	3	4	5	9	10	11	13	14	17
G. inflata	90	768	246	78	62	64	317	72	701
G. truncatulinodies	19	70	205	48	93	121	201	614	963
G. hirsuta	26	99	183	34	62	32	182	27	259
O. universa	1	4	0	0	0	1	0	0	6
G. siphonifera	1	16	10	0	0	7	0	0	29
G. falconensis	0	0	0	0	0	0	1	0	38
G. calida	0	6	1	0	0	0	0	1	5
G. bulloides	7	0	100	0	5	5	0	250	400
G. glutinata	0	0	0	0	0	0	0	7	3
G. ruber	0	0	0	0	0	0	0	0	1

Table A.2: Average foraminifer tissue δ^{15}N from the southeast Atlantic. Leading edge station (10) is classified as "Atlantic," and trailing edge station (3) classified as "Eddy." sd δ^{15}N indicates standard deviation between multiple samples from the same station. For depth estimates and symbiont relationships, see Table A.6

Station	Longitude (°E)	Species	Type	δ^{15}N	sd δ^{15}N
17	2.6	*G. bulloides*	Atlantic	6.7	0.3
17	2.6	*G. glutinata*	Atlantic	7	
17	2.6	*G. hirsuta*	Atlantic	7.2	0.2
17	2.6	*G. truncatulinoides*	Atlantic	7.5	0.1
14	5.1	*G. bulloides*	Atlantic	5.7	0.3
14	5.1	*G. falconensis*	Atlantic	6.2	0
14	5.1	*G. hirsuta*	Atlantic	7.4	0.2
14	5.1	*G. inflata*	Atlantic	6.8	0.6
14	5.1	*G. siphonifera*	Atlantic	8	0.1
14	5.1	*G. truncatulinoides*	Atlantic	7.5	0.6
14	5.1	*O. universa*	Atlantic	7.1	
13	7.5	*G. hirsuta*	Atlantic	6.7	0.2
13	7.5	*G. inflata*	Atlantic	6.5	0.2
13	7.5	*G. truncatulinoides*	Atlantic	6.9	0.1
11	10.2	*G. hirsuta*	Atlantic	7.0	0.1
11	10.2	*G. inflata*	Atlantic	6.6	0.4
11	10.2	*G. truncatulinoides*	Atlantic	7.1	0.2
10	11.2	*G. hirsuta*	Atlantic	6.6	0.5
10	11.2	*G. inflata*	Atlantic	6.3	0.1
10	11.2	*G. truncatulinoides*	Atlantic	6.6	0.2
9	11.8	*G. hirsuta*	Eddy	6.1	0.2
9	11.8	*G. inflata*	Eddy	5.1	0.3
9	11.8	*G. truncatulinoides*	Eddy	6.0	0.3
5	13.6	*G. bulloides*	Eddy	3.4	0.1
5	13.6	*G. hirsuta*	Eddy	5.2	0.3
5	13.6	*G. inflata*	Eddy	4.6	0.1
5	13.6	*G. siphonifera*	Eddy	5.3	0.3
5	13.6	*G. truncatulinoides*	Eddy	5.2	0.4
4	14	*G. bulloides*	Eddy	1.7	0.9
4	14	*G. hirsuta*	Eddy	4.7	0.3
4	14	*G. inflata*	Eddy	2.8	0.7
4	14	*G. siphonifera*	Eddy	4.0	0.7
4	14	*G. truncatulinoides*	Eddy	4.9	0.8
4	14	*O. universa*	Eddy	4.6	
3	14.3	*G. hirsuta*	Eddy	5.3	0.4
3	14.3	*G. inflata*	Eddy	3.3	0.8
3	14.3	*G. siphonifera*	Eddy	5	

Table A.3: Average bulk zooplankton δ^{15}N from the southeast Atlantic.

Station	Latitude (°S)	Longitude (°E)	Size (μm)	Zoo δ^{15}N	sd δ^{15}N	Type
4	-35.25	13.97	250-500	3.2	0.2	Eddy
4	-35.25	13.97	500-1000	4.8	0.2	Eddy
5	-35.25	13.68	250-500	4.7	0.2	Eddy
5	-35.25	13.68	500-1000	5.4	0.1	Eddy
10	-34.51	11.2	250-500	5.8		Leading Edge
10	-34.51	11.2	500-1000	6.6	0.1	Leading Edge
13	-34.51	7.45	250-500	6.0	0.2	Atlantic
13	-34.51	7.45	500-1000	7.7	0.1	Atlantic
14	-34.5	5.11	250-500	6.1	0.0	Atlantic
14	-34.5	5.11	500-1000	6.9	0.0	Atlantic

Table A.4: Weighted average PON δ^{15}N from the southeast Atlantic (profiles 0 - 175m).

Station	Latitude (°S)	Longitude (°E)	PON δ^{15}N	Type
1	-34.5	17.14	1.7	Upwelling
3	-34.75	14.32	2.4	Atlantic
4	-35	14	1.3	Trailing Edge
5	-35.25	13.68	2.7	Eddy
6	-35.41	13.47	3.2	Eddy
7	-35.25	13.07	3.0	Eddy
8	-35	12.44	2.8	Eddy
9	-34.75	11.81	3.0	Eddy
10	-34.51	11.2	4.6	Leading Edge
11	-34.5	10.2	2.1	Atlantic
12	-34.51	8.33	1.6	Eddy
13	-34.51	7.45	2.4	Mixed
13R	-34.51	7.45	2.5	Mixed
14	-34.5	5.11	1.2	Atlantic
17	-34.5	2.62	3.4	Atlantic

Table A.5: Abundance of foraminifera at Agulhas Current System stations.

		Inshore edge		Current core			Offshore edge		Mid-shore			Offshore	
	Station	3	4	5	6	6.5	8	8.5	10	12	14	16	20
Species	Type	B1	B2	B3	B4	B12	B5	B11	B6	B7	B8	B9	B10
O. universa	subtropical	7	9	42	0	2	7	3	11	1	6	0	1
G. bulloides	subtropical	18	21	72	3	49	1	56	113	34	13	7	13
T. sacculifer	tropical	1	41	208	112	45	50	27	19	6	17	0	7
P. obliquiloculata	tropical	5	4	55	29	14	14	5	18	5	9	0	3
N. dutertrei	subtropical	4	4	34	0	12	23	13	28	12	15	2	6
G. ungulata	subtropical	0	3	55	1	0	5	2	3	3	6	0	0
G. tumida	tropical	0	1	15	0	6	1	0	0	0	0	1	0
G. truncatulinoides	subtropical	0	0	6	4	7	2	3	10	2	8	3	1
G. siphonifera	tropical	45	8	60	0	52	6	22	25	7	8	1	3
G. inflata	subtropical	2	0	37	12	72	103	72	334	61	73	72	37
G. hirsuta	subtropical	0	1	0	2	0	2	1	9	0	1	3	0
G. ruber	tropical	13	31	117	38	20	19	29	43	9	9	2	3
G. glutinata	subtropical	0	6	9	5	2	5	33	21	1	6	0	4
G. menardii	tropical	1	7	3	14	63	7	17	21	17	9	1	10
G. calida	subtropical	2	3	24	0	2	2	1	9	6	10	0	0
G. falconensis	subtropical	1	1	3	3	0	0	2	2	0	0	0	0
G. rubescens	tropical	0	0	0	1	0	1	0	5	0	0	0	0
G. adamsi/G. radians	tropical	0	0	0	0	1	0	1	0	0	0	0	0
N. incompta/N. pachyderma	subtropical	0	0	0	3	4	4	0	2	0	0	0	0
G. hexagonus	tropical	0	1	0	0	0	0	0	0	0	0	0	0
G. pelagica	tropical	0	3	2	8	1	0	0	0	0	0	0	0
G. uvula	subtropical	0	0	2	0	0	0	0	0	3	2	0	0
G. scitula	subtropical	0	0	1	5	0	0	0	0	0	0	0	0
G. conglobatus	tropical	0	0	2	1	0	0	0	0	0	0	0	0

Table A.6: Tissue-bound δ^{15}N of Agulhas Current System foraminifera. Depth estimates and symbiont classification are referenced predominantly from Peeters and Brummer (2002); Birch et al. (2013); Kimoto (2015); Rebotim et al. (2017); Takagi et al. (2019) and Stainbank et al. (2019).

Species	Current & Shear δ^{15}N	Mid-shore δ^{15}N	Offshore δ^{15}N	Depth estimates	Symbionts?
G. bulloides	6.8 ± 2.1	6.1 ± 1.1	5 ± NA	0 - 100	No (Unknown)
G. calida	7 ± NA	7.3 ± NA		60 - 80	Unknown
G. crassaformis	6.9 ± NA			40 - 70	No
G. glutinata		6.3 ± 0.3		0 - 80	Facultative (chrysophytes)
G. hirsuta		7.3 ± 0.7		100 - 200	No
G. inflata	7.0 ± 0.5	6.2 ± 0.5	4.5 ± 0.6	80 - 100	Facultative (chrysophytes)
G. menardii	6.3 ± 1.0	6.0 ± 0.5	4.9 ± 0.5	60 - 120	Facultative (chrysophyte/prymnesiophyte)
G. ruber	5.1 ± 0.6	4.9 ± 0.9	3.4 ± NA	<50m	Obligate (dinoflagellate)
G. siphonifera	7.6 ± 1.3	6.7 ± 1.0		80 - 100	Facultative (chrysophytes)
G. truncatulinoides	7.6 ± 0.4	6.4 ± 0.5	4.4 ± NA	80 - 200	No
G. tumida	5.1 ± 0.2			thermocline >100	Facultative (chrysophyte)
G. ungulata	5.4 ± 0.3	5.4 ± 0.4		thermocline <100	No
N. dutertrei	6.5 ± 1.1	6.2 ± 0.4	5.0 ± NA	0 - 80	Facultative (chrysophyte/pelagophyte)
O. universa	5.4 ± 0.7	5.6 ± NA		70 - 100	Obligate (dinoflagellates)
P. obliquiloculata	6.2 ± 0.4	6.3 ± 0.4	5.7 ± NA	30 - 60	Facultative (chrysophyte/prymnesiophyte)
T. sacculifer	5.2 ± 0.5	5.2 ± 0.4	3.5 ± NA	20 - 80	Obligate (dinoflagellate)

References

Birch, H., Coxall, H. K., Pearson, P. N., Kroon, D., and O'Regan, M. (2013). Planktonic foraminifera stable isotopes and water column structure: Disentangling ecological signals. *Marine Micropaleontology*, 101:127–145.

Kimoto, K. (2015). *Marine protists: Diversity and dynamics*.

Peeters, F. J. and Brummer, G. J. A. (2002). The seasonal and vertical distribution of living planktic foraminifera in the NW Arabian Sea. *Geological Society Special Publication*, 195:463–497.

Rebotim, A., Voelker, A. H., Jonkers, L., Waniek, J. J., Meggers, H., Schiebel, R., Fraile, I., Schulz, M., and Kucera, M. (2017). Factors controlling the depth habitat of planktonic foraminifera in the subtropical eastern North Atlantic. *Biogeosciences*, 14(4):827–859.

Stainbank, S., Kroon, D., Rüggeberg, A., Raddatz, J., de Leau, E. S., Zhang, M., and Spezzaferri, S. (2019). *Controls on planktonic foraminifera apparent calcification depths for the northern equatorial Indian Ocean*, volume 14.

Takagi, H., Kimoto, K., Fujiki, T., Saito, H., Schmidt, C., Kucera, M., and Moriya, K. (2019). Characterizing photosymbiosis in modern planktonic foraminifera. *Biogeosciences*, 16(17):3377–3396.

Table A.7: Average bulk zooplankton δ^{15}N from the Agulhas Current System.

Station	Size (μm)	Zoo δ^{15}N	sd δ^{15}N
3	500-1000	6.7	0.1
4	250-500	5.6	0.1
4	500-1000	7.1	0.0
5	250-500	6.0	0.3
5	500-1000	6.0	0.1
6	250-500	5.1	0.1
6	500-1000	5.6	0.1
6.5	250-500	6.0	0.1
6.5	500-1000	6.2	0.0
8	250-500	5.5	0.1
8	500-1000	6.2	0.1
8.5	250-500	5.4	0.2
8.5	500-1000	5.9	0.0
10	250-500	5.8	0.2
10	500-1000	6.0	0.1
12	250-500	5.6	0.1
12	500-1000	6.0	0.1
14	250-500	5.6	0.1
14	500-1000	5.8	0.0
16	250-500	3.3	0.0
16	500-1000	4.0	0.1
20	250-500	3.9	0.0
20	500-1000	4.3	0.0

Table A.8: Weighted average PON δ^{15}N from the Agulhas Current System (profiles 5 - 200m).

Station	PON δ^{15}N	δ^{15}N sd
1	1.36	0.08
2	3.31	0.05
3	2.41	0.31
4	2.27	0.13
5	3.4	0.2
6	1.97	0.22
6.5	2.78	0.12
7	2.52	0.15
8	2.77	0.11
8.5	1.18	0.16
9	2.58	0.18
10	2.49	0.07
11	3.49	0.27
12	2.02	0.17
13	3.92	0.08
14	2.88	0.1
15	3.57	0.08
16	0.93	0.12
17	2.38	0.12
18	1.68	0.19
19	1.21	0.11
20	1.21	0.11

Table A.9: Foraminifera-bound δ^{15}N from South Atlantic core tops.

GeoB	Species	δ^{15}N	[N] nmol/ml
8308	*G. hirsuta*	10.7	5.1
8308	*G. inflata*	10.0	5.0
8308	*G. ruber*	8.5	3.2
8308	*G. siphonifera*	11.2	4.7
8308	*G. truncatulinoides*	10.0	4.6
8308	*N. dutertrei*	10.1	5.3
8308	*O. universa*	7.7	2.9
8308	*T. sacculifer*	9.2	5.0
8311	*G. hirsuta*	10.4	18.1
8311	*G. hirsuta*	11.6	16.0
8311	*G. inflata*	9.5	12.0
8311	*G. truncatulinoides*	12.0	5.0
8311	*O. universa*	10.0	4.4
8317	*G. hirsuta*	9.9	4.9
8317	*G. inflata*	9.5	5.1
8317	*G. truncatulinoides*	9.8	4.9
8317	*O. universa*	9.0	2.1
8336	*G. bulloides*	11.9	3.8
8336	*G. hirsuta*	11.4	23.3
8336	*G. inflata*	11.1	20.7
8336	*G. inflata*	9.7	17.0
8336	*G. inflata*	10.8	4.3
8336	*G. ruber*	10.3	4.6
8336	*G. siphonifera*	11.4	4.6
8336	*G. truncatulinoides*	11.6	12.7
8336	*O. universa*	10.8	8.1
8336	*T. sacculifer*	9.7	6.2
8342	*G. hirsuta*	10.5	5.0
8342	*G. inflata*	10.0	5.0
8342	*G. siphonifera*	11.4	4.8
8342	*G. truncatulinoides*	9.9	4.9
8342	*N. dutertrei*	10.7	4.9
8342	*O. universa*	9.3	4.7
8342	*T. sacculifer*	9.7	3.8